UNIVERSITÀ DEGLI STUDI DI BRESCIA

Dottorato di ricerca in Ingegneria Civile, Ambientale, della Cooperazione internazionale e di Matematica

CICLO
XXXVI

SUSTAINABLE URBAN DRAINAGE SYSTEMS: ASSESSING RAINGARDEN HYDRAULIC BEHAVIOUR USING LOW-COST ELECTRONIC SENSOR TECHNOLOGY AND NUMERICAL MODELLING

Settore scientifico disciplinare ICAR/02

Coordinatore:
Prof. MARCO PILOTTI

Candidata:
ARIANNA DADA

Tutor:
Prof.ssa GIOVANNA GROSSI

Co-tutor:
Dr. BRANDON WINFREY (Monash University, Melbourne)
Prof.ssa MICHÈLE PEZZAGNO

Declaration

I hereby declare that except where specific reference is made to the work of others, the contents of this dissertation are original and have not been submitted in whole or in part for consideration for any other degree or qualification in this, or any other University. This dissertation is the result of my own work and includes nothing which is the outcome of work done in collaboration, except where specifically indicated in the text.

Dott.ssa Arianna Dada

Acknowledgement

My deepest gratitude to my supervisor Professor Giovanna Grossi for her unceasing support, invaluable guidance, and scholarly mentorship throughout the entirety of my doctoral journey and most of all for putting her trust in me.
A special thanks to my family and Simona for their encouragement, understanding, patience and belief in my abilities. Their support has been essential during this path.
I would like to express my sincere appreciation to Brandon Winfrey, for the hospitality, availability and scientific support during my research period at Monash University of Melbourne, especially for giving me the opportunity to spend 6 months in Australia, land I fell in love with.
I would also like to thank all the people I met, and I worked with during this period: Leigh Oliver (for setting up the experiment), Jayden Eddy and Rhizna for your help and support during my stay at the Monash University, Ing. Barbara Zampori, Michele and Mattia from A2A for your technical support and cooperation, Stefano Barontini for your priceless support and for your precious friendship; Carola Marella for your overseas help, for being passionate and sharing with me the difficulties of the sensors project.
Last but not least, thanks to all my Italian colleagues and friends of the DICATAM for sharing with me, joys and sorrows of this journey.

And thanks to me, for all the hard work.

Acknowledgement of Country

I would like to acknowledge the traditional custodians of the land on which I lived and worked during my six months of research period in Australia and pay my respects to their elders, past, present and emerging.

I recognize the ongoing struggles and injustices that the Aboriginal people have faced throughout their history, including colonization, forced removal from their lands, and systemic discrimination. I acknowledge the ongoing effects of these injustices, which continue to impact the Aboriginal people today.

I pay my respects to the ongoing connection that Aboriginal and Torres Strait Islander people have to the land, and recognize their deep and continuing cultural heritage, beliefs and relationship with the land.

Abstract

In the last decades climate change and excessive land exploitation have made stormwater management an increasingly delicate and debated issue, especially in urban areas. Rising temperatures, alterations in rainfall patterns, and soil sealing caused by construction and road infrastructure have a significant impact on the hydrological cycle, increasing the risk of extreme weather events and more frequent flooding.

These phenomena strain conventional urban drainage systems, often designed for previous climatic conditions, leading to emergency situations and considerable material damage. In this context, effective and sustainable management of water resources and the design of resilient urban infrastructure have become urgent necessities to ensure the safety and well-being of communities and ecosystems.

In response to these challenges, public administrations responsible for land management are seeking to implement policies and strategies that promote urban design more attentive to water management and respect for the hydrological cycle, increasing the number of green spaces and permeable surfaces to restore infiltration and evaporation rates to pre-urbanization levels. Decentralized drainage systems, such as green roofs, porous pavements, retention basins, and wetlands, are gaining ground as effective means to mitigate the impacts of urbanization and increased water volumes. Implementing such measures not only helps manage stormwater but also promotes biodiversity conservation, improves urban aesthetics, and provides recreational spaces for residents.

In recent years, one of the green strategies that has gained significant interest due to its low construction cost, low impact, potential effectiveness and ease of integration and adaptation to the urban context, relies on the implementation of Raingarden.

Raingardens (RG), also known as bioretention cells, are vegetated green areas composed of various layers of engineered soil, designed to capture, filter, and slow down surface runoff, promoting sustainable water management practices. The soil and vegetation within RGs act as natural filters, removing pollutants and facilitating water absorption, thus contributing to restoring the natural hydrological cycle. The slowed down and treated runoff can be gradually released into conventional drainage systems or led to infiltrate into the ground, restoring groundwater levels. However, their effectiveness strongly relies on a constant maintenance.

This study addressed two questions: how to ensure proper maintenance aimed at the rapid restoration of hydrological performance of raingardens in case of malfunction due to unpredictable external phenomena, and what are the benefits generated by the use of raingardens in a highly impermeable urban context where the drainage network is still limited to traditional underground collector systems and under non-stationary climate

conditions? The answers to these questions have been assessed through two parallel research projects, one conducted in Australia and one related to an Italian case study.
In the Australian context, the use of these systems has been entrenched in the urban planning process for several years. However, the high number of installations and their spatial distribution within urban areas give rise to numerous issues in terms of management and maintenance. Indeed, the proper functioning of these systems largely depends on the quality and frequency of maintenance interventions performed. While the guidelines for these systems provide specific indications on the type of interventions and their frequency, numerous studies conducted on field installations have revealed that almost 50% of them do not operate correctly and require maintenance interventions or, in more severe cases, even replacement. This can be attributed to the absence of monitoring systems capable of detecting and reporting any malfunctions in real-time, thus enabling a regime of predictive and targeted maintenance.
For this purpose, a 15-column microcosm study was developed to test the reliability of low-cost moisture and temperature sensors in identifying three common biofilter health conditions.
The 15 columns were thus divided in 3 groups: one group representing the healthy biofilter, the second designed to simulate the effect of preferential flow paths due to surface erosion and the last one designed to simulate a surface clogging due to accumulation of stormwater sediment. These operational treatments were validated using falling-head infiltration rate testing.
Each column was constructed to replicate a typical raingarden, consisting of a ponding zone, a surface filter layer of fine sand, a central transition layer made of coarse sand and sugarcane mulch, and a drainage base layer made of gravel with an outflow drainage pipe.
Within each column, 5 sensors were placed: two low-cost “Chameleon Soil Water Sensor” for measuring soil water tension, two temperature probes “DS18B20”, and one “Truebner SMT 100”, a more reliable and robust sensor, for measuring the volumetric water content.
In order to test the sensors ability to detect malfunctions in the columns, a series of rain events corresponding to real low and medium intensity events, characterized by a different number of antecedent dry days, were simulated. The installed sensors were capable of distinguishing the behaviour of the three experimental column groups, providing data that reflect the different reactions to the water infiltration process. Specifically, columns designed with preferential flow pathways showed less significant variations in soil moisture from one event to another but responded with greater instantaneous variations during the simulated rainfall events. On the contrary, columns characterized by surface clogging showed a greater tendency to dry out. This behaviour

led to a reduction in soil moisture to critical minimum levels, potentially dangerous for the health of the plants, and thus for the raingarden itself.
The second part of the study, instead, focuses on hydraulic modelling work conducted using SWMM software to evaluate the effectiveness of raingardens in mitigating the negative impact of climate change and urbanization. An Italian case study was selected to perform the analysis at the urban catchment scale.
In the Italian context, unlike the Australian one, there is still scepticism and a lack of interest in green solutions. This scepticism can be attributed to the scarcity of urban catchment scale studies that highlight the benefits of these strategies.
The research aims to close the gap by providing an understanding of how raingardens can serve as effective tools in the Italian urban context by simulating various storm scenarios, taking into account the effects of climate change and comparing the results with the actual state of the sewerage. To this end, various scenarios of urban de-pavement, i.e., the conversion of a percentage of impermeable surfaces into raingardens, were simulated under non-stationary climate conditions to assess their effectiveness, also considering the impacts of future climate change.
The focus of the study is to quantify the impact of raingardens on key hydrological parameters such as surface runoff reduction, decreased water volumes discharged in the sewer system and reduction in the peak flow.
The simulations conducted shown that raingardens are particularly effective for events with low return periods (2 years), achieving a reduction in peak flows up to 23% and in discharge volumes up to 17.3% on a single-event scale. In continuous simulations (on an annual scale), the benefits of implementing raingardens in terms of surface runoff reduction are enhanced, achieving a reduction of up to 75%.
The obtained results aim to provide tangible evidence supporting the effectiveness of green infrastructures in mitigating the challenges posed by climate change and urbanization.

Sommario

Negli ultimi decenni, il cambiamento climatico e l'eccessivo sfruttamento del suolo hanno reso la gestione delle acque meteoriche, in particolar modo nelle aree urbane, una tematica sempre più delicata e dibattuta. L'aumento delle temperature, le alterazioni dei regimi di pioggia e l'impermeabilizzazione del suolo hanno un impatto negativo sul ciclo idrologico, aumentando il rischio di allagamenti causati da eventi meteorologici estremi sempre più frequenti.

Questi fenomeni mettono a dura prova i tradizionali sistemi di drenaggio urbano, spesso progettati per condizioni climatiche passate, portando a situazioni di emergenza e danni materiali significativi.

In questo contesto, una gestione efficace e sostenibile delle risorse idriche e la progettazione di infrastrutture urbane resilienti diventano una necessità impellente per garantire la sicurezza e il benessere delle comunità e degli ecosistemi.

In risposta a queste sfide, le amministrazioni pubbliche responsabili della gestione del territorio stanno cercando di attuare politiche e strategie che promuovano un design urbano più attento alla gestione dell'acqua e al rispetto del ciclo idrologico, aumentando il numero di spazi verdi e di superfici permeabili per riportare i tassi di infiltrazione ed evaporazione ai livelli precedenti all'urbanizzazione. Sistemi di drenaggio decentralizzati, come tetti verdi, pavimentazioni porose, bacini di raccolta, e zone umide, stanno guadagnando terreno come strategie efficaci per mitigare gli impatti dell'urbanizzazione e dell'aumento dei volumi di deflusso superficiale. L'implementazione di tali misure non solo contribuisce a gestire le acque meteoriche, ma favorisce anche la conservazione della biodiversità, migliora l'estetica urbana e fornisce spazi ricreativi per i residenti.

Negli ultimi anni una delle strategie verdi che ha suscitato maggior interesse per via del suo basso costo di costruzione e per la facilità con cui può essere integrata e adattata al contesto urbano si basa sull'inserimento di Raingardens.

I raingarden (RG), chiamati anche bioretention cells, sono delle aree verdi vegetate, costituiti da diversi strati di terreno ingegnerizzati, progettate per catturare, filtrare e rallentare il deflusso superficiale.

Il terreno e la vegetazione all'interno dei RG agiscono come filtri naturali, rimuovendo inquinanti e favorendo l'assorbimento dell'acqua, contribuendo così a ripristinare il ciclo idrologico naturale. Il deflusso rallentato e trattato può essere rilasciato gradualmente nei sistemi di drenaggio convenzionali o infiltrarsi nel terreno, ripristinando i livelli di falda. Tuttavia, la loro efficacia dipende fortemente da una costante manutenzione.

Questo studio ha affrontato due domande: come fare per garantire una corretta manutenzione finalizzata al rapido ripristino delle prestazioni idrologiche dei raingarden

in caso di malfunzionamento causato da fenomeni esterni imprevedibili, e, quali sono i benefici generati dall'implementazione di raingarden in un contesto urbano altamente impermeabilizzato, dove la rete di drenaggio è ancora limitata ai tradizionali sistemi di collettamento, ed in condizioni climatiche non stazionarie? Le risposte a queste domande sono state valutate attraverso due progetti di ricerca paralleli, uno condotto in Australia e uno relativo a un caso di studio italiano.

In Australia, l'uso di questi sistemi è radicato nel processo di pianificazione urbana da diversi anni. Tuttavia, l'alto numero di installazioni e la loro distribuzione spaziale all'interno aree urbane determina numerose problematiche in termini di gestione e manutenzione. Il corretto funzionamento di questi sistemi infatti dipende in gran parte dalla qualità e frequenza degli interventi di manutenzione che vengono svolti. Le linee guida di questi sistemi forniscono delle indicazioni specifiche sul tipo di interventi e sulla frequenza con cui devono essere svolti, tuttavia, da numerosi studi svolti in installazioni sul campo è emerso che quasi il 50% di questi non funziona correttamente e richiede interventi di manutenzione o, nei casi più gravi, anche di rifacimento. Questo può attribuirsi all'assenza di sistemi di monitoraggio in grado di individuare e segnalare eventuali malfunzionamenti in tempo reale, in modo tale da permettere un regime di manutenzione predittivo e mirato.

A questo scopo, è stato sviluppato uno studio su 15 colonne tipo rappresentanti 15 mini-raingarden per testare l'affidabilità dei sensori economici nell'identificare tre comuni condizioni di salute del biofiltro.

Le 15 colonne sono state divise in 3 gruppi: uno rappresentante il corretto funzionamento di un raingarden, il secondo progettato per simulare l'effetto della presenza di percorsi di flusso preferenziale e l'ultimo progettato per simulare un intasamento superficiale.

Questi tre funzionamenti sono stati validati effettuando numerosi test di infiltrazione.

Ogni colonna è stata progettata in modo tale da riprodurre fedelmente un tipico raingarden, composto da una zona di stagnazione superficiale, uno strato superficiale filtrante di sabbia fine, uno strato centrale di transizione composto da sabbia grossa e pacciame di canna da zucchero, e uno strato drenante di base composto da ghiaia. Sul fondo di ogni colonna è stato inoltre inserito un tubo di drenaggio.

All'interno di ogni colonna sono stati posizionati 5 sensori: due sensori "Chameleon Soil Water Sensor" per la misurazione della tensione idrica del suolo, due sensori di temperatura "DS18B20" e un sensore "Truebner SMT 100", più robusto ed affidabile dei primi due, per la misurazione del contenuto volumetrico di acqua.

Al fine di testare la capacità dei sensori nel rilevare i malfunzionamenti delle colonne sono stati simulati una serie di eventi di pioggia corrispondenti ad eventi reali di bassa e media intensità e caratterizzati da un diverso numero di giorni asciutti antecedenti.

I sensori installati sono stati in grado di distinguere il comportamento dei tre gruppi di colonne sperimentali, fornendo dati che riflettono le diverse reazioni al processo di infiltrazione dell'acqua. In particolare, le colonne predisposte con percorsi preferenziali hanno mostrato variazioni meno significative nell'umidità del suolo tra un evento e l'altro, ma hanno risposto con variazioni istantanee maggiori durante gli eventi di pioggia simulati. Al contrario, le colonne caratterizzate da occlusione superficiale hanno mostrato una maggior tendenza all'essiccamento. Questo comportamento ha portato ad una riduzione dell'umidità del suolo a livelli minimi critici, potenzialmente pericolosi per la salute delle piante, e quindi del raingarden stesso.

La seconda parte dello studio si concentra invece su un lavoro di modellazione numerica condotto utilizzando il software di modellazione idraulica SWMM per valutare e quantificare l'efficacia dei raingarden nel mitigare l'impatto negativo dell'urbanizzazione e dei cambiamenti climatici, a scala di bacino urbano, su un caso studio italiano.

Nel contesto italiano, a differenza di quello australiano, persiste ancora scetticismo e mancanza di interesse verso le soluzioni verdi. Questo scetticismo può essere attribuito alla mancanza di studi che evidenzino i benefici generati dall'adozione di tali strategie.

La ricerca mira quindi a colmare questa lacuna presentando un caso studio che mostri come i raingardens possano essere integrati efficacemente all'interno del contesto urbano italiano. A tal fine sono stati simulati diversi scenari di depavimentazione urbana, ovvero la conversione di una percentuale delle superfici impermeabili in raingardens, in condizione di clima non stazionario per valutarne l'efficacia anche in considerazione degli effetti dei cambiamenti climatici futuri.

L'obiettivo dello studio è quello di quantificare l'impatto positivo dei raingarden su parametri idrologici chiave, quali la riduzione del deflusso superficiale, la riduzione dei picchi di piena e dei volumi d'acqua scaricati all'interno del sistema fognario. Le simulazioni condotte hanno evidenziato che i raingarden sono particolarmente efficaci per eventi con tempi di ritorno bassi (2 anni), registrando una riduzione dei picchi di piena fino al 23% e dei volumi scaricati fino al 17.3% a scala di singolo evento. Nelle simulazioni in continuo (su scala annuale) i vantaggi apportati dall'implementazione dei raingarden in termini di riduzione del deflusso superficiale si accentuano, arrivando ad una riduzione fino al 75%. I risultati ottenuti mirano a fornire evidenze concrete a sostegno dell'efficacia dell'infrastruttura verde nel mitigare le problematiche derivanti dai cambiamenti climatici e dall'urbanizzazione.

CONTENTS

LIST OF ABBREVIATIONS

ADD	Antecedent Dry Days
ARI	Annual Recurrence Interval
BAU	Business As Usual
EIA	Effective Impervious Area
EY	Exceedances per Year
GI	Green Infrastructure
LID	Low Impact Development
NSE	Nash-Sutcliffe Efficiency
PET_D	Daily Potential Evapotranspiration
PET_M	Monthly Potential Evapotranspiration
RG	Raingarden
RCP	Representative Concentration Pathways
RPD	Relative Percentage Difference
RTMs	Real-Time Monitoring systems
SMP	Soil Matric Potential
SUDS	Sustainable Urban Drainage Systems
SWC	Soil Water Characteristic Curve
SWT	Soil Water Tension
SWMM	Storm Water Management Model
TDT	Time Domain Transmission
VWC	Volume Water Content
WSUD	Water Sensitive Urban Design

LIST OF FIGURES

LIST OF TABLES

Chapter 1 - Introduction

Addressing sustainable urban stormwater management is a pivotal challenge within the realm of scientific inquiry. In recent years, the confluence of urbanization and climate change has induced a profound alteration in the natural hydrological cycle, making the cities all over the world increasingly susceptible to the threat of flooding. The escalating occurrence of urban floods brought to light the inadequacies of the traditional urban drainage systems, strongly promoting a transition to more sustainable and resilient urban drainage systems. On this basis, the Ph.D. project focused on deepen the understanding of nature-based solutions, with a particular emphasis on raingardens, their implementation, maintenance, and the benefits derived from their utilization. Recognized for their ability to diminish surface runoff while enhancing evapotranspiration and infiltration rates, these techniques offer valuable options for stormwater management and hydrological restoration in urban areas. However, their utilization poses additional challenges related to their management and maintenance to ensure their consistent functionality and effectiveness over time.

This thesis aims to explore the hydraulic benefits associated with the implementation of raingardens in urban environments. Additionally, it seeks to identify strategies for enhancing post-installation maintenance.

This chapter examines the issues that inspired the project, the new challenges, and possible solutions to urban stormwater management. Then, the aim and objectives of this study will be defined, along with the thesis structure.

1.1 Traditional Stormwater Management challenges

The issue of stormwater management received limited attention until the mid-1990s, remaining largely neglected and unaddressed (Gimenez-Maranges et al., 2020). The surge in impervious surfaces resulting from the ongoing urbanization process stands out as a prominent trend in the last century, carrying substantial environmental repercussions. The alteration of landscapes through development brought to ecosystems impoverishment, heightened flooding risks due to a decreased capacity for a landscape to infiltrate precipitation (Hsu et al., 2000; Hey D. L., 2001), shorter time of concentration, deteriorating water quality, urban heat island effect, altered evapotranspiration regimes due to the removal of vegetation (Dale at al., 2000) and other socio-economic challenges (Shuster et al., 2005; Hellman et al., 2018). From a hydraulic perspective, the exponential growth of built-up areas significantly altered the natural hydrological cycle, especially in urban areas. Beyond imperviousness, other factors contribute affecting the urban hydrological cycle, such as spatial characteristics of impervious areas, including their location, interconnectedness, and proximity to the drainage network (Sheeder et al., 2002; Yang et al., 2011; Jacobson C. R., 2011), the hydrographic network density, soil types, the presence of aquifers and climate conditions (Guan et al., 2015). Furthermore, the incorporation of hydraulic structures, such as modifications to natural pathways and the installation of detention basins, plays a crucial role in influencing urban hydrology (Ravazzani et al., 2014).

Beyond the aspects related to the increase of impervious surfaces, the escalating frequency of extreme rainfall events due to climate change (Kundzewicz et al., 2006, Tamm et al., 2023), combined with urbanization effects, are worsening some of these consequences (Yazdanfar and Sharma, 2015; Moore et al., 2016), which are difficult to assess due to their uncertain nature. The negative impact of these effects is more exacerbated in post-development area, where changes in runoff hydrograph, corresponding to higher volumes and more rapid peak flows, are more pronounced than pre-development conditions.

The excess surface runoff generated overwhelms the traditional drainage system composed of a network of pipes and channels and treatment facilities targeted at the quick removal by receiving and conveying the stormwater volumes from urban areas to water bodies (Zhou, 2014; Chen et al., 2021). However, conventional urban drainage systems have proven ineffective and showed inadequacy to handle the increased runoff volumes making cities susceptible to flooding (Chen et al., 2016).

Recognizing the limitations of traditional systems, Shishegar et al. (2018) emphasize the need for innovative and sustainable approaches to rainwater management. In this

context, stormwater management encompasses strategies to control and limit surface runoff, mitigate water pollution, and restore ecosystem integrity. Consequently, a paradigm shift toward environmentally sustainable urban water management has become imperative (Marsalek et al., 2008; Vairavamoorthy et al., 2015), with various on-site management options available for combined use (Schreier et al., 2009).

1.2 Enhancing Urban Resilience: Integrating Green Strategies to Overcome Traditional Drainage System Challenges

With the increase in urbanization worldwide and the impact of urban stormwater on humans and aquatic ecosystems, urban drainage management has become more complex (Fletcher et al., 2013). Traditional approaches to stormwater management involve large and centralized drainage systems, but as discussed in the previous paragraph, they have proven to be inadequate in addressing the challenges posed by climate change and increasing impervious surfaces. In light of this, a transition towards an innovative, sustainable and resilient urban water management system has become necessary to mitigate the environmental impact of urbanization and climate change.

In recent years, green solutions have gained popularity as an integral component of sustainable stormwater management, offering environmentally friendly alternatives to traditional practices. This shift reflects a growing recognition of the importance of integrating nature-based approaches into various aspects of urban planning and infrastructure, including stormwater management.

These innovative techniques have developed autonomously in different context; therefore, they are defined by various terminologies, such as Sustainable Drainage Systems (SuDS), Best Management Practices (BMPs), Green Infrastructure (GI), Low Impact Developments (LID), and Water Sensitive Urban Designs (WSUD). Throughout this dissertation, the term “LID” is used to describe these systems. They consist of above-ground mechanisms (Wahl, 2009) which emulate natural processes (including infiltration, evapotranspiration, filtration, retention, and reuse) to effectively manage potential flood events, recharge groundwater, reduce water pollutions, in other words, they operate to restore pre-development conditions. (Wong, 2006; Perales-Momparler et al., 2015; Zhang and Chui, 2018).

The implementation of these systems involves measures at different scales starting from regional and urban planning, where the allocation of different land uses is guided by topographical and hydrological characteristics, down to local scale with individual installations (Carmon and Shamir, 2010; Melbourne Water, 2005; Woods-Ballard et al., 2007). The base concept is to reduce stormwater runoff by treating it in close proximity

to its origin, ideally directly on-site (Hoyer et al., 2011). Due to their ability in mitigating urban surface runoff while having more environmentally friendly characteristics, they can be incorporated within the traditional drainage system or even serve as replacement (Liu et al., 2014; Vogel et al., 2015; Yang and Chui, 2016; Bhaskar et al., 2016; Eckart et al., 2017). Because LID-WSUD-GI practices do not need to be connected to conventional drainage systems, they can be located more flexibly and used more readily as retrofits or upgrades. Bioretention cells, green roofs, infiltration trenches, porous pavement, detention, and retention ponds, constructed wetlands are all examples of strategies that fall within the scope of WSUD-LID-SUDS practices (Zhang and Chui, 2018).

The spatial allocation of these practices has become increasingly important due to the large number of and widespread adoption of these practices. With the advancement of Geographic Information Systems (GIS) and distributed hydrological models (Shamsi, 2002; Elliott and Trowsdale, 2007) such allocation has also become easier. However, due to the diverse and decentralized nature of LID practices and the intricate urban landscape, optimizing their spatial allocation poses significant challenges. These practices are frequently constrained by various physical, socio-economic, and institutional factors arising from the intricate interactions among people, urban infrastructure, and the environment (Brown et al., 2009; Kaplowitz and Lupi, 2012; Dhakal and Chevalier, 2017). The availability of space in highly urbanized area remains a major hurdle. Ideally, the implementation of these practices encompasses both private and public lands, sometimes held by different entities. Consequently, achieving widespread adoption of these practices requires time and often leads to conflicts of interest (Brown, 2005). Additionally, the existing urban infrastructure, both above and below ground (such as cables and pipelines), physically constrains potential installation locations.

Beyond the challenge posed by limited space availability, the successful implementation of LID practices may also be hindered by a lack of public interest and support. Although there is a growing awareness of the advantages associated with these practices, the general willingness of the public to contribute financially or actively participate in their planning and management remains relatively low (Lu et al., 2013). In other words, while people are becoming more informed about the positive impact of these practices, there is still a gap in translating this awareness into tangible support or engagement from the public. This disparity in perception and commitment can impede the broader adoption and effective execution of these environmentally beneficial practices in urban areas.

In addition to the aforementioned challenges, another issue begins to arise in the implementation of these strategies, and it pertains to maintenance management. Due to their decentralized and widespread nature, the maintenance of these strategies demands significant human and financial resources. Ensuring their proper functioning necessitates

periodic interventions such as cleaning, vegetation pruning, addition of soil material, and so forth. The decentralized and dispersed nature of these practices poses a logistical challenge in coordinating and efficiently deploying the necessary resources for their upkeep (Erickson et al., 2010). As a result, effective maintenance becomes a crucial aspect of sustaining the functionality and benefits of these decentralized environmental strategies over time (Erickson et al., 2018).

1.3 Research Objectives and Assumptions

Based on the background previously discussed, the overall goal of this research is to address challenges associated with the adoption, or non-adoption, of raingardens in different urban contexts. Two cases studies are considered where stormwater management follows distinct strategic approaches.

The first part of the study aims to identify reliable and cost-effective real-time monitoring tools that can be implemented in green installations scattered across the urban landscape of the city of Melbourne, in order to enhance the planning and management of maintenance regimes. In the Australian context, where nature-based solutions have been integrated into the urban framework for several years, the challenge of managing these strategies is arising. The positive aspects resulting from the adoption of these systems, such as low installation costs, significant environmental and social benefits, reduction of impermeable surfaces, and consequently, runoff volumes, as well as a decrease in pollutant loads discharged into water bodies, are juxtaposed with a negative aspect associated with the maintenance factor.

The specific objectives are 1) to evaluate the reliability of low-cost sensors in providing real-time data on soil moisture and the overall health status of raingardens, 2) to identify characteristic indexes through which it is possible to classify the operational status of the raingarden, distinguishing normal functioning from critical situations arising from erosive phenomena in the soil layers or surface blockages due to the accumulation of stormwater sediments.

The second part of the study, on the other hand, stems from the necessity to assess the applicability of raingardens in the Italian context, particularly in the urban area of the city of Brescia. In Italy, unlike Australia, interest in green solutions is still low due to a lack of studies at the urban basin scale that evaluate and quantify the benefits resulting from their implementation also taking into account the ongoing climate changes.

In this context, this study aims to achieve the following objectives 1) assess the current hydraulic performance of a part of the sewerage system of Brescia identifying the criticalities and weaknesses by developing an hydraulic model through the SWMM

software; 2) integrate raingardens into the sewerage system model to simulate their impact on stormwater management. This will involve evaluating their effectiveness in reducing surface runoff, peak flows, and variation in peak times, thereby and their capacity in mitigating hydraulic risks and coping with criticalities; 3) investigate various climate scenarios to evaluate the resilience of the urban drainage system in the face of changing weather patterns following the adoption of raingardens.
The study is also situated within of the framework of the environmental sustainability project promoted by the Municipality of Brescia and aims to provide support for strategic planning for a climate transition of the city. The objective is to promote greater environmental sustainability and enhance the resilience of the municipal territory and its community.

1.4 Dissertation Structure

In order to give an overview of this thesis the aim of each chapter is below specified. The dissertation is divided into three main chapters, following the first introductive one.
Chapter 2 is dedicated to comprehensive review of existing literature regarding green strategies for sustainable drainage systems, with specific reference to the raingardens. The chapter briefly introduces the concept of nature-based solutions and their relevance in urban areas with a focus on their environmental, social, and economic benefits. It discusses challenges and critiques associated with the implementation of nature-based solutions, including potential limitations and areas for improvement. Finally, the chapter examines the role of raingardens, outlining their key features and functions, such as stormwater management, biodiversity promotion, and aesthetic enhancements.
Chapter 3 addresses the practical aspects of raingardens, focusing on the challenges associated with planning and managing their maintenance. In the chapter a laboratory project conducted during my research tenure at Monash University is presented. The project investigates the utilization of low-cost electronic sensors for establishing a predictive biofilter maintenance regime and successfully implements a system capable of identifying raingarden malfunctions through the definition of indexes. More specifically this study assesses the effectiveness of low-cost sensors in detecting states of poor hydraulic performance linked to common maintenance issues. The project involved the construction of 15 study columns, structured like a traditional raingarden, divided into three groups of 5 each, representing different operational conditions. These conditions include 5 columns depicting normal raingarden functioning, another 5 simulating the effects of soil layer erosion phenomena, and the remaining 5 simulating the effects of surface clogging. The chapter provides details on the experimental setup, electronic

settings, data acquisition and analysis methods. It also discusses the limitation of the sensors used and suggests avenues for future research and improvements in moisture sensor technology.

Chapter 4 investigates the benefits deriving from raingarden implementation within the urban context of the city of Brescia, based on the development of a SWMM-based model. This type of investigation allows for the evaluation, through predictive modelling, of the effects resulting from the adoption of raingardens in terms of surface runoff reduction, peak flow reduction and delay, as well as reduction in the volumes of water discharged at the urban watershed scale. This chapter includes the model construction, calibration, simulation, and analysis of the results.

Chapter 5 provides comprehensive conclusions, highlights the innovative contributions of this study, and suggests directions for future research.

1.5 Research Project Timeline

The research project started in June 2022 with the hydraulic modelling of Brescia industrial area drainage network using the SWMM software. This study represents the culmination of two years of collaborative work with Brescia integrated water service provider, A2A Ciclo Idrico, focusing on modelling the western portion of the city sewerage network. The modelling process identified several critical issues, particularly in the southern part which includes the industrial area, prompting the need for further investigation to comprehensively address the identified challenges.

As a result, the scope of the study expanded to include the assessment of potential interventions to mitigate the identified issues and enhance the overall performance and resilience of the sewerage system. This involved integrating innovative solutions, such as raingardens, into the modelling framework to evaluate their effectiveness in managing stormwater and mitigating flood risks. Additionally, the study explored the impact of climate change on the sewerage system, considering various scenarios to anticipate and adapt to future challenges. Through this holistic approach, the research aims to provide insights and recommendations to support decision-making for sustainable urban water management and climate resilience in the Brescia municipality.

The modelling work continued for several months (until September 2023) during which in-situ investigations and verifications were necessary to validate the geometric and depth data. Parallel to this activity, a monitoring activity (from February 2023 to July 2023) was conducted to collect flow and rainfall values later used for model calibration and validation (see Fig. 1).

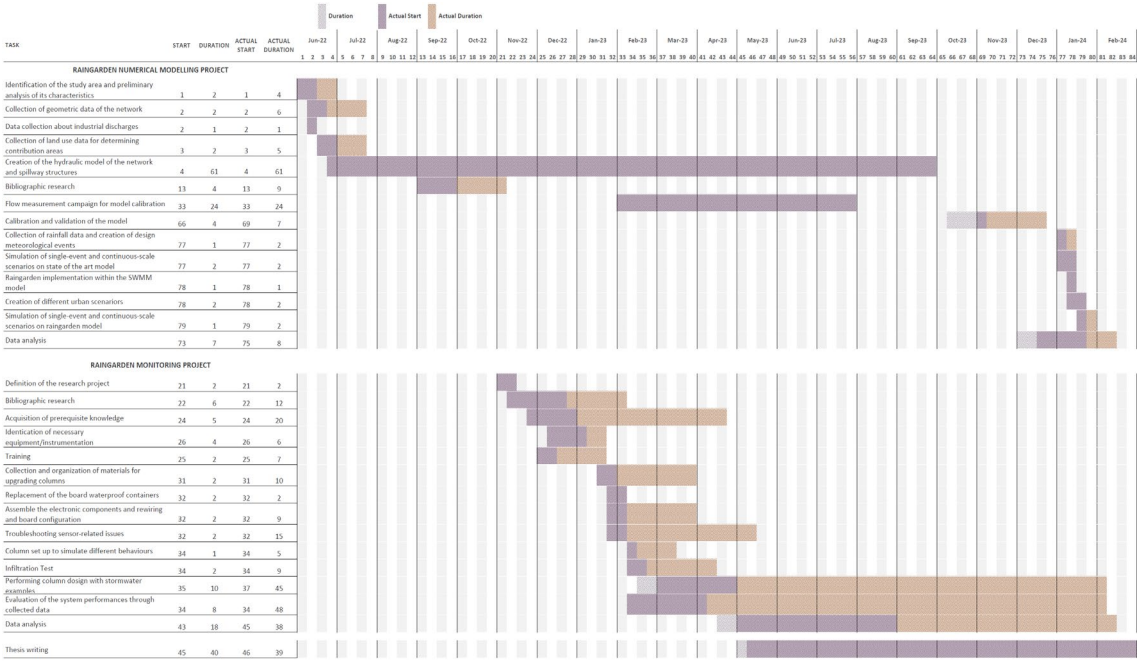

Fig. 1 – Monitoring activity Gantt Chart

The second part of the research work, that of raingarden monitoring activity through sensors, started in November 2022 until May 2023 and continued remotely in the months after my return from Australia the following 9 months.

During the six-months study period at Monash University, the project mainly consisted of three phases: an initial study and training phase, a second phase of system setup, maintenance, and upgrade, and a third phase of storm simulation by dosing the raingarden at predetermined intervals, data collection, processing, and analysis.

The project timeline suffered from several delays due to setting issues, sensor malfunction and limited access to the laboratory for extreme heat conditions.

1.6 References

Bhaskar, A.S., Hogan, D.M., & Archfield, S.A. (2016). Urban base flow with low impact development. *Hydrological Processes, 30,* 3156–3171. doi.org/10.1002/hyp.10808

Brown, R.R. (2005). Impediments to integrated urban stormwater management: the need for institutional reform. *Environmental Management, 36,* 455–468. doi.org/10.1007/s00267-004-0217-4

Brown, R.R., Farrelly, M.A., & Keath, N.A. (2009). Practitioner perceptions of social and institutional barriers to advancing a diverse water source approach in Australia. *International Journal of Water Resources Development, 25 (1)*, 15–28. doi.org/10.1080/07900620802586090

Carmon, N., & Shamir, U. (2010). Water-sensitive planning: Integrating water considerations into urban and regional planning. *Water and Environment Journal, 24,* 181-191. doi.org/10.1111/j.1747-6593.2009.00172.x

Chen, Y., Samuelson, H.W., & Tong, Z. (2016). Integrated design workflow and a new tool for urban rainwater management. *Journal of Environmental Management, 180,* 45–51. doi.org/10.1016/j.jenvman.2016.04.059

Chen, W., Wang, W., Huang, G., Wang, Z., Lai, C., & Yang, Z. (2021). The capacity of grey infrastructure in urban flood management: A comprehensive analysis of grey infrastructure and the green-grey approach. *International Journal of Disaster Risk Reduction, 54,* 102045, ISSN 2212-4209. doi.org/10.1016/j.ijdrr.2021.102045

Dale, V.H., Brown, S., Haueber, R.A., Hobbs, N.T., Huntly, N., Naiman, R.J., Riebsame, W.E., Turner, M.G. & Valone, T.J. (2000). Ecological principles and guidelines for managing the use of land. *Ecological Applications, 10,* 639-670. doi.org/10.1890/1051-0761(2000)010[0639:EPAGFM]2.0.CO;2

Dhakal, K.P., & Chevalier, L.R. (2017). Managing urban stormwater for urban sustainability: barriers and policy solutions for green infrastructure application. *Journal of Environmental Management, 203,* 171–181. doi.org/10.1016/j.jenvman.2017.07.065

Eckart, K., Mcphee, Z., & Bolisetti, T. (2017). Performance and implementation of low impact development: a review. *Science of the Total Environment, 607–608,* 413–432. doi.org/10.1016/j.scitotenv.2017.06.254

Elliott, A.H., & Trowsdale, S.A. (2007). A review of models for low impact urban stormwater drainage. *Environmental Modelling & Software, 22 (3),* 394–405. doi.org/10.1016/j.envsoft.2005.12.005

Erickson, A.J., Gulliver, J.S., Kang, J.-H., Weiss, P.T., & Wilson, C.B. (2010). Maintenance for stormwater treatment practices. *Journal of Contemporary Water Research & Education, 146 (1)*, 75–82. doi.org/10.1111/j.1936-704X.2010.00393.x

Erickson, A.J., Taguchi, V.J., & Gulliver, J.S. (2018). The challenge of maintaining stormwater control measures: A synthesis of recent research and practitioner experience. *Sustainability, 10 (10),* 3666. doi.org/10.3390/su10103666

Fletcher, T.D., Andrieu, H., & Hamel, P. (2013). Understanding, management and modelling of urban hydrology and its consequences for receiving waters; a state of the art. *Advances in Water Resources, 51,* 261–279. doi.org/10.1016/j.advwatres.2012.09.001

Gimenez-Maranges, M., Breuste, J., & Hof, A. (2020). Sustainable Drainage Systems for transitioning to sustainable urban flood management in the European Union: A review. *Journal of Cleaner Production, 255,* 120191, ISSN 0959-6526. doi.org/10.1016/j.jclepro.2020.120191

Guan, M., Sillanpää, N. & Koivusalo, H. (2015). Modelling and assessment of hydrological changes in a developing urban catchment. *Hydrological Processes, 29 (13),* 2880–2894.

doi.org/10.1002/hyp.10410

Hellman, K., Wagner, J., Lass, D., Korfmacher, K., & Hanna, B.G. (2018). Estimating the Economic Impact of Stormwater Runoff in the Allen Creek Watershed. *Ecological Economics, 145,* 420-429, ISSN 0921-8009. doi.org/10.1016/j.ecolecon.2017.11.022

Hey, D.L. (2001). Modern drainage design: the pros, the cons, and the future. Paper presented at the Hydrologic Science: Challenges for the 21st Century, American Institute of Hydrology Annual Meeting, Bloomington, MN.

Hoyer, J., Dickhaut, W., Kronawitter, L., & Weber, B. (2011). *W*ater Sensitive Urban Design. Principles and Inspiration for Sustainable Stormwater Management in the City of the Future. HafenCity Universität Hamburg: JOVIS. ISBN 9783868591064

Hsu, M.H., Chen, S.H. & Chang, T.J. (2000). Inundation simulation for urban drainage basin with storm sewer system. *Journal of Hydrology, 234 (1-2),* 21–37. doi.org/10.1016/S0022-1694(00)00237-7

Jacobson, C.R. (2011). Identification and quantification of the hydrological impacts of imperviousness in urban catchments: A review. *Journal of Environmental Management, 92 (6),* 1438–1448. ISSN 0301-4797. doi.org/10.1016/j.jenvman.2011.01.018

Kundzewicz, Z.W., Radziejewski, M., & Pinskwar, I. (2006). Precipitation extremes in the changing climate of Europe. *Climate Research, 31 (1),* 51-58. doi.org/10.3354/cr031051

Liu, X., Sample, D.J., Bell, C., & Guan, Y. (2014). Review and research needs of bioretention used for the treatment of urban stormwater. *Water, 6 (4),* 1069-1099. doi.org/10.3390/w6041069

Lu, Z., Noonan, D., Crittenden, J., Jeong, H., & Wang, D. (2013). Use of impact fees to incentivize low-impact development and promote compact growth. *Environmental Science & Technology, 47 (19),* 10744–10752. doi.org/10.1021/es304924w

Melbourne Water (2005). *WSUD Engineering Procedures: Stormwater*. Clayton South VIC: CSIRO Publishing, ISBN (electronic) 978-0-643-09989-0. doi.org/10.1071/9780643092235

Moore, T.L., Gulliver, J.S., Stack, L., & Simpson, M.H. (2016). Stormwater management and climate change: vulnerability and capacity for adaptation in urban and suburban contexts. *Climatic Change, 138,* 491–504. doi.org/10.1007/s10584-016-1766-2

Perales-Momparler, S., Andrés-Doménech, I., Andreu, J., & Escuder-Bueno, I. (2015). A regenerative urban stormwater management methodology: the journey of a Mediterranean city. *Journal of Cleaner Production, 109,* 174-189, ISSN 0959-6526. doi.org/10.1016/j.jclepro.2015.02.039

Ravazzani, G., Gianoli, P., Meucci, S., & Mancini, M. (2014). Assessing Downstream Impacts of Detention Basins in Urbanized River Basins Using a Distributed Hydrological Model. *Water Res. Management, 28,* 1033–1044. doi.org/10.1007/s11269-014-0532-3

Shamsi, U.M. (2002). *GIS Tools for Water, Wastewater, and Stormwater Systems*. ASCE (American Society of Civil Engineers) Press. ISBN: 978-0-7844-7084-8. doi.org/10.1061/9780784405734

Sheeder, S.A., Ross, J.D., & Carlson, T.N. (2002). Dual urban and rural hydrograph signals in three small watersheds. *Journal of the American Water Resources Association, 38 (4),* 1027–1040. doi.org/10.1111/j.1752-1688.2002.tb05543.x

Shishegar, S., Duchesne, S., & Pelletier, G. (2018). Optimization methods applied to stormwater management problems: a review. *Urban Water Journal, 15 (3),* 276–286. doi.org/10.1080/1573062X.2018.1439976

Shuster, W.D., Bonta, J., Thurston, H., Warnemuende, E., & Smith, D.R. (2005). Impacts of impervious surface on watershed hydrology: A review. *Urban Water Journal, 2 (4)*, 263–275. doi.org/10.1080/15730620500386529

Tamm, O., Saaremäe, E., Rahkema, K., Jaagus, J., & Tamm, T. (2023). The intensification of short-duration rainfall extremes due to climate change – Need for a frequent update of intensity–duration–frequency curves. *Climate Services, 30*, 100349, ISSN 2405-8807. doi.org/10.1016/j.cliser.2023.100349

Vairavamoorthy, K., Jochen, E., Seneshaw, T., Kebreab, G., & Krishna, K. (2015). *A Paradigm Shift in Urban Water Management: An Imperative to Achieve Sustainability.* Sustainability of Integrated Water resources Management, 51-64. doi.org/10.1007/978-3-319-12194-9_4

Vogel, J.R., Moore, T.L., Coffman, R.R., Rodie, S.N., Hutchinson, S.L., McDonough, K.R., McLemore, A.J., & McMaine, J.T. (2015). Critical review of technical questions facing low impact development and green infrastructure: a perspective from the Great Plains. *Water Envir. Research, 87 (9),* 849–862. doi.org/10.2175/106143015X14362865226392

Wahl, S. (2009). *Stormwater best management practices: a first guide for landscape architects.* Swedish University of Agricultura Sciences, Uppsala. Available in: https://stud.epsilon.slu.se/419/

Wong, T.H.F. (2006). Water sensitive urban design – the journey thus far. Australasian *Journal of Water Resources*, *10 (3)*, 213-222. doi.org/10.1080/13241583.2006.11465296

Woods-Ballard, B., Kellagher, R., Martin, P., Jefferies, C., Bray, R., & Shaffer, P. (2007). *The SuDS Manual*, No C697. London: Construction Industry and Research Association (CIRIA).

Yang, G., Bowling, L.C., Cherkauer, K.A., & Pijanowski, B.C. (2011). The impact of urban development on hydrologic regime from catchment to basin scales. *Landscape and Urban Planning, 103 (2),* 237-247, ISSN 0169-2046, doi.org/10.1016/j.landurbplan.2011.08.003

Yang, Y., & Chui, T.F.M. (2016). Optimal design of green and grey stormwater infrastructure for small urban catchment based on life-cycle cost-effectiveness analysis. American Geophysical Union (AGU), Fall Meeting, San Francisco, CA, Bibcode:

2016AGUFM.H13M1598Y

Yazdanfar, Z., & Sharma, A. (2015). Urban drainage system planning and design-challenges with climate change and urbanization: a review. *Water Science & Technology, 72 (2)*, 165-79. doi.org/10.2166/wst.2015.207

Zhang, K., & Chui, T.F.M. (2018). A comprehensive review of spatial allocation of LID-BMP-GI practices: Strategies and optimization tools. *Science of the total environment, 621,* 915-929. doi.org/10.1016/j.scitotenv.2017.11.281

Zhou, Q. (2014). A Review of Sustainable Urban Drainage Systems Considering the Climate Change and Urbanization Impacts. *Water, 6 (4)*, 976-992. doi.org/10.3390/w6040976

Chapter 2 - Bioretention systems: an overview

In this chapter, an overview of the characteristics, functions, benefits, and potential challenges associated with the implementation of raingardens in urban spaces is presented. Beginning with a general introduction on nature-based solutions techniques, of which raingardens are a part, the chapter progresses to an in-depth description of bioretention systems. This includes an exploration of how they operate, the benefits and advantages derived from their application, as well as the potential problems that may arise from their use.

2.1 LID, WSUD, SUDS: Innovations in Sustainable Urban Water Management

Urbanization and climate change present challenges worldwide, prompting a significant focus on sustainability as a pivotal force in safeguarding and enhancing the urban environment (Chocat et al., 2001). This global shift towards sustainable urban development is underpinned by a range of crucial factors, including the imperative of environmental preservation, the drive for urban regeneration, the economic growth, and the promotion of social health and well-being (Ashley et al., 2013). This cultural transformation recognizes urban drainage not just as a problem to be managed, but as a

wellspring of opportunities for innovation and improvement. These advancements reflect a deeper understanding of urban systems, where the integration of water management into urban design is viewed as a cornerstone of sustainable development, fostering resilience and quality of life in cities (Wong, 2006). In this context, the management of urban drainage, over the past decades, has thus undergone substantial transformation moving from traditional approaches to a more holistic and multifaceted framework that considers a range of urban water management goals and benefits (Chocat et al., 2001; Wong, 2001). Consequently, new terminologies emerged to effectively convey the objectives, strategies, and benefits of these new integrated approaches (Fletcher et al., 2015).

Among the most widespread terms there are Low Impact development (LID), Water Sensitive Urban Design (WSUD), Sustainable Urban Drainage System (SUDS) and many others (Flecther et al., 2015). These terms represent various approaches to sustainable urban drainage, all with the common goal of mimicking natural water cycles within developed areas. WSUD (Water Sensitive Urban Design), primarily used in Australia, emphasizes a holistic approach, integrating water management principles into urban planning and design (Lloyd et al., 2002). LID (Low Impact Development), originating in the US, focuses on implementing small-scale, site-specific practices like raingardens and permeable pavements to manage runoff at its source (Prince George's County, 1999). SUDS (Sustainable Urban Drainage Systems), prevalent in the UK, adopts a similar philosophy, but emphasizes the use of natural elements like swales and wetlands to achieve sustainable drainage (Woods-Ballard et al., 2007). Despite their geographic origins and slight variations in emphasis, the core principles of these approaches remain consistent: reduce runoff, improve water quality, and enhance natural ecosystems within urban environments. Through infiltration, storage, and treatment of rainwater, they aim to mitigate flooding, improve water quality, protect and enhance biodiversity, mitigate urban heat island effects, restore the natural water cycle, reduce energy and water consumption, thus creating more liveable and resilient cities (Dietz, 2007; Hoyer et al., 2011). These benefits are achieved through a variety of specific systems and features, all falling under the umbrella of LID, WSUD, SUDS, and related approaches (Askarizadeh et al., 2015). Examples of such systems include raingardens, porous pavements, bioretention basins, green roofs, bioswales, rainwater harvesting systems and constructed wetlands.

Permeable surfaces, can be made of porous asphalt, porous concrete, or interlocking pavers, are designed to enhance water infiltration, as highlighted in studies by Drake et al. (2013) and Mullaney and Lucke (2014). These materials allow rainwater to pass through them, reducing runoff and promoting groundwater recharge.

Likewise, infiltration trenches, described by Ebrahimian et al. (2021) as narrow, excavated areas, serve as reservoirs to capture and infiltrate water running off from impervious surfaces. Furthermore, rain tanks, a simple and cost-effective solution referenced by Jones and Hunt (2010) and Steffen et al. (2013), are used to collect rainwater from roofs, mitigating stormwater impacts and conserving water.

Some LID practices integrate biological processes with hydrological functions. This approach aims to emulate or restore natural water cycles by employing technologies and strategies that mimic or enhance ecological processes.

Among these vegetative swales, which are essentially planted infiltration trenches, combine the benefits of soil and plant interactions to enhance water quality and control, as discussed by Leroy et al. (2016).

Green roofs are another innovative approach and, as discussed by Cargari et al. (2016), they represent an effective strategy for urban water management. These living roof systems, consisting of vegetation planted over a waterproof membrane, are designed to absorb rainwater, thereby reducing runoff and mitigating the heat island effect in urban areas. These roofs not only contribute to water management but also offer habitat for wildlife, enhance urban green spaces, and improve building energy efficiency (Carter and Jacjkson, 2007; Stovin, 2010; Razzaghmanesh et al., 2016). Especially in densely populated urban areas, green roofs represent a valuable opportunity to reclaim and optimize limited open spaces for environmental benefits (Shafique et al., 2018).

Bioretention cells (or raingardens) are landscaped depressions that utilize a specialized soil mix and, occasionally, gravel layers and drainage pipes to manage stormwater through storage, infiltration, and evaporation (Dunnet & Clayden, 2007). These systems, along with their effectiveness in managing rainfall and runoff, have been extensively studied by many other authors (Roy-Poirier et al., 2010; Ishimatsu et al., 2017; Malaviya et al., 2019; Morash et al., 2019).

The adoption of raingardens, along with other sustainable stormwater management techniques within urban environment primarily seeks to mitigate the overall volume and peak flow of stormwater runoff. This approach significantly reduces the risk of property damage and minimizes the disruption of daily activities caused by flooding. Additionally, these green infrastructure practices play a crucial role in generating green spaces in densely built environments, thereby enhancing the aesthetic appeal and ecological diversity of urban landscapes (Grafton & Hussey, 2011).

Through the strategic integration of such systems, cities can effectively address the emerging water management challenges due to climate change and rapid urbanization while simultaneously promoting environmental sustainability and improving the quality of urban life.

This Ph.D project focuses on assessing the performance of raingardens in urban environments in terms of reducing surface runoff and peak flow rates through implementation in a hydraulic model. It also evaluates potential real-time monitoring systems to remotely monitor the performance of raingardens installation. To this end, the next paragraphs provide a detailed description of these systems.

2.2 Raingardens: an overview

Raingardens, also known as biofilters, bioretention systems or bioretention beds, are one of the most promising green LID technologies, consisting of a depressed, highly dense vegetated area overlaying an engineered porous, sand-based filter layer (Payne et al., 2015; Zhang et al., 2020). These stormwater control measures use plants and soil to capture, filter and significantly reduce pollutants from the stormwater runoff while optimizing water retention for frequent rainfall events. They provide hydrologic losses through infiltration, enhanced evapotranspiration via vegetation and temporary storage of infiltrated runoff volume (Shuster et al., 2017).

One of the key features that make raingardens so widely used is their adaptability to different climatic and urban contexts. This flexibility allows raingardens to be customized to the specific environmental and spatial conditions of a site, enhancing their effectiveness in managing stormwater runoff. Raingardens can vary significantly in shape and size, ranging from small gardens designed to capture and treat water volumes coming from roofs to narrower gardens that extend lengthwise along road or sidewalks, fitting into more restricted urban spaces. This versatility allows to incorporate raingardens into a variety of settings, from residential gardens to larger public spaces (Blecken et al., 2015). Raingardens are usually placed near impermeable surfaces such as buildings and roads, to capture, hold and soak stormwater preventing runoff pollutants from contaminating waterways (Malaviya et al., 2019).

Both plants and filter media play critical roles in the removal of pollutants, according to other studies (Hatt et al., 2009; Read et al., 2010; Shuster at al., 2017). Specifically, filter media captures suspended solids and pollutants using mechanism like sedimentation and filtration (Virahsawmy et al., 2014). These media are intentionally designed with a fine texture not only to facilitate the growth of plants but also to effectively remove pollutants. Additionally, a proper infiltration rate is essential to optimize the water runoff treatment (Le Coustumer et al., 2009). For example, if the soil material allows water to pass through too quickly, it results in brief retention times, which may cause water to flow out immediately, contributing to the overload of the drainage systems during storms. Conversely, if the soil profile is not very permeable, it leads to longer infiltration times,

increasing the risk of the raingarden overflowing. Therefore, the composition of filter media often ranges from fine sand to sandy loam, tailored to fulfill the specific operational needs. The water collected by these systems can be channelled via perforated pipe situated at the bottom, either to nearby water bodies or into the drainage network, typically 24-72 hours following a rainfall event. Alternatively, it can be stored in underground cisterns for various uses, such as flushing toilet or irrigation (Winfrey et al., 2018). In another approach, the treated water is allowed to percolate downward, replenishing the groundwater supply (Read et al., 2010). By delaying the release of stormwater, these systems play a critical role in minimizing flooding risks and alleviating pressure on city drainage systems during heavy rainfall. The storage option not only conserves water but also promotes sustainable practices like reducing the demand for potable water for non-potable applications. On the other hand, allowing water to infiltrate back into the ground helps maintain the natural hydrological cycle, supporting groundwater levels and contributing to the overall health of nearby ecosystems.

The choice of the raingarden size is essential to have system that works properly, ensuring high performance and a long lifespan.

Their size usually is approximately 2 - 4% based on the local climate (Payne et al., 2015) of the Effective Impervious Area (EIA) which is the impervious area directly connected to the drainage system that contributes to increase stormwater volume and runoff (Shuster et al., 2005). Raingardens that are sized as <1% of the impervious catchment area are at risk of clogging and shortened lifespan.

Raingarden are designed to be effective for rainfall event with up to 4 in one year Annual Recurrence Interval (ARI). For region with a temperate climate 5-year ARI representing a minor storm event is suggested. Conversely for tropical climates a 2-year ARI rainfall events are generally used for the design of raingardens Payne et al. (2015). Sizing for larger rainfall events is not required to meet water quality objectives. Oversized systems may demand more frequent maintenance checks to prevent blockages and clogging, as they are more susceptible to accumulating sediment and debris that can limit water flow and infiltration.

Moreover, Payne et al. (2015) highlight a significant drawback of oversizing raingardens: the increased risk of plant mortality due to excessively dry soil conditions. When a raingarden is too large for its typical inflow, it fails to maintain the necessary moisture levels in the soil, leading to conditions that are not conducive for plant health. Plants in an oversized raingarden can struggle to thrive due to the lack of sufficient water, undermining the ecological and aesthetic benefits of the system.

2.3 Structure

All raingardens follow the same fundamental principles, with some essential features shared across designs. Depending on the goals for performance, as well as the advantages or limitations of the location or its catchment area, additional design elements may be integrated or omitted, such as the liner or the underdrain (Fig. 2 and Fig. 3).

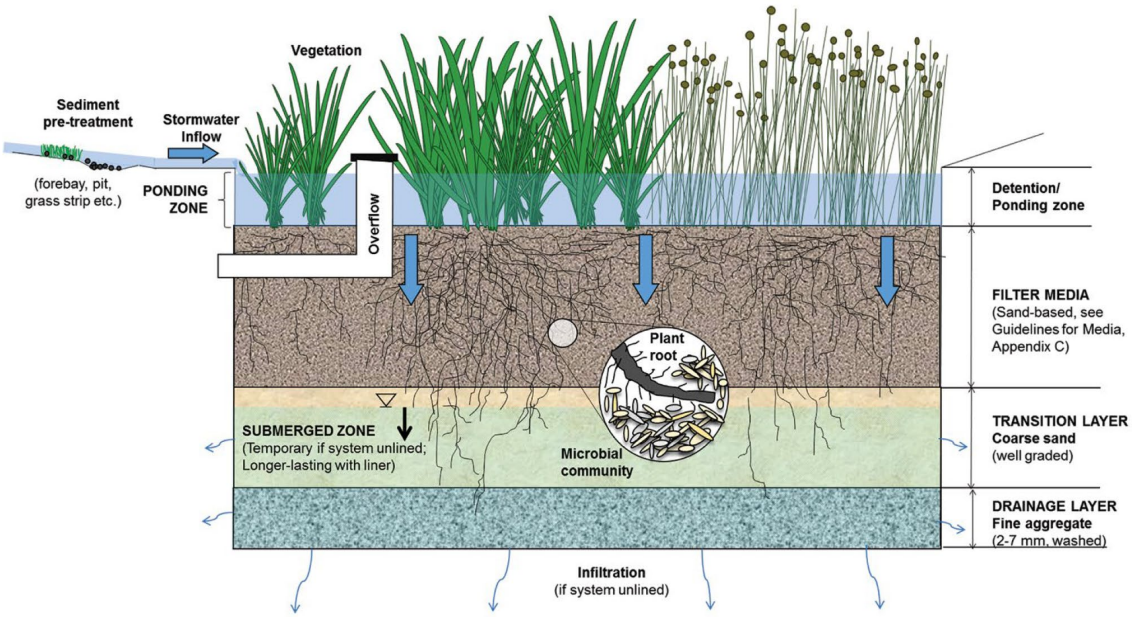

Fig. 2 – Raingarden essential components (Payne et al., 2015)

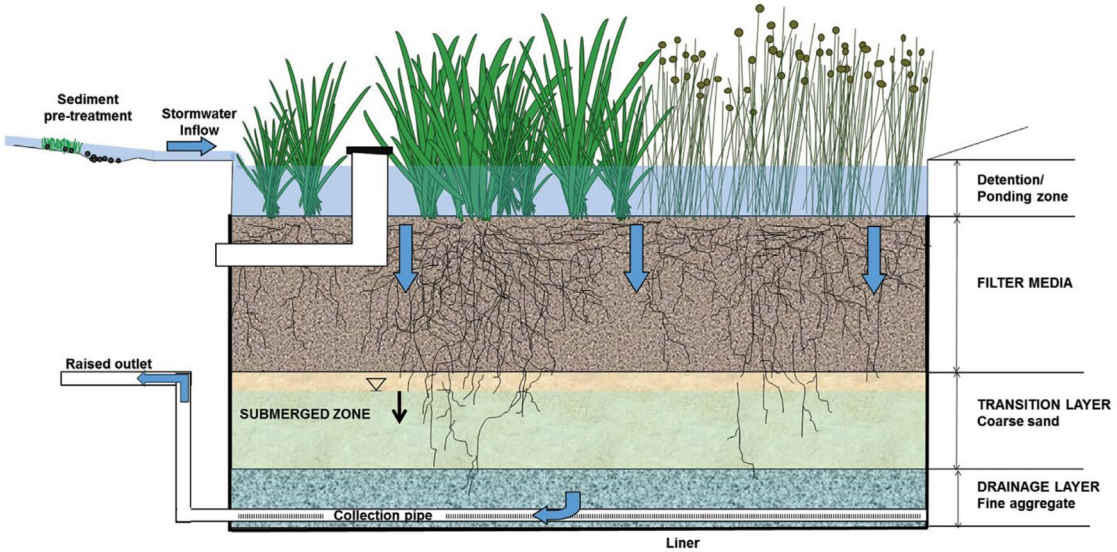

Fig. 3 – Typically biofilter configuration for dense urban areas (Payne et al., 2015)

Every component plays a role in how the system operates, and it's crucial for the proper functioning of the system that each part is properly designed, built, and maintained to fulfill its specific role. Essential and additional components and relative functions are reported in the following table (Tab. 1).

Tab. 1 – Key component of stormwater biofilters and their functional roles

Essential Component	**Function and role**
Inflow	Derivers urban runoff from the surrounding area to the biofilter surface. It can consist of a simple gap in the curb or a more complex piped delivery system.
Overflow	Bypasses flows above the ponding capacity to not damage the system.
Ponding (detention zone)	Allows stormwater to pond on the raingarden surface increasing the treatment capacity.
Vegetation	Plays different roles in water treatment by absorbing substances, converting them into organic forms, providing carbon for microbes, reducing stormwater volume through transpiration, stabilizing the medium's surface, helping maintain infiltration rates, cooling the surrounding area, contributing to the overall amenity, and improving aesthetics.
Filter Media	Typically composed of fine sand, it facilitates water infiltration, filtration, and the removal of pollutants, while also supporting the growth of vegetation. This composition aids in the absorption of stormwater, moderates and reduces the magnitude of the outflow hydrograph. A layer of mulch is often added to cover the soil media and retain solids.
Transition Layer	Generally made of coarse sand and organic matter. Acts as a protective layer to limit fine particles migration from the upper layer to the gravel drainage layer below.
Drainage Layer	Made of gravel. This layer enables the entire system to drain, whether through a drainage pipe leading to an outflow point or by allowing water to seep into the surrounding soil.
Unlined	Enables water to seep into the adjacent soils, applicable to either the entire system or just a portion of it.
Pre-treatment	Gathers large sediment and debris, aiding in safeguarding the biofilter from early clogging and obstructions, and simplifying maintenance tasks. Unnecessary for areas with an impervious catchment smaller than 2 hectares without clear sources of sediment, or for systems that only deal with roof runoff.

Additional Component	Function and role
Underdrain	Perforated pipe installed at the bottom to drain and collect effluent from the system. A higher outlet allows water to accumulate in the biofilter lower layer, creating a submerged zone.
Liner	Creates a longer-lasting submerged zone coupled with a raised underdrain, preventing exfiltration into surrounding soils. In unlined systems, a raised outlet encourages water to seep into the adjacent soils, while in lined systems, it helps maintain a submerged zone for a longer duration.
Submerged zone (Saturated zone)	Established by placing the outlet at some distance from the bottom. It may be temporary (if system unlined) or longer lasting (if lined). Provides a water supply to support plant and microbial survival in dry climate (dry periods exceeding 3 weeks), provides anaerobic conditions for denitrification and prolonged retention for a volume of stormwater which allows longer processing time.

In a temperate climate, the design of a raingarden to meet regulatory load reduction standards involves specific proportions and technical specifications. A raingarden intended to effectively manage stormwater should cover at least a surface area equivalent to 2% (4% for tropical climate) of the drained impervious area it serves. The recommended ponding depth ranges from 100 to 300 mm, which ensures adequate temporary storage for stormwater runoff during rain events. Additionally, to facilitate the efficient infiltration and treatment of this water, the hydraulic conductivity of the soil or filter media within the raingarden should be between 100 to 300 mm/hour. In tropical regions, achieving the desired treatment efficiency within the same land area and ponding depth necessitates a higher hydraulic conductivity (Payne et al., 2015).
Raingarden design guidelines specify three different layers of media for effective stormwater management where: the filter media should range from 400 o 600 mm, the transition layer should be $>$ 100 mm and the drainage layer should cover the underdrain pipe of about 50 mm (Melbourne Water, 2005; Payne et al., 2015).
In order to promote exfiltration into the surroundings soil, the collection pipe should be raised from the bottom of the raingarden of at least 50 mm up to 500 mm.

2.4 Plants

Vegetation in raingardens has proven to play a crucial role in the proper functioning of biofiltration systems (Winfrey et al., 2018).

Design guides from around the world offer detailed recommendations on choosing the right plants to enhance the effectiveness and longevity of these systems. The selection process focuses on identifying plant species that can thrive in the specific climate conditions and resist to environmental stresses of bioretention areas, contribute to water filtration and pollution removal, and support the overall ecosystem health (Roy-Poirier et al., 2010; Dagenais et al., 2018). Grasses, sedges, and small trees, characterized by an extensive and fibrous root system with a high proportion of fine roots, are generally used in these systems. A variety of plants with different functional traits can lead to a more productive ecosystem. This diversity allows for the use of resources in complementary ways, enhancing the system overall efficiency, including its ability to filter pollutants and manage water. Specific plant traits, like how fast a plant grows or the length of its roots, can significantly impact these processes. For example, the Australian shrub *Melaleuca ericifolia* has deep roots that help maintain water flow over time (Le Coustumer et al., 2012), while the Australian sedge *Carex appressa*, with its fast growth and long roots, is particularly good at removing nitrogen, more so than other plants (Read et al., 2010).
The presence of plants has been shown to provide several benefits, such as maintaining soil porosity, enhancing biological processes, sediment filtration, aiding in the absorption of pollutants (nitrogen, phosphorus, metal and pathogens), and, to a lesser extent, promoting evapotranspiration (Read et al., 2010).
The establishment of a robust vegetation cover is not only crucial for the operational effectiveness of these processes but also plays a significant role in improving their visual appeal, contributing positively to the overall aesthetic of the area.

2.5 Benefits

The interest and adoption of raingardens are driven by their multiple benefits.
Extensive studies, both in the lab and in the field, have been carried out to evaluate how well bioretention systems retain stormwater and remove pollutants.
In a field-study conducted by Davis (2008), where 49 storm events were simulated on two bioretention facilities installed at the University of Maryland, significant reduction in stormwater runoff was reported. For the 18% of the simulated events, no outflows were detected, meaning that the total precipitation amount was entirely captured by the raingardens. Furthermore, the research highlighted mean peak flow reductions of 49% and 58% for the two cells under observation, respectively. Notably, there were also significant extensions in the times to peak flow, with average increases by factors of 5.8 and 7.2 for each cell. These longer durations before reaching peak flow are crucial as they more closely replicate the pre-development hydrology within drainage basins,

contributing to a more natural and sustainable water cycle in urban environments. Similar results were documented by Hunt et al. (2006) from a year-long observation study on a field-scale bioretention cell in North Carolina. Over this 12-month period, the annual average ratio of outflow volume to estimated runoff volume was found to be 0.22, indicating that the bioretention cell discharged about 22% of the water it processed. When examining seasonal variations, the study noted significant differences: the mean ratio during summer was just 0.07, suggesting much higher retention rates, whereas it increased to 0.54 in winter months. These findings emphasize the strong influence of seasonal conditions on the hydrologic functionality of bioretention systems. The increase in outflow volume ratios during colder months can be attributed to decreased evapotranspiration rates, as the process is less efficient in lower temperatures. Hatt et al. (2009) investigated the hydrologic and pollutant removal performance on two field-scale biofiltration systems (one in Melbourne, VIC and the other one in McDowall, QLD) and they detected an average reduction in peak flow of 80 %; varying from 37 – 96% across different events. A performance evaluation of a lined biofilter revealed that by retaining inflow volumes within the filter media for later loss through evapotranspiration, runoff volumes were reduced by an average of 33%. Prince George's County's (1999) bioretention design guidelines indicated that a bioretention area comprising 5% of the impervious surface could facilitate the infiltration of the first 1.27 cm of runoff.

Raingardens have also proven effective in removing nitrogen, phosphorus, heavy metals, Total Suspended Solids (TSS), Biochemical Oxygen Demand (BOD), and other pathogens. Nutrients, especially nitrogen and phosphorus, are pollutants of primary concern in the protection of aquatic ecosystems. Davis et al. (2006) explored the nutrient removal capabilities of bioretention systems and they observed a total phosphorus removal from 70 to 85%, corresponding to an average mass removal rate of 86% on a mass basis. They also observed a nitrogen removal rate ranging from 55 to 65 %, equal to an average of 86% on a mass basis. However, the experiments showed poor nitrate reduction, with instances of nitrate production being noted. Hunt et al. (2006) documented varying nutrient removal efficiencies in their study of bioretention cells in North Carolina. The total nitrogen removal efficiency was consistent across two of the bioretention cells, with both achieving a 40% removal rate on a mass basis. However, the efficiency in removing different nitrogen components showed significant variation between the cells.

As for the heavy metal Glass and Bissouma (2005) conducted measurements of inlet and outlet concentrations of a wide range of heavy metals in a bioretention cell located in a parking lot over a three-month period. Their findings highlighted removal efficiencies of 81% for copper, 66% for cadmium, 79% for zinc, 53% for chromium, 75% for lead, 17%

for aluminum, 11% for arsenic, and 53% for iron. Li and Davis (2008b) explored the filtration mechanism of bioretention cells through bioretention column tests and field observations. They discovered that as particulate matter gets trapped by the bioretention media, stratification occurs within the media layers. Specifically, finer soil particles accumulate in the upper layers as suspended solids are captured, altering the media's characteristics and reducing its hydraulic conductivity. The study concluded that the effective lifespan of bioretention filter media is primarily limited by clogging, anticipated to occur before Total Suspended Solids (TSS) breakthrough. To mitigate media clogging, the study suggests annual or biannual replacement of the bioretention soil media to a depth of 5–20 cm, based on laboratory findings.

Despite the typically lower pathogen counts in stormwater compared to sanitary wastewater, the presence of pathogens in urban runoff raises significant health concerns for both humans and aquatic species, drawing attention from regulatory bodies. Column tests conducted by Rusciano and Obropta (2007) indicated that bioretention systems can substantially decrease pathogen levels in stormwater. Across 13 experiments featuring a spectrum of faecal coliform counts, an average reduction of 91.6% was achieved, with removal efficiencies varying between 54.5% and 99.8%. A two-year monitoring study of a bioretention cell in North Carolina, reported by Hunt et al. (2008), corroborated these findings. It showed an average faecal coliform reduction of 69% and a reduction in E. coli counts of 71%, further confirming the effectiveness of bioretention cells in pathogen reduction.

Beyond their effectiveness in mitigating stormwater flow and capturing pollutants, these systems provide in-situ treatment reducing the load on treatment plant. Another appealing aspect of raingardens is their cost-effectiveness. The installation is relatively affordable, and once in place, these systems demand minimal maintenance costs. Based on City of Chicago water management department (https://www.chicago.gov/city/en/depts/water/supp_info/conservation/green_design/bioinfiltration_raingardens.html) a biofiltration system cost can range from $100 to $400 per square meter based on different aspect such as the raingarden depth, the type of plants, and the presence of not of a underdrain, with a lifespan of about 20 years.

Moreover, bioretention systems contribute to the visual and environmental quality of a site. They enhance the landscape aesthetics, dampen noise pollution, and provide beneficial shade and windbreaks. This blend of functionality, cost efficiency, and environmental enhancement positions bioretention systems as a compelling choice for managing urban stormwater.

2.6 Maintenance challenges

Raingardens, and green infrastructure in general, have gained popularity in the field of stormwater management and urban planning in urban areas around the world. Ongoing research endeavours are dedicated to enhancing the fundamental frameworks of practices, aiming to optimize the performance of LID. Research teams keep working on refining the foundational designs to achieve superior outcomes and efficiency in LID applications. The effectiveness of these design enhancements and tools relies on certain fundamental assumptions: that the LID will be constructed and maintained in a proper manner (Blecken et al., 2015). However, it is frequently observed that after their initial construction, these systems tend to be neglected (Al-Rubaei et al., 2013; Hunt et al., 2011) or are assumed to function indefinitely by stormwater managers. Infiltrative raingardens can enhance the retention capacity within sewer catchments. However, the factors contributing to their ability for detention and redistribution of stormwater runoff are dynamic and frequently unverified (Shuster et al., 2017).

The overall hydraulic performance of raingardens has been shown to reduce over time if not regularly inspected and maintained.

Raingardens, like any other nature-based practices whose operation is based on hydrology, can experience different types of degradation, like clogging of the filter media or erosion of the soil layer, that can prevent these systems in delivering hydraulic end ecological benefits and can reduce their effectiveness in managing stormwater runoff (Asleson et al., 2009). As reported in Erickson et al. (2018) common causes of raingardens degradation include:

- Outflow blockage due to accumulation of medium to large-sized material that does not allow water to drain properly, and this can result in overflow leading to flooding the adjacent areas.
- Sediment accumulation and clogging. This represents one of the most prevalent issues is RG. Clogging generally occurs at the surface because of interstitial deposition of fine-grained sediments, mainly comprised of silt and clay particles from the incoming runoff. This phenomenon reduces the ponding volume available on the surface and potentially clogging the filter media, thus reducing the biofilter capacity to infiltrate water effectively (Hatt et al., 2008). Based on field observations this usually occurs closest to the inlet.
- Plant overgrowth leading to crowding and reduced effectiveness in capturing and treating stormwater.
- Invasive species, such as invasive weeds, can outcompete and displace native vegetation and potentially disrupt the local ecosystem.

- Contaminant buildup. The raingarden soil layer can accumulate pollutants, including heavy metals, oil, and chemicals. Over time, these contaminants can affect plant health and water quality.
- Erosion due to inadequate erosion control measures or heavy stormwater flows. This can lead to the loss of soil and vegetation.
- Climate stress due to extreme weather events, such as heavy rainfall or prolonged drought, can disrupt their functioning.
- The hydraulic performance of raingardens has been shown to be mostly affected by the decrease of the infiltration rate mainly due to clogging (Fig. 4), causing the system to overflow (Virahsawmy et al., 2014).

Blocked overflow grate – lead to flooding and damage to the filter and vegetation.

Sediment accumulation – build-up of fine sediments reduces infiltration and treatment.

Blocked inlet – restricts flow entry, reducing proportion of flows receiving treatment.

Plant die-back – severely reduces treatment efficiency and leaves media vulnerable to erosion.

Fig. 4 - Common raingarden issues that require maintenance (Payne et al., 2015)

Observation at operational sites have noted that infiltration rates are higher in the proximity of plants suggesting that they facilitate the water flow through the media

thanks to preferential pathways created by their roots (Archer et al., 2002). This phenomenon can mitigate the impact of surface clogging on infiltration.
Another hypothesis is that wind-induced movement of plant stems or foliage breaks the soil generating surface macropores which create space for the passage of water (Martinez-Meza & Whitford, 1996), lacking filtration and compacting the filter media thereby reducing the overall treatment efficiency of the biofilter (Melbourne Water, 2005).
Since vegetation plays an important role for the treatment processes and supports to maintain the infiltration capacity, healthy and well-established vegetation is essential for a proper functioning of raingardens (Le Coustumer et al., 2012; Blecken et al., 2015). A strong maintenance regime is therefore a crucial requirement for any raingarden.
Common and usual maintenance activities for biofilter include simple tasks as weeds removal, inspection and cleaning of the inlet and overflow devices, litter and debris removal, irrigation, or watering through prolonged dry spells (Payne et al., 2015;). Other tasks instead demand individuals with expertise in stormwater management.
This necessitates either forming a dedicated stormwater work crew or seeking the services of a qualified stormwater engineer.
Even when maintenance needs are not immediately apparent, especially for structures underground or underwater, periodical, and thorough inspections can disclose potential issues (Erickson et al., 2018).
As reported in Hunt and Lord (2006) the frequency of inspection and maintenance is dependent on the watershed land use (e.g., urban, rural, etc), construction in the watershed, and rainfall amounts and intensity. Tab. 2 lists some raingardens maintenance tasks and the frequencies with which they should be conducted.

Tab. 2 – Maintenance requirements and frequencies for bioretention practices (Hunt and Lord, 2006)

Task	**Frequency**	**Notes**
Inspection	1 / year or after 2-year return period storm event	
Pruning	1 – 2 times / year	Nutrients in runoff often cause bioretention vegetation to flourish.
Mowing	2 – 12 times / year	Frequency depends upon location and desired aesthetic appeal.
Mulch removal	1 time / 2 – 3 years	Mulch accumulation reduces available water storage volume and reduce infiltration rates.

Task	Frequency	Notes
		The top layer usually is the cause of clogging Removal of mulch also increases surface infiltration rate of fill soil.
Watering	1 time / 2 – 3 days for first 1 – 2 months. Sporadically after establishment	If droughty, watering after the initial year may be required.
Remove and replace dead plants	1 time / year	Within the first year, 10 %of plants may die. Survival rates increase with time.
Miscellaneous upkeep	12 times / year	Tasks include rubbish collection, spot weeding, and removing mulch from overflow device.

While these activities represent a routine maintenance which is often simple to execute, challenges in the coordination and administration of maintenance crews across raingarden installations have discouraged their upkeep (Erickson et al., 2010). As a result, many biofilter sites experience degradation and reduce infiltration rates due to clogging and erosion (Le Coustumer et al., 2009). As an example, Wardynski and Hunt (2012) conducted a survey on the maintenance requirements of 43 bioretention cells in North Carolina, USA and their findings revealed that over half of the cells exhibited maintenance deficiencies, with surface clogging being the most prevalent issue.

Visual inspection, which is the least complex method of assessment that can be used to quickly identify the cause of poor hydraulic performance and determine the necessary maintenance to restore the proper functioning, in most cases is not enough. Even if there are no outward signs of malfunction, visual inspection cannot guarantee that the biofilter is operating correctly. To properly assess the performance of the biofilter and determine the cause of failure a more complex assessment may be necessary (Erickson et al., 2018). However, an accurate performance assessment of each individual raingarden installed in the field requires a huge amount of economic and human resources. Measurements via infiltrometer are costly due to the high number of measurements required to obtain a confident value of the hydraulic conductivity (Ahmed et al., 2015; Weiss & Gulliver, 2015); moreover, biofilter sites being small and widely distributed coupled with the expertise required to perform these measurements discourages the practice (Erickson et al., 2013).

2.7 References

Al-Rubaei, A.M., Stenglein, A. L., Viklander, M., & Blecken, G.T. (2013). Long-term hydraulic performance of porous asphalt pavements in northern Sweden. *Journal of Irrigation and Drainage Engineering, 139 (6),* 499–505. doi.org/10.1061/(ASCE)IR.1943-4774.0000569

Archer, N.A.L., Quinton, J.N., & Hess, T.M. (2002). Below-ground relationships of soil texture, roots and hydraulic conductivity in two-phase mosaic vegetation in South-east Spain. *Journal of Arid Environments, 52 (4),* 535–553. doi.org/10.1006/jare.2002.1011

Ashley, R., Lundy, L., Ward, S., Shaffer, P., Walker, L., Morgan, C., Saul, A., Wong, T.H. F., & Moore, S. (2013). Water-sensitive urban design: opportunities for the UK. *Proceedings of the ICE - Municipal Engineer, 166 (2),* 65–76. doi.org/10.1680/muen.12.00046

Askarizadeh, A., Rippy, M.A., Fletcher, T.D., Feldman, D., Peng, J., Bowler, P., Mehring, A., Winfrey, B., Vrugt, J., AghaKouchak, A., Jiang, S., Sanders, B.F., Levin, L.A., Taylor, S., & Grant, S.B. (2015). From rain tanks to catchments: Use of low-impact development to address hydrologic symptoms of the urban stream syndrome. *Environmental Science & Technology, 49 (19),* 11264-11280. doi.org/10.1021/acs.est.5b01635

Asleson, B.C., Nestingen, R.S., Gulliver, J.S., Hozalski, R.M., & Nieber, J.L. (2009). Performance assessment of rain gardens. *Journal of the American Water Resources Associations, 45 (4),* 1019–1031. doi.org/10.1111/j.1752-1688.2009.00344.x

Blecken, G.T., Hunt III, W.F., Al-Rubaei, A.M., Viklander, M., & Lord, W.G. (2015). Stormwater control measure (SCM) maintenance considerations to ensure designed functionality. *Urban Water J., 14 (3),* 278–290. doi.org/10.1080/1573062X.2015.1111913

Carter, T., & Jackson, C.R. (2007). Vegetated roofs for stormwater management at multiple spatial scales. *Landscape and Urban Planning, 80 (1–2),* 84-94. doi.org/10.1016/j.landurbplan.2006.06.005

Castonguay, A.C., Urich, C., Iftekhar, S., & Deletic, A. (2018). Modelling urban water management transitions: A case of rainwater harvesting. *Environmental Modelling & Software 105,* 270-285. doi.org/10.1016/j.envsoft.2018.05.001

Chapman, C., & Horner, R.R. (2010). Performance assessment of a street-drainage bioretention system. *Water Environ. Research, 82 (2),* 109-119. doi.org/10.2175/106143009X426112

Chocat, B., Krebs, P., Marsalek, J., Rauch, W., & Schilling, W. (2001). Urban drainage redefined: from stormwater removal to integrated management. *Water Science & Technology, 43 (5),* 61–68. doi.org/10.2166/wst.2001.0251

City of Chicago – Biofiltration: Rain Gardens - https://www.chicago.gov/city/en/depts/water/supp_info/conservation/green_design/bioinfiltration_raingardens.html (Visited on 10/11/2023)

Dagenais, D., Brisson, J., & Fletcher, T.D. (2018). The role of plants in bioretention systems;

does the science underpin current guidance? *Ecological Eng., 120,* 532–545. doi.org/10.1016/j.ecoleng.2018.07.007

Davis, A.P., Shokouhian, M., Sharma, H., & Minami, C. (2006). Water Quality Improvement through Bioretention Media: Nitrogen and Phosphorus Removal. *Water Environment Research, 78(3)*, 284–293. doi.org/10.2175/106143005X94376

Davis, A.P. (2008). Field Performance of Bioretention: Hydrology Impacts. *Journal of Hydrologic Engineering, 13 (2),* 90-95. doi.org/10.1061/(ASCE)1084-0699(2008)13:2(90)

Dietz, M.E. (2007). Low impact development practices: A review of current research and recommendations for future directions. *Water Air Soil Pollution, 186 (1-4),* 351-363. doi.org/10.1007/s11270-007-9484-z

Drake, J.A.P., Bradford, A., & Marsalek, J. (2013). Review of Environmental Performance of Permeable Pavement Systems: State of the Knowledge. *Water Quality Research Journal of Canada*, 48 (3): 203–222. doi.org/10.2166/wqrjc2013.055

Dunnett, N., & Clayden, A. (2007). *Rain Gardens. Managing water sustainably in the garden and designed landscape.* Portland, Oregon: Timber Press. ISBN: 9780881928266

Ebrahimian, A., Sokolovskaya, N., & Wadzuk, B. (2021). Modeling dynamic performance of urban infiltration trench systems: Methodology and a case study in Philadelphia. *J. of Hydrology, 594,* 125938, ISSN 0022-1694. doi.org/10.1016/j.jhydrol.2020.125938

Erickson, A.J., Gulliver, J.S., Kang, J.-H., Weiss, P.T., & Wilson, C. B. (2010). Maintenance for stormwater treatment practices. *Journal of Contemporary Water Research & Education, 146 (1),* 75–82. doi.org/10.1111/j.1936-704X.2010.00393.x

Erickson, A.J., Weiss, P.T., & Gulliver, J.S. (2013). *Optimizing stormwater treatment practices: A handbook of assessment and maintenance.* Springer Science & Business Media. ISBN 978-1-4614-4624-8. doi.org/10.1007/978-1-4614-4624-8

Erickson, A.J., Taguchi, V.J., & Gulliver, J.S. (2018). The challenge of maintaining stormwater control measures: A synthesis of recent research and practitioner experience. *Sustainability, 10 (10),* 3666. doi.org/10.3390/su10103666

Fletcher, T.D., Shuster, W., Hunt, W.F., Ashley, R., Butler, D., Arthur, S., Trowsdale, S., Barraud, S., Semadeni-Davies, A., Bertrand-Krajewski, J-L., Mikkelsen, P.S., Rivard, G., Uhl, M., Dagenais, D., & Viklander, M. (2015). SUDS, LID, BMPs, WSUD and more – The evolution and application of terminology surrounding urban drainage. *Urban Water Journal, 12 (7),* 525-542, doi.org/10.1080/1573062X.2014.916314

Gargari, C., Bibbiani, C., Fantozzi F., & Campiotti, C.A. (2016). Environmental Impact of Green Roofing: The Contribute of a Green Roof to the Sustainable use of Natural Resources in a Life Cycle Approach. *Agriculture and Agricultural Science Procedia, 8,* 646-656. doi.org/10.1016/j.aaspro.2016.02.087

Glass, C., & Bissouma, S. (2005). Evaluation of a parking lot bioretention cell for removal of

storm water pollutants. *Ecosystems and sustainable development,* Transactions on Ecology and the Environment, 81, 699–708. Southampton, U.K.: WIT Press. doi.org/10.2495/ECO050691

Grafton, R.Q., & Hussey, K. (2011). *Water Resources Planning and Management.* Cambridge University Press. Online ISBN: 9780511974304. doi.org/10.1017/CBO9780511974304

Gülbaz, S., & Kazezyilmaz-Alhan, C.M. (2017). Experimental Investigation on Hydrologic Performance of LID with Rainfall-Watershed-Bioretention System. *Journal of Hydrologic Engineering, 22 (1),* 4016003. doi.org/10.1061/(ASCE)HE.1943-5584.0001450

Guo, C., Li, J., Li, H., & Li, Y. (2019). Influences of stormwater concentration infiltration on soil nitrogen, phosphorus, TOC and their relations with enzyme activity in rain garden. *Chemosphere, 233,* 207–215. doi.org/10.1016/j.chemosphere.2019.05.236

Hatt, B.E., Fletcher, T.D., & Deletic, A. (2008). Hydraulic and Pollutant Removal Performance of Fine Media Stormwater Filtration Systems. *Environmental Science & Technology, 42 (7),* 2535-2541. doi.org/10.1021/es071264p

Hatt, B.E., Fletcher, T.D., & Deletic, A. (2009). Hydrologic and pollutant removal performance of stormwater biofiltration systems at the field scale. *Journal of Hydrology, 365 (3-4),* 310-321. doi.org/10.1016/j.jhydrol.2008.12.001

Hoyer, J., Dickhaut, W., Kronawitter, L., & Weber, B. (2011). *Water Sensitive Urban Design. Principles and Inspiration for Sustainable Stormwater Management in the City of the Future.* Manual. JOVIS, HafenCity Universität. ISBN 978-3-86859-106-4

Hunt, W.F., & Lord, W.G. (2006). *Bioretention performance, design, construction, and maintenance.* Urban Waterways, North Carolina Cooperative Extension Service, Raleigh, NC

Hunt, W.F., Jarrett, A.R., Smith, J.T., & Sharkey, L.J. (2006). Evaluating Bioretention Hydrology and Nutrient Removal at Three Field Sites in North Carolina. *Journal of Irrigation and Drainage Engineering, 132 (6),* 600–608. doi.org/10.1061/(ASCE)0733-9437(2006)132:6(600)

Hunt, W.F., Smith, J.T., Jadlocki, S.J., Hathaway, J.M., & Eubanks, P.R. (2008). Pollutant removal and peak flow mitigation by a bioretention cell in Urban Charlotte, N.C. *J. Environ. Eng., 134(5),* 403-408. doi.org/10.1061/(ASCE)0733-9372(2008)134:5(403)

Hunt, W.F., Greenway, M., Moore, T.C., Brown, R.A., Kennedy, S.G., Line, D.E., & Lord, W.G. (2011). Constructed Storm-Water Wetland Installation and Maintenance: Are We Getting It Right? *Journal of Irrigation and Drainage Engineering, 137 (8),* 469–474. doi.org/10.1061/(ASCE)IR.1943-4774.0000326

Ishimatsu, K., Ito, K., Mitani, Y., Tanaka, Y., Sugahara, T., & Naka, Y. (2017). Use of rain gardens for stormwater management in urban design and planning. *Landscape and Ecological Engineering, 13,* 205–212. doi.org/10.1007/s11355-016-0309-3

Jones, M.P., & Hunt, W.F. (2010). Performance of Rainwater Harvesting Systems in the Southeastern United States. *Resources, Conservation and Recycling, 54 (10),* 623-29. doi.org/10.1016/j.resconrec.2009.11.002

Le Coustumer, S., Fletcher, T.D., Deletic, A., Barraud, S., & Lewis, J. (2009). Hydraulic performance of biofilter systems for stormwater management: Influences of design and operation. *J. of Hydrology, 376 (1-2)*, 16 - 23. doi.org/10.1016/j.jhydrol.2009.07.012

Le Coustumer, S., Fletcher, T.D., Deletic, A., Barraud, S., & Poelsma, P. (2012). The influence of design parameters on clogging of stormwater biofilters: A large-scale column study. *Water research, 46 (20),* 6743–6752. doi.org/10.1016/j.watres.2012.01.026

Leroy, M.C., Portet-Koltalo, F., Legras, M., Lederf, F., Moncond'huy, V., Polaert, I., & Marcotte, S. (2016). Performance of vegetated swales for improving road runoff quality in a moderate traffic urban area, *Science of The Total Environment, 566–567,* 113-121. doi.org/10.1016/j.scitotenv.2016.05.027

Li, H., & Davis, A.P. (2008). Urban particle capture in bioretentionmedia. I: Laboratory and field studies. *Journal of Environmental Engineering, 134 (6)*, 409–418. doi.org/10.1061/(ASCE)0733-9372(2008)134:6(409)

Lloyd, S.D., Wong, T.H.F., & Chesterfield, C. (2002). *Water Sensitive Urban Design – A Stormwater Management Perspective.* Cooperative Research Centre for Catchment Hydrology.

Malaviya, P., Sharma, R., & Sharma, P.K. (2019). Rain Gardens as Stormwater Management Tool. In: Shah, S., Venkatramanan, V., Prasad, R. (eds) *Sustainable Green Technologies for Environmental Management*. Springer, 141-166. doi.org/10.1007/978-981-13-2772-8_7

Martinez-Meza, E., & Whitford, W.G. (1996). Stemflow, throughfall and channelization of stemflow by roots in three Chihuahuan desert shrubs. *Journal of Arid Environments, 32(3),* 271-287. ISSN 0140-1963. doi.org/10.1006/jare.1996.0023

Melbourne Water (2005). *WSUD Engineering Procedures: Stormwater*. Clayton South VIC: CSIRO Publishing, ISBN (electronic) 978-0-643-09989-0. doi.org/10.1071/9780643092235

Morash, J., Wright, A., LeBleu, C., Meder, A., Kessler, R., Brantley, E., & Howe, J. (2019). Increasing Sustainability of Residential Areas Using Rain Gardens to Improve Pollutant Capture, Biodiversity and Ecosystem Resilience. *Sustainability, 11(12),* 3269. doi.org/10.3390/su11123269

Mullaney, J., & Lucke, T. (2014). Practical Review of Pervious Pavement Designs. *Clean – Soil, Air, Water, 42 (2),* 111–124. doi.org/10.1002/clen.201300118

Payne, E.G.I., Hatt, B.E., Deletic, A., Dobbie, M.F., McCarthy, D.T., & Chandrasena, G.I. (2015). *Adoption guidelines for Stormwater Biofiltration Systems*. Melbourne, VIC: CRC for Water Sensitive Cities. ISBN: 978-1-921912-27-6

Prince George's County. (1999). *Low-Impact Development Hydrologic Analysis*. Prince George's

County, Maryland. Department of Environmental Resources, Programs and Planning Division. Available in: https://www.princegeorgescountymd.gov/sites/default/files/media-document/dcv87_low-impact-development-hydrologic-analysis-pdf.pdf

Razzaghmanesh, M., Beecham, S., & Salemi, T. (2016). The role of green roofs in mitigating Urban Heat Island effects in the metropolitan area of Adelaide, South Australia. *Urban Forestry & Urban Greening, 15,* 89-102. doi.org/10.1016/j.ufug.2015.11.013

Read, J., Fletcher, T.D., Wevill, T., & Deletic, A. (2009). Plant traits that enhance pollutant removal from stormwater in biofiltration systems. *International Journal of Phytoremediation 12 (1),* 34–53. doi.org/10.1080/ 15226510902767114

Roy-Poirier, A., Champagne, P., & Filion, Y. (2010). Review of bioretention system research and design: Past, present, and future. *Journal of Env. Eng., 136 (9),* 878–889. doi.org/10.1061/(ASCE)EE.1943-7870.0000227

Rusciano, G.M., & Obropta, C.C. (2007). Bioretention Column Study: Fecal coliform and total suspended solids reductions. *Transaction of the ASABE, 50(4)*, 1261–1269.Available in: http://www.water.rutgers.edu/Rain_Gardens/RGWebsite/misc/ColumnStudy.pdf

Shafique, M., Kim, R., & Kyung-Ho, K. (2018). Green Roof for Stormwater Management in a Highly Urbanized Area: The Case of Seoul, Korea. *Sustainability, 10 (3),* 584. doi.org/10.3390/su10030584

Shuster, W.D., Bonta, J., Thurston, H., Warnemuende, E., & Smith, D.R. (2005). Impacts of impervious surface on watershed hydrology: A review. *Urban Water J., 2 (4)*, 263–275. doi.org/10.1080/15730620500386529

Shuster, W.D., Darner, R.A., Shifman, L.A., & Herrmann, D.L. (2017). Factors Contibuting to the Hydrologic Effectiveness of a Rain Garden Network (Cincinnati OH USA). *Infrastructures (Basel), 2(3).* doi.org/10.3390/infrastructures2030011

Steffen, J., Jensen, M., Pomeroy, C.A., & Burian, S.J. (2013). Water Supply and Stormwater Management Benefits of Residential Rainwater Harvesting in US Cities. *Journal of the American Water Resources Association*, 49 (4), 810–824. doi.org/10.1111/jawr.12038

Stovin, V. (2010). The potential of green roofs to manage Urban Stormwater. *Water and Environmental Journal, 24 (3),* 192-199. doi.org/10.1111/j.1747-6593.2009.00174.x

Virahsawmy, H.K., Stewardson, M. J., Vietz, G., & Fletcher, T.D. (2014). Factors that affect the hydraulic performance of raingardens: implications for design and maintenance. *Water Science & Technology, 69 (5),* 982-988. doi.org/10.2166/wst.2013.809

Wardynski, B.J., & Hunt, W.F. (2012). Are Bioretention Cells Being Installed Per Design Standards in North Carolina? A Field Study. *Journal of Env. Eng. 138 (12),* 1210–1217. doi.org/10.1061/(ASCE)EE.1943-7870.0000575

Winfrey, B.K., Hatt, B.E., & Ambrose, R.F. (2018). Biodiversity and functional diversity of Australian stormwater biofilter plant communities. *Landscape and Urban Planning, 170,*

112-137. ISSN 0169-2046. doi.org/10.1016/j.landurbplan. 2017.11.002

Woods-Ballard, B., Kellagher, R., Martin, P., Jefferies, C., Bray, R., & Shaffer, P. (2007). *The SuDS Manual*: C697. London: Construction Industry and Research Association (CIRIA), ISBN: 9780860176978

Wong, T.H.F. (2001). A Changing Paradigm in Australian Urban Stormwater Management. In *Proceedings of 2nd South Pacific Stormwater Conference*, Auckland, New Zealand. Auckland: New Zealand Water & Wastewater Association

Wong, T.H.F. (2006). Water sensitive urban design – the journey thus far. *Australasian Journal of Water Resources, 10 (3),* 213-222. doi.org/10.1080/13241583. 2006.11465296

Zhang, L., Ye, Z., & Shibata, S. (2020). Assessment of Rain Garden Effects for the Management of Urban Storm Runoff in Japan. *Sustainability, 12 (23),* 9982. doi.org/10.3390/su12239982

Chapter 3 - Sensors in green infrastructure

In this chapter, the study concerning the utilization of low-cost electronic sensors for real-time monitoring of raingarden functionality is presented. The study was conducted during the research period at Monash University in Melbourne, during which the experiment setup was established. Data analysis continued remotely in the months following the return, facilitated by a cloud-based data collection system. For the sensor evaluation, a microcosm of 15 study columns was created, designed according to raingarden design guidelines. In each column an electronic sensor system was installed to monitor soil moisture variations, aiming to identify operational indicators and characterize degradation status.

The evaluation was conducted by creating three different raingarden operation scenarios, simulating normal functioning, functioning in case of erosion, and functioning in case of surface clogging. Subsequently, low and medium-intensity meteorological events were simulated on each column to detect soil moisture variations for each operation mode.

At the time of writing, the columns are being studied by other students and are still transmitting real-time data to an online server hosted by Monash University (https://bosl.com.au/IoT/wsudwatch/FYP_SGI/?C=N;O=A).

3.1 Introduction

Bioretention practices (or raingardens) have emerged as an effective solution to restore the natural water cycle in urban areas (Lloyd et al., 2002). They achieve this by enhancing infiltration and evaporation processes, thereby reducing runoff volume urban runoff peak flows (Davis, 2008; Richards et al., 2015). Their function has become increasingly crucial as cities grapple with escalating instances of extreme weather events while their aging and undersized drainage infrastructure struggles to cope with new stormwater management challenges.

While the implementation of bioretention systems within urban drainage networks effectively reduces water volumes impacting traditional sewer infrastructure, their functionality is heavily dependent on the quality and frequency of inspections and maintenance. In fact, despite their benefits, raingardens are prone to clogging from anthropogenic factors such as debris and stormwater sediment accumulation, plant die-off, erosion, and seasonal weather changes (Benedict and McMahon, 2002), issues that require constant and ongoing interventions to ensure their functionality.

The inspection and maintenance of RG garnered increasing attention as integral aspects of sustainable stormwater management initiatives. Currently, these programs predominantly employ manual inspection methods, relying heavily on qualitative assessments. This involves conducting hands-on inspections for each raingarden installation individually, spanning across the entire city (Angelstam et al, 2017). The decentralized nature LID implementation exacerbates this challenge and escalates the financial strain. Moreover, any alterations in the functioning of these practices between inspections, or after a storm event, are challenging to anticipate or even detect (Scarbrough et al., 2023).

Minimizing maintenance requirements by focusing on effective biofilter design has been extensively researched, with significant attention given to large-scale column studies and in-situ evaluations to establish robust guidelines (Davis, 2008; Asleson et al., 2009; Roy-Poirier et al., 2010; Le Coustumer et al., 2012; Payne et al., 2015; Dagenais et al., 2018). While this approach aims to develop biofilter sites that are more resilient to their environmental conditions, it does not adequately address the ongoing maintenance requirements of existing systems. In this context, real-time monitoring systems (RTMs) offer a promising solution to this challenge by enabling remote detection of malfunctions, facilitating prompt interventions to restore proper operation, and allowing for a more quantitative assessment of when maintenance is required. RTM can also reduce the need for extensive inspections and manual labour by staff, thereby making stormwater management more efficient and effective.

While other studies demonstrated the success of real-time monitoring of green infrastructure using electronic systems (Kerkez et al., 2018; Bartos et al., 2018; Mason et al., 2021), their focus was mainly on observing large-scale hydrological patterns, with little exploration into their application for addressing the maintenance needs at the local level.

This study investigates the application of affordable electronic sensors to provide real-time predictive maintenance indicators to enable remote monitoring as an alternative to resource-intensive on-site methods. A 15-column laboratory study was conducted in which two types of electronic sensors (one resistance sensor and one Time Domain Transmission sensor - TDT) for soil moisture and temperature probe were implemented to detect different raingarden behaviours. Specifically, the study evaluated the sensor ability to detect states of poor hydraulic performance in raingardens, commonly associated with maintenance issues. The set of 15 identical columns was divided in three groups characterized by different treatments designed such as to simulate most common biofilter health conditions: normal functioning, surface clogging, and preferential flow path. The treatments were validated through falling-head infiltration rate testing. Once the three different behaviours were validated, the columns were subjected to water dosages of various volumes corresponding to two different meteorological events, specifically a small one and a medium one, corresponding to events that on average occur at least 4 times a year.

It is worth emphasizing that the study did not aim to obtain precise numerical measurements of soil moisture from these sensors; rather, the focus was on their capability to provide maintenance indicators and facilitate timely interventions. This study aimed to address the need to integrate advanced monitoring technologies to enhance the effectiveness and resilience of bioretention systems in urban stormwater management.

3.2 Biofilter common degradations

As discussed in section 2.3, the effectiveness of biofiltration is frequently compromised by two common degradation phenomena: soil layer erosion, which generates preferential flows, and surface clogging. The formation of preferential flow paths in the soil layers is a significant concern in raingarden (RG) maintenance. These paths are channels or routes within the soil layers that allow water to flow more rapidly, thereby reducing the retention and filtration capacity of the RG. This phenomenon reduces efficiency in pollutant removal because water bypasses the filtration process. Additionally, it results in the death of plants (Fig. 5a) (Fletcher et al., 2005).

The main causes of preferential flow path formation are primarily attributed to erosion, particularly in areas where runoff directly enters cells as overland flow instead of passing through a forebay, especially where flow is concentrated along the perimeter of the raingarden (Wardynski and Hunt, 2012; Blecken et al., 2015). The presence of these pathways cannot be easily discerned through simple visual inspection, posing a challenge in identifying the issue without a more thorough investigation.

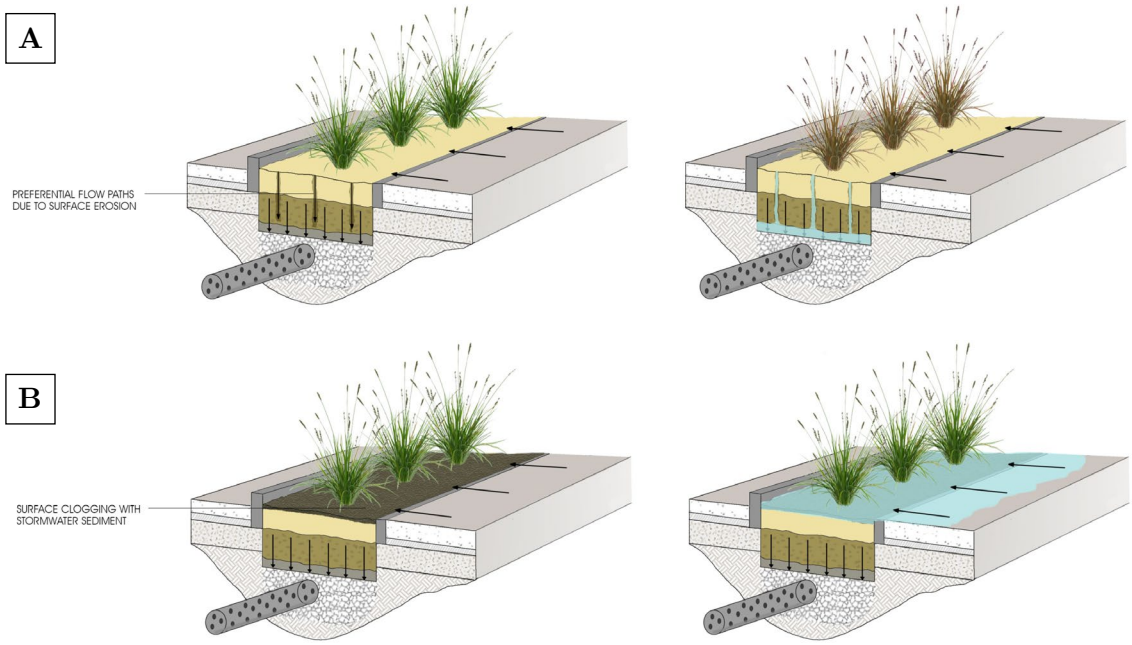

Fig. 5 – Consequences of biofilter health degradation due to a) preferential flow path and b) surface clogging.

The second most common cause of RG performance degradation is surface clogging, defined by Bouwer (2002) as the primary cause of RG failure due to inappropriate pretreatment and maintenance. A field survey conducted by Lindsey et al. (1992) on various infiltration systems revealed that only 38% of infiltration basins were functioning as intended after few years of operation, and two-thirds were identified as clogged and need maintenance. The processes leading to surface clogging of biofilters are attributed to mechanical, biological, and chemical factors (Langergraber et al., 2003). These factors include:

- Sedimentation of solid particles, accumulation of coarse materials and impurities on the surface of the biofilter. These can lead to both a outer blockage and inner blockage due to the deposition in the pores of the substrate. These materials can be removed through mechanical cleaning or by adding pre-treatments to reduce the load on the biofilter (Bouwer, 2002).
- Micro-organism forming the biofilm can proliferate and grow excessively reducing the permeability of the filtering medium, often due to favourable environmental

conditions like excess nutrients or unsuitable pH. Controlling biomass through nutrient regulation, aeration, and pH control measures can help reducing this type of clogging.

- Chemical substances present in the environment influence the formation and development of the biofilm. These may include inorganic or organic compounds, which can alter the physical or biological properties of the biofilter, causing surface clogging. Removing such chemical contaminants may be necessary to maintain the efficiency of the biofilter.
- Other minor factors like the excessively growth of plant roots (Virahsawmy et al., 2014), formation and accumulation of humic substances (Langergraber et al., 2003).

The impact of surface clogging is generally more pronounced in biofilters composed of coarse filter media. The difference in particle size results in the infiltration of sediment into the surface soil layer, reducing its hydraulic conductivity. This phenomenon is less pronounced in biofilters where the surface layer consists of fine soils; in this case, the smaller particle size being similar to that of the sediment proportionally reduce the effect of surface clogging (Le Coustumer et al., 2009). The surface clogging leads to more frequent overflows, reducing treatment capacity as less of the annual flow volume passes through the media and extended ponding time (Fig. 5b). Additionally, clogging can result in stagnant water and aesthetic issues, posing challenges for the acceptance of biofiltration as an integrated system in the built environment.

If a raingarden fails to provide a satisfactory infiltration due to surface clogging, it may necessitate complete or partial reconstruction of the RC itself (Asleson et al., 2009, Brown and Hunt, 2012, Blecken et al., 2015)

3.3 Experiment set up

To assess the effectiveness of low-cost electronic sensors in identifying malfunctions of RG, a total of 15 columns medium-sized were constructed, each with a diameter of 250 mm and a depth of up to 1050 mm as illustrated in Fig. 6. These raingardens columns were designed based on a traditional biofiltration system comprising the following composition:

- A drainage layer at the bottom, consisting of fine aggregate (gravel) with a depth of 100 mm. Within this layer, an 18 mm diameter drainage pipe is connected to serve as emergency outlet of the system;
- A transition layer, composed of a mixture of coarse sand and sugar cane mulch (95:5 ratio), reaching a depth of 350 mm;

- A filter layer, located atop the transition layer, made of fine sand with a depth of 300 mm. This layer acts as a further filtration barrier for water passing through the RG;
- A ponding zone enclosed by a Perspex guard, extending to a depth of 300 mm and featuring vegetation cover. This zone serves to temporarily store water, allowing for enhanced biological treatment and retention within the RG system.

The construction methods employed are consistent with typical practices of biofilter construction and take cues from previous study (Payne et al., 2015; Le Coustumer et al., 2012; Shen et al., 2020). Consequently, the layers were lightly hand-compacted during construction. Following this, the columns were dosed nightly with rainwater using an automated irrigation system.

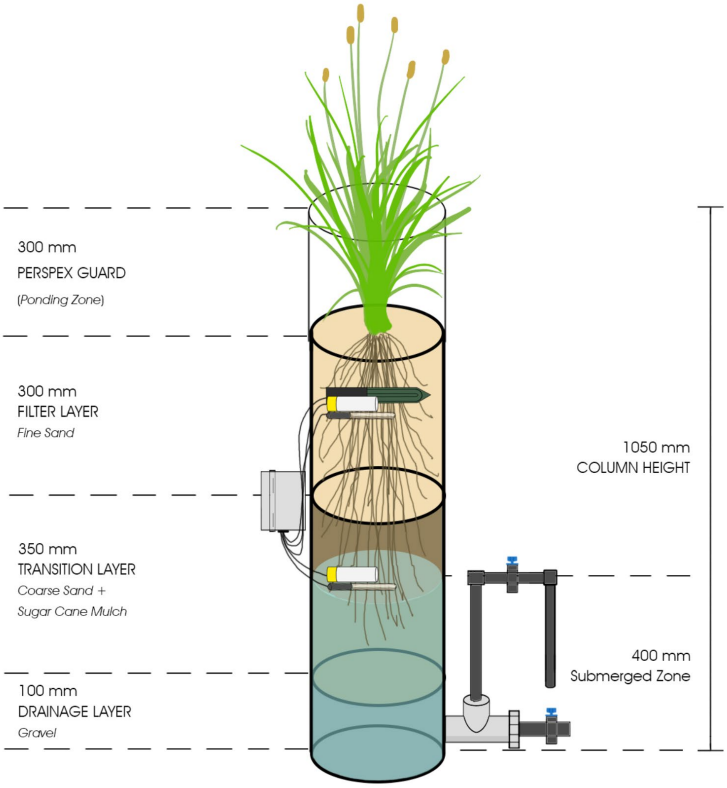

Fig. 6 – Schematic view of biofiltration column with sensor clusters

A tap was placed 400 from the bottom of the column to create a submerged zone and keep a constant saturated level during infiltration tests. During the column construction phase, a total of 5 sensors were placed within the soil layers at two different heights: one cluster of sensors was positioned within the filter media at a depth of approximately 15 cm from the surface, while the second cluster was placed within the transition layer at a

depth of around 350 mm from the surface of the biofilter. The sensor specifications will be discussed later.

The biofilter columns were planted with Carex appressa, the most common plant type for biofilters in Australia (Fig. 7). This selection is attributed to its ability to thrive in wet conditions, filtering capabilities and its ecological advantages, including enhancing water quality, removing pollution, and controlling erosion primarily owing to its dense root system (Melbourne Water, 2005).

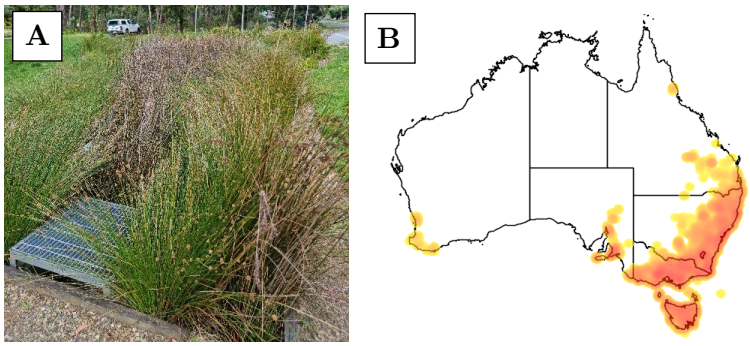

Fig. 7 – A) Carex Appressa plant B) Geographical distribution (https://wtlandcare.org/details/carex-appressa/)

3.3.1 Treatments definitions

To identify health biofilters indicators it was essential to differentiate the column based on different types of operating conditions. To achieve these three common RG health conditions were designed: normal operation, erosion, and surface clogging. The 15 columns were then divided into three groups of five:

- Group C - Control group;
- Group P – Preferential flow group;
- Group S – Surface clogging group.

The Control group is representative of the normal functioning of the raingarden while the two treatment groups represent common modes of biofilter health degradation both of which can significantly affect filter performance if left unmaintained for long periods of time. The group with preferential flow paths was designed by manually creating vertical holes using long wooden stake, typically used for growing tomatoes. The stick was inserted vertically through the filter layers until reaching the gravel of the drainage layer, creating four holes, each placed radially at an angular distance of approximately 90° from each other and about 5 cm from the wall of the column (Fig. 8). This operation was repeated before each water dosing, concurrently with the infiltration tests. In a later

phase of the study, the procedure just described was replaced by inserting a 600 mm long perforated plastic tube inside the biofilter layers. This was done to mitigate uncertainties associated with manual drilling, such as potential soil compaction and settling caused by the continuous passage of the wooden stick.

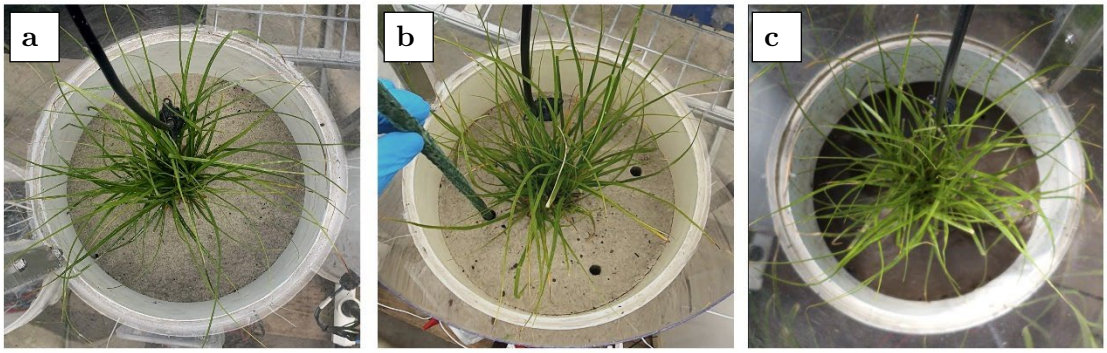

Fig. 8 – a) Control, b) Preferential Flow and c) Surface Clogging treatments (Photo by Leigh Oliver)

The surface clogging group received treatment with stormwater sediment collected for another study at the Monash University Living Laboratory. This sediment, stored in a highly concentrated slurry form, was diluted with water before application to the top of each column. Initially, 200 g of stormwater sediment were deposited on each column. This quantity was subsequently corrected by adding an additional 100 grams, based on the data provided by the infiltration rate tests conducted. The three different design treatments are configured as shown in Fig. 9.

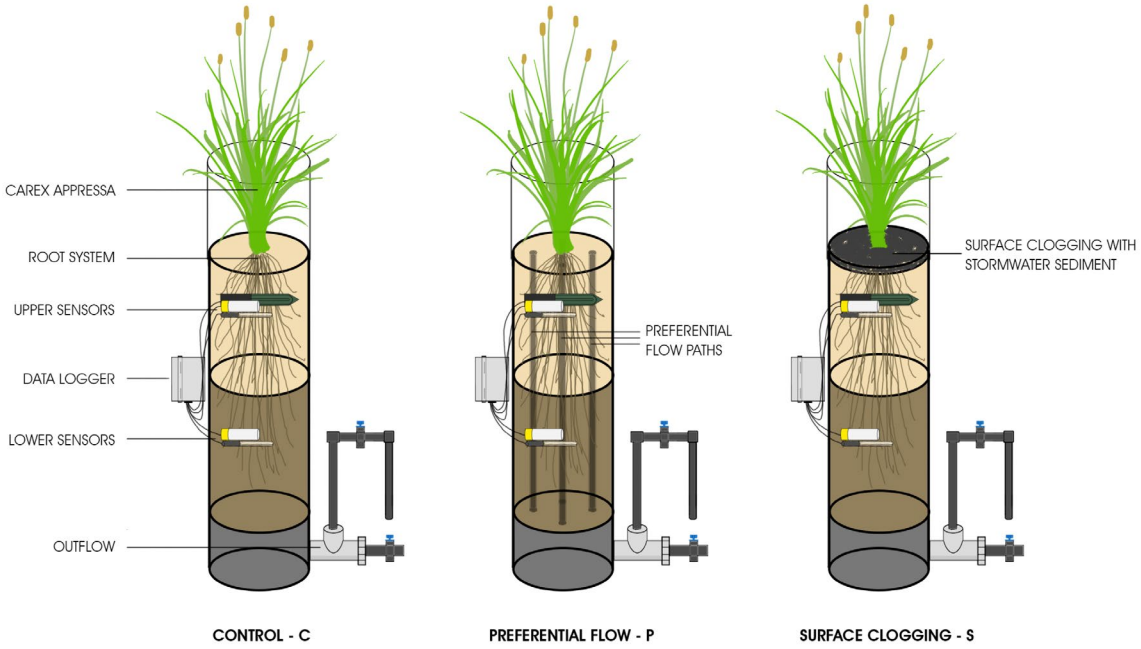

Fig. 9 - Scheme of the three different test conditions

In Fig. 10 the finished columns are arranged in such a way that any bias related to their placement in the laboratory, such as sunlight availability or pedestrian traffic, is evenly distributed across the three experimental groups.

C3 S3 P3 C2 P2 S2 P1 S1 C1 P5 S5 C5 P4 C4 S4

Fig. 10 - The 15-columns study. The three groups are distributed in a random manner to reduce environmental bias. The letter C identifies the control group columns, P those with preferential flow path and S those with surface clogging.

3.3.2 Laboratory infiltration rates test

The hydraulic performance of the columns was assessed through a series of falling-head infiltration rates tests. The methodology used follows the Environmental Protection Agency (EPA) Falling Head Percolation Test Procedure (EPA, 1980).
Given that the soil layers constituting the columns are primarily composed of sand, the pre-soaking phase, as outlined in the EPA guidelines, was deemed unnecessary (EPA, 1980). Each test began by filling the columns with clean water to a minimum level of approximately 25 cm above the surface, corresponding to the ponding zone. Subsequently, water level measurements were taken at 5-minute intervals over a 15-minute period. Beyond this timeframe, the water level had receded too significantly to accurately gauge further variations. The infiltration rate for each column was then determined by dividing the time interval between measurements by the magnitude of each water level drop. Subsequently, the average of all values was calculated. This calculation results in a percolation rate in terms of mm/h as presented in the Tab. 3.

Tab. 3 - Average infiltration values for each column and each treatment group.

Group	Column	Average infiltration rate (mm/h)	Group average infiltration rate (mm/h)
C	C1	134.60*	**186.33**
	C2	198.50	
	C3	161.60	
	C4	210.00	
	C5	175.20	
P	P1	235.60	**244.48**
	P2	246.40	
	P3	265.60	
	P4	238.00	
	P5	236.80	
S	S1	103.50	**100.87**
	S2	166.80*	
	S3	98.40	
	S4	149.40*	
	S5	100.70	

*Columns that exhibited infiltration values outside of the standard range, likely due to construction errors or leaks at the bottom, were therefore excluded from the evaluation.

The values obtained from the infiltration tests allowed for the validation of the three designed treatments. According to the "Guidelines for Stormwater Biofiltration Systems"

(Payne et al., 2015), the hydraulic conductivity of a raingarden under normal conditions should fall within the range of 150 – 200 mm/h. Beyond these values, soil erosion and the presence of preferential flow paths are observed, while below these values, surface clogging occurs.

3.4 Sensor system

The water status inside a soil can be defined by two attributes (Warrick, 2001):

- Volumetric Water Content (VWC);
- Soil Matric Potential (SMP).

The volumetric water content is defined as the volume of water per bulk volume of soil, whereas the soil matric potential is the pressure potential that arises from the interaction between water and the matrix of solid particles in which the water is embedded (Gardner, 1986; Warrick, 2001). These variables are related to each other through a function known as the "soil-water characteristic curve" (SWC).
In this study, two types of sensors were used to characterize the water status within the raingardens: the low-cost "Chameleon Soil Water Sensor" for measuring the soil water tension (SWT), which corresponds to the absolute value of the soil matric potential (Shock and Wang, 2011), and the "Truebner SMT 100", a more reliable and robust sensor, for measuring the volumetric water content. Additionally, a temperature probe DS18B20 was also employed to correlate the measured data with the soil temperature. The sensors are briefly described in the following sections.

3.4.1 Chameleon Soil Moisture Sensor (Resistivity Sensor)

Chameleon sensor is a prototype sensor developed by the Commonwealth Scientific and Industrial Research Organisation (CSIRO) aimed at enhancing water management practices for small-scale irrigators on their farmland (https://www.csiro.au/en/research /plants/crops/Farming-systems/Chameleon-soil-waterwater-sensor).
The sensor was chosen for this project because it is low-cost ($35AUD, approximately 20€), highly reliable, and easily accessible from local suppliers.
The Chameleon Soil Water Sensor is designed to emulate the way a plant perceives water in the soil by measuring the tension required for roots to extract moisture (https://via.farm/chameleon-soil-water-sensor/).
It consists of a central sensing material surrounded by an outer layer of gypsum. Inside the sensor, there are two gold-plated electrodes that measure the resistance across the specialized medium (Fig. 11). The surrounding gypsum material allows moisture to pass

through and reach the sensing material while dissolving a small amount of gypsum into the water, creating a constant electrical conductivity environment thus buffering the sensor (Warrick, 2001). The soil water tension is derived from the measured electrical resistance using a calibration relationship provided by the sensor developer. It is designed to be accurate (±2 kPa) in the range that most plants are sensitive to water stress, from 0 to 80 kPa (Stirzaker and CSIRO, 2014).

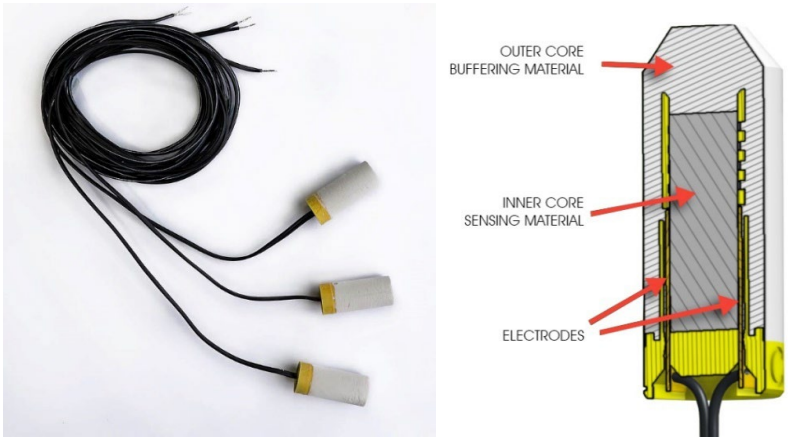

Fig. 11 - Chameleon soil moisture sensors (https://www.pureconnect.co.za/wp-content/uploads/2021/05/Chameleon-Card-three-sensor-pack-800px_2048x2048.jpg)

3.4.2 DS18B20 Digital Temperature Probe

Since the measured resistance in the Chameleon sensor is affected by temperature, a temperature probe input was used for increased accuracy, for this aim a DS18B20 Digital Temperature Probe was chosen (Fig. 12). This is a digital temperature sensor that uses the 1-Wire bus to communicate temperature readings to a microcontroller or computer.

Fig. 12 - DS18B20 Digital Temperature Probe (https://core-electronics.com.au/waterproof-ds18b20-digital-temperature-sensor.html)

It can be used to measure temperature in a variety of applications, including in wet or harsh environments due to its waterproof and pre-wired design. It is precise with an

accuracy of ±0.5°C over much of the range (from – 55 °C to 125 °C) (https://www.analog.com/media/en/technical-documentation/datasheets/ds18b20.pdf).

3.4.3 Truebner SMT 100 soil moisture and temperature probe

The SMT 100 soil moisture probe that uses a Time Domain Transmission (TDT) technology to measure the volumetric water content. This method uses the propagation of electrical signals along the green sensor blade 80 mm long (Fig. 13). A soil temperature sensor is also implemented inside the black part of the sensor.

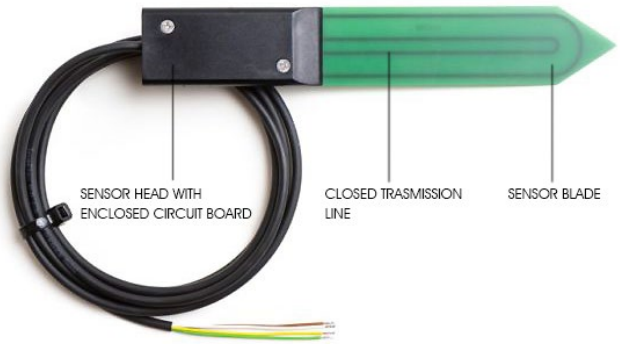

Fig. 13 - SMT 100 Soil Moisture Sensor (https://www.truebner.de/en/smt100.php)

With an accuracy of ±0.1% for volumetric water content and ±0.01 °C for temperature, and a range of 0 - 100% for volumetric water content and -40°C to +80°C for temperature, the SMT-100 sensor combines the cost-effectiveness (about 150€) of capacitance sensor systems with the precision of a TDR (time domain reflectometry) system. It operates by measuring the signal travel time, similar to TDR, to determine soil relative permittivity, and then converts this into a frequency, akin to capacitance sensors.

The SMT-100 measurements are less influenced by soil temperature, electrical conductivity, and texture, leading to more accurate readings of VWC without siter-specific calibration (https://www.truebner.de/ assets/download/Manual_SMT100_V1. 0.pdf). It is a reliable and well-documented device, and it was used in this study as a benchmark against the less known Chameleon.

3.4.4 Sensor clusters

As mentioned in section 3.3 a total of 5 sensors were placed within each column. The 5 sensors are divided in two different sensor cluster placed at two different heights: the

lower cluster comprised of 1 Chameleon Soil Water Sensor and 1 DS180B20 digital temperature probe is placed within the transition layer at a depth of 350 mm from the surface of the biofilter; the upper cluster, comprised of 1 Chameleon Soil Water Sensor, 1 DS180B20 digital temperature probe and 1 Truebner SMT 100 soil moisture and temperature probe, is positioned within the filter media at a depth of 150 mm from the surface (Fig. 14).

Fig. 14 – a) Lower sensor cluster comprised of 1 Chameleon Soil Water Sensor and 1 DS180B20 digital temperature probe, b) Upper sensor cluster comprised of 1 Chameleon Soil Water Sensor, 1 DS180B20 digital temperature probe and 1 Truebner SMT 100 soil moisture and temperature probe (Photo by Leigh Oliver)

3.5 Electronic system

Each column is equipped with its own independent data logging system, which collects readings from two sensor clusters positioned at the top and bottom of the column. The entire electrical system is connected and managed by a microcontroller BoSL board, a device very similar to an Arduino Uno but developed by Monash University. Each board is installed inside a waterproof plastic enclosure attached to the side of the column. Power to the entire system is supplied by a 3.7 V Lithium-Polymer battery.

3.5.1 BoSL Board VO.3

The entire electrical system is managed by the open source BoSL microcontroller board (Fig. 15). The BoSL board is developed by researchers at the Monash University that stands for "Bio-Oxidation Sensor and Logger Board" (https://www.bosl.com.au/wiki/BoSL_Board_v0.3). The board is designed to be a low-cost, easy-to-use platform for collecting and analysing data on water quality and quantity in real-time.

The board contains multiple sensors for measuring environmental parameters such as temperature, humidity, and gas concentrations, as well as a data logger for recording the sensor data over time. It also has built-in wireless communication capabilities, allowing for remote data transmission and real-time monitoring.

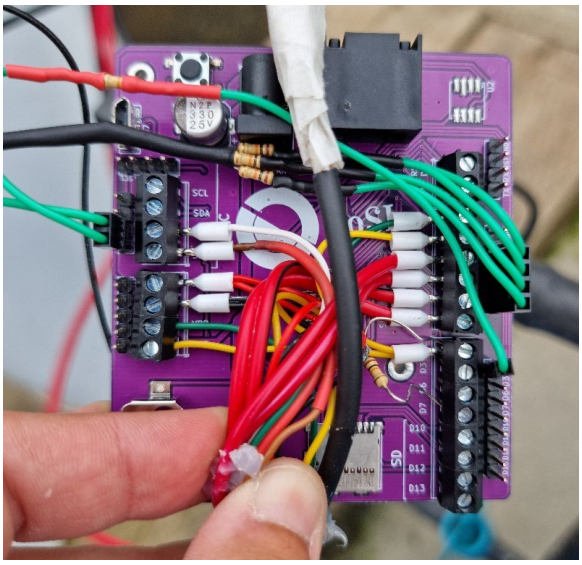

Fig. 15 - A configured and operational BoSL board

On the BOSL board the pins that can do analog-to-digital conversion are the ones with "A" in front of their label (A0 through A5) to indicate that these pins can read analog voltages, and it is to these that both Chameleon sensors and the Truebner SMT are connected to (Fig. 16).

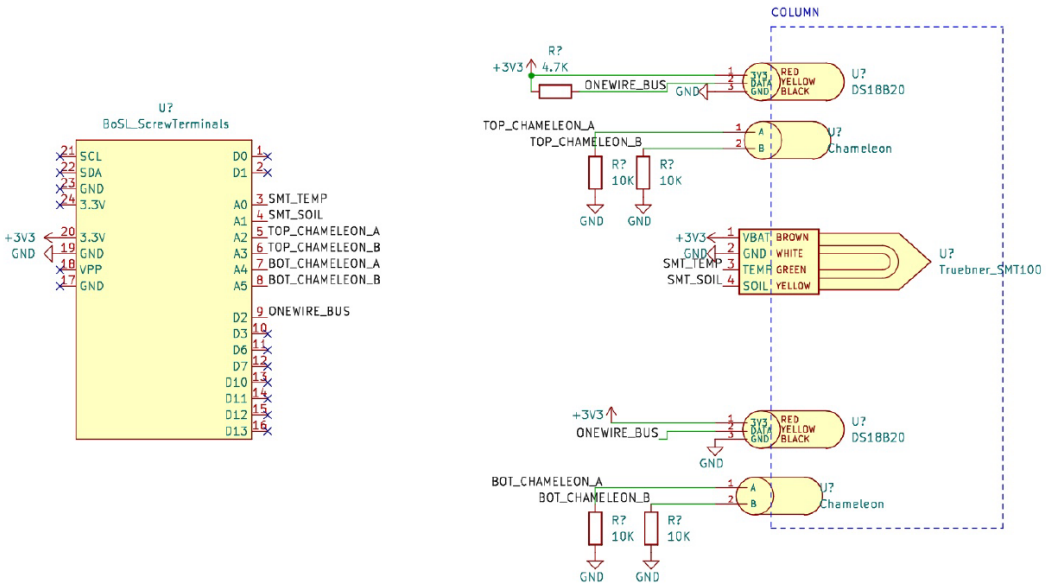

Fig. 16 - Diagram of the electrical system (designed by Leigh Oliver)

3.5.2 Data Logging

The data logging system is embedded in the firmware of each BoSL board, written in C++ within the Arduino IDE framework.
Each board sends data via the 3G cellular network using a SIM card installed directly on the board itself. Data collected by the sensors are transmitted to a web server on the internet, hosted by the Monash BoSL teams server, where a PHP script is used to store the data into two different types of files: json and csv (Fig. 17) (https://bosl.com.au/IoT/wsudwatch/FYP_SGI/?C=N;O=A).

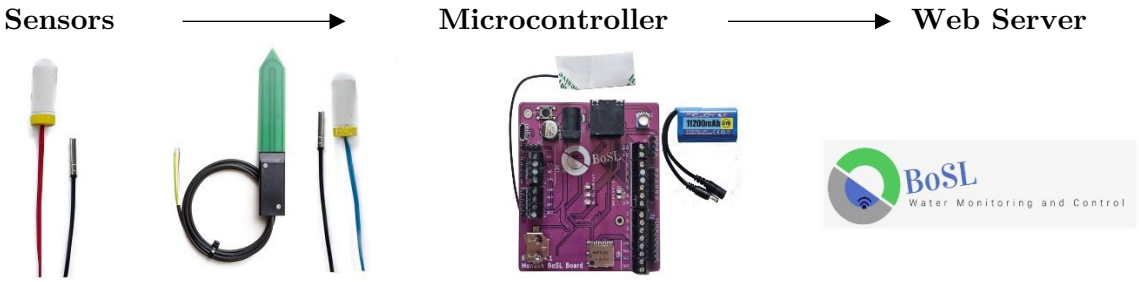

Fig. 17 - Data transfer connectivity flowchart

Data are transmitted at regular intervals pre-set in the card scrip. Given the needs of the study and given the short battery life due to the power required by the Truebner SMT 100 sensor, the interval was set equal to 15 minutes.

3.6 Data Conversion

The data sent by the sensors are raw data that require the use of specific equations to convert the units of measurement and obtain the soil water tension for the Chameleon sensor and the volumetric water content for the SMT 100 sensor. Below are all the steps adopted.

3.6.1 Chameleon conversion equations

The chameleon sensor measures electrical resistance to determine soil water tension by using a reference resistance of 10 KΩ, embedded within the electronic system, and alternating the voltage driven across the sensor with the BoSL board firmware. The resistance of both gold-plated electrodes (called channel A and channel B) can then be calculated by reading the analog pin, converting the reading to volts, and solving for the unknown resistance using the known resistance (10K Ω). To convert the analog voltage

signal on a pin into digital values an Analog-to-Digital Converter (ADC), integrated into the BOSL board, was used. The general equation that governs this process is the following:

$$\frac{\text{Resolution of the ADC}}{\text{System Voltage}} = \frac{\text{ADC}_{\text{reading}}}{\text{Analog Voltage Measured}} \quad (3.1)$$

The ADC on the BOSL board is a 10-bit ADC, meaning it can detect 1024 discrete analog levels ranging from 0 to 1023. This resolution determines the precision of a measurement. The higher the digitizer resolution, the more precise the measurement values (www.arduino.cc/reference/en/language/functions/analog-io/analogread/). In this case with a 10-bit ADC divides the vertical range of the input amplifier into 1024 discrete levels. With a vertical range of 1 V, the 10-bit ADC can ideally resolve voltage differences as small as 0.98 mV. Because the BoSL board used for this study has a 10-bit ADC of the BOSL with a 3.3V system, the previous equation became:

$$\frac{1023}{3.3\ \text{V}} = \frac{\text{ADC}_{\text{reading}}}{\text{Analog Voltage Measured}} \quad (3.2)$$

The ADC reading, representing the raw values provided by the board were then calculated with the following equation:

$$\text{ADC}_{\text{reading}} = \frac{1023 \cdot \text{Analog Voltage Measured}}{3.3\ \text{V}} \quad (3.3)$$

This equation was used to calculate the ADC reading for both the electrodes of the sensor. Subsequently, to obtain the resistance value for each sensor, the average of the values detected by the two electrodes (channel a and channel b) was calculated:

$$\text{ADC}_{avg} = \frac{(\text{ADC}_{\text{reading A}} + \text{ADC}_{\text{reading B}})}{2} \quad (3.4)$$

where:

- ADC_{Avg} is the average between the $\text{ADC}_{\text{reading}}$ of channels A and B;
- $\text{ADC}_{\text{reading A}}$ is the raw value read by the channel A
- $\text{ADC}_{\text{reading B}}$ is the raw value read by the channel B

The sensor raw average value was then converted into electrical resistance (ohm) using an electrical engineering formula given by the partition of voltage across the circuit, derived by the Ohm's law, to obtain the resistance:

$$R = 10\,000\ \Omega \cdot \frac{\text{ADC Avg}}{(1023 - \text{ADC Avg})} \quad (3.5)$$

The resistance is then converted to kilopascals using four different calibration equations, depending on the resistance value, that take into account both the soil temperature at the time of measurement and the calibration temperature (temp Calib) of 24°C:

$$\text{If } R < 550 \longrightarrow \text{SWT} = 0 \quad (3.6)$$

$$\text{If } R < 1000 \longrightarrow \text{SWT} = \text{abs}\left\{\left[\left(\frac{\text{Ohms Avg}}{1000}\right) 23.156 - 12.736\right] \cdot [(-)(1 + 0.018\ (\text{temp C} - \text{temp Calib}]\right\} \quad (3.7)$$

$$\text{If } R < 8000 \longrightarrow \text{SWT} = \text{abs}\left\{\frac{\left[-3.213\left(\frac{\text{Ohms Avg}}{1000}\right) - 4.093\right]}{\left[1 - 0.009733\left(\frac{\text{Ohms Avg}}{1000}\right)\right]} - 0.01205\ \text{temp C}\right\} \quad (3.8)$$

$$\text{If } R < 35000 \longrightarrow \text{SWT} = \text{abs}\left\{-2.246 - 5.236\left(\frac{\text{Ohms Avg}}{1000}\right) \cdot [1 + 0.018\ (\text{temp C} - \text{temp Calib})]\right\} - 0.06756\left(\frac{\text{Ohms Avg}}{1000}\right)^2 [1 + 0.018\ (\text{temp C} - \text{temp Calib})(1 + 0.018\ (\text{temp C} - \text{temp Calib})] \quad (3.9)$$

$$\text{If } R > 35000 \longrightarrow \text{Not considered}$$

Values exceeding 35000 are deemed non-significant and were consequently excluded from consideration. High values could result from various factors, including measurement errors or instability caused by fluctuations in electrical voltage.

Temperature correction is often necessary for gypsum-based sensors, such as the Chameleon sensor. Specifically, for the Chameleon sensor, this correction involves a 1.8 percent decrease in reported soil tension for each degree above 24 degrees Celsius (Stirzaker and CSIRO, 2014). However, the manufacturer provided an alternative calibration equation (see Fig. 18) that doesn't depend on temperature, which is deemed negligible for temperatures below 24°C.

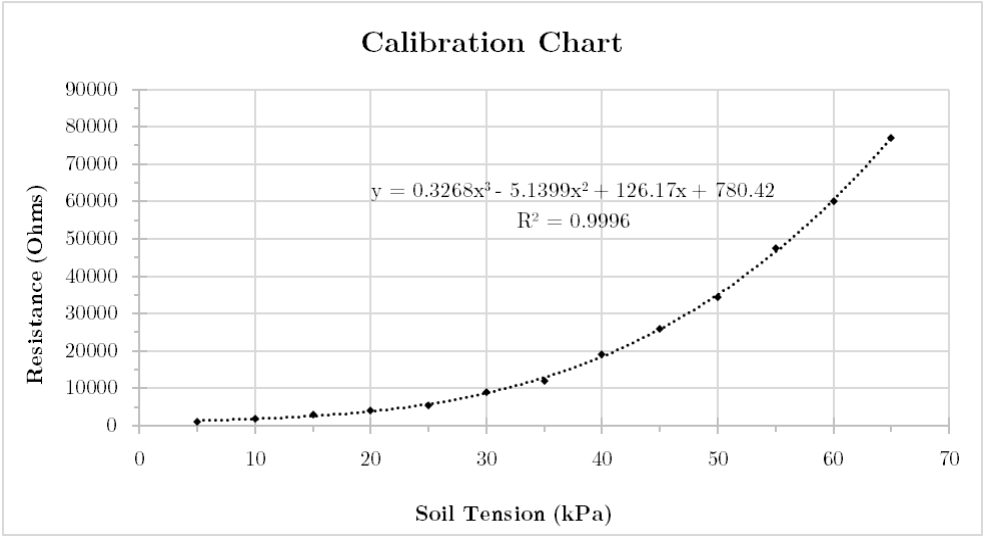

Fig. 18 – Chameleon Soil Water Sensor calibration chart

The reference soil water tension data are presented in Tab. 4 - Reference soil water tension values representative of soil moisture levels.

Tab. 4 - Reference soil water tension values representative of soil moisture levels.

Tension (kPa)	SOIL CONDITION
0-10	Saturated soil
10-30	Soil is wet (except coarse sands, which are beginning to lose water)
30-60	Usual range for irrigation (most soils)
60-100	Soil is becoming dangerously dry

3.6.2 SMT 100 Sensor conversion unit

Similarly to the Chameleon sensor, the value measured by the SMT 100 are provided in the form of raw data that require a conversion equation to obtain the Volumetric Water Content (VWC). Given the 10-bit resolution of the ADC and the board tension at 3.3 V, the following unit conversion was used to obtain VWC values in percentage:

$$\text{VWC}\,(\%) = \left(\frac{\text{VWC}_{raw}}{1023}\right) 3.3\,\text{V} \cdot 100 \qquad (3.10)$$

Where VWC_{raw} is the volumetric water content raw value measured by the SMT 100. Likewise, the conversion of raw temperature values has been done to Celsius degrees using the following formula:

$$\text{Temp}\,(°\text{C}) = \left[\left(\left(\frac{\text{Temp}_{raw}}{1023}\right) 3.3 \cdot 10\right) - 4.0\right] \cdot 10 \qquad (3.11)$$

where Temp_{raw} is the temperature raw value measured by the sensor.

3.6.3 Soil Water Characteristics Curve (SWC)

The relationship between Soil Water Tension (SWT) and Volumetric Water Content (VWC) is known as the Soil Water Characteristic Curve (SWC), or Soil Water Retention Curve, which is subject to variations contingent upon soil type and its specific attributes, including texture, structure, and organic matter content. Since this relationship is a highly nonlinear function is relatively difficult to obtain accurately (Warrick, 2001).

As briefly outlined in section 3.4, Soil Water Tension (SWT) is typically measured in kilopascals (kPa) or Centibar. It represents the energy required to draw water from the soil, reflecting the soil particles' ability to retain water. Put simply, kPa gauges the soil's grip on water: higher values suggest drier soil, as it demands more force to extract water from soil particles.

On the other hand, Volume Water Content (VWC), also known as Soil Moisture Content, represents the ratio of water volume to the total soil volume, typically expressed as a percentage. It can range from 0 (for soil extremely dry) to the value of the porosity at full saturation (Shuckla, 2013).

The relationship between SWT and VWC in a soil is generally inverse, as the kilopascal value increases (indicating drier soil), the volume water content decreases. The soil water characteristic (SWC) can be derived by plotting the soil water tension (representing the absolute value of the soil matric potential) on the Y-axis against the volumetric soil water content on the X-axis, or vice versa. Panayiotopoulos and Mullins (1985) examined various types of sand, from which they established distinct SWC curves based on the particle size of the soil (refer to Fig. 19).

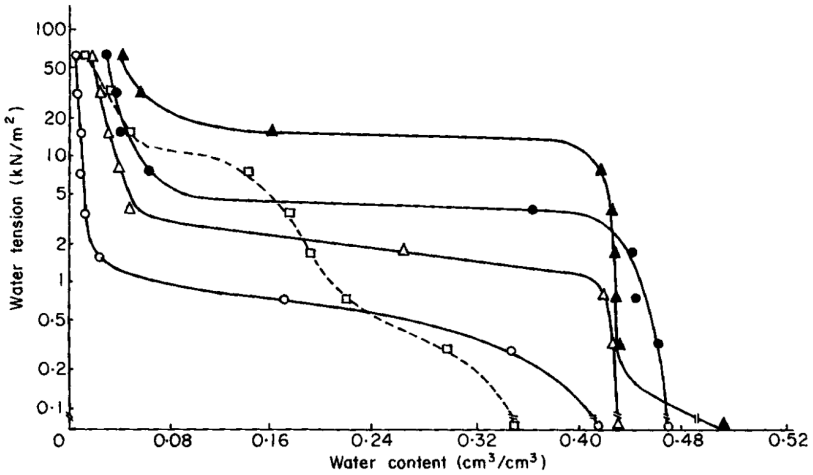

Fig. 19 – Soil Water Characteristics Curve recorded for coarse sand (circle), medium sand (triangle), fine sand (filled circle), very fine sand (filled triangle) and optimum mixture (square) (Panayiotopoulos and Mullins, 1985)

Considering this, the relationship between measurements taken by the Chameleon and SMT sensors was derived by plotting the values of SWT against the values of VWT. The resulting outcome is the specific SWC for each column group, as will be illustrated in the following paragraphs.

3.7 Design of dosing events

Different dosing events were designed to simulate recurring rain events in the urban area of Melbourne. The selection of meteorological events was conducted based on rainfall data collected over the past 17 years (2007-2024) recorded by the Melbourne Burnley station (https://www.melbournewater.com.au/water-and-environment/water-management/rainfall-and-river-levels#/).

According to Green et al. (2015), the design of Water Sensitive Urban Design (WSUD) features such as raingardens is carried out using design meteorological events characterized by probabilities greater than 4 Exceedances per Year (EY). Based on this guidance, two meteorological events were identified, one small size and one medium size, each with a recurrence frequency of greater than or equal to 4 EY. Another key parameter is represented by the Antecedent Dry Days (ADD), which represent the period between two events with no rain.

As already highlighted by other studies (Hatt et al., 2009; McCarthy et al., 2013; Ebrahimian et al., 2019), the number of Antecedent Dry Days (ADD) has an effect on the performance of raingardens in terms of both water quantity and quality. A prolonged dry period preceding rainfall events can lead to a depletion of soil moisture below safe levels for plant health. Conversely, a very short antecedent dry period can prevent the raingarden soil layers from effectively disposing water, reducing the storage capacity for consecutive events.

For the simulation phase, the selection of the number of antecedent dry days was determined by the frequency of such occurrences over the two decades considered (Fig. 20).

In Melbourne climate, a notable recurrence of a one-day antecedent dry period was identified in all seasons except for summer. Conversely, the 7-day dry period is more characteristic of the autumn and spring climates, while an antecedent dry period exceeding seven days is typical during the summer months, marked by less frequent but more intense events.

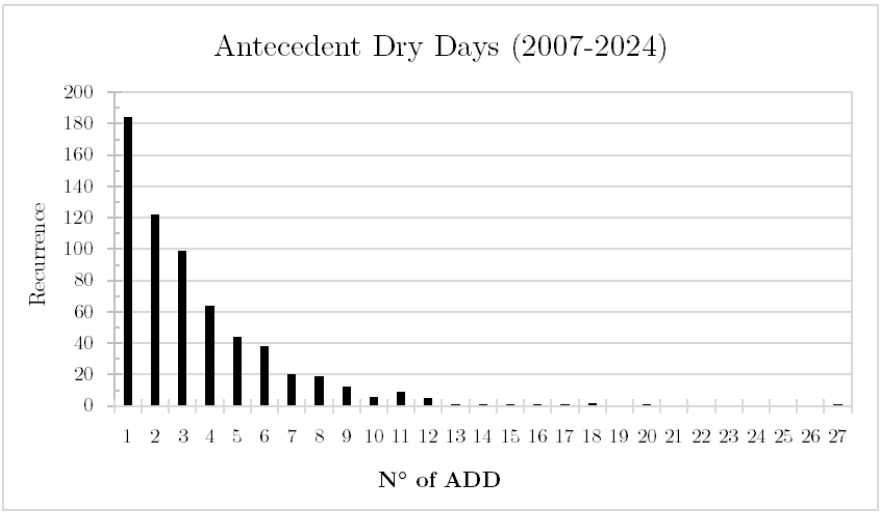

Fig. 20 – Number of antecedent dry days and their recurrence over a 10-years period (2007-2024) based on rainfall data provided by the Bureau of Meteorology Australian Government.

The simulations of the events took place in two different phases. In the first simulation phase 4 designed rainfall events were simulated selected among the historical rainfall events that occurred in the decade from 2007 to 2016 (Tab. 5). The simulated events are characterized by two different event sizes and different number of ADD:

- Small size (S), with around 4.42 mm per event (corresponding to 11.05 L of dosing volume considering a contribution area of 2.5 m^2);
- Medium size (M,) with around 8.84 mm per event (corresponding of 22.1 L of dosing volume considering a contribution area of 2.5 m^2).
- Both the events are characterised by a recurrence of 1 in 1 month ARI.

The four events also have two different length of antecedent dry weather period:

- Short dry (S), with 1 antecedent dry day (24 hours between two dosing processes);
- Medium dry (M) with 7 antecedent dry days.
-

Tab. 5 - First phase of simulation. Characteristics of each dosing event including dosing volume, size, antecedent dry length. "S", "M" respectively stands for "small/short" and "medium".

Event No.	**1**	**2**	**3**	**4**
Dosing volume (L)	11.0	22.1	11.0	22.1
Size type	S	M	S	M
Antecedent dry drays (-)	1	1	7	7
Dry type	S	S	M	M

As for the second simulation phase 8 different rainfall event were simulated selected among the historical rainfall events that occurred in the decade from 2014 to 2024 (Tab. 6). These events are characterized by different sizes and antecedent weather conditions:

- Small size (S), with around 3.12 mm per event (corresponding to 7.8 L of dosing volume considering a contribution area of 2.5 m^2);
- Medium size (M,) with around 7.36 mm per event (corresponding to 18.4 L of dosing volume considering a contribution area of 2.5 m^2).

The four events also have three different number of ADD:

- Short dry (S), with 1 day < ADD < 3 days;
- Medium dry (M) with 7 ADD.

Tab. 6 - Second phase of simulation. Characteristics of each dosing event including dosing volume, size, antecedent dry length. “S”, “M”, “L” respectively stands for “small/short” and “medium”, “long”**.**

Event No.	**1**	**2**	**3**	**4**	**5**	**6**	**7**	**8**
Dosing volume (L)	7.8	18.4	7.8	18.4	7.8	18.4	7.8	18.4
Size type	S	M	S	M	S	M	S	M
Antecedent dry drays (-)	1	1	1	1	3	3	7	7
Dry type	S	S	S	S	S	S	M	M

3.8 Result and discussion

All the sensors transmitted data consistently, with some short periods of downtime due to many setbacks such as battery replacement, connectivity lag, server breakdowns or BoSL board blockages over the two testing periods. To "fill in" the gaps left by the sensor down times, a linear interpolation function of the data was used.

Out of the 15 constructed columns, column S4 displayed bizarre sensor values as well as continuous water leaks. Consequently, it was decided to exclude the column from the dataset. In the following sections, plots of the temperature, soil water tension and volume water content values are displayed during the two-simulation periods. All sensors showed good responsiveness and clearly highlighted the differences between the three designed treatments. However, the Chameleon sensors experienced a progressive loss of functionality over time, especially in the columns of group P (preferential flow path), likely due to excessive drying that compromised their functionality or due to damages induced during the manual drilling process of soil layers for the creation of flow paths. The values measured by these sensors were not considered in the second phase of the

study. The battery charge proved insufficient to ensure continuity in monitoring, necessitating constant replacement every 5-6 days. This may have affected the data quality, particularly on the Chameleon sensor, which was found to be extremely sensitive to voltage variations.

3.8.1 First phase simulations

The DS18B20 sensors exhibited temperature gradients between the top and bottom of each column (see Fig. 21). These data were utilized to calibrate the Chameleon readings during the conversion phase from Ohms to kilopascals.

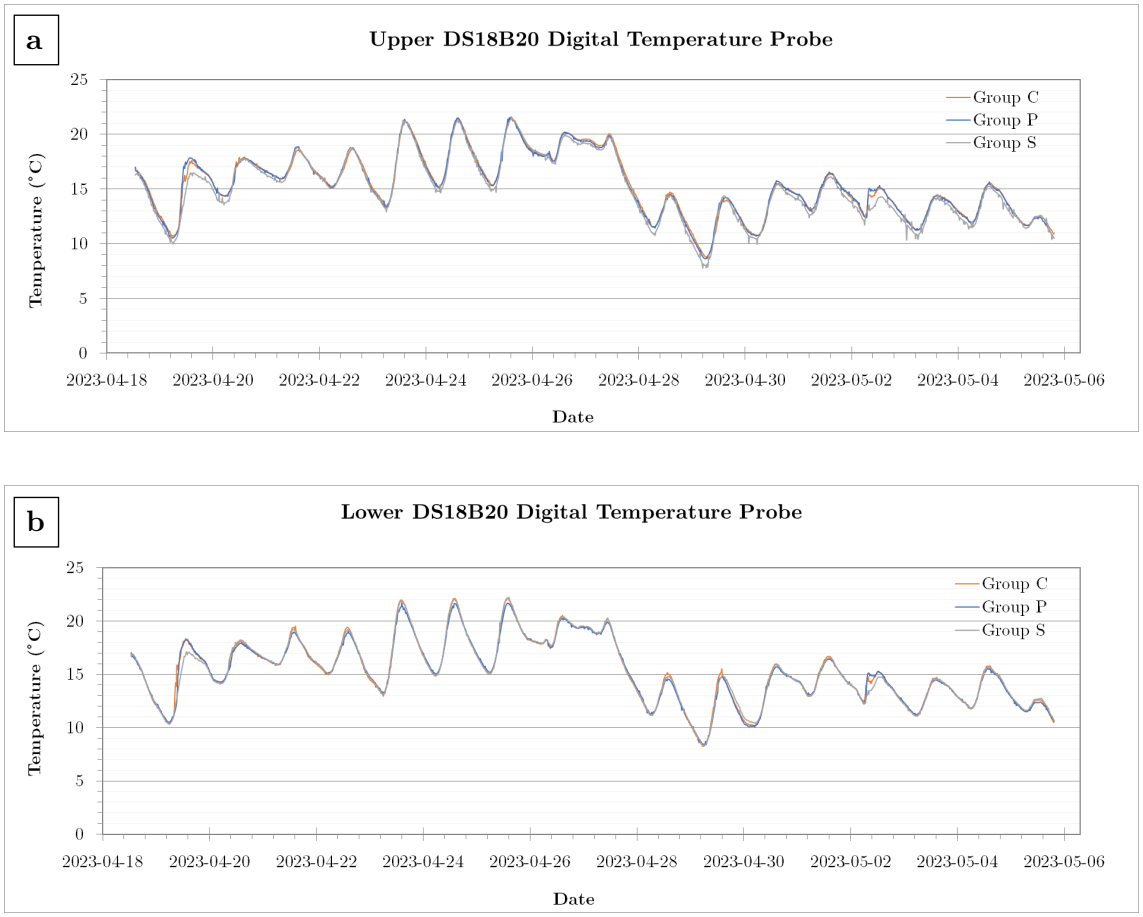

Fig. 21 - a) Upper and b) Lower DS18B20 temperature readings, from the three group of columns

The data presented in Fig. 22 highlight clear differences in the three biofilter performances. Data provided by the Chameleon Soil water sensor placed in the upper sensor cluster clearly displays soil water tension variation, with distinct negative spikes corresponding to simulated meteorological events.

The jumps observed in the measurements are caused by instabilities in the electrical circuit of the board, as well as other unidentified factors.

On the contrary, the data from the Chameleon soil water sensor in the lower cluster did not show significant soil water tension variations during the simulation period. The recorded variations were on the order of a few kilopascals. It is believed that this is due to a design error, specifically that the sensors were positioned at a level too close to the saturated zone. It is thought that through capillarity, the soil surrounding the sensor remained consistently at high saturation levels, resulting in no variations being recorded in terms of soil water tension.

Fig. 22 – a) Upper Chameleon values b) Lower Chameleon values from first phase simulations

Volumetric water content (VWC) measured by the SMT 100 sensor as a percentage is shown in Fig. 23. The dosing events can be clearly observed through the peaks in the VWC data. The effects of different ADDs are mainly noticeable in the variations of VWC over time, which are naturally greater for larger ADDs.

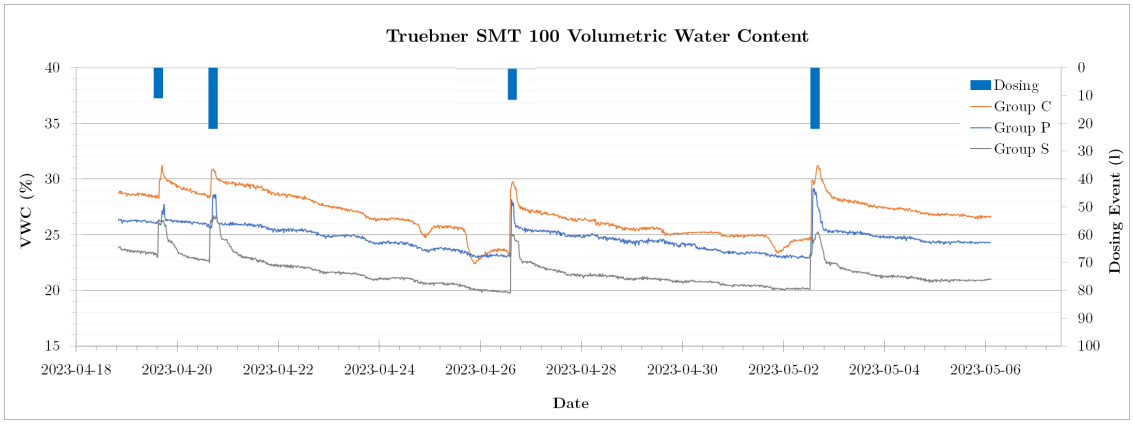

Fig. 23 – Truebner SMT 100 measured values in the first simulation phase

Fig. 24 shows the SWC obtained from the correlation between volumetric water content (VWC) and soil water tension (SWT) for each treatment group.

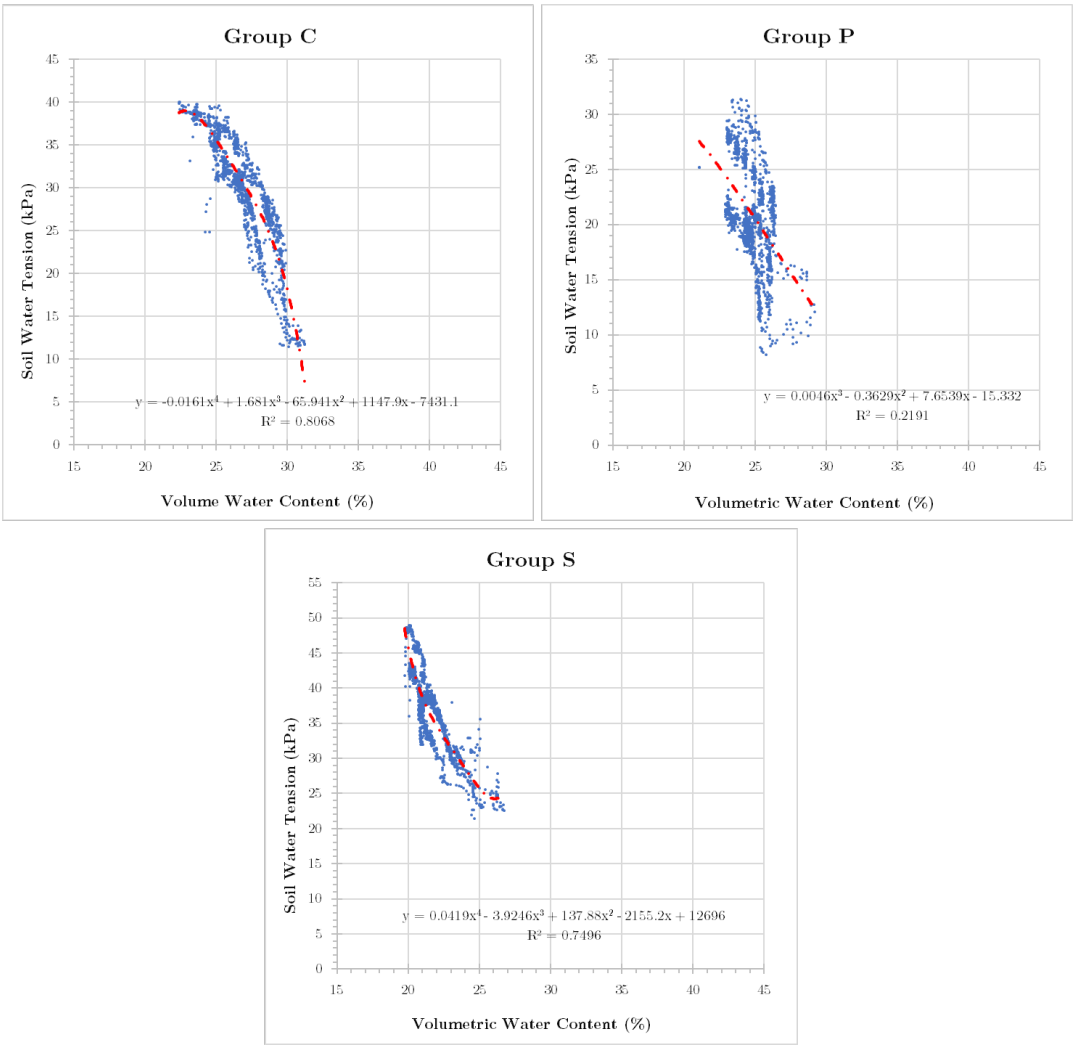

Fig. 24 – Soil water characteristic curve of the three treatments group (Group C, P and S)

The data measured by the two Chameleon and SMT 100 sensors closely replicate the trend of the soil water retention curve for sand. Some outlying values, particularly in group P, distort the SWC curve described by the third-degree polynomial. Removing these values would result in a curve more consistent with the curve reported in the literature (refer to Fig. 20).
Moreover, the graphs clearly illustrate the phenomenon of hysteresis in soil-water dynamics. During wetting and drying cycles, the relationship between soil water content and soil water tension exhibits noticeable differences: the water content in the drying curve is higher for a given soil tension (matric potential) than that in the wetting branch. This hysteresis effect is indicative of variations in soil structure, pore size distribution, and surface properties during different moisture conditions (Warrick, 2001). This confirms the validity of the sensors in measuring fluctuations in soil water tension (SWT) and volumetric water content (VWC).

3.8.2 Second phase simulations

The second phase of simulations occurred approximately 9 months after the first one. Throughout this period, the columns received consistent irrigation through an automated system, promoting plant growth and the expansion of root systems within each column. Consequently, changes were observed in soil water tension, accompanied by a reduction in infiltration rates across all columns compared to the first phase. It is hypothesized that this may be attribute to the growth of the dense root system of Carex appressa, which could have obstructed the pores of the filter media. While this hypothesis has not been validated yet by practical tests, similar results have been obtained in previous studies (Le Coustumer et al., 2012; Virahsawmy et al., 2014).
Additionally, as previously mentioned, Chameleon sensors experienced a significant decline in their operational capabilities. This deterioration rendered the data collected from these sensors unreliable and unsuitable for subsequent analyses. In Fig. 25, the volumetric water content values measured by the SMT 100 sensors during the second phase of simulations are presented.
In the second simulation phase as well, significant differences are evident among the three column treatments. However, during the initial three events, the distinctions between Group P and Group S values are less prominent, showing a noticeable degree of overlap.

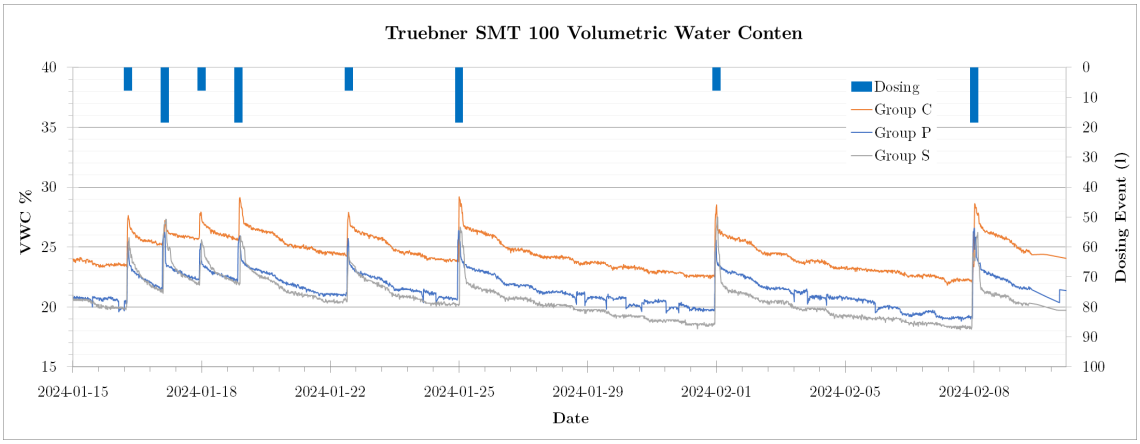

Fig. 25 - Truebner SMT 100 measured values in the second simulation phase

3.8.3 Data analysis

The data measured in the first and second simulation phase confirm a clear differentiation between the normal functioning of the raingarden (group C) and the two designed degraded states. Although in the first phase there was also a noticeable differentiation between group P and group S, in the second simulation phase, this difference narrowed, making it more difficult to identify descriptive indices of the raingarden behaviours.

During the first simulation phase, data were collected regarding the inflow, corresponding to the volumes of water used to simulate the 4 events, and the outflow, that is the total volume discharged from the column following the simulation. The measurement of this volume was taken at the end of the outflow dripping from the column, occurred approximately 2 hours after dosing for columns C, 1 hour and 30 minutes for columns P, and 3 hours and 30 minutes for columns S. Measured data are reported in Tab. 7.

The measurement of outflow volumes has revealed that the S columns, those with surface clogging, retain larger volumes of water compared to the other two groups, C and P, regardless of the number of antecedent dry days and the incoming volume. This can be justified by the lower volume water content present in group S. This also suggests that the sediments used to simulate the surface clogging effect contribute to retaining some of the water, resulting not only in reduced infiltration rates but also in greater evaporation loss during dry periods.

As can be seen from the data reported in Tab. 7, group S is characterized by losses, in terms of the difference between inflow and outflow, of percentages exceeding 10% for a medium event with 1 ADD, up to exceeding 35% for a small event with 7 ADD.

In contrast to group S, groups C and P showed lower losses, with percentages ranging from 1 to 7.6%. The columns of group P retained the lowest percentages of water. This

is attributed to the presence of preferential pathways that cause water to flow quickly through the soil layers, preventing its absorption.

Tab. 7 – Total volumes and losses for the first phase during the four simulated storm events.

	Simulation Event	Inflow (l)	Outflow (l)	Loss (l)	Loss (%)	ADD (days)
Group C	1	11.0	10.6	0.4	3.4%	1
	2	22.1	21.8	0.3	1.4%	1
	3	11.0	10.2	0.8	7.6%	7
	4	22.1	21.3	0.8	3.5%	7
Group P	1	11.0	10.7	0.3	2.5%	1
	2	22.1	21.8	0.3	1.1%	1
	3	11.0	10.4	0.6	5.7%	7
	4	22.1	21.5	0.6	2.9%	7
Group S	1	11.0	8.9	2.1	19.0%	1
	2	22.1	19.5	2.6	11.8%	1
	3	11.0	7.1	3.9	35.5%	7
	4	22.1	17.4	4.6	20.8%	7

The measurement of losses can therefore provide a preliminary indication of the functioning of the raingarden; in particular, high percentage values indicate potential surface clogging issues. However, this parameter alone is not sufficient to characterize raingarden operations. Therefore, the trends of the values were analysed throughout the simulations to identify characteristic indices for each group column operation.

The variables considered for identifying these indices are reported in Fig. 26 and include:

- Peak amplitude, in hours (ΔPk);
- Variation of VWC between two events (ΔVWC_{ADD});
- Variation of initial VWC from dosing until reaching the peak (ΔVWC_i);
- Variation in final VWC, namely from the peak to the point where the variation no longer follows a linear trend and subsequently undergoes a change in curve shape (ΔVWC_f);
- Average of water content volume values in the hour preceding column dosing ($VWC_{1h,Avg}$);
- Number of Antecedent Dry Days (ADDs).

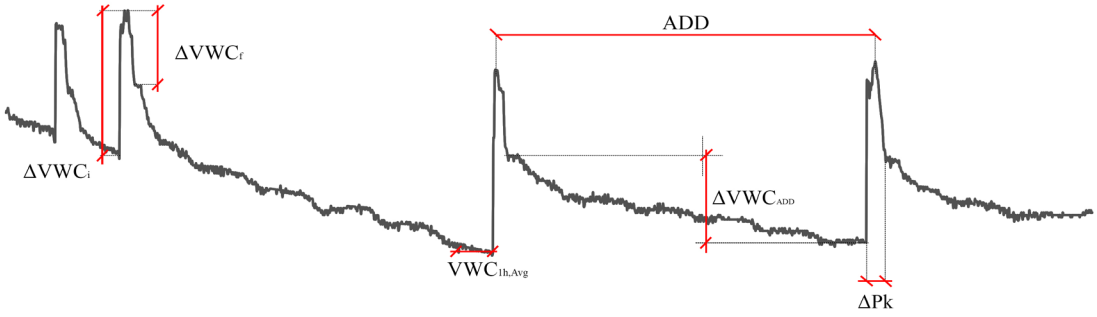

Fig. 26 - Variables considered for identifying characterization indices of the raingarden behaviour.

Regarding the Peak amplitude value, in both simulation phases, it was noted that the peak amplitudes are shorter for the P group columns, as shown in Tab. 8 and Tab. 9, indicating a more rapid variation of VWC caused by the presence of preferential flow paths. The peak width was taken from the moment dosing began, to the point, after the peak, where the decrease in VWC stops having a linear trend and the curve changes its course. The peak amplitude was calculated using the following formula:

$$\Delta \mathrm{Pk} = T_i - T_e \qquad (3.12)$$

where T_i corresponds to the dosage start time and T_e is the instant when the decrease in VWC changes trend.

Tab. 8 - Peak amplitude (ΔPk) for each columns group and for all the simulated events in the first testing phase.

First simulation phase - Peak amplitude ΔPk (h)

Group	Simulated rainfall events			
	1	**2**	**3**	**4**
C	5.00	3.75	5.25	11.25
P	2.25	2.50	2.00	4.75
S	6.25	5.75	6.00	9.00

Tab. 9 – Peak amplitude (ΔPk) for each columns group and for all the simulated event in the second testing phase.

Second simulation phase - Peak amplitude ΔPk (h)

Group	Simulated rainfall events							
	1	**2**	**3**	**4**	**5**	**6**	**7**	**8**
C	2.58	6.50	4.75	5.33	4.08	4.25	3.30	7.50
P	1.92	2.83	2.00	2.58	1.92	2.92	2.08	2.66
S	4.50	7.25	4.17	3.92	4.42	4.83	5.17	8.00

As illustrated in Fig. 27 the peak amplitude values for the P columns oscillate around 2 hours, while they are more variable for the other two groups of columns (C and S).

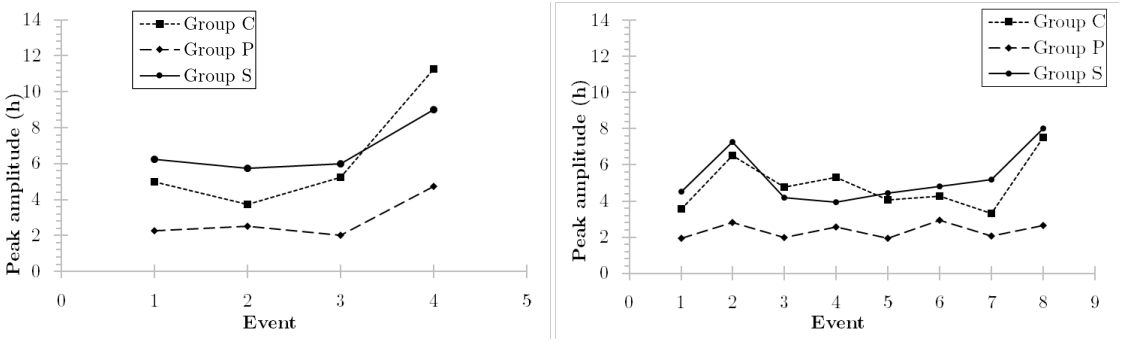

Fig. 27 – Peak amplitude ΔPk (h) of each columns group (C, P and S) for all the simulated events (first and second simulation phases)

Regarding the variation in VWC during dosing time, an index of variation, I_{VWC}, ranging from 0 to 1, was calculated using the following formula:

$$I_{VWC} = \frac{\Delta VWC_f}{\Delta VWC_i} \quad (3.13)$$

It represents the quotient of the variation in volumetric water content after dosing (ΔVWC_f) divided by the variation in volumetric water content at the dosing instant (ΔVWC_i).

During the first simulation phase, the index consistently resulted higher for the columns in group P as shown in Tab. 10. It was observed that columns with preferential flow paths tend to return to VWC values prior to dosing, resulting in an I_{VWC} index greater than 0.5. The columns in groups C and S, showed a smaller difference between ΔVWCi and ΔVWCf, resulting in lower values of the index I_{VWC}.

In the second simulation phase, an opposite behaviour was observed in the columns of group S.

Specifically, as the number of ADDs increased, the columns of group S exhibited larger variations in VWC_i at the time of water dosing, as well as a greater tendency to return to lower VWC levels compared to the other two groups of columns as shown by the value reported in Tab. 11 for the last three simulated events.

Tab. 10 – Ratio between ΔVWC_f and ΔVWC_i for each columns group and for all the simulated events in the first testing phase.

First simulation phase – VWC variation index I_{VWC} (-)				
Group	Simulated rainfall events			
	1	**2**	**3**	**4**
C	0.524	0.418	0.368	0.311
P	0.789	0.857	0.544	0.636
S	0.585	0.456	0.467	0.473

Tab. 11 - Ratio between ΔVWC_f and ΔVWC_i for each columns group and for all the simulated events in the second testing phase.

Second simulation phase - VWC variation index I_{VWC} (-)								
Group	Simulated rainfall events							
	1	**2**	**3**	**4**	**5**	**6**	**7**	**8**
C	0.252	0.535	0.561	0.614	0.341	0.461	0.348	0.372
P	0.453	0.593	0.599	0.630	0.536	0.489	0.395	0.324
S	0.379	0.503	0.432	0.500	0.221	0.706	0.631	0.587

Fig. 28 shows the trend of the I_{VWC} index at the time of dosing. In the first phase of the simulation, the behaviours of the three groups of columns were more differentiated, with lower values for the columns in group C, which were not much different from the values of the S columns.

Higher values, tending towards 1, were observed for the columns in group P. However, this trend is completely altered in the second phase of the simulation.

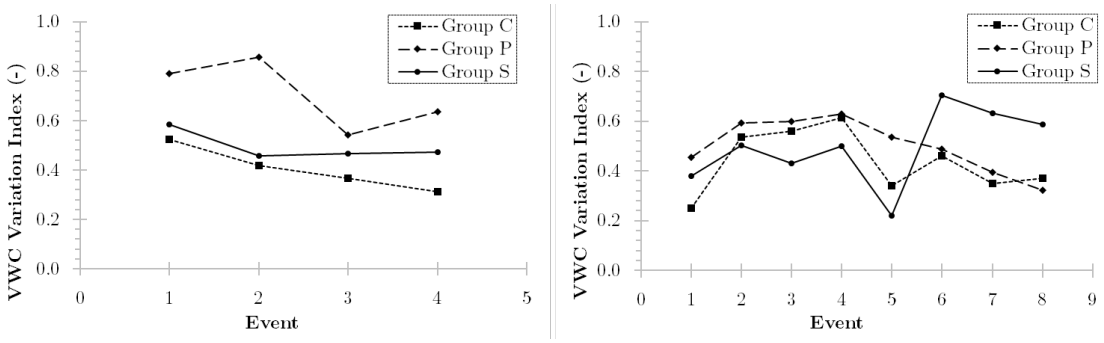

Fig. 28 – I_{VWC} index values (-) of each columns group (C, P and S) for all the simulated events (first and second simulation phases)

Another index that was evaluated is the hourly variation of volumetric water content ΔVWC_D during the dry period. The hourly percentage variation was calculated by dividing the total variation of the volumetric water content observed during each dry period (ΔVWC_{ADD}) by the number of hours between two dosages as follows.

$$\Delta VWC_D = \frac{\Delta VWC_{ADD}}{ADD} \quad (3.14)$$

During the first phase of simulation, the P group columns showed smaller variations in VWC during the dry period as shown by the values reported in Tab. 12. This behaviour was not observed in the second phase of simulations, where the C group, representing normal operation, exhibited smaller variations than the P group (see Tab. 13). The columns of the S group show in general greater VWC variations for short ADD.
For longer ADD, the S group values also approach those of the other two groups.
For longer dry periods (7 days), the three groups of columns showed similar water content variations. This is more evident from the graphs in Fig. 29, where it is observed that the curves, in both the first and the second phase, converge towards the same value.

Tab. 12 – VWC variation over the ADD for each columns group and for all the simulated events in the first testing phase.

First simulation phase – Hourly VWC variation (ΔVWC_D)

Group	Simulated rainfall events			
	1	**2**	**3**	**4**
C	4.76%	5.66%	3.78%	1.70%
P	1.31%	1.21%	1.79%	1.17%
S	6.26%	6.87%	2.89%	1.50%

Tab. 13 - VWC variation over the ADD for each columns group and for all the simulated events in the second testing phase.

Second simulation phase - Hourly VWC variation (ΔVWC_D)

Group	Simulated rainfall events							
	1	**2**	**3**	**4**	**5**	**6**	**7**	**8**
C	2.11%	3.07%	1.15%	5.21%	3.70%	3.99%	2.49%	2.21%
P	0.15%	6.72%	2.33%	5.51%	3.52%	4.15%	2.27%	2.72%
S	1.77%	8.81%	6.45%	8.53%	5.80%	4.80%	2.28%	2.00%

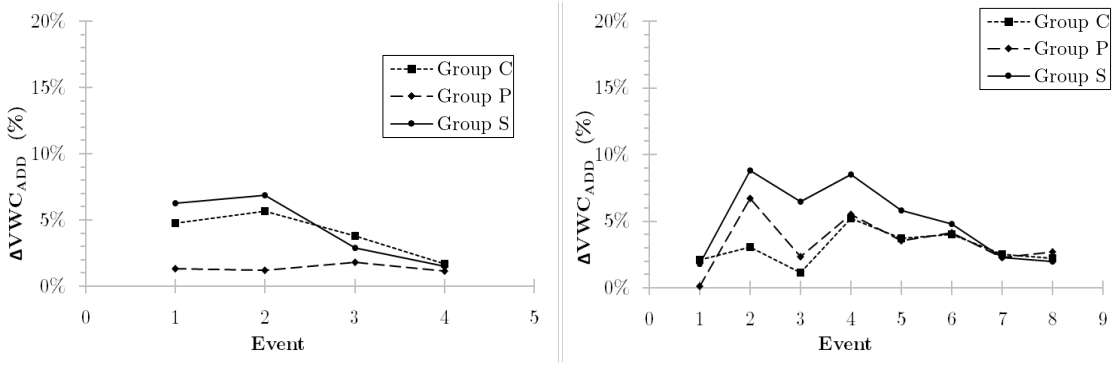

Fig. 29 - Hourly VWC variation (ΔVWC_D) of each columns group (C, P and S) for all the simulated events (first and second simulation phases)

An additional index that was analysed is the ratio between the peak amplitude and the number of antecedent dry days in hours. The index in question, which was named as "Peak Amplitude Index" (I_{pk}), is calculated using the following formula:

$$I_{pk} = 1 - \frac{\Delta Pk}{ADD} \quad (3.15)$$

Where ΔPk represents the peak amplitude in hours and ADD denotes the antecedent dry periods also in hours. The index value can vary from 0 to 1.

The results from both the first and the second simulation phases reveal that for the columns belonging to group P, the index tends to be closer to 1, as indicated in Tab. 14 and Tab. 15. Conversely, the columns categorized under group S exhibit lower index values initially, with a reversal of behaviour as the number of antecedent dry days increases. As the duration without rainfall extends, the indices for the S group columns begin to rise, eventually surpassing those calculated for the C group columns (Fig. 30).

Tab. 14 – Peak amplitude index equal to 1 – the ratio between the peak amplitude (**ΔPk**) and the number of antecedent dry days for each columns group and for all the simulated events in the first testing phase.

First simulation phase - Peak apmplidute index I_{pk} (-)

Group	Simulated rainfall events			
	1	**2**	**3**	**4**
C	0.792	0.844	0.969	0.933
P	0.906	0.896	0.988	0.972
S	0.740	0.760	0.964	0.946

Tab. 15 - Peak amplitude index equal to 1 – the ratio between the peak amplitude (ΔPk) and the number of antecedent dry days for each columns group and for all the simulated events in the second testing phase.

Second simulation phase - Peak amplitude index I_{pk} (-)

Group	Simulated rainfall events							
	1	**2**	**3**	**4**	**5**	**6**	**7**	**8**
C	0.893	0.729	0.802	0.778	0.943	0.941	0.980	0.955
P	0.920	0.882	0.917	0.893	0.973	0.959	0.988	0.984
S	0.813	0.698	0.826	0.837	0.939	0.933	0.969	0.952

The difference is more pronounced for shorter antecedent dry periods.

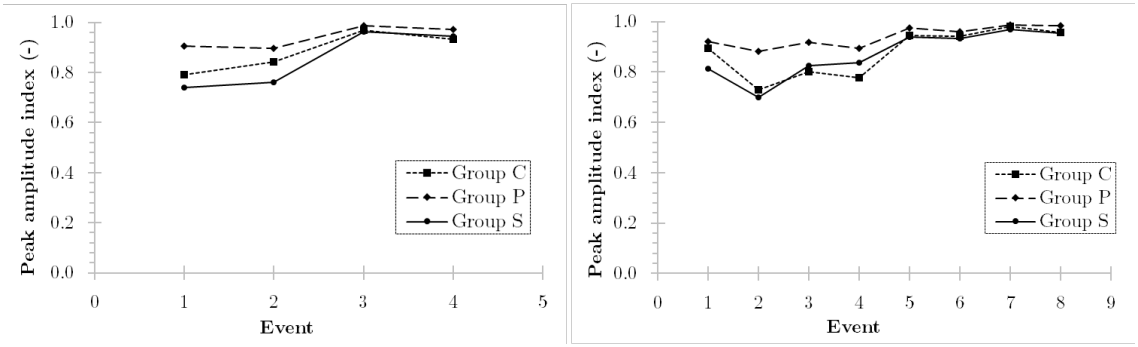

Fig. 30 - Peak amplitude index I_{pk} equal to 1 – the ratio between the peak amplitude (**ΔPk**) and the antecedent dry period in hours for each columns group (C, P and S) for all the simulated events (first and second simulation phases)

The last index calculated to characterize the raingarden performance is ΔVWC_{Pk} which is calculated as the ratio between the average of the Volumetric Water Content values 1 hour prior to dosing ($VWC_{1h,Avg}$) and the peak VWC value reached (Pk).

$$\Delta VWC_{Pk} = \frac{VWC_{1h,Avg}}{Pk} \qquad (3.16)$$

This index did not reveal substantial differences among the three groups. The only notable observations are that for the columns of group S, this ratio is generally lower compared to the other two groups, indicating greater VWC variations during the dosing phase in the S columns compared to the others (see Tab. 16 and Tab. 17).
Between the first and second simulation phases, no significant differences emerged; the behaviour of the columns remained consistent across both simulation phases.

However, a greater disparity between the behaviour of the C and P columns was observed in the second simulation phase. In this case, the C columns exhibited higher ratios between the average values 1 hour prior to dosing and the peak values, indicating smaller VWC variations during the dosing phase (Fig. 31).

Tab. 16 – Ratio between the VWC average values of one hour preceding the peak, $VWC_{1h,Avg}$, and the peak value for each columns group and for all the simulated events in the first testing phase.

First simulation phase - ΔVWC_{Pk} (-)

Group	Simulated rainfall events			
	1	**2**	**3**	**4**
C	0.91	0.92	0.79	0.82
P	0.94	0.90	0.80	0.77
S	0.88	0.86	0.79	0.81

Tab. 17 - Ratio between the VWC average values of one hour preceding the peak, $VWC_{1h,Avg}$, and the peak value for each columns group and for all the simulated events in the in the second testing phase.

Second simulation phase - ΔVWC_{Pk} (-)

Group	Simulated rainfall events							
	1	**2**	**3**	**4**	**5**	**6**	**7**	**8**
C	0.83	0.91	0.90	0.87	0.84	0.82	0.79	0.79
P	0.79	0.86	0.89	0.85	0.81	0.77	0.77	0.73
S	0.74	0.82	0.88	0.85	0.83	0.76	0.69	0.71

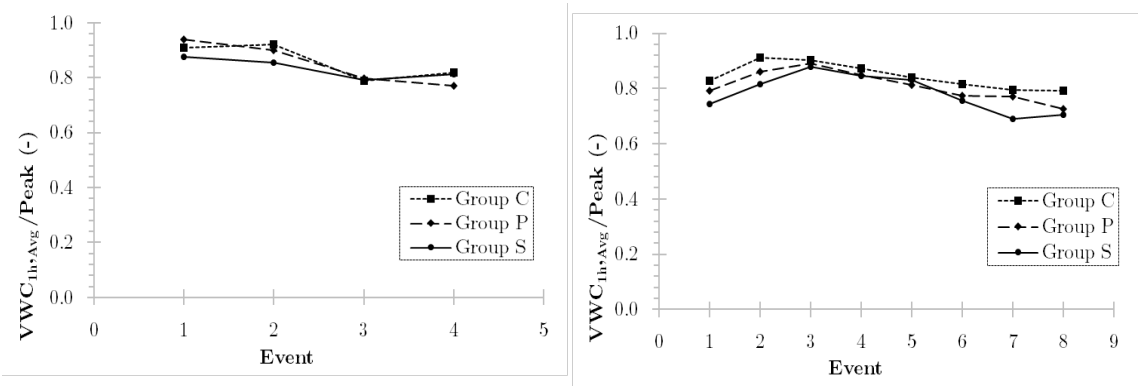

Fig. 31 - Ratio between the VWC average values of one hour preceding the peak, $VWC_{1h,Avg}$, and the peak value of each columns group (C, P and S) for all the simulated events (first and second simulation phases)

The overall results obtained do not allow for a clear classification of the columns functionality. The assessments provided offer general guidelines for detecting and quantifying potential malfunctions in raingardens equipped with real-time monitoring systems. Measuring outflow volumes and calculating the above-mentioned indices can help identify malfunctions, but further analysis is required to differentiate the behaviours of raingardens more distinctly with preferential flow paths and surface clogging.
Additionally, as the number of dry days between events increases, dynamics such as excessive soil drying occur, leading to the formation of macropores in all three groups indistinctly, which narrows the differences in functionality among the three different operations, making characterization more challenging.

3.9 References

Angelstam, P., Pedersen, S., Manton, M., Garrido, P., Naumov, V., & Elbakidze, M. (2017). Green infrastructure maintenance is more than land cover: Large herbivores limit recruitment of key-stone tree species in Sweden. *Landscape and Urban Planning, 167*, 368-377. ISSN 0169-2046. doi.org/10.1016/j.landurbplan.2017.07.019

Arduino (Open-source hardware and software prototyping platform). https://www.arduino.cc/reference/en/language/functions/analog-io/analogread/ (Visited on 11/02/2023)

Asleson, B.C., Nestingen, R.S., Gulliver, J.S., Hozalski, R.M., & Nieber, J.L. (2009). Performance assessment of rain gardens. *JAWRA Journal of the American Water Resources Association, 45 (4)*, 1019–1031. doi.org/10.1111/j.1752-1688.2009.00344.x

Bartos, M., Wong, B., & Kerkez, B. (2018). Open storm: A complete framework for sensing and control of urban watersheds. *Environmental Science: Water Research & Technology, 4 (3)*, 346–358. doi.org/10.1039/C7EW00374A

Benedict, M.A., & McMahon, E.T. (2002). Green infrastructure: smart conservation for the 21st century. *Renewable Resources Journal, 20 (3),* 12–17.

Blecken, G.T., Hunt III, W.F., Al-Rubaei, A.M., Viklander, M., & Lord, W.G. (2015). Stormwater control measure (SCM) maintenance considerations to ensure designed functionality. *Urban Water J., 14 (3),* 278–290. doi.org/10.1080/1573062X.2015.1111913

BOSL Board v0.3 - https://www.bosl.com.au/wiki/BoSL_Board_v0.3 (Visited on 11/02/2023)

Bouwer, H. (2002). Artificial recharge of groundwater: hydrogeology and engineering. *Hydrogeology Journal, 10,* 121–142. doi.org/10.1007/s10040-001-0182-4

Brown, R.A., & Hunt, W.F. (2012). Improving bioretention/biofiltration performance with restorative maintenance. *Water Science & Technology, 65 (2),* 361–367.

doi.org/10.2166/wst.2012.860

CSIRO (Commonwealth Scientific and Industrial Research Organisation) - Chameleon soil water sensor. https://www.csiro.au/en/research/%20plants/crops/Farming-systems/Chameleon -soil-water-sensor (Visited on 10/02/2023)

CORE Electronics - Waterproof DS18B20 Digital temperature sensor. https://core-electronics.com.au/waterproof-ds18b20-digital-temperature-sensor.html (Visited on 10/02/2023)

Dagenais, D., Brisson, J., & Fletcher, T.D. (2018). The role of plants in bioretention systems; does the science underpin current guidance? *Ecological Engineering, 120,* 532–545. doi.org/10.1016/j.ecoleng.2018.07.007

Davis, A.P. (2008). Field Performance of Bioretention: Hydrology Impacts. *Journal of Hydrologic Engineering, 13 (2),* 90-95. doi.org/10.1061/(ASCE)1084-0699(2008)13:2(90)

DS18B20 Dveloped by Analog Device Inc. Wire Digital Thermometer, Technical documentation. https://www.analog.com/media/en/technical-documentation/data-sheets/ds18b20.pdf (Visited on 10/02/2023)

Ebrahimian, A., Wadzuk, B., & Traver, R. (2019). Evapotranspiration in green stormwater infrastructure systems. *Science of The Total Environment, 688,* 797 - 810, ISSN 0048-9697. doi.org/10.1016/j.scitotenv.2019.06.256

U.S. Environmental Protection Agency - EPA (1980). *Falling Head Percolation Test Procedure.* In: Design Manual Onsite Wastewater Treatment and Disposal Systems, Cincinnati OH, 41-43. Online source: https://nepis.epa.gov/Exe/ZyPURL.cgi?Dockey=300043XO.txt

Fletcher, T.D., Wong, T.H.F., & Breen, P.F. (2006). Buffer strips, vegetated swales and bioretention systems. In: In T.H.F. Wong (Ed.), *Australian Runoff Quality - A Guide to Water Sensitive Urban Design,* 10.1–10.14, New South Wales: Engineers Media.

Gardner, W.H. (1986). Water Content. In: *Methods of Soil Analysis: Part 1—Physical and Mineralogical Methods, 5.1, Chapter 21,* 493-544. Klute A. (Ed.). Madison, WI: American Society of Agronomy - Soil Science Society of America. doi.org/10.2136/sssabookser5.1.2ed.c21

Green, J., Beesley, C., The, C., & Podger, S. (2015). New Design rainfalls for Australia. In: *36th Hydrology and Water Resources Symposium: The art and science of water.* Engineers Australia. Hobart, 7-10 December 2015. Online: http://www.bom.gov.au/water/designRainfalls/document/Green-et-al-2015a.pdf

Hatt, B.E., Fletcher, T.D., & Deletic, A. (2009). Hydrologic and pollutant removal performance of stormwater biofiltration systems at the field scale. *Journal of Hydrology, 365 (3-4),* 310-321. doi.org/10.1016/j.jhydrol.2008.12.001

Kerkez, B., Gruden, C., Lewis, M., Montestruque, L., Quigley, M., Wong, B., Bedig, A., Kertesz, R., Braun, T., Cadwalader, O., Poresky, A., & Pak, C. (2016). Smarter stormwater

systems. *Environmental Science & Technology, 50 (14)*, 7267–7273. PMID: 27227574. doi.org/10.1021/acs.est.5b05870

Langergraber, G., Haberl, R., Laber, J., & Pressl, A. (2003). Evaluation of substrate clogging processes in vertical flow constructed wetlands. *Water Science & Technology, 48 (5),* 25–34. doi.org/10.2166/wst.2003.0272

Le Coustumer, S., Fletcher, T.D., Deletic, A., Barraud, S., & Lewis, J. (2009). Hydraulic performance of biofilter systems for stormwater management: Influences of design and operation. *J. of Hydrology, 376 (1-2)*, 16-23. doi.org/10.1016/j.jhydrol.2009.07.012

Le Coustumer, S., Fletcher, T.D., Deletic, A., Barraud, S., & Poelsma, P. (2012). The influence of design parameters on clogging of stormwater biofilters: A large-scale column study. *Water research, 46 (20)*, 6743–6752. doi.org/10.1016/j.watres.2012.01.026

Lindsey, G., Roberts, L. & Page, W. (1992). Inspection and maintenance of infiltration facilities. *Journal of Soil and Water Conservation, 47 (6)*, 481 – 486.

Lloyd, S.D., Wong, T.H.F., & Porter, B. (2002). The planning and construction of an urban stormwater management scheme. *Water Science & Technology, 45 (7)*, 1–10. doi.org/10.2166/wst.2002.0111

Mason, B.E., Schmidt, J., & Kerkez, B. (2021). S*ensor networks for real-time green infrastructure monitoring.* Paper presented at the 15th International Conference on Urban Drainage, Melbourne, VIC.

McCarthy, D.T., Deletic, A., Mitchell, V.G., & Diaper, C. (2013*).* Predicting Between-Event Variability of Escherichia coli in Urban Storm Water. *Journal Environmental Engineering, 139 (5)*, 728-737. doi.org/10.1061/(ASCE)EE.1943-7870.0000674

Melbourne Water (2005). *WSUD Engineering Procedures: Stormwater*. Clayton South, VIC: CSIRO Publishing, 305, ISBN (electronic) 978-0-643-09989-0. doi.org/10.1071/9780643092235

Melbourne Water. Rainfall and river levels. [Data file]. https://www.melbournewater.com.au/water-and-environment/water-management/rainfall-and-river-levels#/reader/ (Visited on 05/03/2023)

Panayiotopoulos, K.P., & Mullins, C.E. (1985). Packing of sands. *Journal of Soil Science, 36 (1),* 129–139. doi.org/10.1111/j.1365-2389.1985.tb00318.x

Payne, E.G.I., Hatt, B.E., Deletic, A., Dobbie, M.F., McCarthy, D.T., & Chandrasena, G.I. (2015). *Adoption guidelines for Stormwater Biofiltration Systems.* Melbourne, VIC: CRC for Water Sensitive Cities. ISBN: 978-1-921912-27-6

PureConnect. Chameleon card three sensor pack R450.00. https://www.pureconnect.co.za/products-page/chameleon-card-three-sensor-pack/ (Visited on 10/02/2023)

Richards, P.J., Farrell, C., Tom, M., Williams, N.S.G., & Fletcher, T.D. (2015). Vegetable raingardens can produce food and reduce stormwater runoff. *Urban Forestry & Urban Greening, 14 (3),* 646-654, ISSN 1618-8667. doi.org/10.1016/j.ufug.2015.06.007

Roy-Poirier, A., Champagne, P., & Filion, Y. (2010). Review of bioretention system research and design: Past, present, and future. *Journal of Environmental Engineering, 136 (9),* 878–889, doi.org/10.1061/(ASCE)EE.1943-7870.0000227

Scarbrough, K., Padmini, P., Fletcher, I., Akin, A.A., Hathaway, J., & Khojandi, A. (2021). Real-Time Sensor-Based Prediction of Soil Moisture in Green Infrastructure: A Case Study. *Environmental Modelling & Software, 162,* 105638, ISSN 1364-8152. doi.org/10.13140/RG.2.2.27887.30885

Shen, P., Deletic, A., Bratieres, K., & McCarthy, D.T. (2019). Real time control of biofilters delivers stormwater suitable for harvesting and reuse. *Water Research, 169,* 115257. doi.org/10.1016/j.watres.2019.115257

Shock, C.C., & Wang, F-X. (2011). Soil Water Tension, a Powerful Measurement for Productivity and Stewardship. *Horticultural Science, 46 (2),* 178-185. doi.org/10.21273/HORTSCI.46.2.178

Shuckla M.K. (2013). *Soil Physics – An Introduction.* Boca Raton, Florida: CRC Press. ISBN 9781482216868

Stirzaker, R., Car, N., Chilundo M., & CSIRO Land and Water (2014). *A traffic light soil water sensor for resource poor farmers: proof of concept – Final Report.* Canberra, ACT: Australian Centre for International Agricultural Research (ACIAR), ISBN 978-1-925133-37-0

Truebner - SMT 100 Soil moisture sensor. https://www.truebner.de/en/smt100.php (Visited on 11/02/2023)

Truebner - SMT 100 Soil moisture sensor, Manual. https://www.truebner.de/assets/download/Manual_SMT100_V1.0.pdf (Visited on 11/02/2023)

Virtual Irrigation Academy (VIA). Chameleon Soil Water Sensor. https://via.farm/chameleon-soil-water-sensor/ (Visited on 31/01/2023)

Virahsawmy, H.K., Stewardson, M.J., Vietz, G., & Fletcher, T.D. (2014). Factors that affect the hydraulic performance of raingardens: implications for design and maintenance. *Water Science & Technology, 69 (5),* 982. doi.org/10.2166/wst.2013.809

Warrick, A.W. (2001). *Soil Physics Companion (1st edition).* Boca Raton, Florida: CRC Press. doi.org/10.1201/9781420041651

Wardynski, B.J., & Hunt, W.F. (2012). Are Bioretention Cells Being Installed Per Design Standards in North Carolina? A Field Study. *Journal of Environmental Engineering, 138 (12),* 1210 - 1217. doi.org/10.1061/(ASCE)EE.1943-7870.0000575

Chapter 4 - Numerical Modelling of Raingardens

Water Sensitive Urban Design (WSUD) approach is changing stormwater management in cities that are adopting it, providing adaptable solutions for reducing runoff, and enhancing biodiversity. Among these strategies, raingardens stand out for their ability to capture, treat, and manage rainwater runoff, alleviating water pollution and easing pressure on stormwater systems. While various studies highlight the efficacy of raingardens in mitigating runoff in urban areas (Bąk and Barjenbruch, 2022; Basdeki et al., 2016; Jiake et al., 2016; Kasprtzyk et al., 2022; Richards et al., 2015) their adoption in Italy remains limited.

This chapter assesses the potential benefits that would result from the introduction of raingarden in the industrial area of Brescia; a highly impermeable zone and prone to flooding during medium to intense rainfall events. Using the EPA Storm Water Management Model (SWMM) software, raingardens were integrated into the urban context. The "Businnes As Usual" scenario, representing the state of the art of the sewerage, was calibrated and validated based on the field flow measurements provided by the local integrated water service management body, A2A Ciclo Idrico, measured in different points within the network. The simulations were carried out using as input rainfall data both synthetic hyetographs derived for three different return period (T=2, 5 and 10 years) and continuous based on the measured rainfall data collected by ARPA

Lombardia for the years 2022 and 2023. Possible future climate scenarios were also considered. The raingarden performance was evaluated in term or runoff volume and peak flow reduction, and peak flow delay. The comparative analysis pre- and post-raingarden implementation showed consistent effectiveness across all simulated rainfall events, including those with a 10-year return period. However, under climate change conditions, the performance of raingardens slightly diminishes when more intense rainfall events.

4.1 Introduction

The rapid urbanization in recent decades has led to significant changes in land use. This has exacerbated the impact on the water cycle, particularly due to alterations in precipitation patterns due to climate change, resulting in more frequent occurrences of flooding (Zhou et al., 2019). Increased imperviousness and decreased native vegetation altered the hydrologic cycle, leading to higher water discharge into the traditional sewage infrastructure, faster runoff concentration, and decreased infiltration and evapotranspiration rates (Shuster et al., 2005; Jacobson, 2011; Salerno et al., 2018). The increase in runoff volumes also results in a washout of pollutants, such as heavy metals, suspended solids, and other organic pollutants, which are conveyed directly into water bodies (Walters et al., 2011). The reduction in impervious surfaces compensates for the impact of urbanization and climate change on urban hydrology and on the efficiency of drainage systems, as several other authors have highlighted (McGrane, 2015; Li et al., 2016; Zeng et al., 2018; Campisano et al, 2020; Dada et al., 2021; Palermo et al., 2023). In this context, a growing attention has been paid to strategies aimed at reducing flows and water volumes discharged into the sewage system based on the adoption of green infrastructures. In many countries this interest has been embraced by government departments who have introduced tax breaks or economic incentives to facilitate the introduction of green solutions and limit land use exploitation (Grant, 2018; Newburn and Alberini, 2016). These economic measures are designed to encourage property owner to adopt technologies such as raingarden, green roofs, or any other sustainable stormwater control strategies.

While these systems may come at higher cost than conventional stormwater infrastructure, they offer different social, environmental, and economic benefits (Faivre et al., 2017). In fact, unlike conventional stormwater systems, green infrastructure reduces peak flow, improves runoff quality, reduces water volumes on the surfaces by increasing the infiltration into the subsurface and the evapotranspiration restoring in this

way the pre-development watershed regular water cycle and ecosystem services (Hunt et al., 2012, McPhillips et al., 2023; Coutts et al., 2012).

In order to encourage investment on green solutions and to motivate widespread use for these green strategies, it is necessary to identify valuable methods to evaluate the effectiveness of their implementation, with the goal of providing the tools to properly introduce these systems within urban planning (Ahiablame and Shakya, 2016).

EPA Storm Water Management Model (SWMM) is one of the most widely used hydraulic and hydrological simulation model for analysing and managing stormwater runoff. Starting from its last release, SWMM5 (v. 5.1.007) it was updated with a module for LID (Low Impact Development) modelling (McCutcheon and Wride, 2013). As for the Australian term WSUD, the American term LID embodies the concept of minimizing the cost of stormwater management by controlling storm water runoff at its source with a "nature approach" (Fletcher et al., 2015). In other words, LIDs are techniques that aim to mimic natural hydrological processes in order to mitigate the impacts of urbanization on water quality and quantity (Chang, 2010, Peng et al., 2018). LID Modules in SWMM can simulate the regulation effects of these green strategies on runoff volumes, peak flow and water pollution removal by simulating the hydrological processes including infiltration, evaporation, storage and drainage (Peng et al., 2018). SWMM has the capability to provide both single event and continuous simulations of hydraulic and hydrologic performance of various types of stormwater control measures including grey and green infrastructure.

In the present study, among LID solutions, raingardens were selected as source of control systems to be applied to a case study area, the industrial zone of Brescia, in order to reduce the impact of urbanization.

Raingarden (also called bioretention pond), as LID measures, are evaluated for their effectiveness in managing stormwater quantity issues, by promoting the reduction of surface runoff volume, delaying and reducing the peak flow and increasing the control of pollutants loads washed-off from urban surfaces. The adopted modelling approach is meant to provide valuable insights for urban planners and engineers to access the performances and benefits of these green infrastructure features in the overall stormwater management strategy. Studies on raingarden applications are mostly limited to small-area or residential applications (Burszta-Adamiak et al., 2023; Ebrahimian et al., 2019; Kasprzyk et al., 2022) demonstrating their effectiveness in reducing stormwater volume as well as limiting the pollutants load delivered into the drainage system. However, raingarden implementation at the urban catchment scale is still subject of debate. In light of this, evaluations based on a modelling study would provide insight about their potential efficiency in a more complex environment such as the urban one, characterized

by increased impervious surfaces, higher population density and more complex drainage systems. Other modelling studies at urban catchment have already demonstrated the effectiveness of other LIDs (green roofs, rain barrels and porous pavements) in reducing surface runoff volume (Palla and Gnecco, 2015; Ahiablame and Shakya, 2016; Bursztа-Adamiak and Mrowiec, 2013; Lee et al., 2013; Raimondi et al., 2021).
The aim of this study is to investigate the effects of raingarden at urban catchment scale in reducing surface water volume and minimizing the impact of the impervious surfaces on the formation of the hydraulic loads that the underground drainage network must handle. For this purpose, an EPA SWMM model of the sewerage system was created and incorporated with raingardens as LID control devices, in order to evaluate their effectiveness under different rainfall events scenarios, in the current and future climate.

4.2 Study area

The study area selected as a test site for the raingarden modelling is the industrial area of the city of Brescia (Italy). This area is located south-west of the city centre and covers approximately 240 hectares. Accessible vis the western ring road, SP BS 11 marks its eastern boundary towards Fornaci. To the west, beyond the Mella River, it borders the municipalities of Roncadelle and Castelmella (Onzato). On the south and east sides, the area borders land designated for agricultural purposes (see Fig. 32).

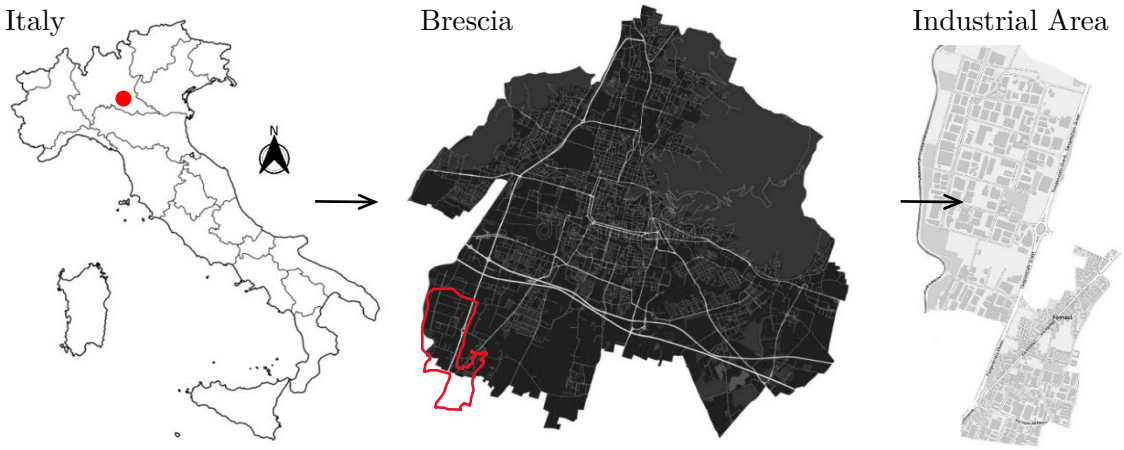

Fig. 32 – Map of the study area

The urban development of the area began in the 1970s with the construction of the first industrial complexes. Nowadays, the area is entirely urbanized, with an impermeability rate of about 85%. It is predominantly occupied by the road network and industrial facilities, along with associated car parks and concrete areas. Downstream from the

industrial area there is the suburb of Fornaci, a residential neighbourhood with approximately 2.650 inhab.

The drainage network of the area consists of a traditional grey infrastructure which includes manholes, pipes, spillways and pumps. The system type is combined, with a main collector that runs from north to south across the entire area before diverting eastward to reach the wastewater treatment plant. Discharge occurs through a pumping station designed to handle a maximum flow of 274 l/s. Several secondary collectors branch off the main collector, delivering flows into the main collector after passing through 18 overflow points distributed along the network (Fig. 33).

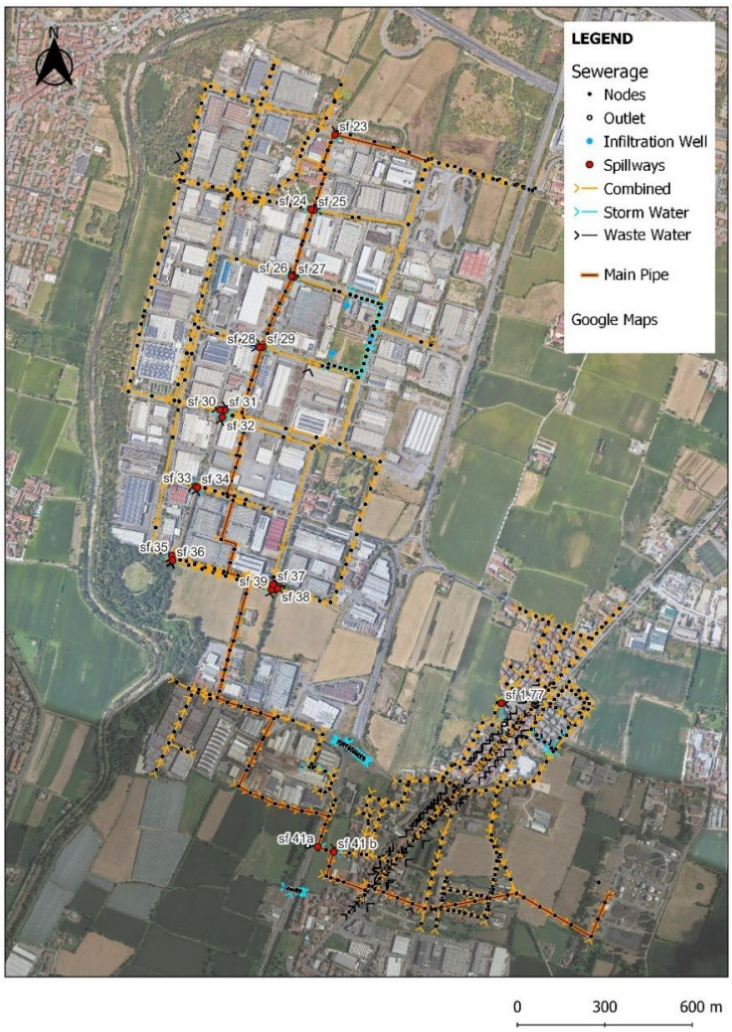

Fig. 33 – Sewerage system of the case study area

The drainage network develops from north to south following the natural slope of the terrain, so that water in the collectors flows by gravity from the northern part of the catchment (with a maximum elevation of 124 m above sea level) to the southeastern part

of the catchment (elevation of 107 m above sea level), with an average slope of 3 ‰. Due to the high degree of impermeability, combined with the low slopes of the terrain, the area is prone to flooding even during meteorological events of relatively low intensity. Additionally, the lack of separate networks channelling blackwater to a treatment plant and stormwater directly into surface waterbodies makes the existing infrastructure unsuitable to cope with increased intensity of high frequency rainfall events. The climate of the area, classified as Cfa – where C corresponds to "Temperate", f to "no dry season" and, a to "hot summer" - by the Koppen-Geiger[1], is warm and temperate, with warm summer and cold, damp winters. The city is located at the foot of the Pre-Alps, whose proximity increases thunderstorms during late spring and summer. The average annual precipitation is 1090 mm (https://en.climate-data.org/europe/italy/lombardy/brescia-1096/).

4.3 Determination of potential evapotranspiration

Evaporation plays an important role in the hydrological process since it represents the amount of water that goes from the ground back to atmosphere and is considered within the hydraulic model as a hydrological loss. It combines two important processes, evaporation from the soil surface and transpiration from plants (Anggraini and Slamet, 2021). The monthly potential evapotranspiration (PET_D in mm per day) was computed using the method proposed by Pereira and Pruitt (2004), an improved version of the daily Thornthwaite and Mather (1957) equation. The Thornthwaite equation developed by Thornthwaite (1948) uses air temperature and latitude from meteorological observations.

The PET_D is a daily time scale of the standard monthly potential evapotranspiration (PET_M) which is a function of the month average temperature T (°C) and, as reported in Thornthwaite (1948) and Willmott et al. (1984), for a standard month of 30 days each day with 12 h of photoperiod, is well expressed by the equation:

$$PET_M = \begin{cases} 0 & if\ T < 0\,℃ \\ 16\left(10\,\frac{T}{I}\right)^a & if\quad 0℃ \le T \le 26\,℃ \\ -415.85 + 32.24\,T - 0.43\,T^2 & if\ T > 26\,℃ \end{cases} \qquad (4.1)$$

[1] The Köppen-Geiger climate classification system, developed by climatologists Wladimir Köppen and Rudolf Geiger, is a widely used method to categorize and classify Earth's climates based on various climatic parameters. The classification system divides the Earth's climates into several main groups and subgroups based on the annual and monthly averages of temperature and precipitation.

Where:

- PET_M is the monthly evapotranspiration (mm/day);
- T is the mean monthly temperature (°C);
- I is the annual heat index characteristic of the local climatic temperature;
- a is the exponent function of I.

The annual I index is calculated as the sum of the monthly heat index, function of the monthly average temperature, as shown in the next equation:

$$I = \sum_{n=1}^{12} \left(\frac{T}{5}\right)^{1.514} \qquad \text{T} > 0\ ^\circ\text{C} \qquad (4.2)$$

While this index varies from 0 to 160, the exponent a varies from 0 to 4.25 and the relation between the two is closely approximated by the equation:

$$a = 0.000000675\, I^3 - 0.0000771\, I^2 + 0.01792\, I + 0.49239 \qquad (4.3)$$

In order to convert the values of PET_M from a monthly (mm/month) to a daily time scale (mm/day) a correction factor (C) which depends on the actual number of sun hour of each day was introduced (Thornthwaite & Mather, 1957). The factor was computed as follows:

$$C = \frac{N}{360} \qquad (4.4)$$

where N is the photoperiod (h) for a given day, varying with season and latitude.
The equation then became:

$$PET_D = \begin{cases} 0 & if\ T_d < 0\ ^\circ C \\ 16\ \frac{N}{360} \left(10 \frac{T_d}{I}\right)^a & if\ 0\ ^\circ C\ \leq T_d \leq 26\ ^\circ C \\ \frac{N}{360} \left(-415.85 + 32.24\ T_d - 0.43\ {T_d}^2\right) & if\ T_d > 26\ ^\circ C \end{cases} \qquad (4.5)$$

where T_d is the daily average temperature equals to $T_d = \frac{1}{2}\ (T_{max} + T_{min})$.

Camargo et al. (1999) found that the values obtained with the Thornthwaite approach could be improved using an "effective" temperature (T_{ef}) computed as a function of the average temperature and of the daily amplitude as shown in the following equation:

$$T_{ef} = \frac{1}{2}\ k\ (3\ T_{max} - T_{min}) \qquad (4.6)$$

Where:

- k is a statistical value obtained experimentally equal to 0.72;
- T_{max} is the daily maximum temperature;
- T_{min} is the daily minimum temperature.

Pereira and Pruitt (2004) suggested to correct T_{ef} introducing the day-night ratio. So, the previous equation became as follows:

$$T_{ef}{}^{*} = T_{ef}\ \frac{N}{24 - N} \qquad \text{with } T_d \leq T_{ef}^{*} \leq T_{max} \qquad (4.7)$$

where T_{ef}* in °C is the corrected T_{ef}, and N is the daylight hours.
The values of PET_D obtained for the case study are reported in the following table (Tab. 18) and they are graphically represented in the Fig. 34. As mentioned above, the PET_D values that were used in the SWMM model are those derived by the Pereira and Pruitt (2004) method.

Tab. 18 - Values of monthly average PET_D in mm/day

PET_D [mm/day]	Jan	Feb	Mar	Apr	May	Jun	Jul	Aug	Sep	Oct	Nov	Dec
Thornthwaite	0.12	0.23	0.57	1.15	2.16	3.31	3.85	3.57	2.17	0.95	0.41	0.32
Pereira & Pruitt	0.35	0.60	1.08	1.66	2.63	3.64	3.80	3.52	2.19	1.03	0.53	0.16

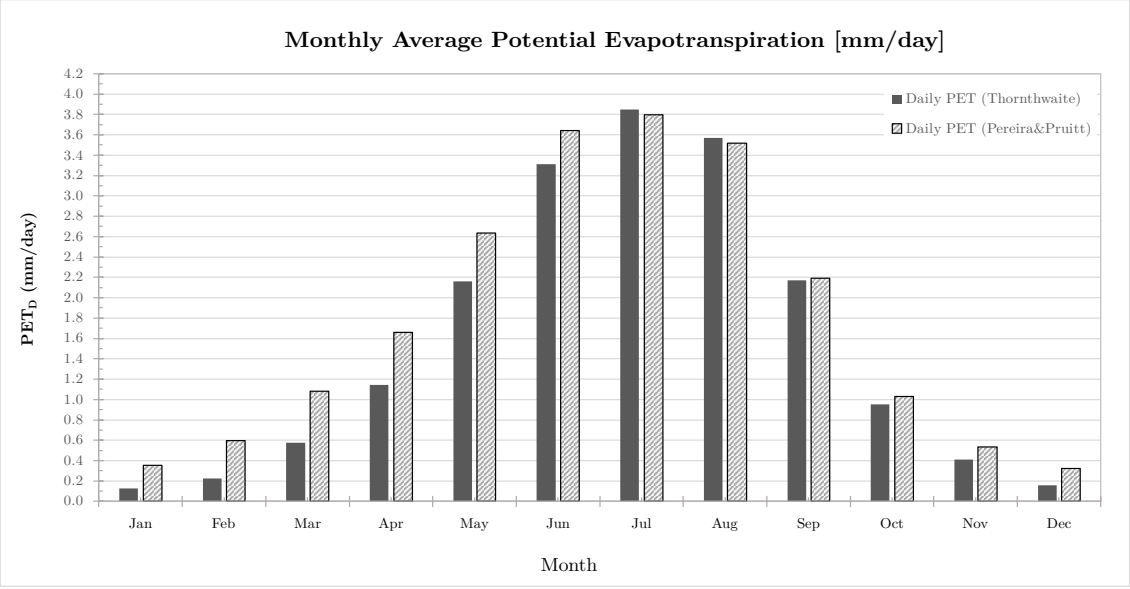

Fig. 34 – Monthly average of PET_D in mm/day

The temperature values (daily maximum and minimum) used to calculate the PET_D refer to historical data from 1991 to 2021 while the values of the average daily sun hours refer to historical data from 1999 to 2019 (Climate Data - https://en.climate-data.org/europe/italy/lombardy/brescia-1096/).

4.4 Rainfall events designed and dry weather flows

The selection of design rainfall events used in the simulation phase was carried out by deriving Chicago hyetographs for three different return periods (namely 2, 5 and 10 years) based on the rainfall probability curve. The identification of synthetic design rainfall events was conducted as described in the following paragraphs.

4.4.1 Estimation of rainfall DDF Curves (Rainfall analysis)

To define the rainfall depth-duration-frequency curves, the rainfall data available on the ARPA Lombardia website were used. Assuming a homogeneous distribution of rainfall over the study area, the DDF curves were defined and the T-year rainfall depth h_T was calculated using the following equations:

$$h_T(D) = a_1 \, w_T \, D^n \qquad (4.8)$$

$$w_T = \varepsilon + \frac{\alpha}{k}\left\{1 - \left[ln\left(\frac{T}{T-1}\right)\right]^k\right\} \qquad (4.9)$$

Where:

- $h_T(D)$ is the rainfall depth;
- D is the duration of the rainfall event;
- T is the return period;
- a_1 is the hourly rainfall coefficient;
- w_T is the probabilistic coefficient linked to the return period;
- n is the exponent of the curve (parameter of scale, lower than 1);
- α, ε, k are the parameters of the adopted GEV probabilistic law.

The n value provided by ARPA relates to a rainfall event lasting > 1 h. For an event of duration <1 h, instead, n was considered equal to 0.5, as required by the regional law "Regolamento Regionale 23 novembre 2017, n. 7" (updated on 21/12/2019 - BURL, 2019 – "Reporting criteria and methodologies to comply with the hydraulic and hydrologic

invariance in accordance with the article 58 bis of the regional law of 11th March 2005 n.12 (the so called "Law for the territorial administration").
The LIRIS WebGIS tool provided by ARPA Lombardia was used to collect the data (https://iris.arpalombardia.it/gisINM/common/webgis_central.php?TYPE=guest).
This tool provides not only the hydro-nivo-weather observations in real time, but also the characteristic parameters of the rainfall possibility curves as a function of the area of interest. Fig. 35 shows the cell from which the parameters for constructing the curves were obtained, representative of the area under examination.

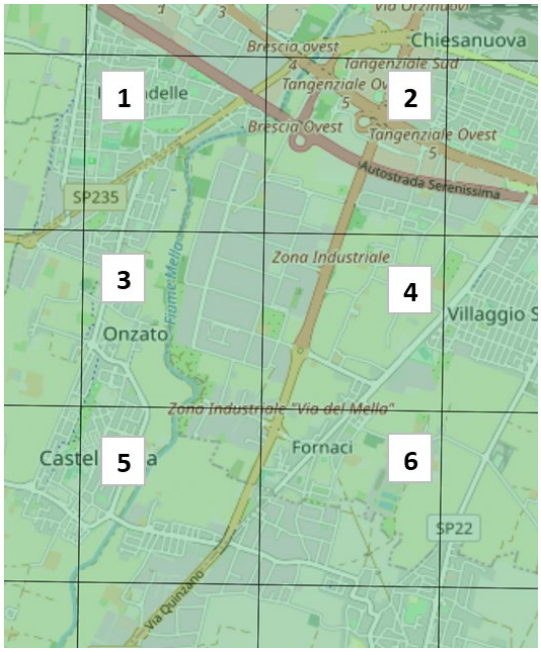

Fig. 35 – Study area cells for DDF curves parameters

The characteristic parameters of the DDF curves representative of the study area is shown in Tab. 19.

Tab. 19 – DDF curves characteristic parameters for the study area

LSPP Parameters		**1**	**2**	**3**	**4**	**5**	**6**	**Mean**
Hourly Rainfall Coefficient	a_1	28.26	28.12	28.11	28.08	28.09	28.13	28.13
Parameter of scale	n	0.275	0.2762	0.2757	0.2755	0.2749	0.2728	0.275
GEV - alpha parameter	α	0.2813	0.2811	0.2809	0.2804	0.2801	0.2799	0.280
GEV - kappa parameter	k	0.0281	0.0226	0.0248	0.0286	-0.031	-0.031	0.027
GEV - epsilon parameter	ε	0.8295	0.8311	0.8307	0.8297	0.8292	0.8295	0.830

The representation of the curves is shown in the Fig. 36 below. Given the purpose of the study, meteoric events with return period of 2, 5 and 10 years were examined.

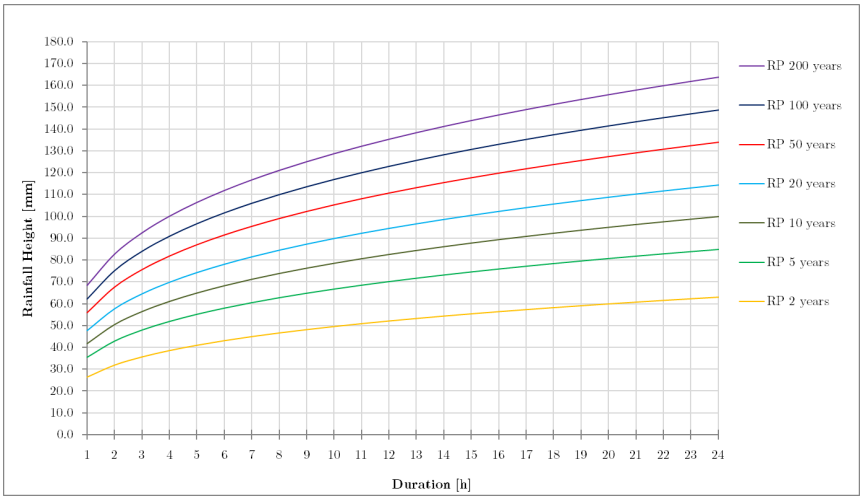

Fig. 36 – Rainfall depth-duration-frequency curves for events of 1-24 hours.

The rainfall obtained (point storm rainfall) was then related to the whole study area by applying a correction factor (areal reduction factor) to the parameters in order to evaluate the areal storm rainfall. To evaluate the new parameters a' and n' reference was made to the formulas proposed by Marchetti (1964), valid for areas between 100 and 500 ha:

$$a' = a\left[1 - 0.06\left(\frac{A}{100}\right)^{0.4}\right] \quad (4.10)$$

$$n' = n + 0.003\left(\frac{A}{100}\right)^{0.6} \quad (4.11)$$

where A is the area expressed in hectares. The value obtained are shown in Tab. 20.

Tab. 20 - Values of the parameters of the rainfall depth-duration-frequency curves for **Brescia**

Return Period	Point storm rainfall		Areal storm rainfall	
	a	n	a'	n'
2 yrs.	26.255624	0.275	24.017949	0.325
5 yrs.	35.436740	0.275	32.416591	0.325
10 yrs.	41.675983	0.275	38.124086	0.325

The Chicago hydrograph was then created assuming a rainfall duration equal to 30 min (duration of the rainfall events for which raingardens are usually designed) and a time-to-peak ratio equal to 0.4. The selected return periods refer to high-intensity rainfall events characterized by a frequency smaller than the ones used for dosing the raingardens in the laboratory. The reason for this lies in the fact that, during this phase of the study, the aim was to assess the effectiveness of raingardens for less frequent but more intense

meteorological events. Fig. 37 shows the Chicago hyetographs evaluated for the three selected return period (T=2, 5 and 5 years).

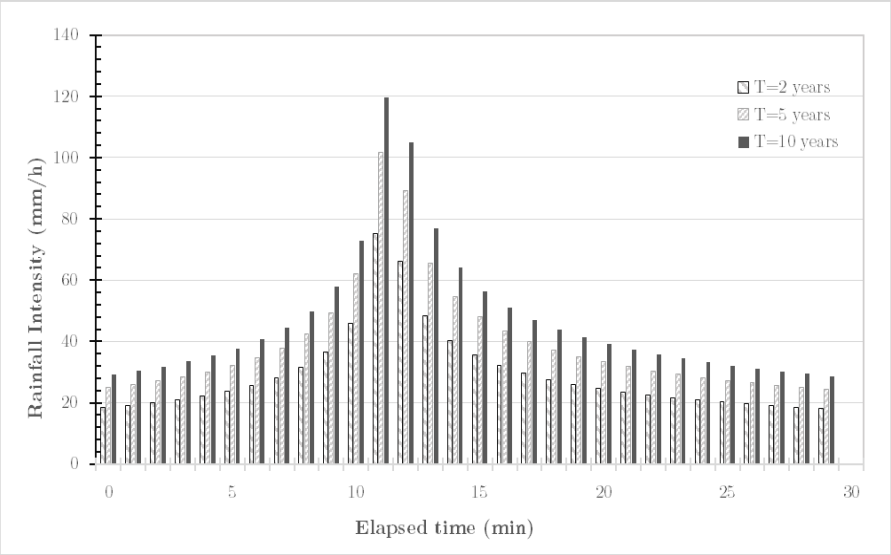

Fig. 37 – Chicago hyetograph for three return periods: 2, 5 and 10 years.

For continuous simulations the data recorded at the "Brescia -v.Ziziola" weather station, managed by the regional Agency ARPA Regione Lombardia (https://www.arpalombardia.it/), were used. Rainfall data used for simulation ranged from 1 January 2022 to 31 December 2023 (2 years with 10 min time step). Fig. 38 and Fig. 39 shows the distribution of rainfall intensity and the air temperature measured in the 10 min time interval for both years.

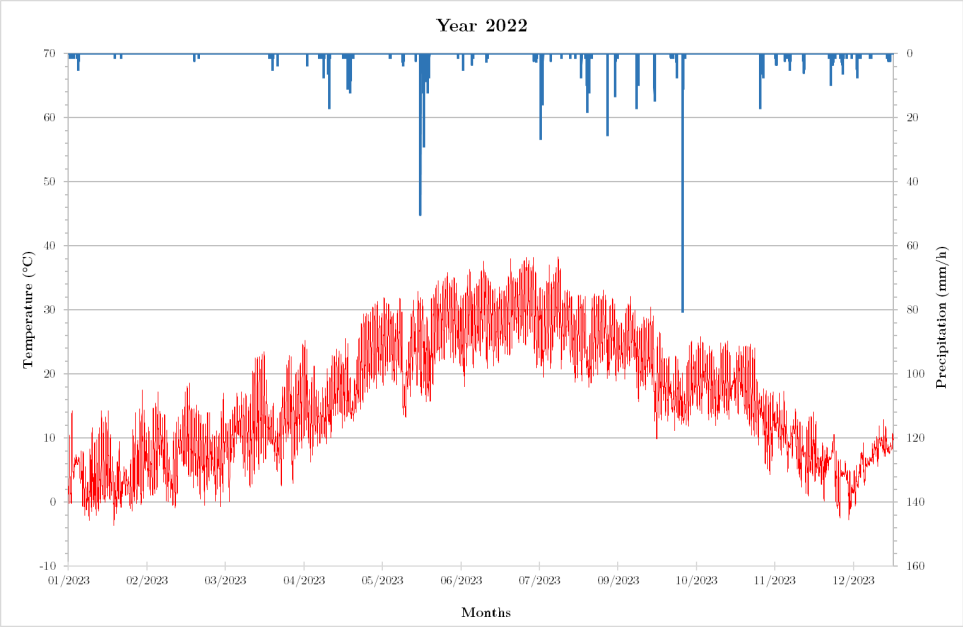

Fig. 38 – Histogram of the rainfall intensity (mm/h) and the air temperature measured in the 10 min time interval for the year 2022.

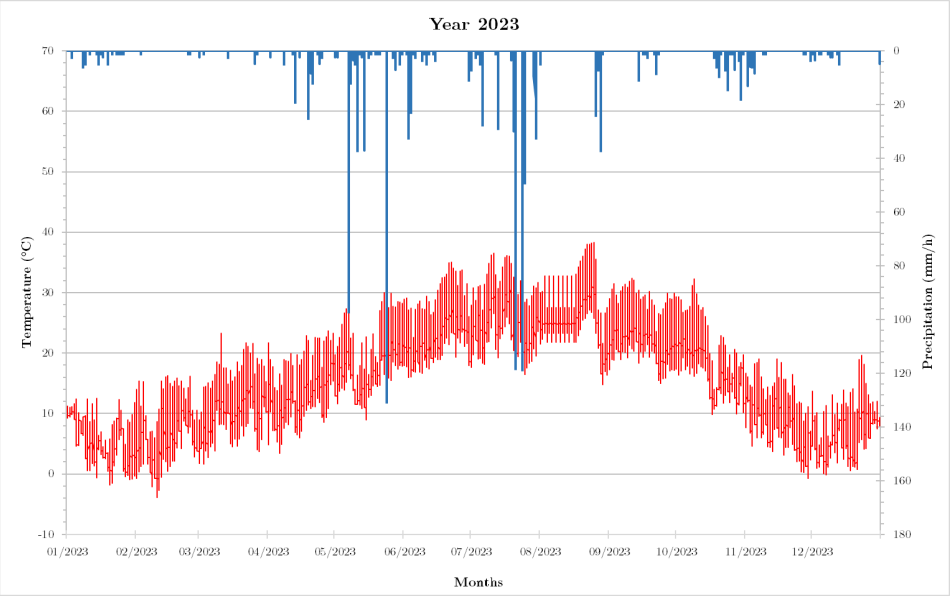

Fig. 39 - Histogram of the rainfall intensity (mm/h) and the air temperature measured in the 10 min time interval for the year 2023.

In 2023 the total precipitation recorded was 788.4 mm, significantly higher than the 455.6 recorded in 2022 corresponding to about 120 wet days per year in 2023 and 90 wet days per year in 2022.

It is important to note that Brescia typically experiences an average annual precipitation of about 1090 mm, according to data from Climate-Data (https://en.climate-data.org/europe/italy/lombardy/brescia-1096/).

4.4.2 Dry weather flows

The water inflows entering the nodes during dry weather were calculated based on the number of inhabitants and industrial water consumption.

The time patterns for both domestic and industrial wastewater, illustrate in Fig. 40, whose factors adjust the baseline inflow on a daily basis, were provided by the integrated water service management body (A2A Ciclo Idrico). These factors were entered in the model as timeseries.

The baseline black flows have been included starting from the water supply consumption, reduced by a portion equal to 20%. The deduction of 20% from the water consumption accounts for factors such as leakages, evaporation, or non-return flows, thereby providing a more accurate estimate of the actual wastewater discharge.

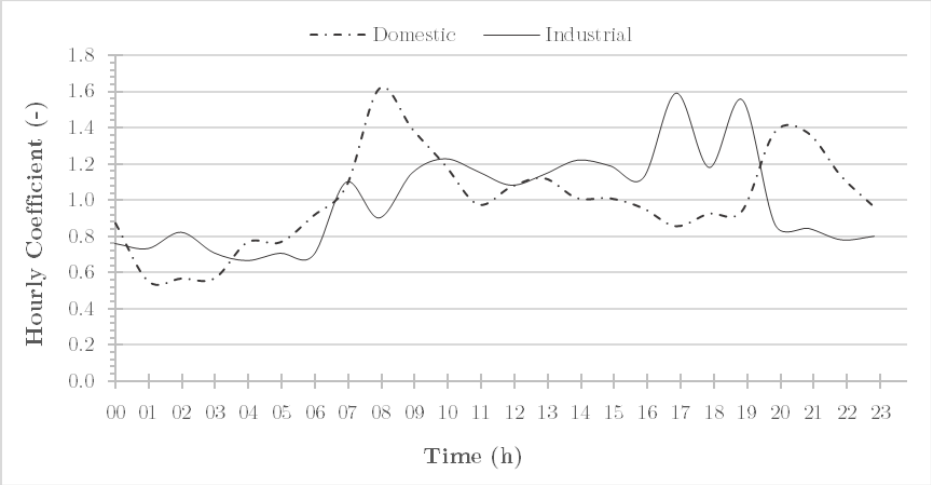

Fig. 40 – Wastewater daily patterns

4.5 Future Climate scenario

Climate change significantly impacts precipitation patterns, altering the frequency, intensity, and distribution of rainfall. Sewage networks are commonly designed for a service life of 50-100 years; however, climate change has been putting a strain on the existing infrastructures due to an increased occurrence of extreme rainfall events associated with climate change (Moore et al., 2016). These events can disrupt the efficiency of urban drainage systems, increasing the risk of localized flooding, overwhelming stormwater infrastructure, and causing potential damage to property and public spaces. The inadequacy of drainage systems to handle intensified and concentrated rainfall poses a substantial threat to the resilience of urban areas in the face of changing precipitation patterns (Hughes et al., 2021). In this context, assessing the impact of climate change on future precipitation scenarios represents a crucial step for effective stormwater management.

CORDEX data (Coordinated Regional Downscaling Experiment), were used to simulate future climatic scenarios at regional scale, in order to evaluate the efficiency of the raingardens implemented within the network in facing climate change impacts.

CORDEX was firstly introduced by the World Climate Research Programme (WCRP) to address the need for improving climate change information at regional and local scale (Giorgi et al., 2009). CORDEX experiments consist of Regional Climate Models (RCMs) simulations representing different future socio-economic scenarios, different combinations of Global Climate Models (GCMs) and RCMs and different ensemble members of the same GCM-RCM combinations (Copernicus Climate Change Service). CORDEX data provide a timeseries of values of different parameters (such as precipitation,

temperatures, wind speed, relative humidity etc.) at specific grid points (https://esg-dn1.nsc.liu.se/search/cordex/).

In this study the MOHC-HadGEM2-ES Global Climate Models (GCM) from the CMIP5 (5th phase of the Coupled Model Intercomparison Project) archive was used, along with the RCA4 (the Rossby Centre regional Atmospheric climate model) regional downscaling model used to downscale the GCM model and to provide information on higher spatial resolution. Since the case study area is located in northern Italy, the EUR-11i (central Europe) domain was used. he numeric value "11" in the "EUR" abbreviation signifies the grid resolution in the original CORDEX simulation, which is 0.11 degrees with rotated poles. The addition of the letter "i" to the domain name indicates that the poles have been readjusted back to their original positions, and the grid resolution has been slightly altered through interpolation. Consequently, the data associated with EUR-11i now possess a resolution of 0.125 degrees (about 12.5 km) in both latitude and longitude (https://portal.enes.org/). Three different climate scenarios (or climate projections) were considered, according to the Representative Concentration Pathways (RCP) set by IPCC Intergovernmental Panel on Climate Change (https://ar5-syr.ipcc.ch/topic_future_changes.php): RCP 2.6, RCP 4.5, and RCP 8.5, representing respectively three different future scenarios characterised by a greenhouse gas concentration pathways equivalent to a radiative forcing of 2.6 W/m^2, 4.5 W/m^2 and 8.5 W/m^2. The periods considered are the twenty-years period from 1980 to 1999 for the historical, from 2040 to 2059 and from 2080-2099 for the future scenarios.

In the following figures (Fig. 41, Fig. 42, Fig. 43 and Fig. 44) observed values are compared with values derived from future scenarios for each RCP (2.6, 4.5 and 8.5) and for the two time periods considered (2040-2059 and 2080-2099), for the precipitation and temperature variables.

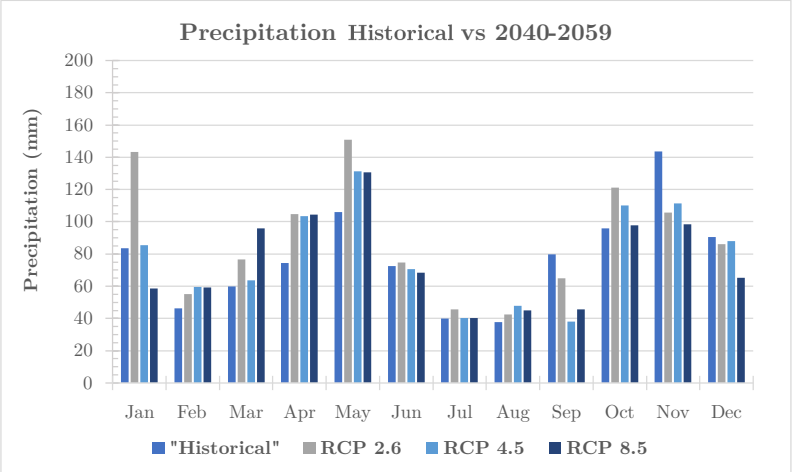

Fig. 41 – Historical and future (2040 – 2059) scenarios simulation (monthly precipitation)

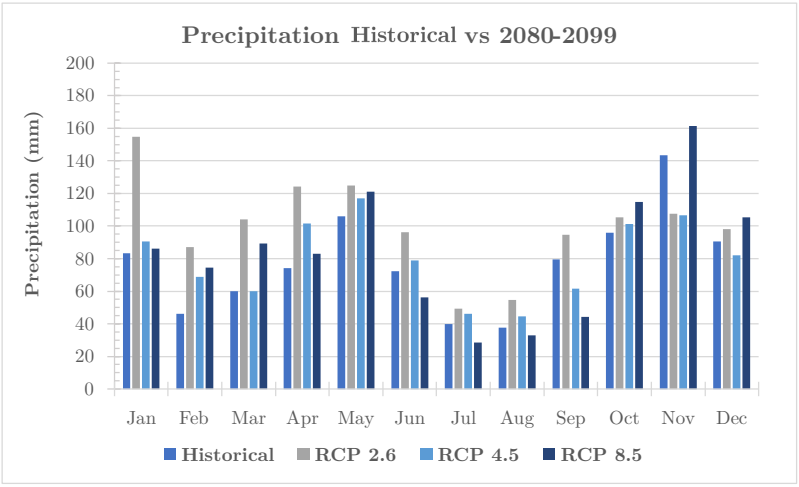

Fig. 42 - Historical and future (2080 – 2099) scenarios simulation (monthly precipitation)

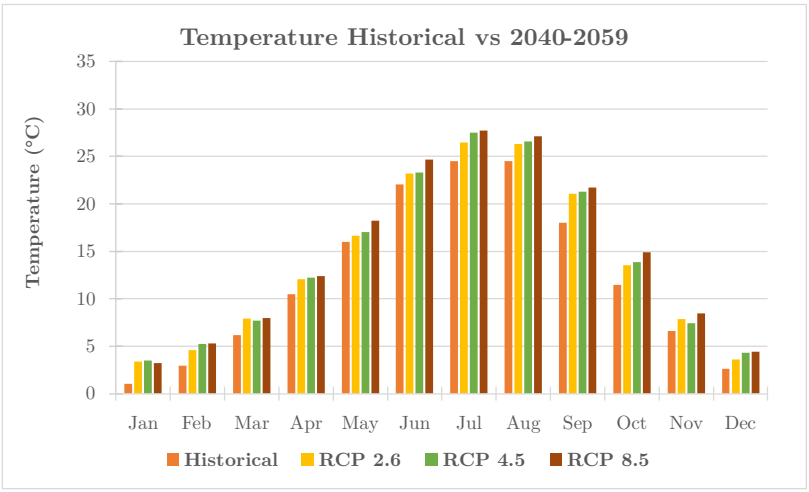

Fig. 43 – Historical and future (2040 – 2059) scenario simulation (monthly average temperature)

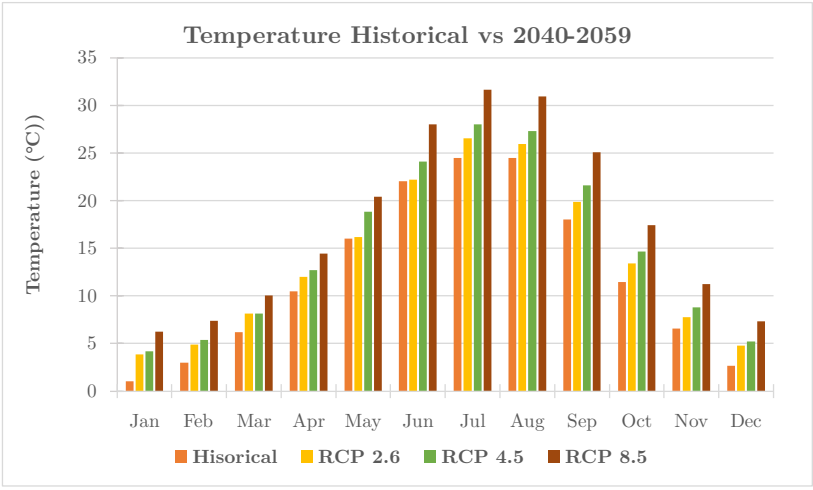

Fig. 44 - Historical and future (2080 – 2099) scenario simulation (monthly average temperature)

Through the comparison of observed rainfall amounts with values derived from future climate projections, it was possible to estimate a correction factor K. This factor is determined as the ratio of the monthly projected rainfall to the observed values, as follows:

$$K = \frac{P_{(ith-month)\ RCP\ Scenario}}{P_{(ith-month)\ Historical\ Scenario}} \quad (4.12)$$

where $P_{(ith\text{-}month)\ RCP\ Scenario}$ represents the monthly precipitation for each month in each climate projection scenario and $P_{(ith\text{-}month)\ Historical\ Scenario}$ is the monthly precipitation for each month based on historical values.

A similar procedure was adopted in Berteni et al., 2021 as well. The obtained K values are reported in Tab. 21.

Tab. 21 – K coefficients for precipitation. The values are a ratio between the historical and the future values derived from each RCP.

	2040-2059			**2080-2099**		
Month	**RCP 2.6**	**RCP 4.5**	**RCP 8.5**	**RCP 2.6**	**RCP 4.5**	**RCP 8.5**
January	1.72	1.02	0.70	1.86	1.09	1.03
February	1.19	1.29	1.28	1.88	1.49	1.61
March	1.28	1.06	1.60	1.74	1.00	1.49
April	1.41	1.39	1.41	1.67	1.37	1.12
May	1.42	1.24	1.24	1.18	1.10	1.14
June	1.03	0.97	0.94	1.33	1.09	0.78
July	1.15	1.01	1.01	1.24	1.16	0.72
August	1.13	1.27	1.20	1.45	1.19	0.88
September	0.82	0.48	0.57	1.19	0.77	0.56
October	1.26	1.15	1.02	1.10	1.06	1.20
November	0.74	0.78	0.69	0.75	0.74	1.12
December	0.95	0.97	0.72	1.09	0.91	1.17

Based on the monthly correction factor K, a seasonal correction factor J was calculated to take into account the seasonal variation in precipitation patterns. J is computed as the average of the K factors related to the 4 reference months of each season. The obtained values are reported in the following table (Tab. 22).

Tab. 22 - J coefficients for seasonal precipitation. The values came from the average value of the monthly correction factors K.

	2040-2059			2080-2099		
Season	**RCP 2.6**	**RCP 4.5**	**RCP 8.5**	**RCP 2.6**	**RCP 4.5**	**RCP 8.5**
Summer	1.10	1.08	1.05	1.34	1.15	0.79
Autumn	0.94	0.80	0.76	1.01	0.86	0.96
Winter	1.29	1.09	0.90	1.61	1.16	1.27
Spring	1.37	1.23	1.42	1.53	1.16	1.25

The monthly temperature coefficient ΔT, that is the difference in degrees Celsius between the historical and derived from future climate scenario values, was calculated using the following equation:

$$\Delta T_{ith-month} = T_{(ith-month)\ RCP\ Scenario} - T_{(ith-month)\ historical\ Scenario} \quad (4.13)$$

where $T_{(ith\text{-}month)RCPScenario}$ represents the average monthly temperature for each month in each climate projection scenario and $T_{(ith\text{-}month)HistoricalScenario}$ is the average monthly temperature for each month based on historical values. The monthly variation calculated for each RCP are reported in the Tab. 23.

Tab. 23 – ΔT temperature variation between historical values and values of future scenarios for each RCP.

	2040-2059			2080-2099		
Month	**RCP 2.6**	**RCP 4.5**	**RCP 8.5**	**RCP 2.6**	**RCP 4.5**	**RCP 8.5**
January	+ 2.36 °C	+ 2.47 °C	+ 2.16 °C	+ 2.79 °C	+ 3.12 °C	+ 5.18 °C
February	+ 1.63 °C	+ 2.29 °C	+ 2.31 °C	+ 1.91 °C	+ 2.4 °C	+ 4.43 °C
March	+ 1.76 °C	+ 1.53 °C	+ 1.82 °C	+ 1.99 °C	+ 1.99 °C	+ 3.85 °C
April	+ 1.61 °C	+ 1.76 °C	+ 1.9 °C	+ 1.51 °C	+ 2.24 °C	+ 3.98 °C
May	+ 0.64 °C	+ 1.02 °C	+ 2.21 °C	+ 0.17 °C	+ 2.84 °C	+ 4.42 °C
June	+ 1.17 °C	+ 1.28 °C	+ 2.59 °C	+ 0.18 °C	+ 2.04 °C	+ 5.96 °C
July	+ 1.97 °C	+ 3.03 °C	+ 3.24 °C	+ 2.04 °C	+ 3.51 °C	+ 7.13 °C
August	+ 1.8 °C	+ 2.1 °C	+ 2.65 °C	+ 1.47 °C	+ 2.86 °C	+ 6.49 °C
September	+ 3.04 °C	+ 3.27 °C	+ 3.71 °C	+ 1.87 °C	+ 3.61 °C	+ 7.09 °C
October	+ 2.05 °C	+ 2.38 °C	+ 3.44 °C	+ 1.94 °C	+ 3.17 °C	+ 5.95 °C
November	+ 1.26 °C	+ 0.83 °C	+ 1.86 °C	+ 1.19 °C	+ 2.2 °C	+ 4.67 °C
December	+ 0.97 °C	+ 1.66 °C	+ 1.79 °C	+ 2.14 °C	+ 2.58 °C	+ 4.68 °C

As for the seasonal precipitation correction factors, the temperature variation in terms of Celsius degrees for each season were calculated. The values are reported in the following table (Tab. 24).

Tab. 24 - ΔT seasonal temperature variation. The values came from average values from the monthly variation.

	2040-2059			2080-2099		
Season	**RCP 2.6**	**RCP 4.5**	**RCP 8.5**	**RCP 2.6**	**RCP 4.5**	**RCP 8.5**
Summer	+1.64°C	+2.13°C	+2.82°C	+1.23°C	+2.8°C	+6.53°C
Autumn	+2.11°C	+2.16°C	+3.00°C	+1.67°C	+2.99°C	+5.9°C
Winter	+1.65°C	+2.14°C	+2.09°C	+2.28°C	+2.70°C	+4.76°C
Spring	+1.33°C	+1.43°C	+1.98°C	+1.22°C	+2.36°C	+4.08°C

4.6 SWMM Model

EPA Storm Water Management Model (EPA SWMM) is a dynamic rainfall-runoff simulation model developed by the U.S. Environmental Protection Agency widely used for designing and analysing stormwater management infrastructure based on single event or long-term (continuous) simulation (Rossman and Simon, 2022). The SWMM model version 5.2.4 was used for this study, available from the EPA website (https://www.epa.gov/water-research/storm-water-management-model-swmm). SWMM was selected because it is an open-source software with a good versatility and capability in modelling a wide range of stormwater management scenarios and because of its well-known accuracy in simulating the hydrologic performance of low impact development practices (Platz et al. 2020; Palla and Gnecco, 2015). It consists of different components that allow to simulate the complex processes involved in stormwater management.

The mail modules include a hydrological module which estimates the flow generated by a given precipitation and represents the territory as a mosaic of sub-basins. Each basic subcatchment has dimensional and functional characteristics and represents a land area that collects rainwater and allows infiltration, evapotranspiration, and drainage to a specific node or another subcatchment. The hydraulic module deals with propagating flows through the sewerage conveyance network, including pipes, channels, and storage structures. It calculates flow rates, water level, and velocities throughout the system, considering factors such as pipe roughness, slope, and geometry.

SWMM also include a quality module that simulates the transport of pollutants in stormwater runoff. It can track various pollutants such as sediment, nutrients, heavy metals, and pathogens, allowing users to assess water quality impacts and the effectiveness of pollution control measures.

The EPA has recently expanded the capabilities of the SWMM software to model the hydrologic response characteristics of specific low-impact intervention techniques, such as permeable pavement, raingardens, green roofs, rainwater harvesting basins and

infiltration trenches. The model allows to accurately represent any combination of these intervention techniques within a study area to determine their effectiveness in managing stormwater and combined sewer systems (Rossman and Simon, 2022).

4.6.1 SWMM Processes scheme

The process scheme in SWMM encompasses the key components and the various hydrological and hydraulic processes involved in stormwater management. Six primary environmental components can be used to construct a modelling project: 1. external forcing information such as precipitation, temperature, and evaporation; 2. a land surface runoff component; 3. a subsurface groundwater component; 4. a conveyance system of pipes, channels, flow regulators, and storage units; 5. contaminant buildup, wash off, and treatment; 6. LID controls. The processes modelled by SWMM and their interactions can be schematized as in the following diagram (Fig. 45).

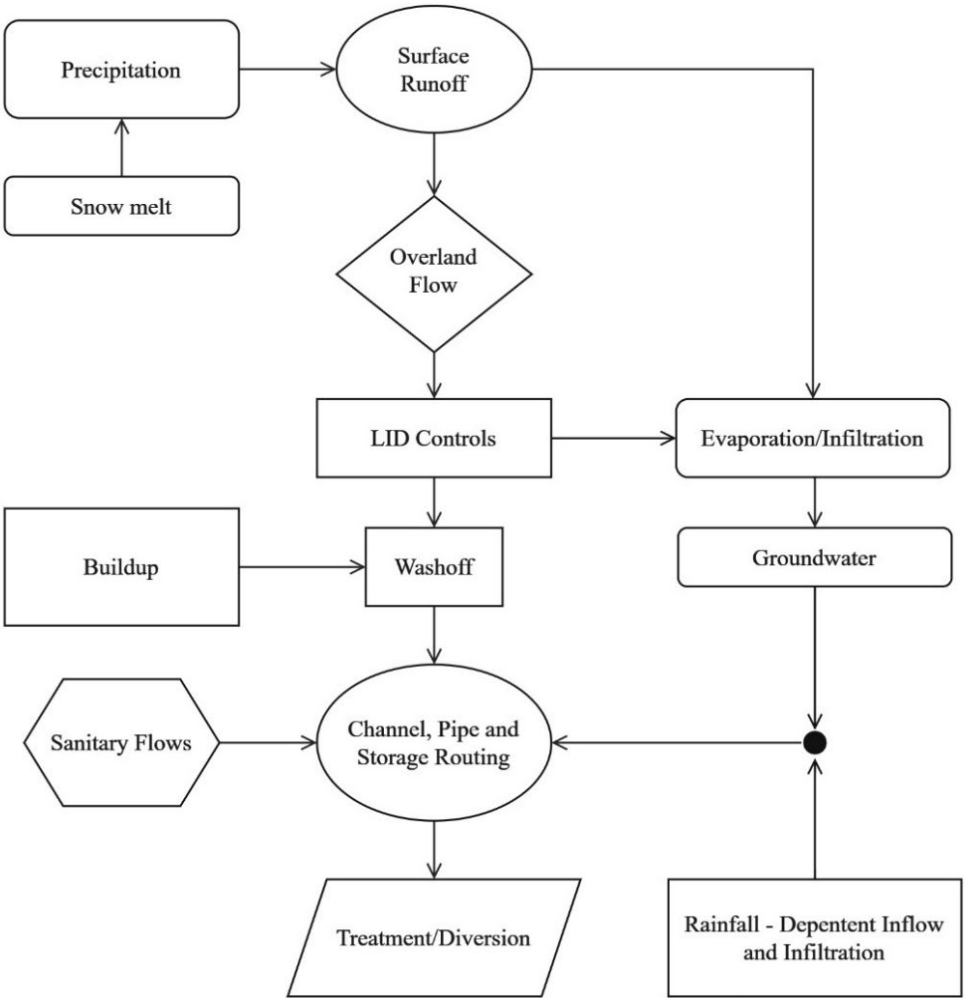

Fig. 45 – Processes modelled by SWMM

Rainfall as precipitation entered the model as a time series function represented by a rain gage within the model. In SWMM both single-event and long-term precipitation can be used for the simulations.

In order to simulate the snowmelt process, temperature data and windspeed are also needed. Another parameter that can be used is the evaporation which can be introduced in the model in various way: as a single constant value, as a monthly average value, or as a time series daily data. Precipitation is considered in the form of snow when the temperature is falls below a specific threshold chosen by the user.

SWMM divides the study area into one or more sub-areas called "subcatchments". The rain falls on each subcatchments and either infiltrates into the subsurface, evaporates, or flows on the surfaces directly into the receiving system (sewer, culvert, or natural water body). SWMM computes the infiltration process using either Horton's method, Green-Ampt method or Curve Number method.

Infiltration can also rise the water table underneath a subcatchment, causing ground water to slowly leak back into a conveyance system. By using this feature, the model can reproduce long recession periods associated with runoff hydrographs for unlined and natural channels.

To model subsurface flow, two reservoirs are assigned to each subcatchment: one representing vadose zone and the other representing deeper groundwater. Upper (vadose zone) compartment moisture content is assumed to be uniformly distributed, while lower (groundwater) compartment moisture content is assumed to be fully saturated. Water is directed from the vadose zone compartment into the groundwater compartment. Groundwater can percolate downward or be directed into the conveyance system. Both reservoirs can be affected by evapotranspiration, which is dependent on the depth of each one.

Modelling the dynamics of storage and flow from each reservoir is accomplished by performing a water balance while solving the model.

There are two primary options for modelling flow routing in SWMM: kinematic wave routing and dynamic wave routing. The kinematic wave routing model solves the continuity equation by assuming that the friction slope along a conduit is equal to its bottom slope. However, flow reversal, backwater effects, and pressurized flow cannot be accounted for by this method.

The dynamic wave model solves the full St. Venant equations for conservation of mass and momentum, and therefore does not have the restrictions. St. Venant equations can be solved by expressing them in finite-difference form, which depends on nodal heads at either end of conduit. In addition, continuity equations account for the change in nodal head based on the net nodal inflow and the surface area of the connecting conduits. At

each time step, these two sets of equations are solved together to provide an updated hydraulic solution.

Pollutant buildup and wash-off are governed by a functional relationship selected by the user. Surface buildup is modelled using a power function, exponential function, or Langmuir saturation function.

The rate of pollutant wash-off is a function of overland flow rate and proportional to the pollutant mass remaining. As an alternative, wash-off can be modelled with a rating curve in which mobilization is solely dependent on flow, independent of buildup, or by a constant concentration (the so-called Event Mean Concentration). It is possible to model the pollutant treatment (as a result of settling or filtration) as a removal rate at each node, making it a function of water depth, hydraulic residence time, and other variables. Mass balance and advection are then used to model the fate and transport of pollutants in the conveyance system. The user can specify the rate constant for the first-order reaction of pollutant decay.

In the LID Module, surface, pavement, soil, storage, and underdrain portions of a LID unit are modelled as several interconnected, fully mixed layers. Each layer's storage is dynamically controlled by infiltration, drainage, and overflow. Bioretention cells, infiltration trenches, porous pavement, rain barrels, vegetated swales, green roofs, and street planters can all be explicitly modelled by SWMM through the LID Module.

Hydraulic conductivity and moisture content are assumed to have an exponential relationship for determining infiltration rates in soil layers. An outflow from the storage zone into the native soil beneath the unit occurs at a constant rate determined by the user while the underdrain flow is represented by an orifice-type equation. Depending on the type of LID, each layer type is present or absent; for example, vegetative swales only have the surface layer, whereas bioretention systems can have surface, soil, storage, and underdrain layers.

4.6.2 Model Overview

The study area was divided into 374 subcatchments, 402 conduit link, 417 nodes, and 19 outfall nodes (red spots on the map) located at spillways locations distributed throughout the network (see Fig. 46).

The impervious fraction calculation was performed within a GIS environment, taking into account various surface types identified, while excluding areas where stormwater management occurs through alternative infiltration systems. These excluded areas were not considered in the model. Additionally, within the GIS environment, the average slope and area of each basin were calculated alongside the impervious fraction.

Fig. 46 – a) Generalized map of the study area with subcatchments and sewerage network, b) SWMM Model with background.

The analysis of land use data revealed that 83% of the industrial area is covered with impervious surfaces where rooftops represent the 33% while road and parking lot represent the 50%.

4.6.3 Subcatchments

SWMM simulates runoff quantity and quality by modelling a catchment as a collection of irregularly shaped subcatchment areas that receive the rainfall and generate different hydrologic responses including surface runoff, infiltration, and evaporation.
The subdivision in small areas allow to better evaluate the effect of spatial variability in topography, drainage pathways, land use and soil characteristics have on runoff generation. SWMM conceptualizes each subcatchment as a rectangular surface characterised by site-specific properties like area, constant slope S, width W, percent of imperviousness and soil properties that conveys the water to a single discharge point as shown in Fig. 47. The surface runoff produces by rainfall over a surface is generated by modelling the subcatchment as a non-linear reservoir (Rossman and Simon, 2022).

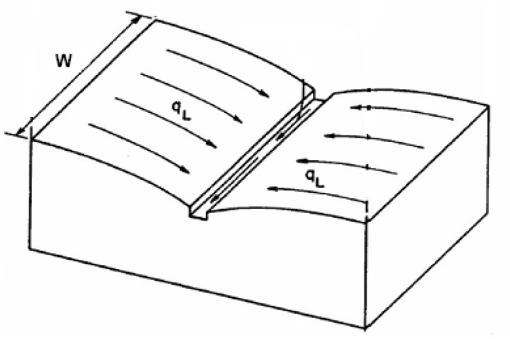

Fig. 47 – Conceptual representation of a subcatchment (Rossman and Simon, 2022)

Subcatchments are divided into pervious and impervious subareas where the surface runoff can infiltrate into the upper soil zone of the pervious subarea, but not through the impervious one. Impervious areas can be also divided into two subareas characterized by different depression storage values.

SWMM tracks the runoff generated from each subcatchment during a simulation period marked by regular time steps. In this scheme, each subarea receives inflows from precipitation and accounts for water losses due to evaporation and infiltration processes. The water pond on the subcatchment surface to the depth d (Fig. 48)

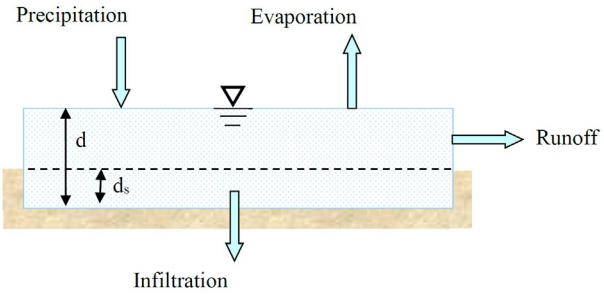

Fig. 48 - Conceptual view of surface runoff (Rossman and Simon, 2022)

The excess volume between the depth d_s, which is the maximum storage depth, and the depth d become runoff outflow q. The depression storage takes into consideration of the initial rainfall abstractions such as surface ponding, interception by flat roofs and vegetation. By solving numerically, a water balance equation over the subcatchment, the depth of water over the subcatchment d is continuously updated with time.

From the conservation of mass, the net change in depth d per unit of time t is the difference between the inflow and outflow rates over each subcatchment (Rossman and Simon, 2022):

$$\frac{\partial d}{\partial t} = p - e - f - q \qquad (4.14)$$

where:

- p is the rainfall plus the snowmelt rate (mm/h);
- e is the surface evaporation rate (mm/h);
- f is the infiltration rate (mm/h);
- q is the runoff rate per unit area (mm/h).

The Manning's equation is used to express the runoff volumetric flow rate Q (m^3/s) as follows, assuming that flow occurs uniformly along the subcatchment surface as a rectangular channel with width W (m), height d–d_s, and slope S:

$$Q = W \frac{1.49}{n} S^{\frac{1}{2}} (d - d_s)^{\frac{5}{3}} \quad (4.15)$$

where:

- W is the width of subcatchment overland flow (m);
- n is the surface Manning's coefficient (s/m1/3);
- S is the average slope of the subcatchment (m/m);
- d is the depth of water over the subcatchment (m);
- d_s is the maximum depression storage.

The area of each subcatchment, along with the slope and the percentage of impervious surface, was calculated within a GIS environment. In Fig. 49, an excerpt from the SWMM table regarding the subcatchments and their respective geometric characteristics is shown.

[SUBCATCHMENTS]

;;Name	Rain Gage	Outlet	Area	%Imperv	Width	%Slope	CurbLen	SnowPack
Sub_S_235	Continuo	S_235	0.07500	56.0000	15.4	2.00000	0.00000	
Sub_S_236	Continuo	S_236	0.15600	64.7435	22.3	1.10000	0.00000	
Sub_S_2_10	Continuo	S_2_10	0.15400	70.7792	22.2	0.80000	0.00000	
Sub_S_237	Continuo	S_237	0.15700	91.7197	22.3	0.20000	0.00000	
Sub_S_238	Continuo	S_238	0.15500	89.0322	22.3	0.10000	0.00000	
Sub_S_2_9	Continuo	S_2_9	0.07100	88.7323	15	0.70000	0.00000	
Sub_S_239	Continuo	S_239	0.22000	61.3636	26.4	0.40000	0.00000	
Sub_S_240	Continuo	S_240	0.03700	62.1621	10.7	0.20000	0.00000	
Sub_S_247	Continuo	S_247	0.39100	39.6419	35.3	0.20000	0.00000	
Sub_S_245	Continuo	S_245	0.30100	46.8438	30.9	0.10000	0.00000	
Sub_S_249	Continuo	S_249	0.21900	44.2922	26.4	0.10000	0.00000	
Sub_S_241	Continuo	S_241	0.06900	84.0579	14.7	0.20000	0.00000	

Fig. 49 – Extract from tables of the .inp file concerning the geometric characteristics of each subcatchments.

To calculate the percentage of imperviousness, all types of surfaces falling within the study area were categorized into four main classes: rooftops, roads, green urban areas (such as flowerbeds, public and private gardens), and extra-urban green areas (agricultural greenery) as shown in Fig. 50.

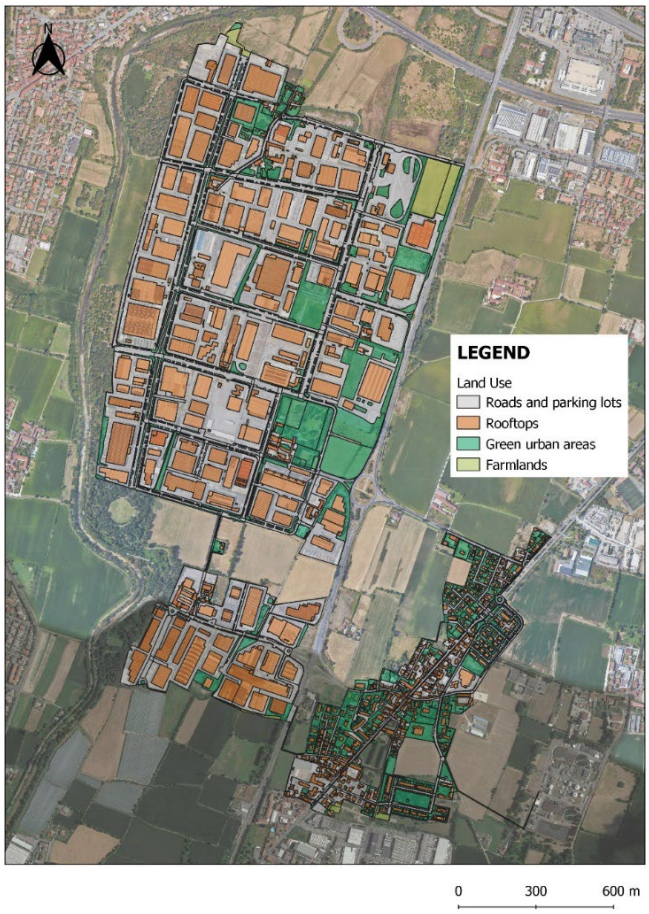

Fig. 50 – Land use of the study area

Infiltration model – Modified Horton Method

Infiltration occurs when rainfall penetrates the ground surface and fills the pores of the soil beneath (Akan and Houghtalen, 2003). In pervious areas, it is usually responsible for the greatest portion of rainfall losses. For this study the Horton Modified Method was used to estimate how much rainfall infiltrates into the soil, affecting the runoff and flow patterns. Horton's infiltration model is a widely known method for simulating the infiltration of water into the soil. This method relies on empirical observations through which it was noted that infiltration rate decreases exponentially over time as the soil becomes saturated, starting from an initial peak rate and reaching a minimum rate during an extended rainfall event.

SWMM 5 includes a modified version of the Horton infiltration method developed by A. O. Akan (Rossman and Simon, 2022).

The method uses the same parameters as the Horton method, but instead of tracking the time along the Horton decay curve it measures the incremental infiltration volume exceeding the minimum infiltration rate. According to this method, part of the water

infiltrating the soil will percolate deeper into the soil at a minimum infiltration rate (the saturated hydraulic conductivity of the soil). Therefore, the difference between actual and minimum infiltration rates accumulates just below the surface, causing the infiltration capacity to decrease over time. Infiltration estimates are supposed to be more accurate with this method when rainfall intensities are low.
As with the original Horton method, the modified method starts with an exponential decay equation:

$$f_p = f_\infty + (f_0 - f_\infty)e^{-k_d t} \quad (4.16)$$

where:

- f_p is the infiltration capacity into soil (mm/s)
- f_∞ is the minimum or equilibrium value of f_p at t = ∞ (mm/s)
- f_0 is the maximum or initial value of f_p at t = 0 (mm/s)
- t is the time from beginning of storm (s)
- k_d is the decay coefficient (s^{-1})

As a result of multiple storm events occurring in a set period, infiltration capacity will be regenerated (recovered) during dry weather periods and it can be assumed that the instantaneous recovery rate is proportional to the difference between the current capacity and the maximum capacity:

$$f_r = f_0 - (f_0 - f_{r0})e^{-k_r t} \quad (4.17)$$

Where:

- f_r is the infiltration capacity during recovery (mm/s)
- f_{r0} is the infiltration capacity at some time during the recovery (mm/s)
- t is the recovery time (s)
- k_r is the decay coefficient for the recovery curve (s^{-1})

Essential input parameters for this method encompass the maximum and minimum infiltration rates, a decay coefficient which govern the rate at which infiltration decreases over time, and the time it takes for a fully saturated soil to undergo complete drying:

- The initial infiltration capacity f_0 is the maximum infiltration rate on the Horton curve (mm/h) and depends primarily on soil type, initial moisture content and surface vegetation conditions.
- The minimum infiltration rate on the Horton curve f_∞ (mm/h) is essentially equal to the soil's saturated hydraulic conductivity, K. The value is also the limiting

infiltration rate when water is ponded on the surface, at low depths.

- Decay Constant k_d represents the infiltration rate decay constant for the Horton curve (h^{-1}). This value is considered a constant for the soil independent of initial moisture content.
- Drying Time is the time in days for a fully saturated soil to dry completely. Drying times are typically longer than wetting times, implying $k_r < k_d$. Typical values range from 2 to 14 days.
- Max. Infil. Vol. is the maximum infiltration volume possible (mm). It can be estimated as the difference between a soil's porosity and its wilting point times the depth of the infiltration zone.

Even though the Horton equation is probably the most used of the several infiltration equations, there is little guidance to help users determine the values of the parameters f_0 and k_d (nevertheless, some guidance are available for value f_∞). It is ideally recommended to estimate the actual values of f_0 and k_d based on results from field infiltrometer tests conducted at several sites in the watershed and for several different antecedent wetness conditions since these parameters depend on soils, vegetation, and initial moisture content, but no field measurements were available for the case study area. As reported in the "Carta Idrogeologica. V.I.-ALall 04c1" of the Brescia municipality land management plan (PGT) the soil of the industrial area is mostly composed of gravels, sands and silts and it is characterized by a high infiltration rate. According to the SWMM 5.2 user's manual (Rossman and Simon, 2022) 127 mm/h and 50.0 mm/h were selected as the maximum and minimum infiltration rates. The maximum infiltration value refers to sandy soils with little vegetation, whereas the minimum infiltration rate refers to an average value between sand and loamy sand values (Tab. 25).
The corresponding decay constant and drying time were 4 and 2 days, respectively, as suggested in the SWMM user's manual for sandy soil in case of no field data available.

Tab. 25 – Soil Characteristics (Rawls, W. J. et al., 1983)

Soil Texture Class	**K**	**Ψ**	**ϕ**	**FC**	**WP**
Sand	120.40	49.02	0.437	0.062	0.024
Loamy Sand	29.97	60.96	0.437	0.105	0.047

*K is the saturated hydraulic conductivity [mm/h], Ψ is the suction head [mm], ϕ is the porosity [-], FC is the field capacity [-], WP is the wilting point [-]

4.6.4 Conduits and nodes

SWMM uses uniform, kinematic, or dynamic routing to model the water flow into the pipes modelled as conduits (Rossman and Simon, 2022). In this study the dynamic wave routing was used to solve the complete one-dimensional Saint Venant flow equations and to represent the water flow within the pipes. These equations consist of the continuity and momentum equations (reported below) for conduits and a volume continuity equation at nodes:

$$\text{Momentum Equation: } \frac{\vartheta Q}{\vartheta t} + \frac{\vartheta(\frac{Q^2}{A})}{\vartheta x} + gA\frac{\vartheta H}{\vartheta x} + gAS_f = 0 \quad (4.18)$$

$$\text{Continuity Equation: } \frac{\vartheta Q}{\vartheta x} + \frac{\vartheta A}{\vartheta t} = 0 \quad (4.19)$$

where:

- x is the distance (m)
- t is the time (s)
- A is the flow cross-sectional area (m^2)
- Q is the flow rate (m^3/s)
- H is the hydraulic head of water in the conduit (equal to Z+Y) (m)
- Z is the conduit invert elevation (m)
- Y is the conduit water depth (m)
- S_f is the friction slope (head loss per unit length)
- g is the acceleration of gravity (m/s^2)

The friction slope S_f is expressed by the Manning equation:

$$S_f = (n)^2 \frac{Q\,|U|}{AR^{4/3}} \quad (4.20)$$

where:

- n is the Manning roughness coefficient ($s/m^{1/3}$)
- R is the hydraulic radius of the flow cross-section (m)
- U is the flow velocity equal to Q/A (m/s). The absolute sign makes S_f a directional quantity (since Q can be either positive or negative) and ensures that the frictional force always opposes the flow.

As a result of this form of routing, it is possible to represent pressurized flow when a closed conduit becomes full, so that flows can exceed the full normal flow value. Moreover, with the dynamic wave routing, channel storage, backwater, entrance/exit losses, flow

reversal, and pressurized flow can be also considered. This method fit perfectly for the case study system since it is subjected to backwater effects due to downstream flow restriction and the presence of flow regulation (weirs and orifices). Manning's coefficients used for the case study are reported in the Tab. 26.

Tab. 26 - Coefficients for closed conduits adopted in the SWMM Model

Material	**Manning's Coefficient**	**Strickler's Coefficient**
Concrete	0.01800 $s/m^{1/3}$	55 $m^{1/3}/s$
PVC	0.01205 $s/m^{1/3}$	80 $m^{1/3}/s$
GRES	0.01538 $s/m^{1/3}$	65 $m^{1/3}/s$

In SWMM there is also a continuity relationship at nodes (junctions) that connect pipes (conduits) together. Nodes and links are grouped in "node assemblies" that consist of one node and half the length of each link connected to it. In each assembly the difference between the inflow and outflow must be equal to the change in volume over time as expressed by the following equation:

$$\frac{\vartheta V}{\vartheta t} = \frac{\vartheta V}{\vartheta H}\frac{\vartheta H}{\vartheta t} = A_s \frac{\vartheta H}{\vartheta t} = \sum Q \qquad (4.21)$$

where:

- V is the node assembly volume (m^3)
- As is the node assembly surface area (m^2)
- ΣQ is net flow into the node assembly (m^3/s)

Wet weather runoff or dry weather sanitary flow are included in the ΣQ term in addition to the flow in the conduits connected to the node.
It is assumed that there is a continuous water surface between the water elevation at a node and the conduit that enter and leave it: flood occurs when a node's water depth exceeds the maximum available depth, and the excess flow pond on top of the node, re-entering the drainage system as capacity permits.

4.7 Validation and Calibration

The calibration and validation processes of the SWMM model were carried out using flow rate measured at two different points within the sewer network, along with rainfall data measured by a rain gauge installed in the northern part of the study area.

The calibration and validation strategy were based on comparing observed hydrographs with those simulated at the monitored cross-section. The Code of Practice for the Hydraulic Modelling of Urban Drainage Systems (2017) states that the model accuracy is satisfactorily when:

- The Relative Percentage Difference (RPD) of the peak flow rate value range between +25% to -15%;
- General shape of the hydrographs should be similar.

In addition to these criteria, Moriasi et al. (2015) also states that the Nash-Sutcliffe Efficiency index (NSE) value should be greater than 0.5. To assess the model performance with respect to the above-mentioned criteria, the RPD and NSE were calculated to quantitatively assess the model accuracy in reproducing the outflow hydrograph.
The RPD index, which is the ratio of the difference between the simulated and the observed values to the observed one, was calculated using the following equation:

$$RPD\ (\%) = \frac{(V - V_{ref})}{V_{ref}} \cdot 100 \qquad (4.22)$$

where:

- V is the simulated value;
- Vref is the measured value;
- (V – Vref) is the actual change.

This index was evaluated for each rainfall event for some particularly intense rainfall events that occurred during the observation period.
As for the NSE index proposed by Nash and Sutcliffe (1970), who approached the model calibration from a linear regression point of view, it was calculated using the following formula:

$$NSE = 1 - \frac{\sum_{t=1}^{T}(Q_o^t - Q_m^t)^2}{\sum_{t=1}^{T}(Q_o^t - \overline{Q_o})^2} \qquad (4.23)$$

where:

- Q_o^t is the observed flow (m^3/s);
- Q_m^t is the modelled flow (m^3/s);
- $\overline{Q_o}$ is the mean of the observed flow (m^3/s).

The NSE coefficient is a measure of how closely the ratio between observed and modelled values approaches the 45° linear regression line (Krause et al., 2005). The values of NSE ranges between 1 (comprised) and -∞, where 1 corresponds to a perfect match between

the observed and the modelled data. Values from 0 to 1 are generally considered optimal while negative values indicate that the mean value of the observed date is a better predictor.

Continuous simulations were initiated on 1/02/2023 and concluded on 31/07/2023. This choice allowed for the use of the entire dataset derived from the measurement campaign. The model was calibrated based on data measured over a six-month period, during which four particularly intense events occurred: the first event on 7th May with a peak intensity of 97.2 mm/h, the second event on 24th May with a peak intensity of 130.8 mm/h, the third event on 21st July with a peak intensity of 118.8 mm/h, followed by another event on 24th July with a peak intensity of 118.8 mm/h. These four events plus one additional moderate event, which occurred on June 4th with a peak intensity of 48 mm/h, were used for model calibration and validation. Fig. 51 shows the placement points of measuring instruments within the sewer network.

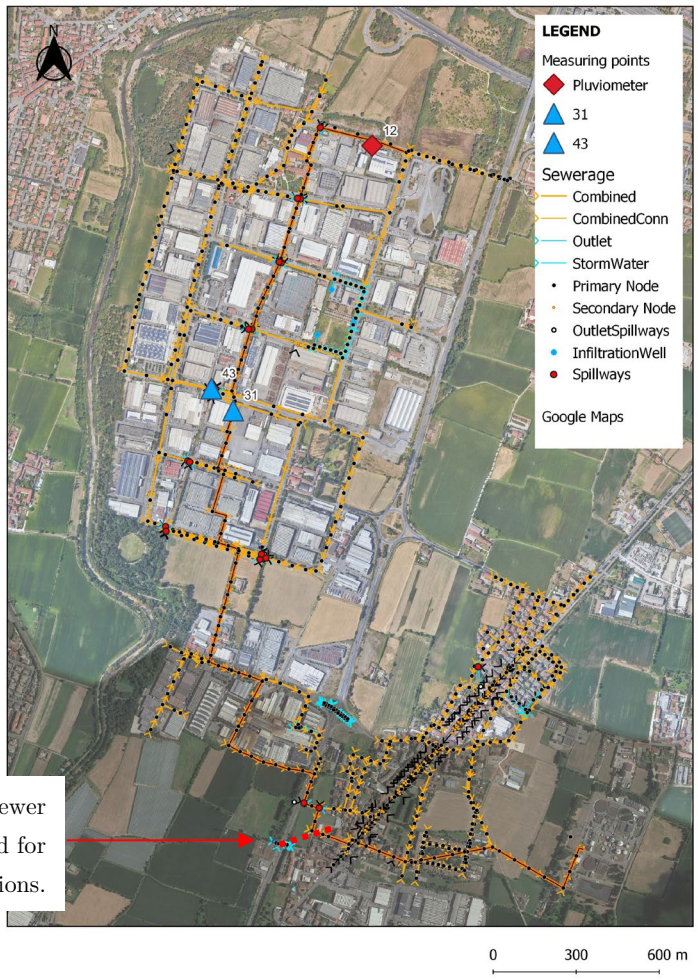

Ending point of the sewer network considered for the simulations.

Fig. 51 - Position of measurement points within the sewer network

The model reproduced with acceptable matching capabilities the shape of the observed hydrographs presented in Fig. 52 and Fig. 53 which shows the rainfall events used during the calibration and validation phases. In particular, the timing and magnitude of peak flow rate are accurately predicted.

Despite a good correspondence between the measured and simulated data, some differences in peak flows and volumes are still evident, likely attributed to a malfunction (blockage) of the measuring instruments that occurred during the increased inflow associated with intense rainfall events.

The quantitative assessment of the model performance is summarized in Tab. 27 where the RPD values and the NSE index of the peak flow rate are reported for both calibration and validation events, revealing that the model effectively captures the hydraulic behaviour of the network.

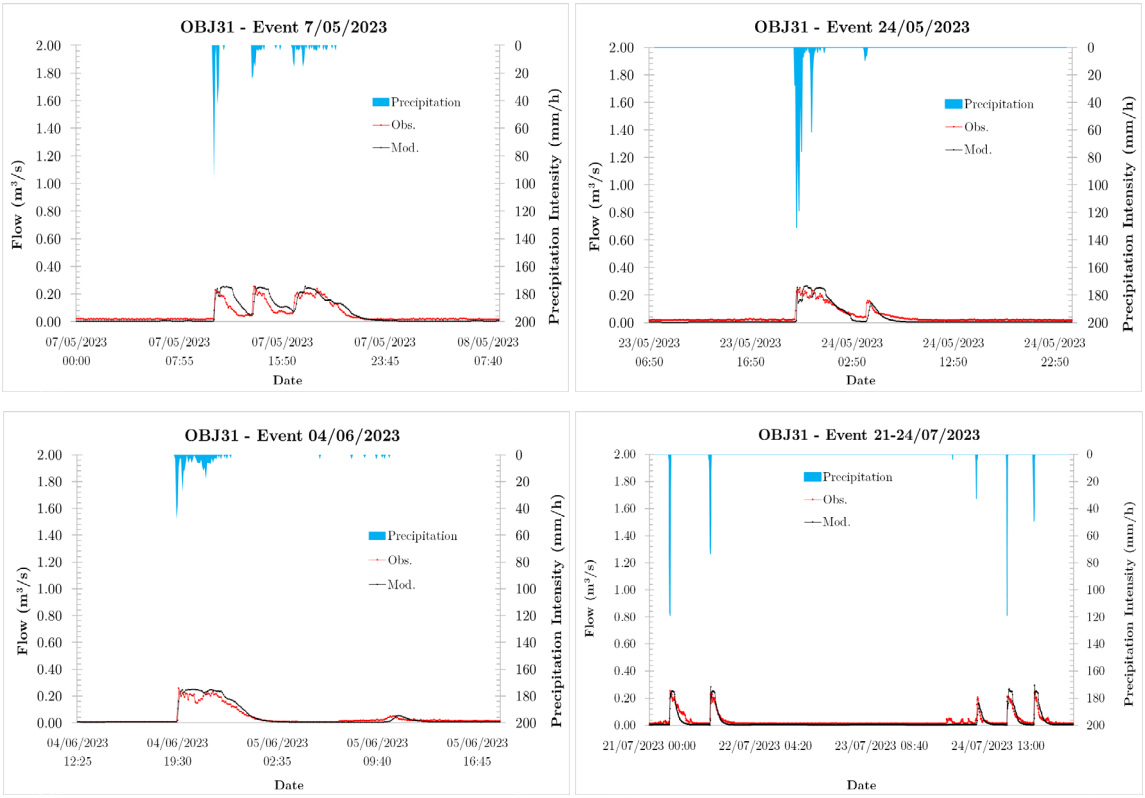

Fig. 52 - Precipitation hyetograph for five events and comparison between simulated flows (black line) and measured flows (red line) for the point 31.

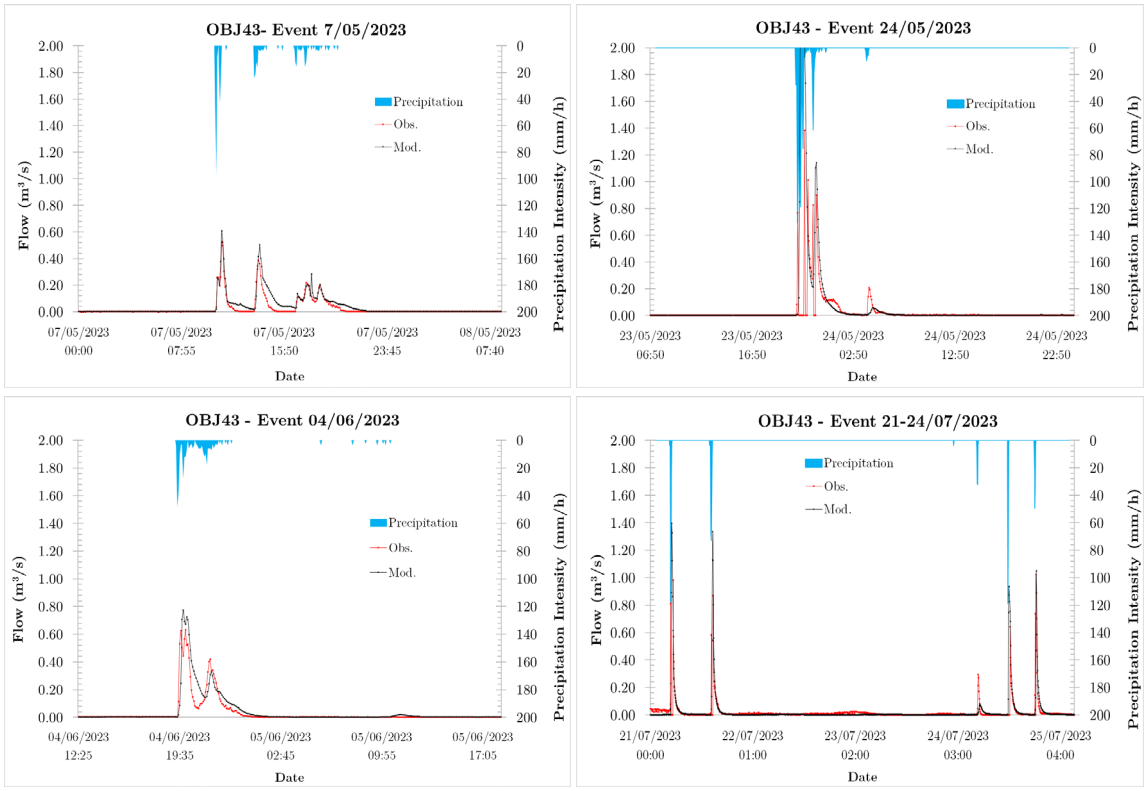

Fig. 53 - Precipitation hyetograph for five events and comparison between simulated flows (black line) and measured flows (red line) for the point 43.

The results show that the model can simulate with an acceptable accuracy the shape of the hydrographs observed. Specifically, the Relative Peak Differences (RPD) values for the measurement point OBJ31 are under 25%, demonstrating that the model accurately represents both the flood peak and the hydrograph shape.

As for the RPD values related to the other measurement point, (Point 43), it is observed that during three out of the five events (May 24th, July 21st, and July 24th), where rainfall intensities exceeded 100 mm/h, the instrument experienced a temporary blockage causing a brief interruption in flow measurement for a few minutes. The reported RPD value in the table corresponds to the last measured flow value before the blockage occurred. Results of the validation procedure reveal the suitability of the model to describe the response of the sewerage as confirmed by the NSE values greater than 0.5.

Tab. 27 - Relative Percentage Difference (RPDs) and Nash-Stutcliffe Efficiency (NSE) index of the peak flow rate for the rainfall events used for the calibration and validation of the model. The asterisk marks events where instrument experienced issues or blockages.

Object	Event	Peak Flow Obs. (m^3/s)	Peak Flow Mod. (m^3/s)	RPD (%)	NSE (Flow) (-)
Point 31	7th May 2023	0.228	0.251	9.94	0.64
	24th May 2023	0.254	0.258	1.46	0.70
	4th June 2023	0.258	0.246	-4.51	0.88
	21st July 2023	0.254	0.252	-0.79	0.74
	24th July 2023	0.224	0.269	20.09	0.71
Point 43	7th May 2023	0.527	0.609	15.51	0.78
	24th May 2023*	1.382	2.436	76.22	0.66
	4th June 2023	0.625	0.774	23.85	0.67
	21st July 2023*	0.983	1.396	42.06	0.65
	24th July 2023*	0.643	0.937	45.20	0.55

* The measuring instrument has experienced a blockage

The parameters that significantly influence calibration predominantly pertain to the characteristics of subcatchments, particularly Dstore-Imperv and Dstore-Perv. These parameters signify the depth of depression storage on impervious and pervious areas of the subcatchments, respectively, along with Width, representing the characteristic width of the overland runoff flow path. Additionally, hydrological parameters associated with the infiltration model, notably the Min. Infil. Rate played a crucial role in calibration. From the calibration and validation process, the following reference values were established (Fig. 54):

- For the Manning's Coefficient (n), a value of 0.012 was utilized for impervious surfaces, while a value of 0.15 was applied for pervious surfaces, in line with recommendations from the SWMM User's Manual for smooth concrete and grass surfaces respectively.
- Depression storage values were standardized at 1.5 mm for impermeable surfaces (Dstore-Imperv) and 3.0 mm for permeable surfaces (Dstore-Perv).

```
673   [SUBAREAS]
674   ;;Subcatchment   N-Imperv   N-Perv     S-Imperv   S-Perv     PctZero    RouteTo    PctRouted
675   ;;-------------- ---------- ---------- ---------- ---------- ---------- ---------- ----------
676   Sub_S_345        0.012      0.15       1.50       3.00       0.0        OUTLET
677   Sub_S_344        0.012      0.15       1.50       3.00       0.0        OUTLET
678   Sub_S_352        0.012      0.15       1.50       3.00       0.0        OUTLET
679   Sub_S_351        0.012      0.15       1.50       3.00       0.0        OUTLET
680   Sub_S_349        0.012      0.15       1.50       3.00       0.0        OUTLET
```

Fig. 54 – Extract from tables of .inp file concerning the subareas characteristics adopted as a result of the calibration process.

4.8 SWMM LID Module

The LID (Low Impact Development) module in SWMM is designed to simulate and analyse the impact of various low-impact development practices on stormwater runoff and water quality (Rossman and Simon, 2022). Specifically, these systems capture, infiltrate, and convey water preventing the subcatchment from flooding while removing pollutants from runoff.

The LID practices can be added in the model as separated sub catchments (fully allocated to the function of LID) or as a fraction of the impervious, and/or pervious surface, of an existing sub catchment as shown in Fig. 55.

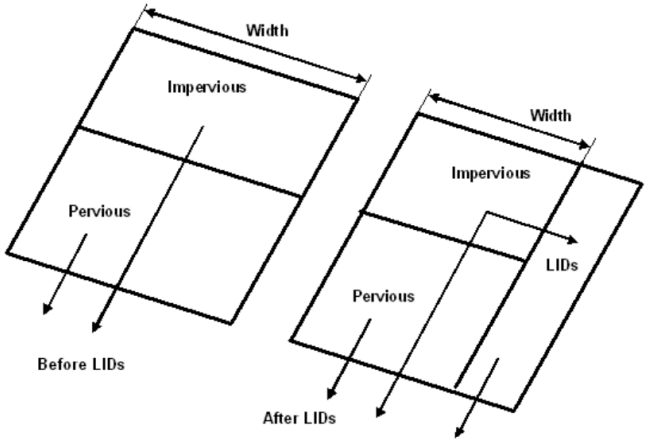

Fig. 55 – Adjustment of subcatchment after LID placement (Rossman and Simon, 2022)

All the LID controls based on nature technologies provide some amount of rainfall/runoff storage, evaporation of stored water and infiltration through the soil layers. They are schematized as a combination of vertical layers, corresponding to different soil types, whose properties (such as thickness, porosity, void ratio, hydraulic conductivity, and underdrain parameters) are defined on a per-unit-area basis, where the processes of infiltration, percolation, and storage take place. In Fig. 56 are shown the layers used to model a bio-retention cell and the flow pathways between them.

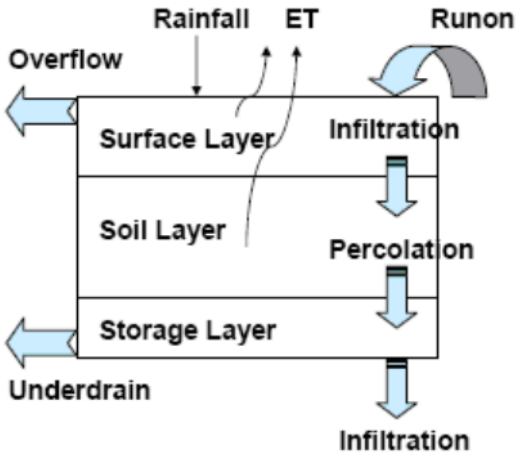

Fig. 56 - Conceptual model of a bio-retention cell in SWMM (Rossman and Simon, 2022)

The surface layer corresponds to the ground surface that receives direct rainfall and inflow from upstream impermeable areas. This layer is usually vegetated and it stores excess inflow in depression storage. Water leaves the surface as outflow that either enters the drainage system or flows onto downstream land areas, or via evaporation to the atmosphere or infiltration to the soil layer. The intermediate soil layer is an engineered soil mixture or native soil used to support vegetative growth. The storage layer is a generally made of gravel that provides storage and it could be equipped with a drainage pipe which conveys water out of system into a common outlet pipe or chamber. Rainfall and runoff volume are infiltrated, evaporated, or stored in the LID until the volume entering exceeds its capacity. LID unit can also have an underdrain that enhances the functionality of the system by providing a means to manage and control water levels. In the following study, a single type of Low Impact Development (LID) practice was employed, and it will be described in the following paragraph.

4.8.1 Raingardens (or Bio-retention Cells) modelling

Raingardens are depressions that contain vegetation grown in an engineered soil mixture placed above a gravel drainage bed. They provide storage, infiltration and evaporation of both direct rainfall and runoff captured from surrounding areas. The raingarden system studied in the preceding section of this study can be accurately modelled using the SWMM LID type "Bio-Retention Cell" (Fig. 57) primarily due to the inclusion of the underdrain system, a feature absents in the software LID system labelled Raingarden. Zhang et al. (2020) also adopted this modelling approach for their raingarden study.

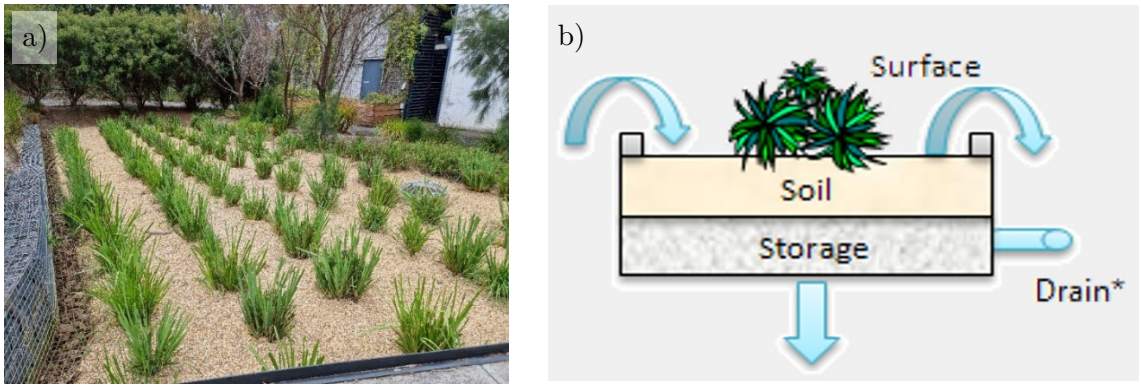

Fig. 57 – a) Bio-filter Garden located at the Monash University, Clayton Campus, b) Scheme of a Bio-retention cell in LID Control Editor (Rossman and Simon, 2022)

Their modelling involves defining a set of parameters associated with the soil types within them and the vegetation type in the surface layer.

The *Surface Layer Properties* page is used to describe the surface properties which include:

- Berm Height (or Storage Depth) is the maximum depth to which water can pond above the surface of the unit before overflow occurs.
- Vegetative Volume Fraction is the fraction of the volume within the storage depth filled with vegetation. For very dense vegetative growth it may be equal to 0.1 – 0.2.
- Surface Roughness is the Manning's roughness coefficient (n) for overland flow over surface soil cover.
- Surface Slope. This value must be less than 30% (Payne et al., 2015)

The *Soil Layer properties* page describes the properties of the engineered soil mixture. These properties encompass:

- Thickness of the soil layer. Typical values range from 450 to 900 mm for raingardens, street planters and other types of land-based bio-retention units.
- Porosity is the volume of pore space relative to total volume of soil (as a fraction).
- Field Capacity is the volume of pore water relative to total volume after the soil has been allowed to drain fully. Below this level, vertical drainage of water through the soil layer does not occur.
- Wilting Point is the volume of pore water relative to total volume for a well dried soil where only bound water remains. The moisture content of the soil cannot fall below this limit.

- Conductivity is the hydraulic conductivity for the fully saturated soil.
- Conductivity Slope is the average slope of the curve of log(conductivity) versus soil moisture deficit (porosity minus moisture content). Typical values range from 30 to 60.
- Suction Head is the average value of soil capillary suction along the wetting front.

In the *Storage Layer Properties* page, the properties of the gravel layer are described. The following data fields are displayed:

- Thickness (or Barrel Height) is the thickness of a gravel layer or the height. Crushed stone and gravel layers are typically 150 to 450 mm thick.
- Void Ratio is the volume of void space relative to the volume of solids in the layer. Typical values range from 0.5 to 0.75 for gravel beds. Note that porosity = void ratio / (1 + void ratio).
- Seepage Rate is the rate at which water seeps into the native soil below the layer. This would typically correspond to the Minimum Infiltration Rate for Horton infiltration.
- Clogging Factor is the total volume of treated runoff it takes to completely clog the bottom of the layer divided by the void volume of the layer. Clogging progressively reduces the Infiltration Rate in direct proportion to the cumulative volume of runoff treated.

The last properties page is the *Storage Drain Properties*. Raingardens usually have a drainage system that collects water that flows through the soil layers and conveys it to a water body or other location. This outlet can be different than the outlet of the LID's subcatchment. The drainpipe can be placed at some distance above the bottom of the storage layer, allowing a volume of runoff to be stored and infiltrated before any excess is captured by the drain. The Drain page of the LID Control Editor contains the following data entry fields:

- Drain Flow Coefficient and Drain Flow Exponent determines the rate of flow through a drainpipe as a function of the height of stored water above the drain's offset.
- Drain Offset Height is the height of the drain line above the bottom of a storage layer.
- Open Level is the height in the drain's Storage Layer that causes the drain to automatically open when the water level rises above it. The value 0 means that this feature is disabled.
- Closed Level it the height in the drain's Storage Layer that causes the drain to

automatically close when the water level falls below it. The default is 0.

- Control Curve is an optional curve that adjusts the computed drain flow as a function of the head of water above the drain.

The Green-Ampt equation is used to model infiltration into growth media of bioretention cells. SWMM models the flow through the underdrain pipe as a function of the hydraulic head accumulated above its base. It is calculated as a flow rate per unit area of the LID as described in the following equation:

$$q = Ch^n \quad (4.24)$$

where:

- q is outflow (mm/h);
- h is the height of saturated media above the drain (mm);
- C is the underdrain discharge coefficient ($mm^{1/2}/h$);
- n is the underdrain discharge exponent (-). A typical value for n would be 0.5 (making the drain act like an orifice).

To calculate the flow coefficient C the Torricelli's formula was used, which calculates the flow rate from a orifice as follows:

$$Q = C_c\, C_v\, A \sqrt{2gh} \quad (4.25)$$

where:

- Cc is the contraction coefficient equal to 0.61 (-),
- Cv is the velocity coefficient that ranges from 0.97 to 0.99 (-) and represents the relationship between the effective velocity v_e and the Torricellian velocity v_t;
- A is the cross-sectional area of the outlet (m^2);
- g is the acceleration of gravity (m/s^2);
- h is hydraulic head above the underdrain invert (m).

In order to have as unit mm/h, the acceleration of gravity unit was converted from m/s^2 to mm/h^2 and the underdrain discharge coefficient was calculated with the following equation:

$$C = 301444.88\, \frac{A}{A_{LID}} \quad (4.26)$$

where A is the orifice area (mm^2) and A_{LID} is the footprint area of the LID unit (mm^2). The raingardens implemented in the model have the same characteristics of those created in the laboratory for the previous part of the study related to the raingarden maintenance. In the detailed the stratigraphy is primarily comprised of a surface layer

made of fine sand (total depth of 30 cm), a soil layer made of coarse sand and sugar cane mulch mixture (depth of 35 cm) and a drainage layer made of gravel (depth of 10 cm). The parameter used for modelling the raingarden were chosen based on the literature, laboratory tests, or default values provided by the software manual. These parameters are detailed in the following table (Tab. 28).

Tab. 28 – SWMM parameters values used in the model for the Raingarden LID Control

Parameters	**Value**	**Source**
Surface		
Berm height (mm)	300	Design
Vegetation volume (-)	0.30	Calculated
Surface Roughness ($s/m^{1/3}$)	0.24	Rossman and Simon (2022)
Surface Slope (%)	0.50	Design
Soil		
Thickness (mm)	300	Design
Porosity (-)	0.437	Rossman and Simon (2022)
Field Capacity (-)	0.062	Rossman and Simon (2022)
Wilting Point (-)	0.024	Rossman and Simon (2022)
Conductivity (mm/h)	127.00	Rossman and Simon (2022)
Conductivity Slope (-)	48.00	Rossman and Simon (2022)
Suction Head (mm)	49.02	Rossman and Simon (2022)
Storage		
Thickness (mm)	400	Design
Void Ratio (Voids/Solids)	0.10	Design
Seepage Rate (mm/h)	5	
Clogging Factor (-)	-	Not considered
Drain		
Flow Coefficient ($mm^{1/2}/h$)	800	Calculated
Flow Exponent (-)	0.50	Rossman and Simon (2022)
Offset (mm)	10.00	Design

Raingardens were modelled and incorporated into the existing network as distinct subcatchments, serving as outlets for the current subareas, thereby effectively managing water from impervious surfaces and overflow from permeable ground within the existing subcatchments. The size of each raingarden was determined to be equal to the 2%, 3% or 4% (depending on the urban scenario simulated) of the effective impervious area EIA (Fig. 58).

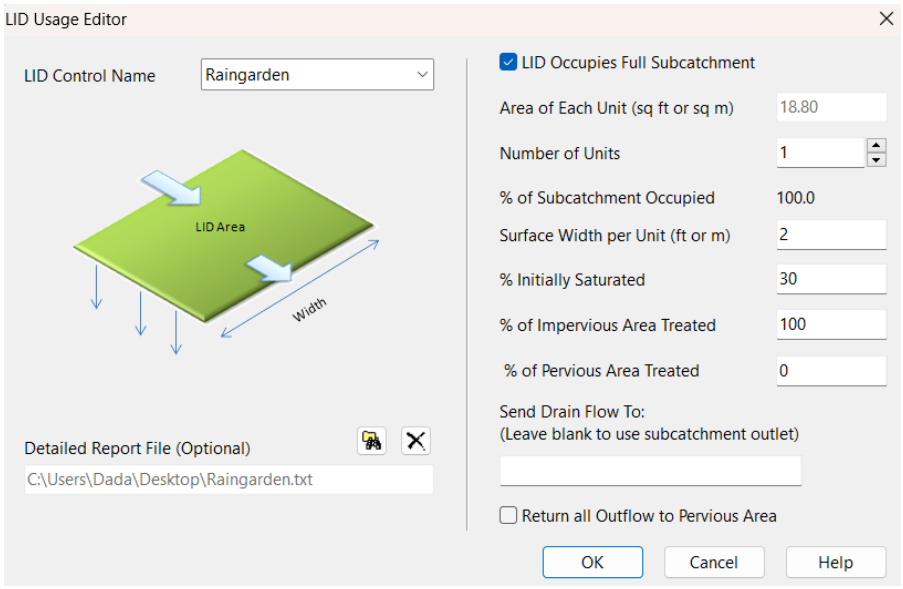

Fig. 58 – LID Usage editor window in SWMM

Since the simulation were performed both at rainfall event scale and in continuous mode, the initial saturation accounts for the retention recovery that occurs during the inter-event periods (Lucas and Sample, 2015). In the former case (rainfall event scale) the initial saturation of the raingarden was assumed equal to 0.3 (30%), while on the continuous simulations, the value was set to 1 (100%), assuming full saturation, which occurs after an intense meteorological event.

4.8.2 Raingarden Urban Integration: study context

Integrating raingardens into a densely urbanized industrial area, such as the one in the case study, poses significant challenges.

Firstly, the study area is characterized by an extensive transportation infrastructure specifically designed to accommodate the passage of large vehicles, thereby constraining the available space for implementing green infrastructures like raingardens. Furthermore, the predominant architectural feature comprises industrial buildings, often surrounded by parking lots and transit yards, further constraining potential sites for raingarden implementation. It is worth noting that some of the industrial properties in this area already manage rainfall runoff autonomously through other infiltration systems or internal water treatment facilities. In this context, the assessment of potential areas for raingarden implementation necessitates meticulous design considerations to ensure compatibility with existing infrastructure and operations. Given the limited available space, identifying suitable locations for raingardens becomes of primary importance, necessitating careful evaluation to ensure they effectively managing stormwater runoff

while seamlessly blending into the existing urban landscape. Additionally, the impact of transportation infrastructure on stormwater flow must be taken into account to ensure the effectiveness of these strategies.

A key strategy involves converting into raingarden existing flower beds especially those adjacent to roads or acting as road separators. Repurposing these green spaces offers several advantages, notably minimizing disruption to the surrounding environment (see example in Fig. 59 a) and b)). The areas outlined in red and blue can be replaced with two raingardens that collect and treat runoff coming from the road as shown in the figure on the right This allows for the smooth integration of raingardens into the urban landscape while enhancing water retention and filtration capacities, thereby improving the ecological functionality of this urban area.

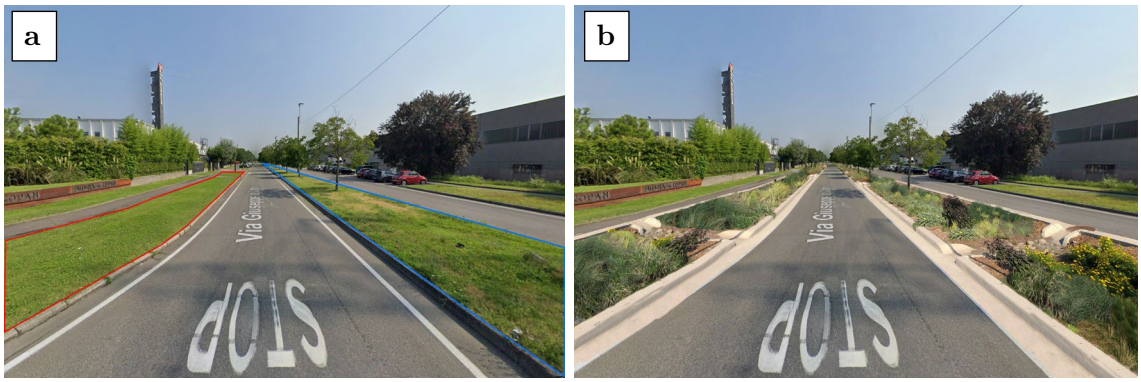

Fig. 59 - Example of raingarden implementation along Via Giuseppe di Vittorio. a) Current situation, b) Transformation of the road with the implementation of two raingardens.

Furthermore, considering the extensive transportation infrastructure, incorporating raingardens along roadside, sidewalks, or parking lot edges can effectively intercept and treat runoff from impervious surfaces. These locations serve as natural buffers, filtering pollutants before they reach water bodies or stormwater drainage systems, thereby contributing to reduce surface runoff and improving water quality.

Another effective approach involves identifying vacant spaces such as unused corners or areas between buildings and transforming them into raingarden installations. These spaces often have limited functionality but possess the potential to contribute significantly to stormwater management and environmental enhancement.

An example can be seen in Fig. 60, where a green corner (outlined in red) at the intersection of two roads in the study area that is currently neglected.

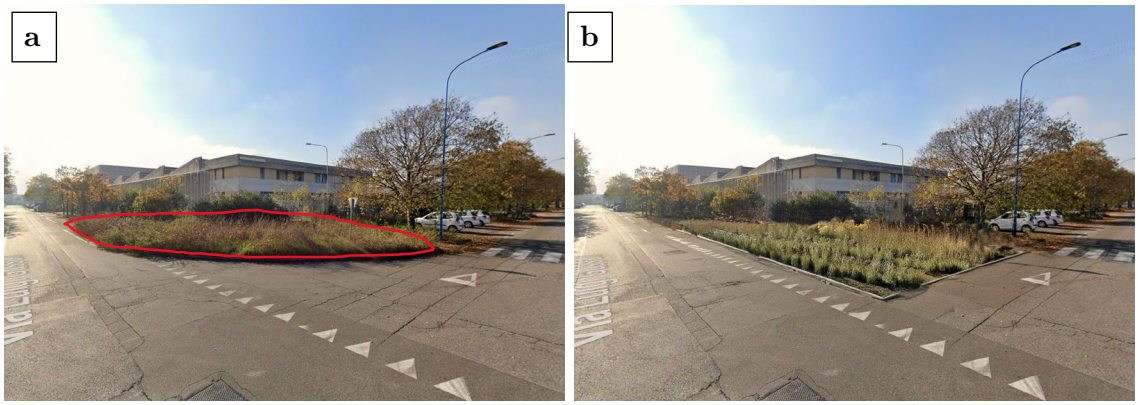

Fig. 60 - Example of raingarden implementation at the intersection of Via Serpente and Via Luigi Gussalli. a) current situation, b) transformation of the green area into a raingarden.

The rain gardens modelled in the study vary in size, ranging from a minimum of 3 m^2 (in the scenario with a 2% EIA reduction) to a maximum of 690 m^2 (in the scenario with a 4% EIA). This range reflects the flexibility and scalability of rain garden design, allowing for adaptation to different spatial constraints and stormwater management needs within the industrial context. By accommodating various sizes, rain gardens can be tailored to specific site conditions and contribute effectively to mitigating stormwater runoff across a spectrum of industrial settings. The integration of rain gardens not only provides effective stormwater management solutions but also enhances the aesthetic appeal of the industrial landscape, as shown in the previous image, in line with principles of sustainable urban development.

4.9 Results and discussion

Model simulations outcomes consist of outflow hydrographs for the reference and simulated scenarios. The reference scenario, BAU (Business as Usual) corresponds to the "do nothing" scenario, that is the current state of the sewerage and of the urban catchment. The other three scenario simulated differ in term of EIA reduction percentage of the catchment area.

As discussed in section 2.3 a raingarden is usually designed to manage the runoff volumes incoming from the impervious surface it serves. For an effective management, the area of the raingarden should range from 2 to 4% of the impervious area, depending on climate conditions. In this study the effectiveness of raingardens with an area equal to the 2%, 3% and 4% of the impervious area of the urban catchment was evaluated creating three different urban de-sealing scenarios.

The simulations were conducted both at the scale of single events (characterized by three different return periods equal to 2, 5, and 10 years) and continuous simulations using rainfall data from 2022 and 2023 collected by ARPA Lombardia.
Moreover, other six different climate scenarios were simulated to evaluate the hydrological capacity of raingarden to cope with the effects of climate change. In detail, three different Representative Concentration Pathways (RCP 2.6, 4.5, and 8.5), corresponding to 2.6, 4.5 and 8.5 W/m^2 greenhouse gas emissions scenarios, were simulated for two different time periods: 2040-2059 and 2080-2099.
These scenarios were developed on a seasonal scale, wherein correction factors for precipitation and temperature were calculated. These factors were used to simulate future precipitation and temperature variations for each season (summer, autumn, winter, and spring). These correction factors were derived from the ratio between projected precipitation and temperature values for the future period and historical precipitation and temperature values from the reference period of 1980-1999. For precipitation, the identified factors were used as multiplicative factors for the parameters of the rainfall probability lines, while the temperature correction factors were applied as temperature increments in degrees Celsius.
Finally, simulations were conducted to assess the influence of the initial saturation value on the performance of raingardens for three events with return periods of 2, 5, and 10 years, each lasting 30 minutes. The benefits of raingardens implementation were carried out comparing the total volumes, the timing and magnitude of peak flow of the of the model before and after their implementation.

4.9.1 Results for different return period events and EIA

The impact of different rainfall intensities is analysed here through three distinct simulations corresponding to different return periods: 2, 5, and 10 years. The hydrological performance, as presented in Tab. 29, demonstrates that the reduction in peak flow and volume is influenced by the return period of the rainfall event. Volume reduction, in particular, is significantly affected by the water retention capacity of the raingarden (RG), which is closely linked to the physical attributes of the Low Impact Developments (LIDs), such as void ratio and storage depth.
As noted by Qin et al. (2013), the effectiveness of LIDs is closely tied to their specific characteristics. Notably, an increase in effective storage capacity of the systems results in improved performance, especially when analysing flood volumes corresponding to escalating rainfall event magnitudes.

Tab. 29 – Hydrologic performance of the de-sealing scenario at assigned rainfall event return period (RP = 2, 5 and 10 year)

Hydrologic performance rate (-)	**Actual Climate** EIA reduction		
	2%	3%	4%
Rainfall event T = 2 years			
Peak reduction (%)	10.5	17.0	22.9
Volume reduction (%)	7.4	9.5	12.2
Hydrograph relay (min)	6	10	12
Rainfall event T = 5 years			
Peak reduction (%)	8.3	12.7	17.3
Volume reduction (%)	4.7	6.0	7.7
Hydrograph relay (min)	5	8	9
Rainfall event T = 10 years			
Peak reduction (%)	4.8	9.2	13.0
Volume reduction (%)	4.2	5.3	7.1
Hydrograph relay (min)	1	4	4

Observing the hydrograph depicted in Fig. 61, considering the 2% EIA scenario as an example, the transition from a 2-year to a 10-year return period event results in a reduction in performance by 4.8 % out of 10.5 % for peak flow reduction and by 4.2 % out of 7.4 % for volume reduction. Additionally, the results reported in Tab. 29 highlight that a raingarden with an area equal to the 2% of the EIA corresponds to peak reduction benefits ranging from 5 % to 10%. Conversely, with a 4% EIA decrease, these benefits double, ranging from a minimum of 13 % to a maximum of 23%. Moreover, significant advantages are observed in terms of reduced total discharge volumes and delayed peak flows.

This phenomenon becomes more pronounced from the hydrograph depicted in Fig. 60a: as the imperviousness of the urban catchment decreases, the simulated hydrograph flattens out, indicating a trend towards a hydrograph resembling pre-urbanization conditions. However, this effect diminishes as the return period increases, making raingardens less effective for higher return periods. Fig. 61b shows that the hydrologic performances in terms of peak and volume reductions are linearly dependent on the EIA reduction.

These findings are consistent with those obtained in previous studies (Kleidorfer et al., 2014; Palla and Gnecco, 2015). Regarding the peak flow delay, the relationship between the variation in EIA and the delay is better described by a second-degree polynomial curve.

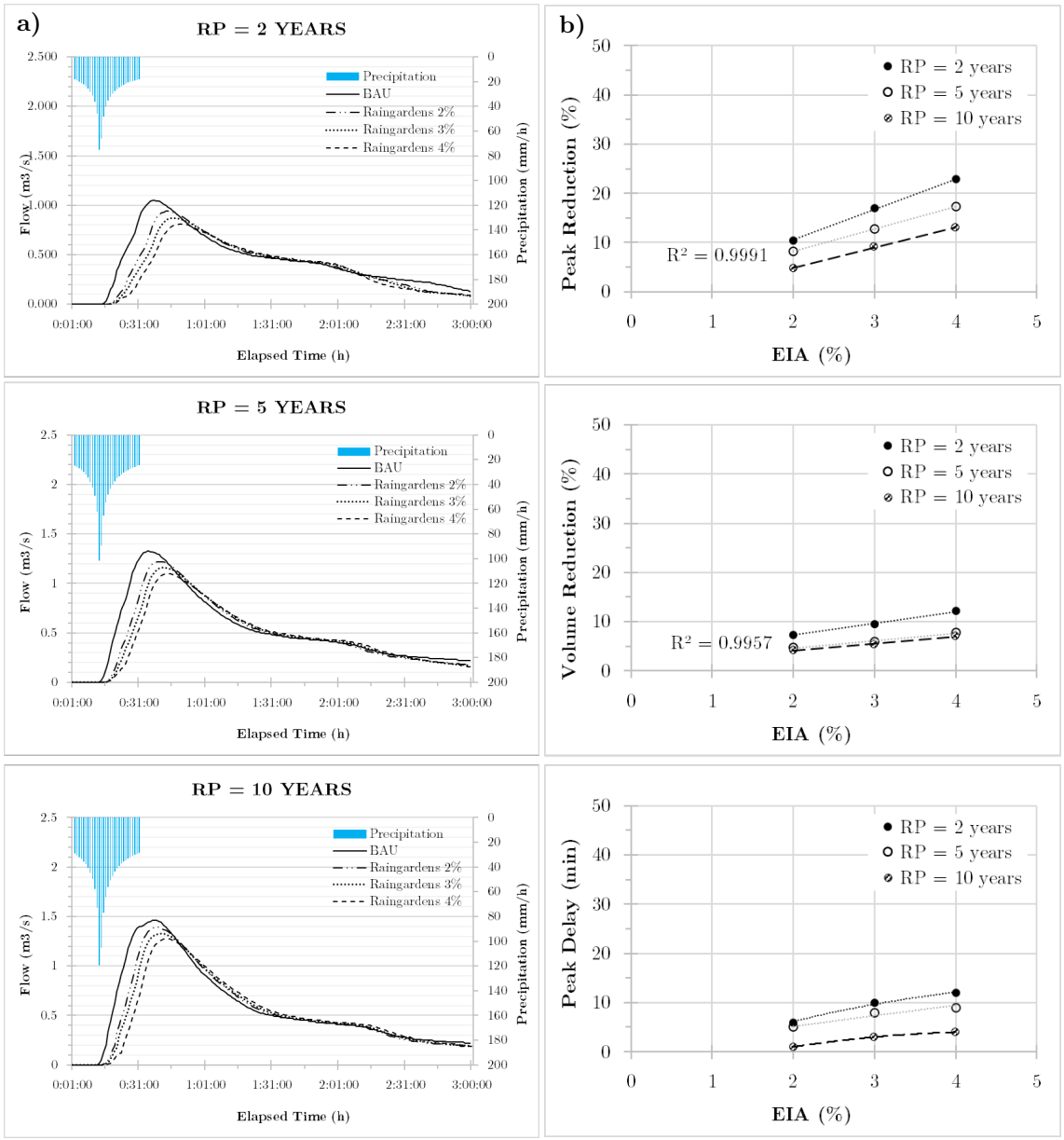

Fig. 61 – a) Hydrograph corresponding to the different EIA reduction scenarios at assigned rainfall event return period (T=2, 5 and 10 years). The reference BAU scenario indicates the "do nothing" scenario**. b)** Hydrologic performance vs. EIA reduction and return period.

4.9.2 Results for different initial saturation percentages

As highlighted in other studies (Sun et al, 2011; Palla and Gnecco, 2015; Lucas and Sample, 2015), the initial saturation represents one of the parameters that most influences the performance of LIDs.

In order to assess the impact of initial saturation on the effectiveness of RG, four different scenarios were simulated, varying the percentage of initial saturation from 30% to 60%, at intervals of 10. The simulations were conducted only in the urban scenario

corresponding to 4% EIA. Fig. 62a reports the comparison between the reference hydrograph and the hydrographs simulated at different initial saturation conditions.

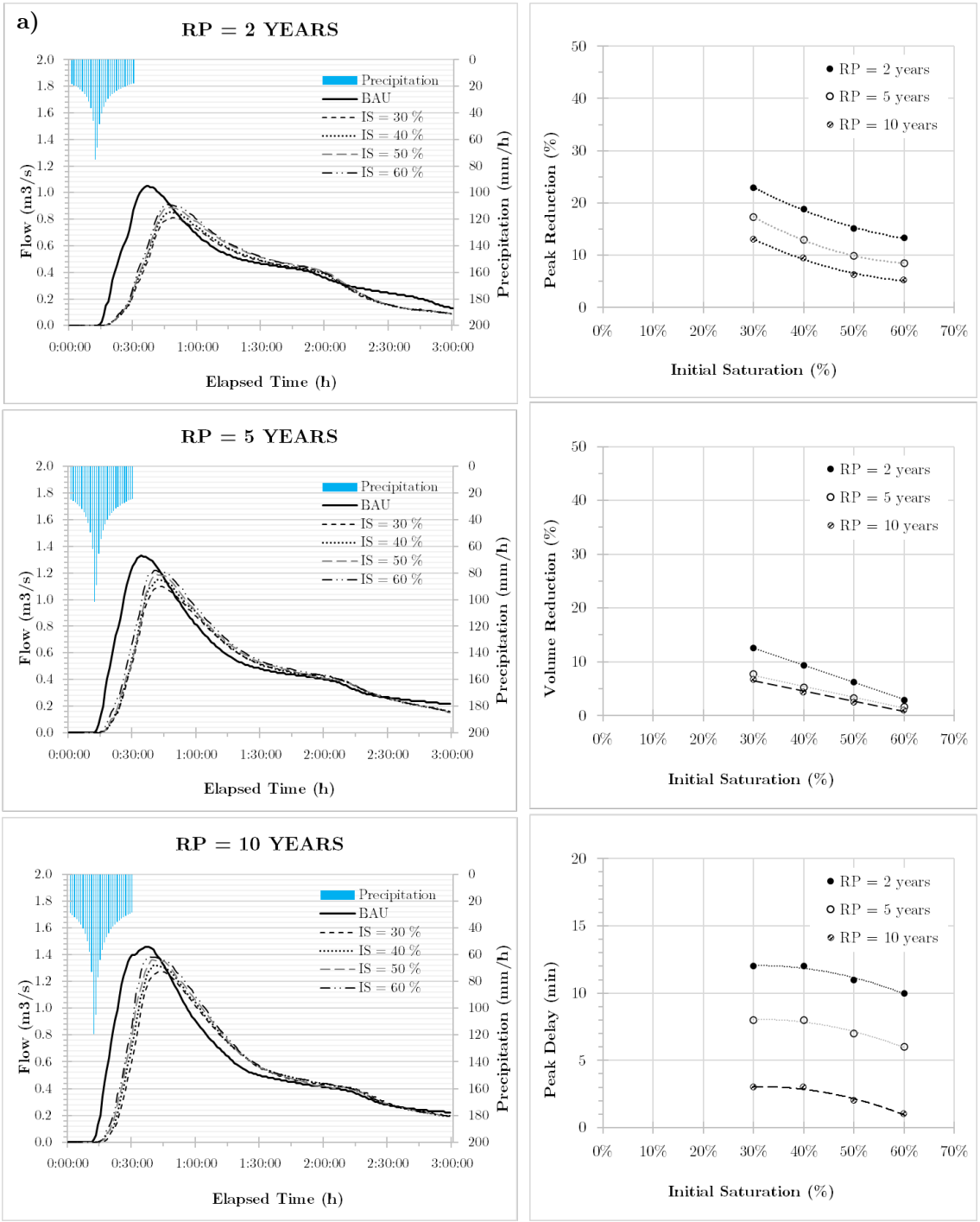

Fig. 62 – a) Comparison between the reference hydrograph and the hydrographs simulated at different initial saturation percentages of the raingardens; b) Hydrologic performance vs. initial saturation percentages for three rainfall event return period (2, 5 and 10 years). The simulations are referred to the EIA reduction scenario of 4%.

Simulation results shows that the variation in the initial saturation value is particularly noticeable in the changes to the peak and the behaviour of the two tails of the curve.
As the saturation level increases, the initial tail grows more rapidly, while there are no substantial differences observed in the final tail, which decreases uniformly for all four simulated saturation levels. This phenomenon is mor pronounced in the 10-return period event. The reduction in peak flow rate is less pronounced for higher saturation levels, while the delay of the peak shows no significant differences among the various simulated scenarios.
Fig. 62b shows the hydrologic performance as a function of initial saturation value. The percentage change in volume decreases linearly with increasing initial saturation percentage, consistent with the findings from simulations conducted varying the EIA (smaller EIA correspond to a smaller volume reduction effect).

The variations in terms of peak flow reduction and delay do not follow a linear trend. Although the limited data points do not allow for precise identification of the relationship between the variation in initial saturation level and the percentage decrease in peak flow or the delay of the peak flow, the function that best describes the trend of the values is represented by a second-degree polynomial function. A similar result was obtained by Palla and Gnecco (2015) for green roofs.

4.9.3 Results under different future climate scenarios

According to Tab. 22 the precipitation regime will undergo distinct variations depending on the season. For instance, there is an observed increase in precipitation during the winter season, exceeding 50% in the RCP 2.6 scenario for the period 2080-2099. Simultaneously, a reduction in precipitation will occur, particularly in autumn, for all analysed scenarios except for RCP 2.6 2080-2099, where the precipitation regime will remain relatively unchanged.
Based on these future climate scenarios, 96 simulations were conducted to compare the current state of the network ability to cope with climate change-induced variations. The results were then compared with two urban scenarios where raingardens were implemented with an EIA reduction of 2% and 4%.
Nie et al. (2009) conducted a similar study to assess the potential impact of climate change on sewer system performance. They explored scenarios involving increased rainfall intensities of +20%, +30%, and +50%, and investigated parameters such as surface flooding and combined sewer overflow (CSO). Their findings revealed a notable escalation in flooding volume, which they characterized as "dramatic.

The following figures (from Fig. 63 to Fig. 74) depict the output hydrographs obtained from all simulations, categorized by season and future climate scenario.

SUMMER

RCP 2.6 - (2040-2059)	RCP 2.6 - (2080-2099)

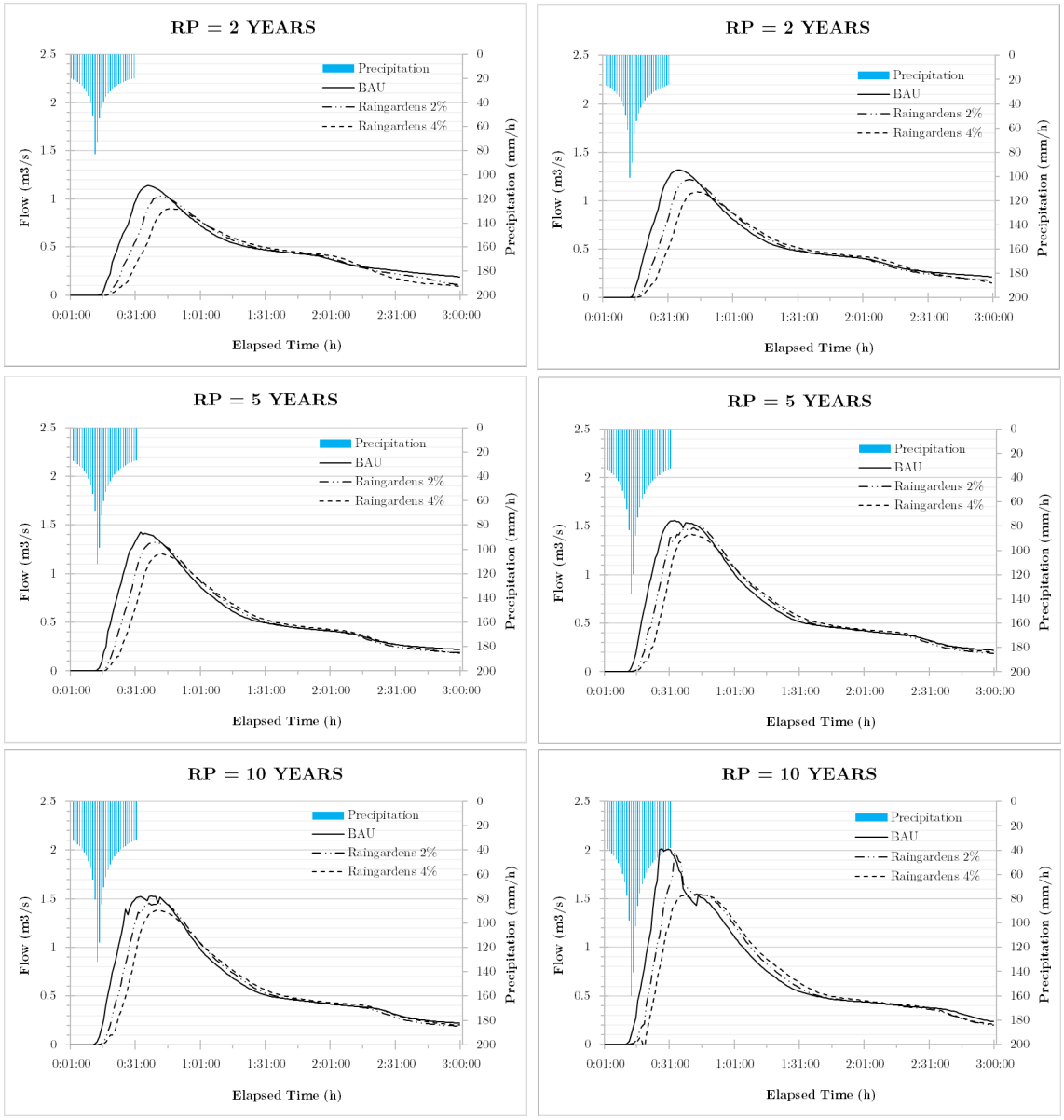

Fig. 63 – Hydrograph corresponding to the different EIA reduction scenarios at assigned rainfall event return period (T=2, 5 and 10 years) in the RCP 2.6 scenario for the refence period 2040-2059 and 2080-2099, summer season. The reference BAU scenario indicates the "do nothing" scenario.

SUMMER

RCP 4.5 - (2040-2059)	RCP 4.5 - (2080-2099)

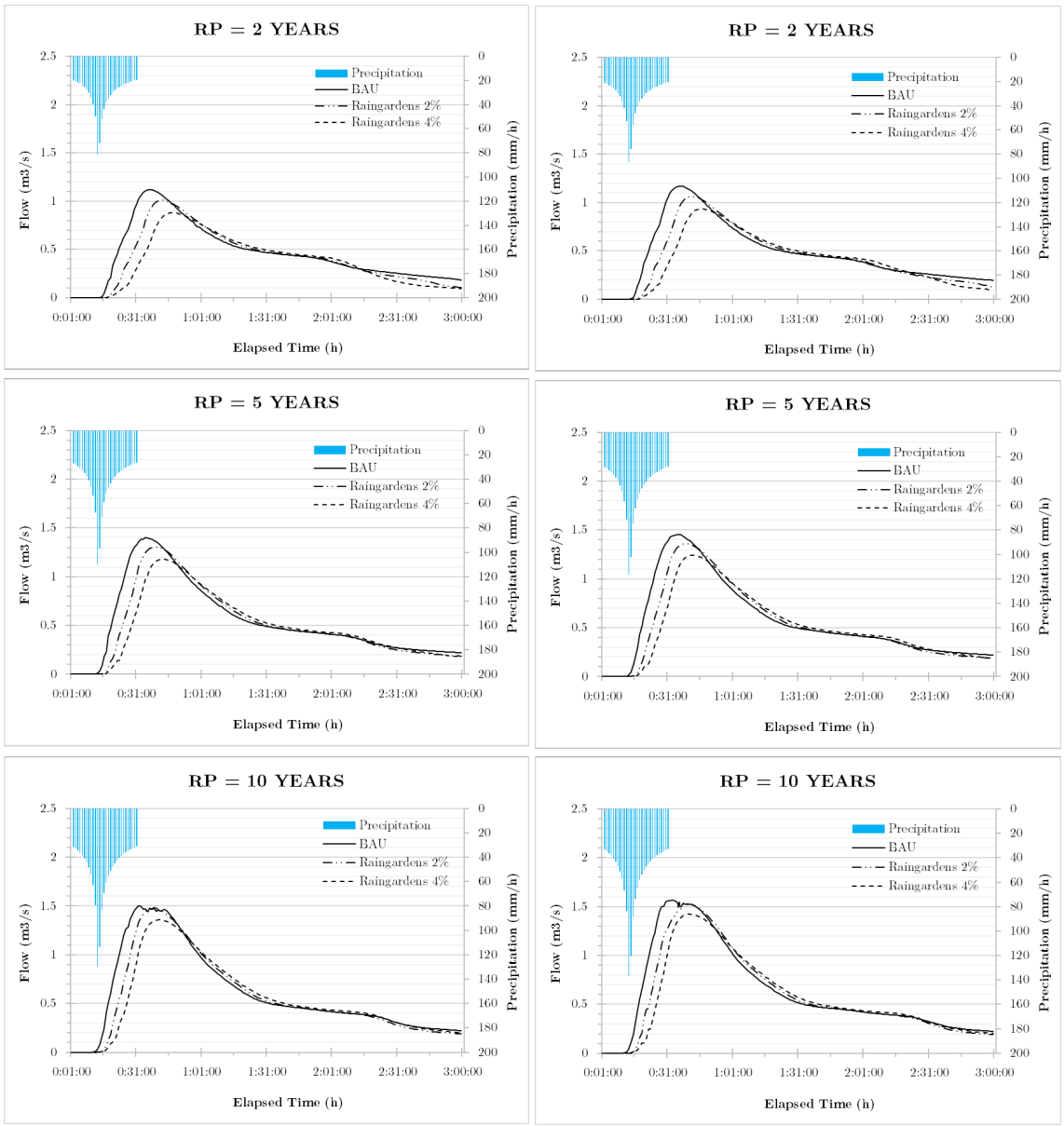

Fig. 64 - Hydrograph corresponding to the different EIA reduction scenarios at assigned rainfall event return period (T=2, 5 and 10 years) in the RCP 4.5 scenario for the refence period 2040-2059 and 2080-2099, summer season. The reference BAU scenario indicates the "do nothing" scenario.

SUMMER

RCP 8.5 - (2040-2059)	RCP 8.5 - (2080-2099)

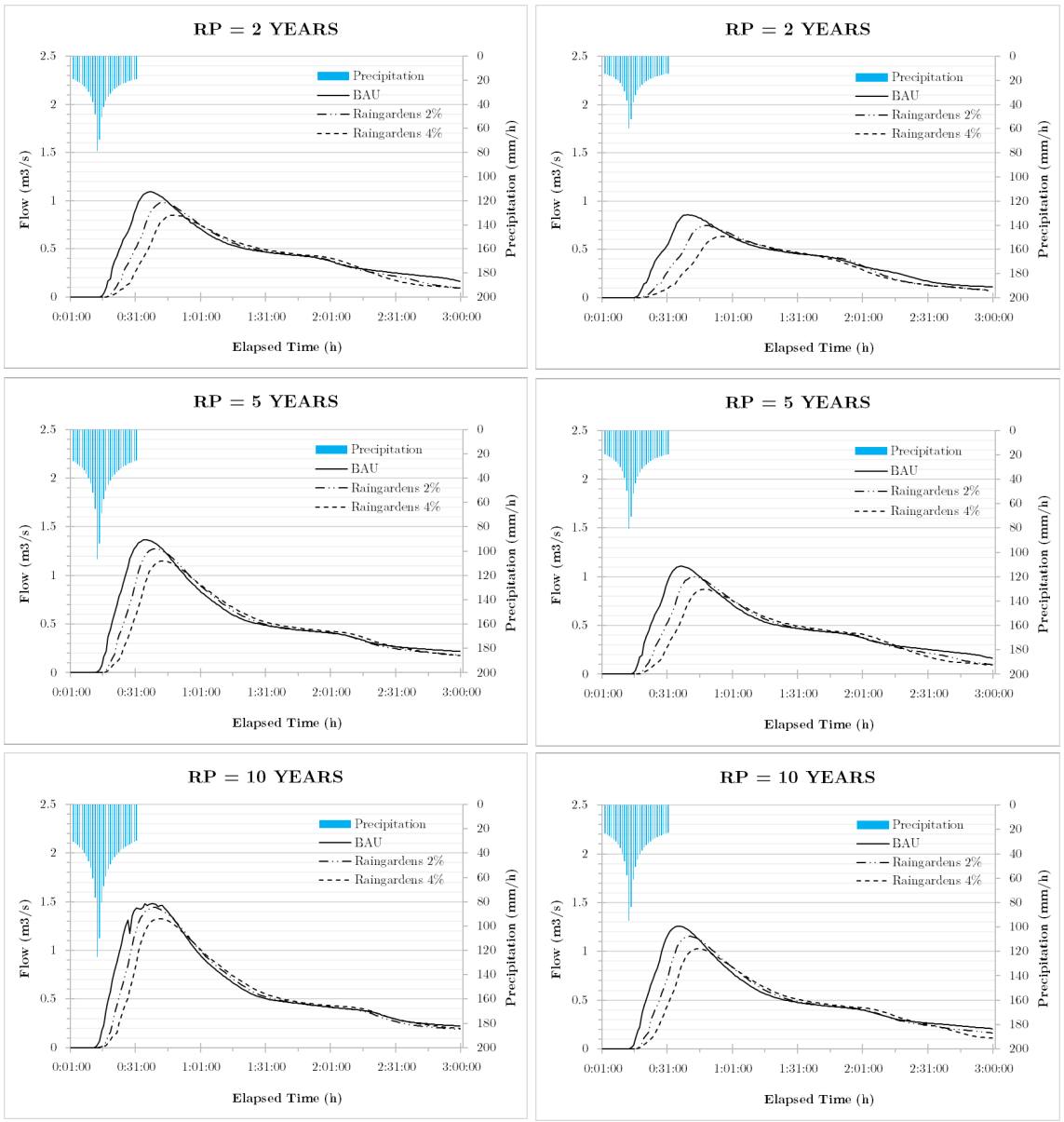

Fig. 65 - Hydrograph corresponding to the different EIA reduction scenarios at assigned rainfall event return period (T=2, 5 and 10 years) in the RCP 8.5 scenario for the refence period 2040-2059 and 2080-2099, summer season. The reference BAU scenario indicates the "do nothing" scenario.

AUTUMN

RCP 2.6 - (2040-2059)	RCP 2.6 - (2080-2099)

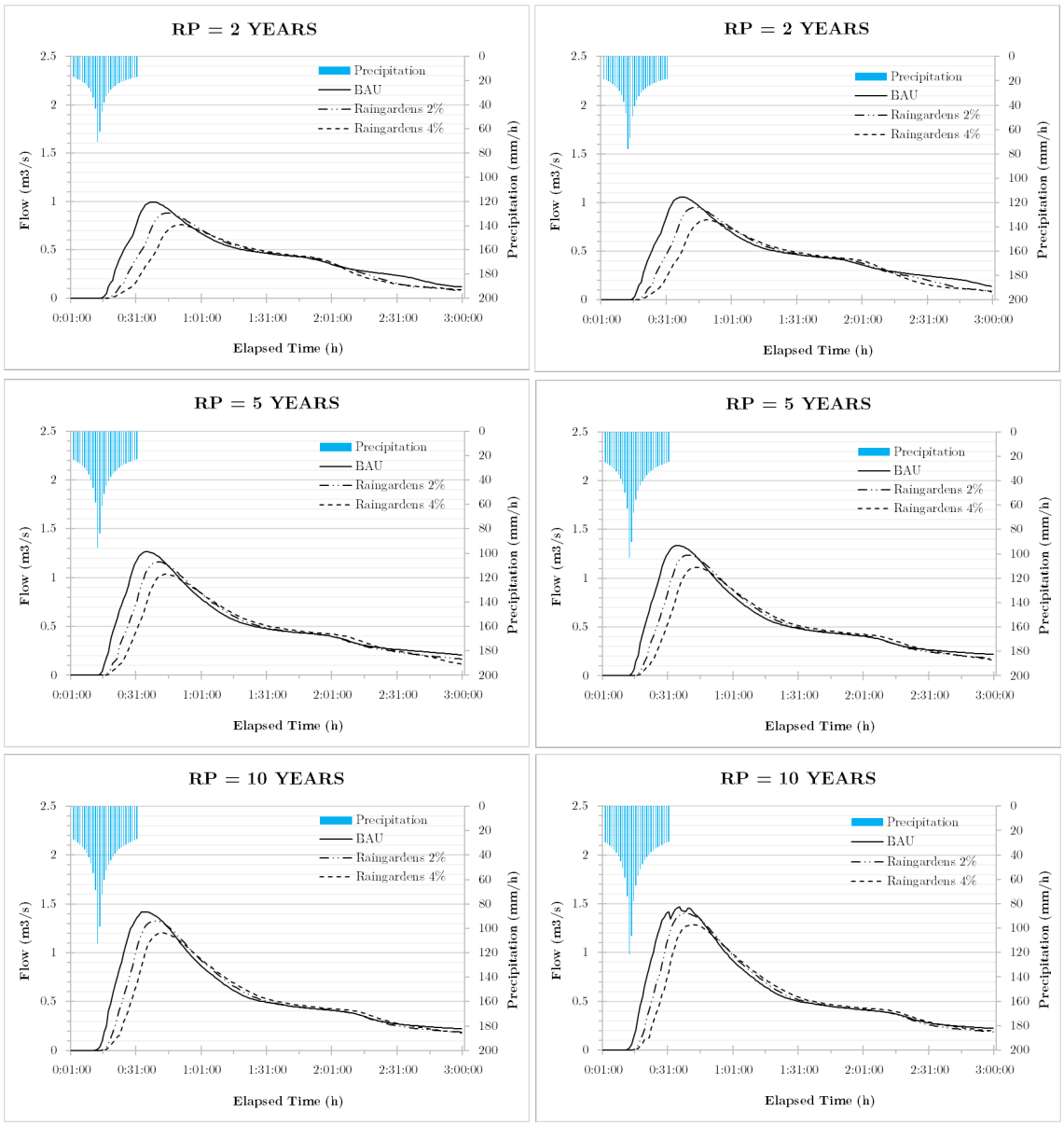

Fig. 66 – Hydrograph corresponding to the different EIA reduction scenarios at assigned rainfall event return period (T=2, 5 and 10 years) in the RCP 2.6 scenario for the refence period 2040-2059 and 2080-2099, autumn season. The reference BAU scenario indicates the "do nothing" scenario.

AUTUMN

RCP 4.5 - (2040-2059)	RCP 4.5 - (2080-2099)

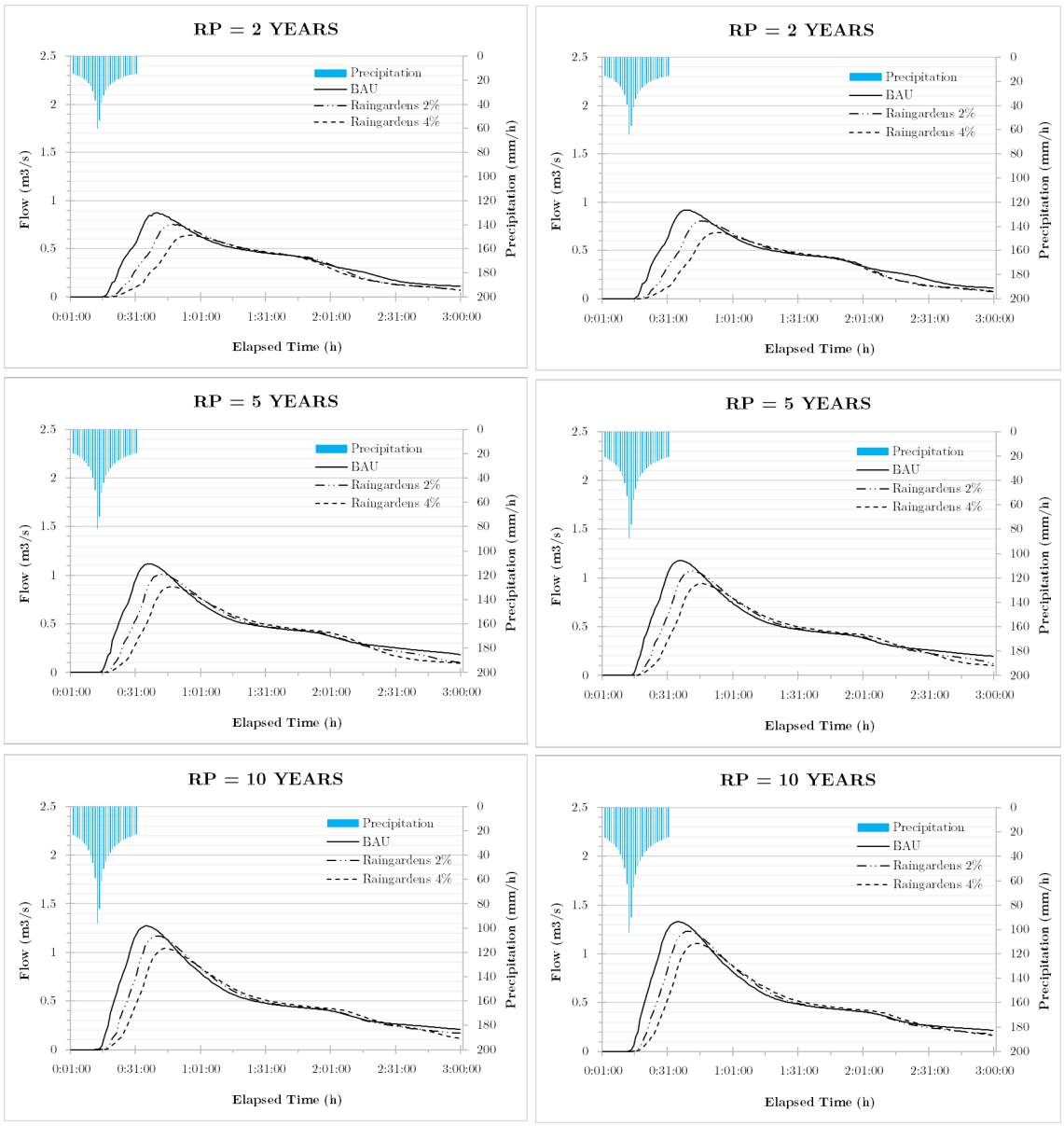

Fig. 67 - Hydrograph corresponding to the different EIA reduction scenarios at assigned rainfall event return period (T=2, 5 and 10 years) in the RCP 4.5 scenario for the refence period 2040-2059 and 2080-2099, autumn season. The reference BAU scenario indicates the "do nothing" scenario.

AUTUMN

RCP 8.5 - (2040-2059)	RCP 8.5 - (2080-2099)

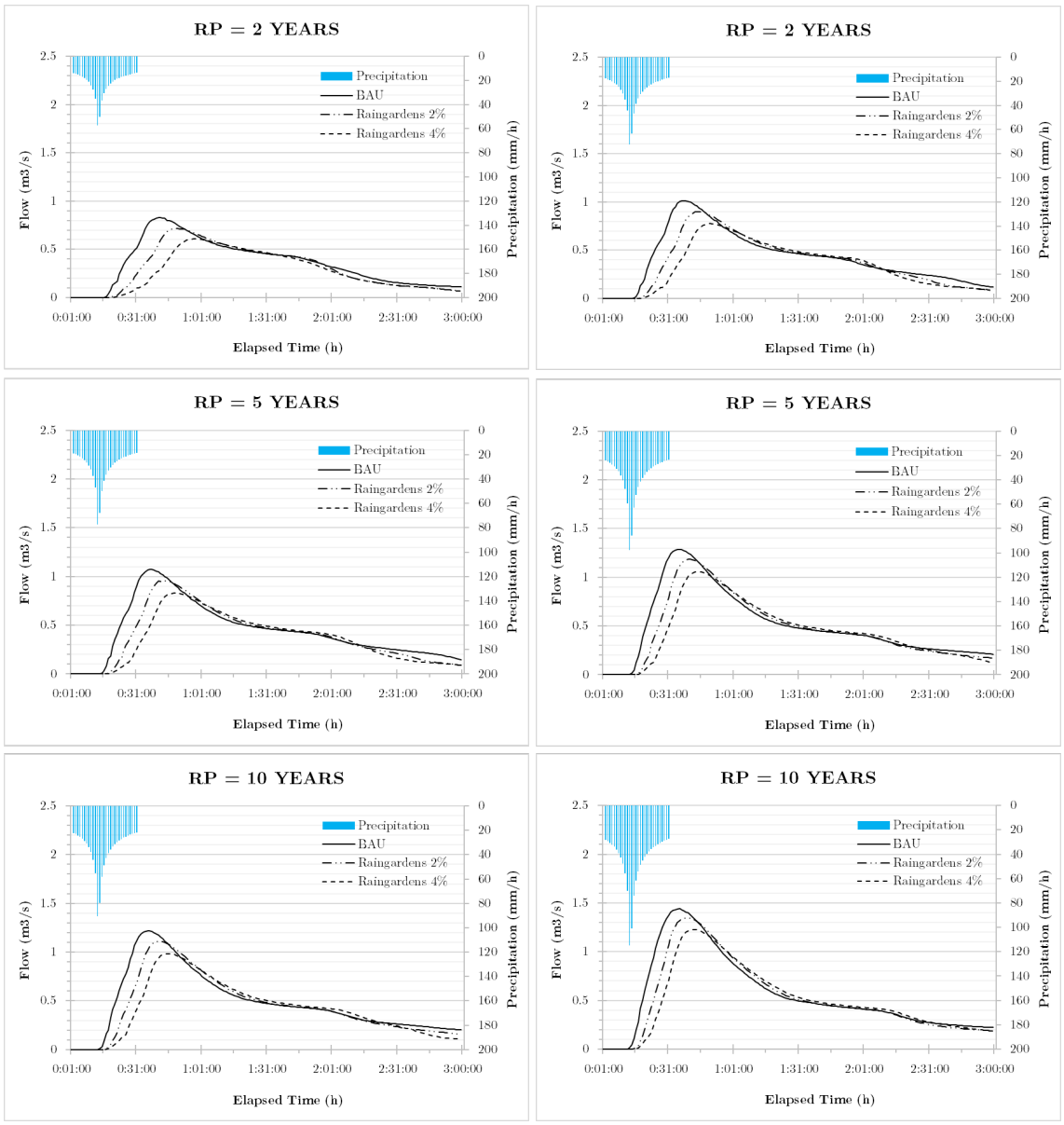

Fig. 68 - Hydrograph corresponding to the different EIA reduction scenarios at assigned rainfall event return period (T=2, 5 and 10 years) in the RCP 8.5 scenario for the refence period 2040-2059 and 2080-2099, autumn season. The reference BAU scenario indicates the "do nothing" scenario.

WINTER

RCP 2.6 - (2040-2059)	RCP 2.6 - (2080-2099)

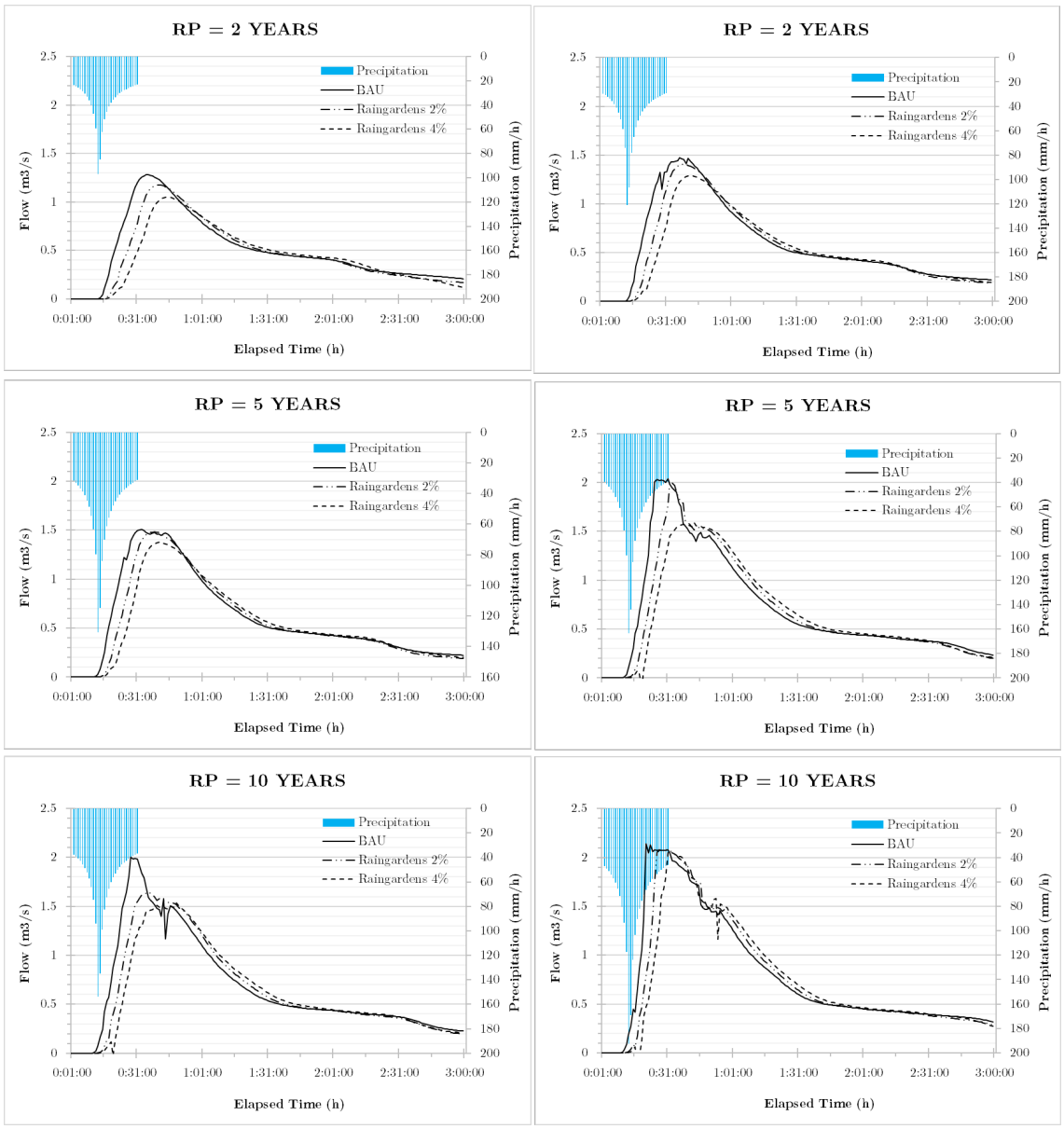

Fig. 69 – Hydrograph corresponding to the different EIA reduction scenarios at assigned rainfall event return period (T=2, 5 and 10 years) in the RCP 2.6 scenario for the refence period 2040-2059 and 2080-2099, winter season. The reference BAU scenario indicates the "do nothing" scenario.

WINTER

RCP 4.5 - (2040-2059)	RCP 4.5 - (2080-2099)

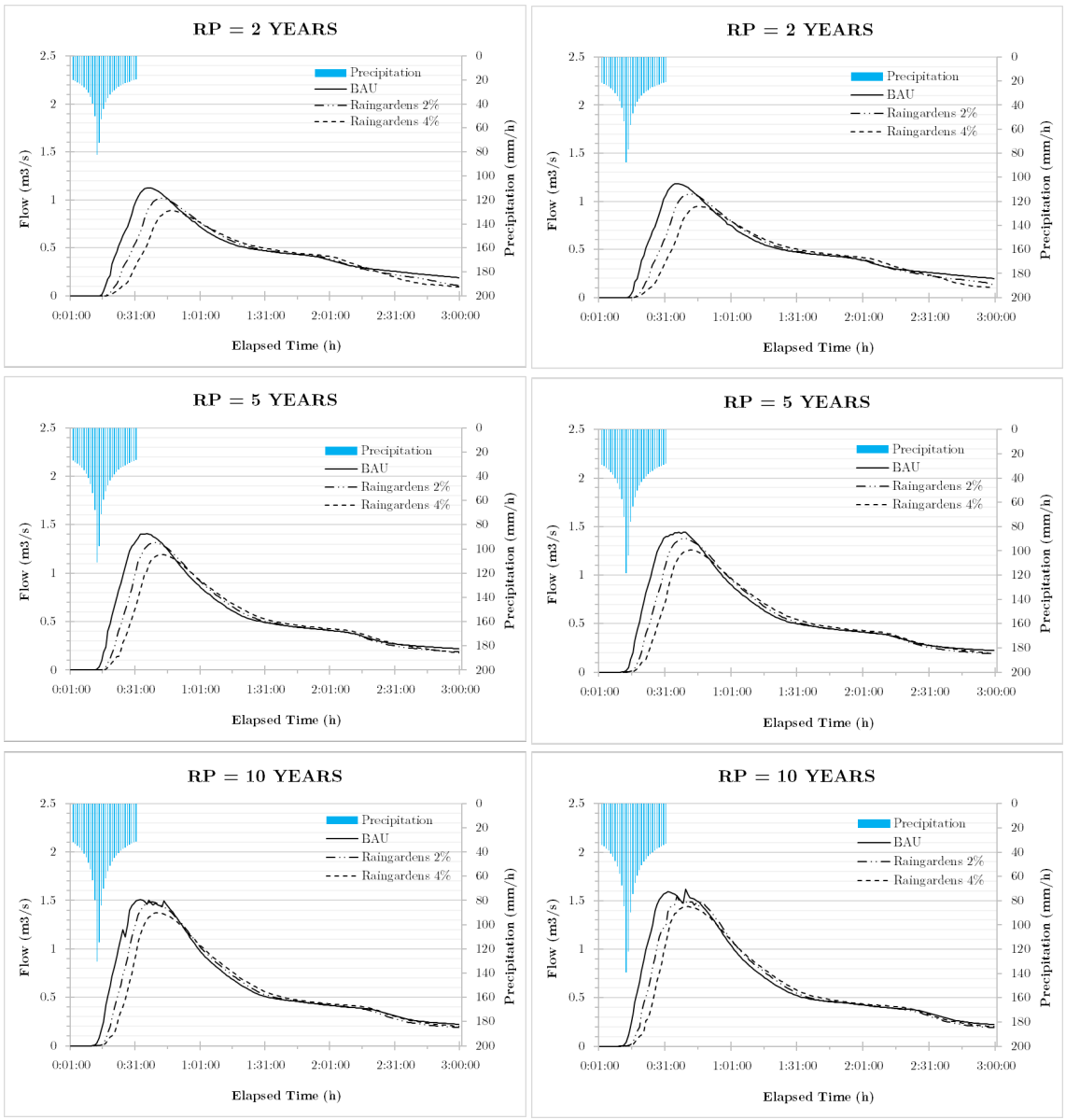

Fig. 70 - Hydrograph corresponding to the different EIA reduction scenarios at assigned rainfall event return period (T=2, 5 and 10 years) in the RCP 4.5 scenario for the refence period 2040-2059 and 2080-2099, winter season. The reference BAU scenario indicates the "do nothing" scenario.

WINTER

RCP 8.5 - (2040-2059)	RCP 8.5 - (2080-2099)

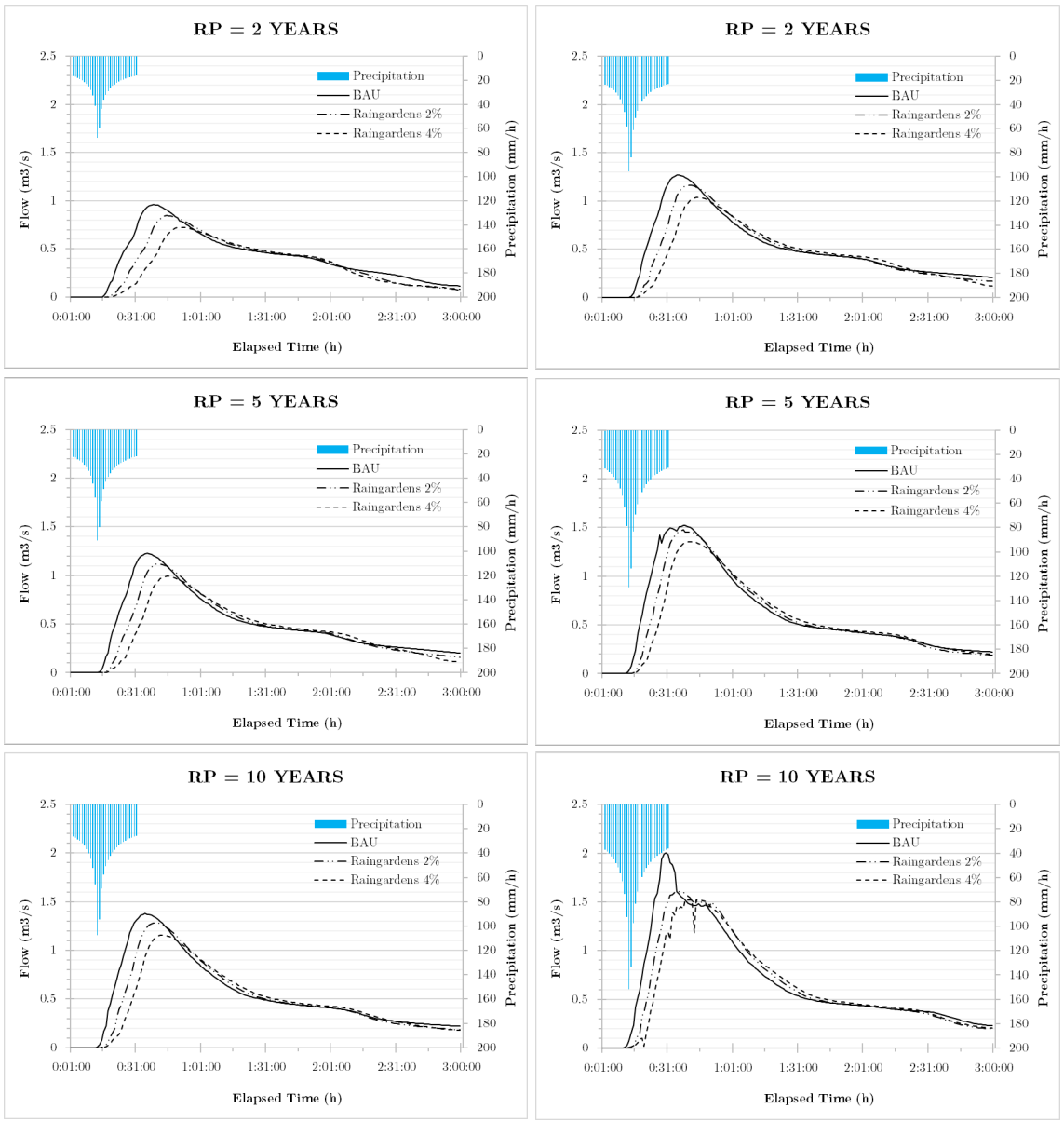

Fig. 71 - Hydrograph corresponding to the different EIA reduction scenarios at assigned rainfall event return period (T=2, 5 and 10 years) in the RCP 8.5 scenario for the refence period 2040-2059 and 2080-2099, winter season. The reference BAU scenario indicates the "do nothing" scenario.

SPRING

RCP 2.6 - (2040-2059)	RCP 2.6 - (2080-2099)

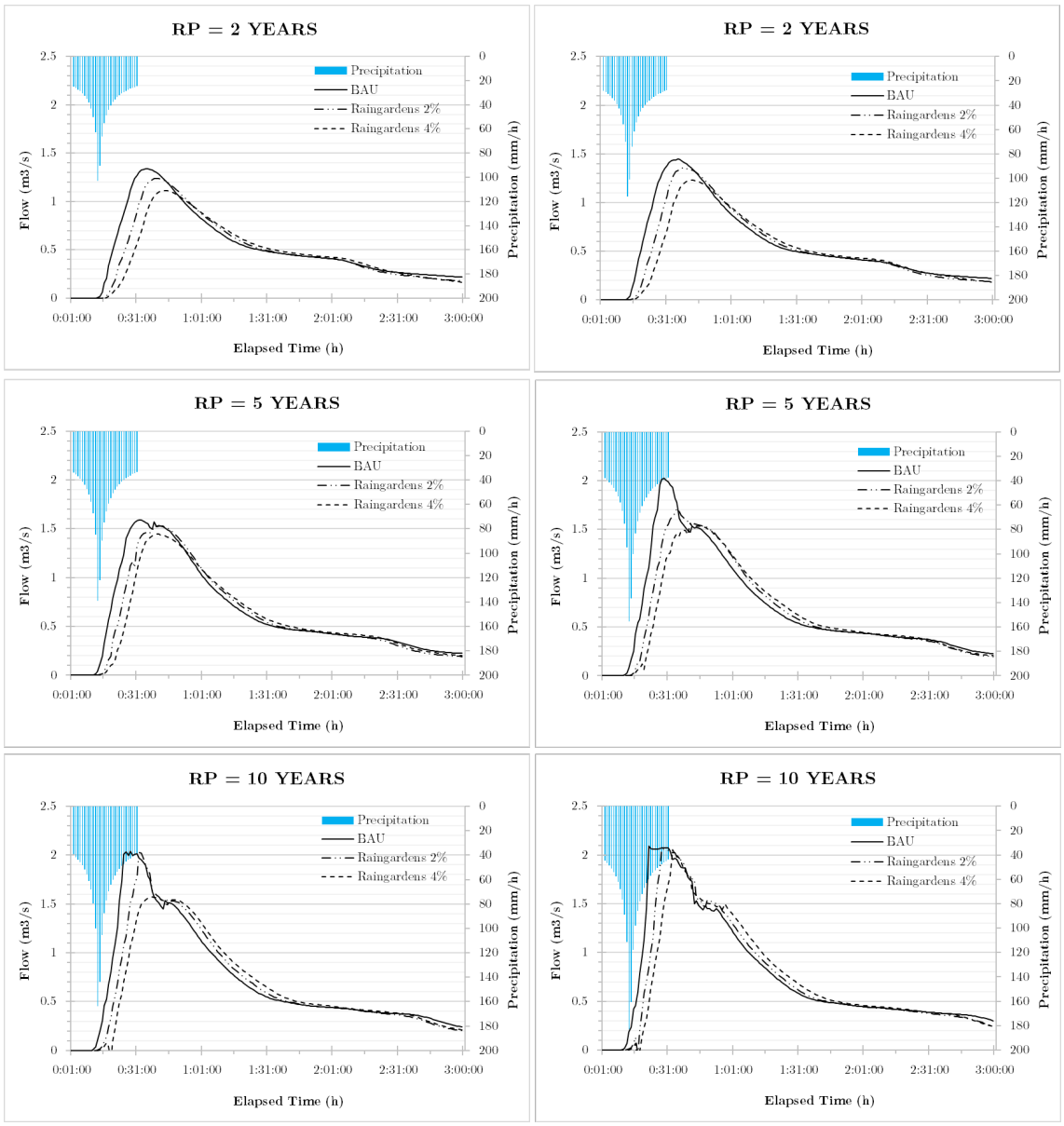

Fig. 72 – Hydrograph corresponding to the different EIA reduction scenarios at assigned rainfall event return period (T=2, 5 and 10 years) in the RCP 2.6 scenario for the refence period 2040-2059 and 2080-2099, spring season. The reference BAU scenario indicates the "do nothing" scenario.

SPRING

RCP 4.5 - (2040-2059)	RCP 4.5 - (2080-2099)

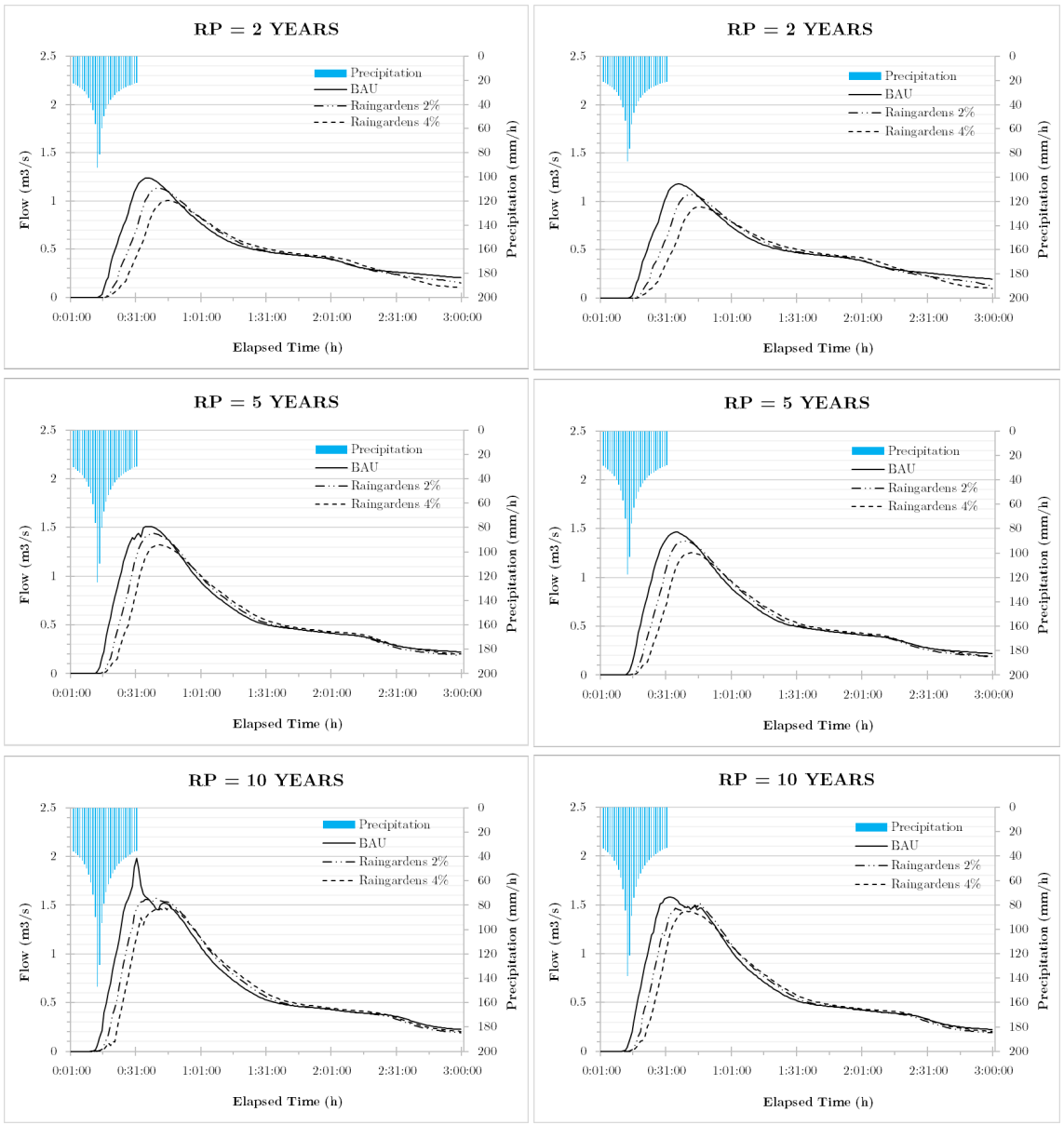

Fig. 73 - Hydrograph corresponding to the different EIA reduction scenarios at assigned rainfall event return period (T=2, 5 and 10 years) in the RCP 4.5 scenario for the refence period 2040-2059 and 2080-2099, spring season. The reference BAU scenario indicates the "do nothing" scenario.

SPRING

RCP 8.5 - (2040-2059)	RCP 8.5 - (2080-2099)

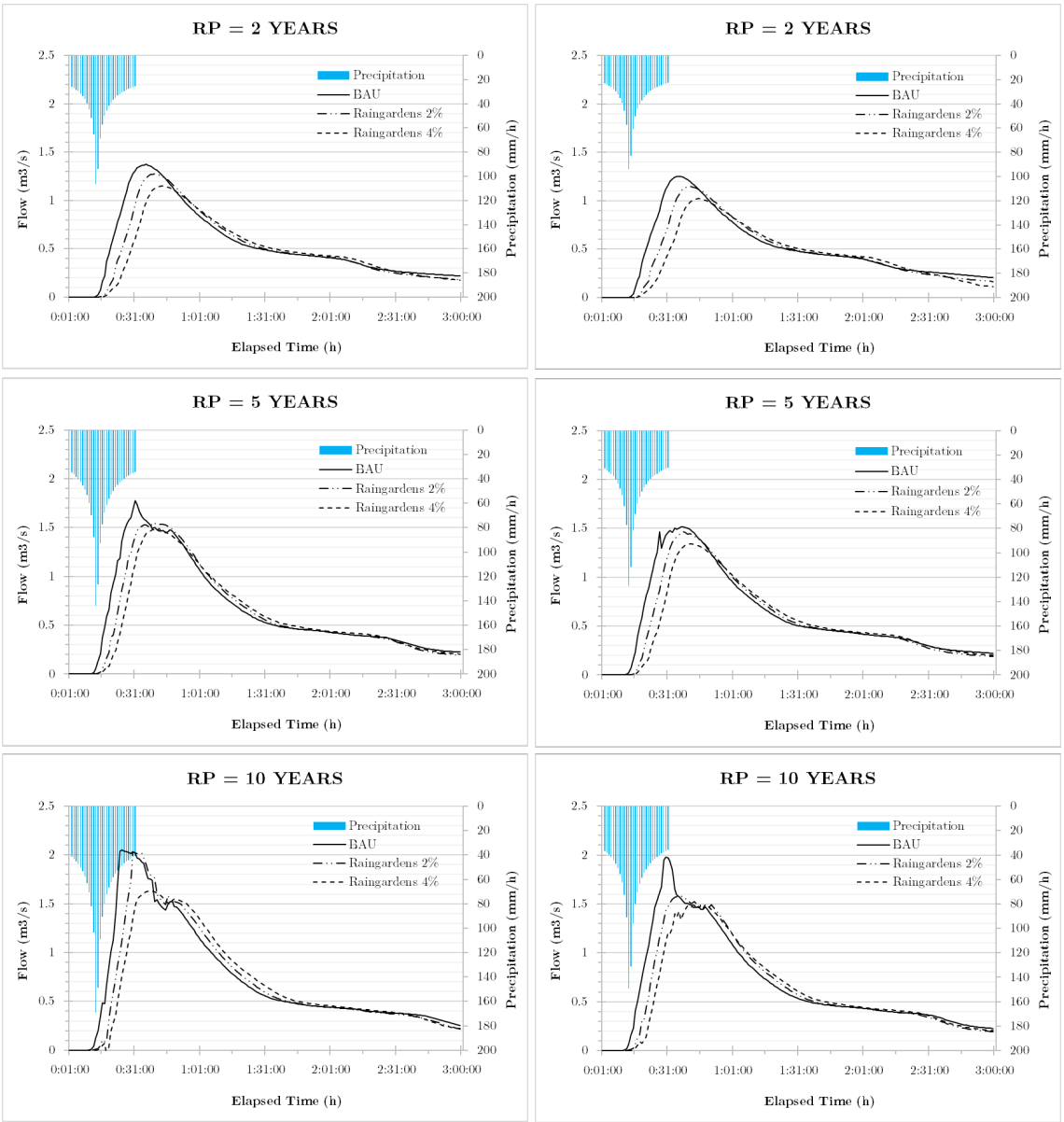

Fig. 74 - Hydrograph corresponding to the different EIA reduction scenarios at assigned rainfall event return period (T=2, 5 and 10 years) in the RCP 8.5 scenario for the refence period 2040-2059 and 2080-2099, spring season. The reference BAU scenario indicates the "do nothing" scenario.

The findings indicate that raingardens are effective in decreasing both the total volume and peak flow of urban runoff, while also delaying the peak flow. Nevertheless, the efficacy of raingardens diminishes with higher rainfall intensity and longer return periods.

In the next four tables (from Tab. 30 to Tab. 33), the hydrologic performance of raingardens under future climate scenarios (RCP 2.6, 4.5 and 8.5) is presented, focusing on selected indicators such as peak flow reduction, volume reduction and peak flow delay. In the first three tables, results are presented on a seasonal scale for the corresponding urban scenario with 4% EIA, divided by future climate scenario (RCP 2.6, 4.5, and 8.5). In the last table, a summary is provided on the performance of raingardens in both the 2% and 4% scenarios, regarding annual variations in precipitation for each future climate scenario.

The hydrographs depicted in the preceding figures illustrate the occurrence of flood peaks reaching 2 m^3/s during meteorological events with a 10-year return period. This is consistent across all three future climate scenarios for the spring season, the RCP 2.6 future climate scenario during the 2080-2099 summer, and in scenarios RCP 2.6 and 8.5 during the winter season. These flood peaks are primarily attributed to the inadequate capacity of the current drainage network to manage incoming water volumes effectively, resulting in surface flooding. This vulnerability is particularly pronounced in the business-as-usual scenario, where the existing drainage infrastructure struggles to cope with increased precipitation. However, even in scenarios with a 2% EIA reduction instances of surface flooding are observed although to a lesser extent. Conversely, the scenario featuring a 4% EA reduction consistently demonstrates the ability to manage flood volumes effectively, except for specific instances, such as the 10-year return period event in the RCP 2.6 2080-2099 winter and spring scenarios.

These findings underscore several key points:

- Raingardens demonstrate greater efficacy under conditions of lower precipitation intensity;
- The projected increase in precipitation outlined in the RCP 2.6 future climate scenario notably impacts rain garden performance, particularly in terms of peak flow reduction, although some delay in peak flow persists;
- As return periods increase, the benefits derived from raingardens decrease by approximately 10 percentage points for summer season about 15 percentage points for winter and spring, and less than 10 percentage points for autumn;
- For future climate scenario RCP 2.6 (2080-2099) the benefits for a rainfall event with a 10-years return period are nearly negligible in spring and winter. A similar situation is noted for the RCP 2.6 (2040-2060);
- On the annual scale results, the urban scenario with raingardens featuring 2% EIA often exhibit limited effectiveness in terms of peak flow delay, yet still provide notable benefits in reducing peak and outflow volumes.

Tab. 30 - Hydrologic performance of 4 % EIA Raingarden implementation under the future climate scenarios RCP 2.6 (for the periods 2040 – 2059 and 2080 – 2099) at assigned rainfall event return period (T = 2, 5, 10 years). Seasonal evaluation.

Hydrologic performance	**RCP 2.6 (2040 - 2059)**				**RCP 2.6 (2080 - 2099)**			
	Summer (Jul - Sept)	Autumn (Oct - Dec)	Winter (Jan - March)	Spring (Apr - Jun)	Summer (Jul - Sept)	Autumn (Oct - Dec)	Winter (Jan - March)	Spring (Apr - Jun)
Rainfall event T = 2 years								
Peak reduction (%)	20.83	23.72	17.98	16.82	17.27	22.28	12.51	15.05
Volume reduction (%)	11.10	12.79	8.22	7.64	7.77	11.95	6.84	7.05
Hydrograph relay (min)	00:10	00:13	00:09	00:09	00:09	00:11	00:05	00:07
Rainfall event T = 5 years								
Peak reduction (%)	15.65	18.28	8.76	8.88	9.16	16.79	8.05	6.86
Volume reduction (%)	7.21	8.35	6.01	5.09	5.26	7.61	2.09	2.73
Hydrograph relay (min)	00:10	00:09	00:08	00:07	00:08	00:09	00:03	00:
Rainfall event T = 10 years								
Peak reduction (%)	9.81	15.15	4.32	3.95	6.17	12.28	3.44	1.83
Volume reduction (%)	5.81	7.05	2.82	1.94	2.42	6.60	1.37	1.48
Hydrograph relay (min)	00:04	00:08	00:06	00:03	00:03	00:06	00:02	00:02

Tab. 31 - Hydrologic performance of 4 % EIA Raingarden implementation under the future climate scenarios RCP 4.5 (for the periods 2040 – 2059 and 2080 – 2099) at assigned rainfall event return period (T = 2, 5, 10 years). Seasonal evaluation.

Hydrologic performance	RCP 4.5 (2040 - 2059)				RCP 4.5 (2080 - 2099)			
	Summer (Jun - Aug)	Autumn (Sept - Nov)	Winter (Dec - Feb)	Spring (Mar - May)	Summer (Jun - Aug)	Autumn (Sept - Nov)	Winter (Dec - Feb)	Spring (Mar - May)
Rainfall event T = 2 years								
Peak reduction (%)	21.25	26.14	20.98	18.83	20.13	25.35	19.91	19.95
Volume reduction (%)	11.34	14.67	10.85	9.38	9.98	13.73	9.71	9.85
Hydrograph relay (min)	00:11	00:15	00:10	00:09	00:10	00:15	00:10	00:10
Rainfall event T = 5 years								
Peak reduction (%)	15.59	21.23	15.31	12.29	14.58	20.04	12.89	14.39
Volume reduction (%)	7.32	11.20	7.15	6.28	6.85	9.79	6.92	6.89
Hydrograph relay (min)	00:08	00:10	00:07	00:05	00:07	00:10	00:04	00:06
Rainfall event T = 10 years								
Peak reduction (%)	9.36	18.13	8.95	5.76	8.88	16.86	10.70	9.38
Volume reduction (%)	6.12	8.31	6.05	3.83	5.23	7.66	5.19	5.25
Hydrograph relay (min)	00:07	00:08	00:06	00:02	00:06	00:08	00:02	00:05

Tab. 32 - Hydrologic performance of 4 % EIA Raingarden implementation under the future climate scenarios RCP 8.5 (for the periods 2040 – 2059 and 2080 – 2099) at assigned rainfall event return period (T = 2, 5, 10 years). Seasonal evaluation.

Hydrologic performance	**RCP 8.5 (2040 - 2059)**				**RCP 8.5 (2080 - 2099)**			
	Summer (Jun - Aug)	Autumn (Sept - Nov)	Winter (Dec - Feb)	Spring (Mar - May)	Summer (Jun - Aug)	Autumn (Sept - Nov)	Winter (Dec - Feb)	Spring (Mar - May)
Rainfall event T = 2 years								
Peak reduction (%)	21.84	26.62	24.54	16.36	26.34	23.32	18.22	18.48
Volume reduction (%)	11.53	15.61	13.12	7.40	15.02	12.37	8.34	8.66
Hydrograph relay (min)	00:12	00:17	00:14	00:07	00:16	00:12	00:09	00:09
Rainfall event T = 5 years								
Peak reduction (%)	15.90	22.06	19.15	12.25	21.39	17.86	10.78	11.70
Volume reduction (%)	7.38	11.73	8.83	4.53	11.13	8.17	6.05	6.22
Hydrograph relay (min)	00:07	00:13	00:09	00:11	00:11	00:09	00:05	00:05
Rainfall event T = 10 years								
Peak reduction (%)	10.62	19.16	15.90	7.42	18.42	15.05	5.90	6.37
Volume reduction (%)	6.51	9.17	7.43	1.67	8.72	6.98	3.33	3.52
Hydrograph relay (min)	00:03	00:09	00:06	00:06	00:09	00:06	00:02	00:03

Tab. 33 – Hydrologic performance of the EIA de-sealing (2% and 4%) and future climate scenarios (RCP 2.6, 4.5, 8.5 for the periods 2040 – 2059 and 2080 – 2099) at assigned rainfall event return period (T = 2, 5, 10 years). Yearly evaluation.

	ACTUAL CLIMATE		**RCP 2.6 (2040 - 2059)**		**RCP 2.6 (2080 - 2099)**		**RCP 4.5 (2040 – 2059)**		**RCP 4.5 (2080 - 2099)**		**RCP 8.5 (2040 - 2059)**		**RCP 8.5 (2080 - 2099)**	
	EIA reduction		EIA reduction		EIA reduction		EIA reduction		EIA reduction		EIA reduction		EIA reduction	
Hydrologic performance	2 %	4 %	2 %	4 %	2 %	4 %	2 %	4 %	2 %	4 %	2 %	4 %	2 %	4 %
Rainfall event T = 2 years														
Peak reduction (%)	10.3	22.3	8.6	19.8	7.0	16.6	9.8	21.8	9.4	21.1	9.8	22.1	9.6	21.5
Volume reduction (%)	7.5	12.2	5.3	9.6	4.6	7.6	6.6	11.4	6.2	11.3	7.0	11.9	6.5	11.1
Hydrograph relay (min)	5	11	6	9	5	8	6	10	6	10	6	10	6	11
Rainfall event T = 5 years														
Peak reduction (%)	7.3	17.0	6.3	14.4	6.1	9.2	6.7	15.7	6.7	15.6	6.8	16.3	6.6	15.8
Volume reduction (%)	4.7	7.7	4.2	6.8	2.9	5.0	4.6	7.5	4.5	7.2	4.6	7.5	4.5	7.3
Hydrograph relay (min)	5	9	-	3	8	8	5	8	5	8	5	9	4	7
Rainfall event T = 10 years														
Peak reduction (%)	12.9	12.9	9.9	9.9	22.4	22.4	11.7	11.7	12.8	12.8	11.3	11.3	9.0	9.0
Volume reduction (%)	4.2	6.7	3.0	5.0	1.8	1.9	4.1	6.4	3.9	6.2	4.2	6.5	2.9	5.2
Hydrograph relay (min)	-	2	5	11	3	8	-	-	2	6	-	4	-	3

4.9.4 Result for continuous simulation

Continuous simulations were conducted on an annual scale using precipitation and temperature data collected by ARPA Lombardia. Specifically, two continuous simulations were performed for the years 2022 and 2023, characterized by significantly different total annual precipitation values: 788.4 mm for 2023 and 455.6 mm for 2022 (below the annual average for Brescia, which is approximately 900 mm per year). The simulations were conducted to evaluate the effectiveness of raingardens in reducing surface runoff, increasing infiltration rates, and enhancing evapotranspiration. Three different urban scenarios were simulated, where raingardens were implemented with a total area equal to the 2%, 3%, and 4% of EIA respectively (Fig. 74).

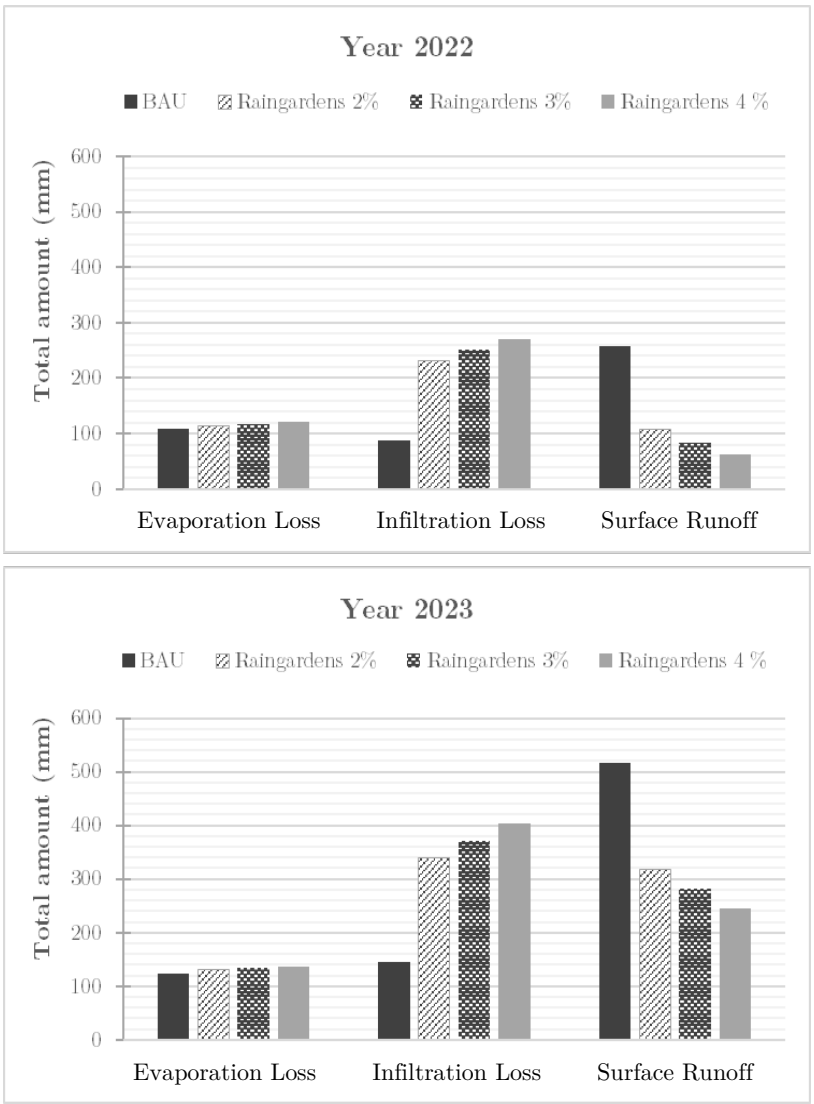

Fig. 75 – Hydrologic performance vs. year of simulation (2022 and 2023) based on three different EIA conversion (2, 3 and 4 %)

The results presented in Tab. 34 and Tab. 35 demonstrate improvements in terms of surface runoff reduction and infiltration rate increase. No significant improvements were observed in terms of evaporation losses, likely due to the underdrain system of the raingarden, which disposes of accumulated water within the raingarden through discharge into the network, thereby reducing accumulated water over time and the potential evapotranspiration rate.

Brown and Hunt (2011a; 2011b) achieved a similar finding, determining that evaporation accounted for less than 5% of the water budget in bioretention systems. They used the Thornthwaite method (1948) to calculate potential evapotranspiration (PET) and applied the Zhang et al. (2001) formula to estimate the actual evapotranspiration derived from PET.

It is worth clarifying that in each simulation, a slight discrepancy of a few millimetres in the final mass balance occurs. This discrepancy is caused by a continuity error within the SWMM model, which arises during the solving of differential equations.

Tab. 34 – Modelling **r**esults of continuous simulations for the four urban scenarios (BAU, 2, 3 and 4% EIA) for the years 2022 and 2023.

	2022				**2023**			
		EIA				**EIA**		
	BAU	**2%**	**3%**	**4%**	**BAU**	**2%**	**3%**	**4%**
Total Precipitation	455.6				788.4			
Evaporation Loss	111.8	116.5	119.4	122.3	125.0	131.6	134.9	138.3
Infiltration Loss	88.6	233.1	253.9	271.9	145.6	339.3	371.4	403.7
Surface Runoff	257.1	108.0	84.1	63.2	517.2	316.9	281.5	245.9
Final Storage	1.2	1.1	1.0	0.9	1.7	1.5	1.4	1.3

Tab. 35 – Hydrologic performance of the urban scenarios assessed through continuous simulation at the yearly scale (2022 and 2023)

	2022			**2023**		
	EIA			**EIA**		
Hydrologic Performance	**2%**	**3%**	**4%**	**2%**	**3%**	**4%**
Evaporation Loss increase	4.2	6.8	9.4	5.3	7.9	10.7
Infiltration Loss increase	163.2	186.7	207.0	133.0	155.1	177.2
Surface Runoff reduction	58.0	67.3	75.4	38.7	45.6	52.5

In addition, the results also demonstrate a linear relationship between variations in terms of evapotranspiration, infiltration, and surface runoff and the percentage of EIA conversion (Fig. 76) as already highlighted by the results at the single-event scale.

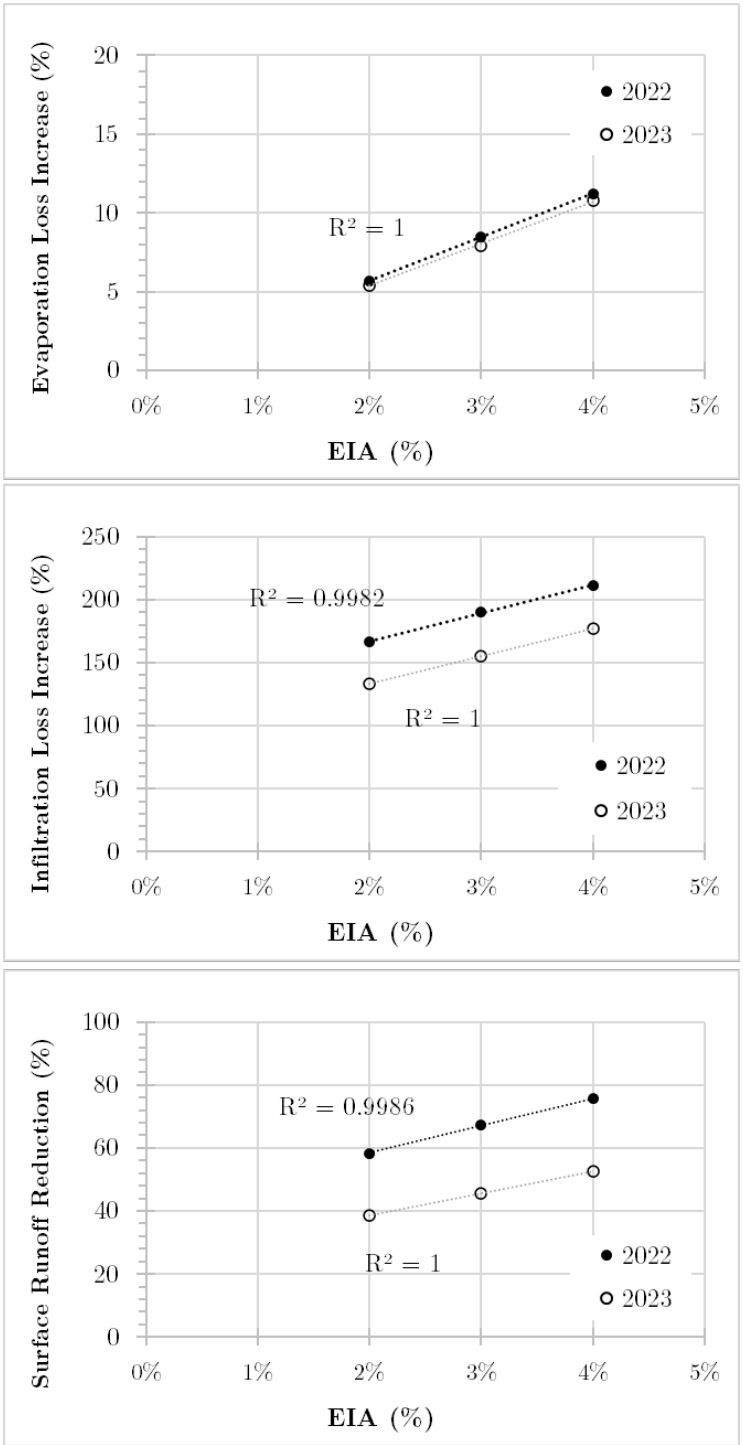

Fig. 76 - Hydrologic performance vs. EIA conversion (2, 3 and 4%) for the two simulated years (2022 and 2023)

4.10 References

Ahiablame, L., & Shakya, R. (2016). Modeling flood reduction effects of low impact development at a watershed scale. *Journal of Environmental Management*, *171*, 81-91. ISSN 0301-4797. doi.org/10.1016/j.jenvman.2016.01.036

Akan, A.O., & Houghtalen, R.J. (2003). Urban Hydrology, Hydraulics, and Stormwater Quality: Engineering Applications and Computer Modeling. *John Wiley & Sons*, Inc. ISBN: 978-0-471-43158-9

Anggraini, N., & Slamet, B. (2021). Thornthwaite Models for Estimating Potential evapotranspiration in Medan City. *IOP Conference Series: Earth and Environmental Science*. 912. 012095. doi.org/10.1088/1755-1315/912/1/012095

ARPA Regione Lombardia [data file]. https://www.arpalombardia.it/temi-ambientali/meteo-e-clima/form-richiesta-dati/ (Visited on 07/09/2023).

Bąk, J., & Barjenbruch, M. (2022). Benefits, Inconveniences, and Facilities of the Application of Rain Gardens in Urban Spaces from the Perspective of Climate Change—A Review. *Water, 14 (7)*, 1153. doi.org/10.3390/w14071153

Basdeki, A., Katsifarakis, L., & Katsifarakis, K.L. (2016). *Rain Gardens as Integral Parts of Urban Sewage Systems-a Case Study in Thessaloniki, Greece*. Procedia Engineering, *162*, 426-432. ISSN 1877-7058. doi.org/10.1016/j.proeng.2016.11.084

Berteni, F., Dada, A., & Grossi, G. (2021). Application of the MUSLE Model and Potential Effects of Climate Change in a Small Alpine Catchment in Northern Italy. *Water*, *13,* 2679. doi.org/10.3390/w13192679

Burszta-Adamiak, E., & Mrowiec, M. (2013). Modelling of Green roofs' hydrologic performance using EPA's SWMM. *Water Science and Technology, 68 (1),* 36–42. doi.org/10.2166/wst.2013.219

Burszta-Adamiak, E., Biniak-Pieróg, M., Dąbek, P.B., & Sternik, A. (2023). Rain Garden hydrological performance - Responses to real rainfall events. *Science of The Total Environment*, *887*, 164153. ISSN 0048-9697. doi.org/10.1016/j.scitotenv.2023.164153

Brown, R.A., & Hunt, W.F. (2011a). Underdrain configuration to enhance bioretention exfiltration to reduce pollutant loads. *Journal of Environmental Engineering, 137 (11)*, 1082–1091. doi.org/10.1061/(ASCE)EE.1943-7870.0000437

Brown, R.A., & Hunt, W.F. (2011b). Impacts of media depth on effluent water quality and hydrologic performance of undersized bioretention cells. *Journal of Irrigation and Drainage Engineering, 137 (3)*, 132–143. doi.org/10.1061/(ASCE)IR.1943-4774.0000167

Camargo, A.P., Marin, F., Sentelhas, P., & Picini, A.G. (1999). Adjust of the Thornthwaite's method to estimate the potential evapotranspiration for arid and superhumid climates, based on daily temperature amplitude. *Rev. Bras. Agrometeorol.* 7. 251-257.

Campisano, A., Modica, C., & Gullotta, A. (2020). Long-term experiments for the evaluation of

the potential for storm water control of modular blue roofs in Mediterranean climate. *Urban Water Journal, 18 (1)*, 33-42. doi.org/10.1080/1573062X.2020.1850807

Chang, N. B. (2010). Hydrological Connections between Low-Impact Development, Watershed Best Management Practices, and Sustainable Development. *Journal of Hydrologic Engineering (ASCE Archive), 15 (6)*, 10.1061. HE.1943-5584.0000236. doi.org/10.1061/(ASCE)HE.1943-5584.000023

Chartered Institution of Water and Environmental Management (CIWEM) – Urban Drainage Group. (2017). *Code of Practice for the Hydraulic Modelling of Urban Drainage Systems.* Version N. 01.

Climate Data [Data file]. https://en.climate-data.org/europe/italy/lombardy/brescia-1096/ (Visited on 26/01/2023).

Comune di Brescia (2020). Adeguamento della componente geologica, idrogeologica e sismica del PGT al Piano di Gestione del Rischio Alluvioni (P.G.R.A.) - Carta Idrogeologica. V.I.-ALall 04c1

Copernicus Climate Change Service, Climate Data Store (2019). CORDEX regional climate model data on single levels. Copernicus Climate Change Service (C3S) Climate Data Store (CDS). doi.org/10.24381/cds.bc91edc3 (Visited on 07-01-2023)

Coutts, A.M., Tapper, N.J., Beringer, J., Loughnan, M., & Demuzere, M. (2013). Watering our cities: The capacity for Water Sensitive Urban Design to support urban cooling and improve human thermal comfort in the Australian context. *Progress in Physical Geography: Earth and Environment, 37 (1)*, 2-28. doi.org/10.1177/0309133312461032

Dada, A., Urich, C., Berteni, F., Pezzagno, M., Piro, P., & Grossi, G. (2021). Water Sensitive Cities: An Integrated Approach to Enhance Urban Flood Resilience in Parma (Northern Italy). *Climate*, *9*, 152. doi.org/10.3390/cli9100152

Ebrahimian, A., Wadzuk, B., & Traver, R. (2019). Evapotranspiration in green stormwater infrastructure systems. *Science of The Total Environment*, *688,* 797-810. ISSN 0048-9697. doi.org/10.1016/j.scitotenv.2019.06.256

ENES – European Network for Earth System Modelling [Data file]. https://portal.enes.org/ (Visited on 06/07/2023)

ESGF@LiU – [Data file]. https://esg-dn1.nsc.liu.se/search/cordex/ (Visited on 06/07/2023)

EPA – Environmental Protection Agency – [Software]. https://www.epa.gov/water-research/storm-water-management-model-swmm

Faivre, N., Fritz, M., Freitas, T., de Boissezon, B., & Vandewoestijne, S. (2017). Nature-Based Solutions in the EU: Innovating with nature to address social, economic and environmental challenges. *Environmental Research*, *159,* 509-518, ISSN 0013-9351. doi.org/10.1016/j.envres.2017.08.032

Fletcher, T.D., Shuster, W., Hunt, W.E., Ashley, R., Butler, D., Arthur, S., Trowsdale, S.,

Barraud, S., Semadeni-Davies, A., Bertrand-Krajewski, J.L., Mikkelsen, P.S., Rivard, G., Uhl, M., Dagenais, D., & Viklander, M. (2015). SUDS, LID, BMPs, WSUD and more – The evolution and application of terminology surrounding urban drainage. *Urban Water Journal*, *12 (7)*, 525-542. doi.org/10.1080/1573062X.2014.916314

Giorgi, F., Jones, C., & Asrar, G. (2008). Addressing climate information needs at the regional level: The CORDEX framework. WMO Bull. 53.

Grant, G. (2018). Chapter 1.3 – Incentives for Nature-Based Strategies. In: Pérez, G., & Perini, K. (Eds.), *Nature Based Strategies for Urban and Building Sustainability*, Butterworth-Heinemann, 29-41. ISBN 9780128121504. doi.org/10.1016/B978-0-12-812150-4.00003-3

Hughes, J., Cowper-Heays, K., Olesson, E., Bell, R., & Stroombergen, A. (2021). Impacts and implications of climate change on wastewater systems: A New Zealand perspective, *Climate Risk Management*, *31*, 100262. ISSN 2212-0963. doi.org/10.1016/j.crm.2020.100262

Hunt, W., Davis, A., & Traver, R. (2012). Meeting Hydrologic and Water Quality Goals through Targeted Bioretention Design. *Journal of Environmental Engineering*, *138*, 698-707. doi.org/10.1061/(ASCE)EE.1943-7870.0000504

IPCC - Future Climate Changes, Risks and Impacts. https://ar5-syr.ipcc.ch/topic_futurechanges.php (Visited on 30/06/2023)

Jacobson, C.R. (2011). Identification and quantification of the hydrological impacts of imperviousness in urban catchments: A review. *Journal of Environmental Management, 92 (6),* 1438–1448. doi.org/10.1016/j.jenvman.2011.01.018

Kasprzyk, M., Szpakowski, W., Poznańska, E., Boogaard, F.C., Bobkowska, K., & Gajewska, M. (2022). Technical solutions and benefits of introducing rain gardens - Gdańsk case study. *Science of the Total Environment*, *835*, 155487. doi.org/10.1016/j.scitotenv.2022.155487

Kleidorfer, M., Mikovits, C., Jasper-Tönnies, A., Huttenlau, M., Einfalt, T., & Rauch, W. (2014). Impact of a Changing Environment on Drainage System Performance, Procedia *Engineering, 70*, 943-950. ISSN 1877-7058. doi.org/10.1016/j.proeng.2014.02.105

Krause, P., Boyle, D., & Bäse, F. (2005). Comparison of Different Efficiency Criteria for Hydrologic Models. *Advances in Geosciences, 5*, 89-97. doi.org/10.5194/adgeo-5-89-2005

Lee, J.M., Hyun, K.H., & Choi, J.S. (2013). Analysis of the impact of low impact development on runoff from a new district in Korea. *Water Science and Technol*ogy, *68 (6)*, 1315-1321. PMID: 24056429. doi.org/10.2166/wst.2013.346

Li, J., Li, Y., & Li, Y. (2016). SWMM-based evaluation of the effect of rain gardens on urbanized areas. *Environ Earth Sci.* 75, 17. doi.org/10.1007/s12665-015-4807-7

Lucas, W.C., & Sample, D.J. (2015). Reducing combined sewer overflows by using outlet controls for Green Stormwater Infrastructure: case study in Richmond. Virginia. *Journal of Hydrology*, *520*, 473–488. doi.org/10.1016/j.jhydrol.2014.10.029

McCutcheon, M., & Wride, D. (2013). Shades of Green: Using SWMM LID Controls to Simulate Green Infrastructure. *Journal of Water Management Modeling,* R246-15. doi.org/10.14796/JWMM.R246-15

McGrane, S.J. (2015). Impacts of urbanisation on hydrological and water quality dynamics, and urban water management: a review. *Hydrological Sciences Journal*, *61 (13)*, 2295-2311. doi.org/10.1080/02626667.2015.1128084

McPhillips, L., Wu, H., Rojas, C., Rosenzweig, B., Sauer, J., & Winfrey, B. (2023). Nature-Based Solutions as Critical Urban Infrastructure for Water Resilience. *Nature-Based Solutions for Cities*, 147-166. Edward Elgar Publishing Ltd. doi.org/10.4337/9781800376762.00017

Moore, T.L., Gulliver, J.S., Stack, L., & Simpson, M.H. (2016). Stormwater management and climate change: vulnerability and capacity for adaptation in urban and suburban contexts. *Climatic Change, 138*, 491–504. doi.org/10.1007/s10584-016-1766-2

Moriasi, D.N., Gitau, M.W., Pai, N., & Daggupati, P. (2015). Hydrologic and Water Quality Models: Performance Measures and Evaluation Criteria. Transactions of the *American Society of Agricultural and Biological Engineers, 58*, 1763–1785. doi.org/10.13031/trans.58.10715

Nash, J.E., & Sutcliffe, J.V. (1970). River flow forecasting through conceptual models part I — A discussion of principles. *Journal of Hydrology*, *10 (3)*, 282-290. doi.org/10.1016/0022-1694(70)90255-6

Newburn, D.A., & Alberini, A. (2016). Household response to environmental incentives for rain garden adoption, *Water Resources Res., 52,* 1345–1357. doi.org/10.1002/2015WR018063

Nie, L., Lindholm, O., Lindholm, & G., Syversen, E. (2009). Impacts of climate change on urban drainage systems – a case study in Fredrikstad, Norway. *Urban Water Journal*, *6 (4)*, 323–332. doi.org/10.1080/15730620802600924

Palermo, S.A., Turco, M., Behrouz, P., Presta, L., Falco, S., de Stefano, A., Frega, F., & Piro, P. (2023). Nature-based solutions for urban stormwater management: an overview. *IOP Conference Series: Earth and Environmental Science,* 1196, 012027. doi.org/10.1088/1755-1315/1196/1/012027

Palla, A. & Gnecco, I. (2015). Hydrologic modeling of Low Impact Development systems at the urban catchment scale. *Journal of Hydrology, 528,* 361-368. doi.org/10.1016/j.jhydrol.2015.06.050

Peng, Z., Jinyan, K., Wenbin, P., Xin, Z., & Yuanbin, C. (2018). Effects of Low-Impact Development on Urban Rainfall Runoff under Different Rainfall Characteristics, *Polish Journal of Environmental Studies, 28 (2)*, 771-783. doi.org/10.15244/pjoes/85348

Qin, H.P., Li, Z.X., & Fu, G. (2013). The effects of low impact development on urban flooding under different rainfall characteristics. *Journal of Environmental Management*, *129*, 577-585. ISSN 0301-4797. doi.org/10.1016/j.jenvman.2013.08.026

Pereira, A.R., & Pruitt, W.O. (2004). Adaptation of the Thornthwaite scheme for estimating

daily reference evapotranspiration. *Agricultural water Management*, *66 (3)*, 0–257. doi.org/10.1016/j.agwat.2003.11.003

Platz, M., Simon, M., & Tryby, M. (2020). Testing of the Storm Water Management Model Low Impact Development Modules. *Journal of American Water Resources Association, 56 (20)*, 283-296. doi.org/10.1111/1752-1688.12832

Raimondi, F., Marchioni, M., Raimondi, A., & Becciu, G. (2021). Comparison of Urban Retrofitting Scenarios for Sustainable Stormwater Control: A Case Study in Milan, Italy. Sustainable Water Resources Management XI, 131-142. ISBN: 978-1-78466-421-3. doi.org/10.2495/WRM210121

Rawls, W.J., Brakensiek, D.L., & Miller, N.L. (1983). Green-ampt Infiltration Parameters from Soils Data. *Journal of Hydraulic Engineering, 109*, 62-70. doi.org/10.1061/(ASCE)0733-9429(1983)109:1(62)

Richards, P.J., Farrell, C., Tom, M., Williams, N.S.G., & Fletcher, T.D. (2015). Vegetable raingardens can produce food and reduce stormwater runoff. *Urban Forestry & Urban Greening*, *14 (3)*, 646-654. ISSN 1618-8667. doi.org/10.1016/j.ufug.2015.06.007

Rossman, L.A., & Simon, M.A. (2022). Storm Water Management Model User's Manual Version 5.2. US-EPA, Center for Environmental Solutions and Emergency Response, EPA/600/R-22/0030

Salerno, F., Viviano, G., & Tartari, G. (2018). Urbanization and climate change impacts on surface water quality: Enhancing the resilience by reducing impervious surfaces. *Water Research, 144*, 491-502. ISSN 0043-1354. doi.org/10.1016/j.watres.2018.07.058

Shuster, W.D., Bonta, J., Thurston, H., Warnemuende, E., & Smith, D.R. (2005). Impacts of impervious surface on watershed hydrology: A review. *Urban Water Journal, 2 (4)*, 263–275. doi.org/10.1080/15730620500386529

Sun, Y.W., Wei, X.M., & Pomeroy, C.A. (2011). Global analysis of sensitivity of bioretention cell design elements to hydrologic performance. *Water Science and Engineering, 4 (3)*, 246-257. doi.org/10.3882/issn.1674-2370.2011.03.002

Thornthwaite, C.W. (1948). An Approach Toward a Rational Classification of Climate. *Soil Science*, *66 (1)*, 77. doi.org/10.1097/00010694-194807000-00007

Thornthwaite, C.W., & Mather, J. (1957). Instructions and Tables for Computing Potential Evapotranspiration and the Water Balance. *Laboratory of Climatology*, 10.

Walters, S.P., Thebo, A.L., & Boehm, A.B. (2011) Impact of urbanization and agriculture on the occurrence of bacterial pathogens and stx genes in coastal waterbodies of central California, *Water Research*, *45 (4)*, 1752-1762. ISSN 0043-1354. doi.org/10.1016/j.watres.2010.11.032

Web GIS LIRIS ARPA Lombardia, [Data file]. https://iris.arpalombardia.it/gisINM/common/webgis_central.php?TYPE =guest (Visited on 18/05/2023)

Willmott, C.J., Rowe, C.M., & Mintz, Y. (1985). Climatology of the terrestrial seasonal water cycle. *Journal of Climatology, 5 (6)*, 589–606. doi.org/10.1002/joc.3370050602

Zhang, L., Dawes, W.R., & Walker, G.R. (2001). Response of mean annual evapotranspiration to vegetation changes at catchment scale. *Water Resources Research, 37 (3)*, 701–708. doi.org/10.1029/2000WR900325

Zhang, L., Ye, Z., & Shibata, S. (2020). Assessment of Rain Garden Effects for the Management of Urban Storm Runoff in Japan. *Sustainability, 12 (23),* 9982. doi.org/10.3390/su12239982

Zheng, P., Kem J., Pan, W., Zhan, X., & Cai, Y. (2018). Effects of Low-Impact Development on Urban Rainfall Runoff under Different Rainfall Characteristics. *Journal of Environmental, 129*, 577-585. doi.org/10.15244/pjoes/85348

Zhou, Q., Leng, G., Su, J., Ren, Y. (2019). Comparison of urbanization and climate change impacts on urban flood volumes: Importance of urban planning and drainage adaptation. *Science of the total Environment, 658,* 24-33. ISSN 0048-9697. doi.org/10.1016/j.scitotenv.2018.12.184

Chapter 5 - Conclusions

In this dissertation, the two following aspects were evaluated:

- the capability of electronic sensors to provide real-time data for monitoring the hydraulic performance of raingardens and detecting malfunctions. This was aimed at developing a predictive maintenance regime to guarantee the continuous optimal functioning of these systems.
- the effectiveness of the raingardens, through their implementation into an hydraulic model of the sewer network of a portion of the city of Brescia, in reducing the urban runoff and the peak flow resulting from rainfall events and thus contributing in the creation of a more resilient and sustainable urban environment against the effects of climate change.

The motivation behind this research stems from an increasing global need to identify solutions that are economically, socially, and environmentally sustainable. These solutions are essential for tackling the challenges posed by rapid urbanization and the escalating threats of climate change. Raingardens emerge as a promising solution in this context. However, their adoption, especially in Italy, has been slow. This is primarily due to a lack of awareness and understanding of the significant benefits they offer when implemented in urban settings, along with concerns about the possibility of facing high and practically demanding maintenance costs.

By contrast, in countries like Australia, where raingardens have been widely adopted for years, the focus has shifted towards enhancing their monitoring and maintenance processes. This helps to ensure the maintenance of high performance of the raingardens

over time. In this regard, the use of electronic sensors to quantify the hydrological performance of these systems represents an innovative and cost-effective approach. This not only facilitates remote monitoring, significantly cutting down on the time and human resources required, but it also paves the way for establishing a predictive maintenance regime. Such a regime leverages real-time data to anticipate and address potential issues before they escalate, ensuring the long-term effectiveness and sustainability of raingardens as a tool for urban climate resilience.

5.1 Sensor on Biofilter

The capability of low-cost electronic sensors to provide real-time data on the hydraulic performance of raingardens was assessed through a laboratory experiment. Specifically, 15 columns were created, designed according to the guidelines for a typical raingarden design, consisting of three different soil layers: a filter layer made of fine sand, a transition layer made of coarse sand and sugarcane mulch, and a bottom drainage layer made of gravel. The columns also had a ponding area created by inserting a plexiglass barrier sealed with silicone, which allows for water accumulation on the surface, and a storage area (saturation zone) created by inserting an outflow pipe at 40 cm from the bottom. The columns were then divided into three different groups, characterized by three different operations: one group representing the normal functioning of a raingarden, a second group representing functioning with preferential flow paths in the soil layers, and the last group representing functioning in case of surface clogging. The three operations were validated through infiltration tests.

Additionally, three different types of sensors were placed inside the columns: one for measuring Soil Water Tension (Chameleon Soil Water Sensor), one for measuring Volumetric Water Content % (Truebner SMT 100 soil moisture and temperature sensor), and one for measuring temperature (DS18B20). Two sensor clusters were placed into each column, one in the upper part within the filter media and the other in the middle part of the column within the transition layer. To test the reliability of the sensors, two simulation sessions were planned: the first consisted of 4 dosing events characterized by different intensities and different antecedent dry days (ADD), and a second phase of simulations consisting of 8 events, also characterized by different rain intensities and ADD. The choice of events and ADDs was based on an analysis of rainfall data from the last 17 years recorded by a rain gauge station in central Melbourne.

The sensors of the upper cluster demonstrated their ability to deliver real-time data that clearly differentiated between the three distinct operational scenarios.

On the contrary, the sensors placed in the central part of the column did not show any differences between the three operations, probably due to a design error. Specifically, the

sensors were positioned too close to the saturation zone. It is believed that, due to capillarity, the soil around the sensors maintained constant moisture levels, preventing the sensors from detecting variations during the simulation of events.

The relationship between the SWT values measured by the Chameleon sensor and the VWC values measured by the SMT 100 sensor led to the creation of three different soil characteristic curves representative of the three different column operations. The curve of the group representing normal operation accurately follows the characteristic curves for sandy soils reported in the literature, validating the accuracy of the data measured by both sensors. The other two curves obtained also refer to the curves reported in the literature but are limited to describing only part of the curve.

The data measured by the SMT 100 sensor, which is also cost-effective but more reliable and tested compared to the Chameleon sensor, underwent a more thorough analysis aimed at finding specific indices that could characterize the individual operations of the columns.

Specific descriptive parameters were identified to trace the trends of values throughout the simulation periods. The analysis of these parameters, such as the variation in Volumetric Water Content (VWC) at the time of water dosing, the change in VWC during the dry period between simulations, or the magnitude of the peak corresponding to the instant change in soil moisture, were examined to identify characteristic recurring values for each type of operation.

From the data analysis, it was possible to characterize the operation of columns more distinctly with preferential flow paths, which stood out due to larger and quicker VWC variations compared to the other two groups of columns. They also exhibited sharper peaks and smaller VWC changes over the dry period. At this stage, the identified indices are not considered useful for accurately distinguishing between normal operation and operation with surface occlusion.

A particularly effective parameter for characterizing the operation of columns with surface occlusion is the measurement of outflow volume. These columns have demonstrated a greater capacity to retain inflow water, generating smaller outflow volumes compared to other columns. Specifically, the outflow was always about the 85 - 90% of the volume of water introduced for the simulation. In contrast, the columns of the preferential flow path group showed an almost complete inability to retain any of the water added to simulate the rainfall event, nearly always discharging the 98% of the inflow volume.

The values just mentioned, however, vary with the increase in the number of dry days between two simulated events, showing in all three groups a greater water retention capacity. In the case of the columns with surface occlusion, this exceeds even 20% up to the 35 % of the inflow volume.

By using real-time data collected by electronic sensors, this system facilitates the early identification of potential malfunctions or decreases in performance. As a result, it enables prompt actions that prevent problems from worsening, guaranteeing that raingardens and their associated infrastructure maintain optimal performance consistently. This strategy not only prolongs the service life of these green infrastructure elements but also enhances their environmental, social, and economic advantages, aiding in the sustainability and resilience of urban environments.

5.1.1 Sensor consideration

The Chameleon sensor, which provided Soil Water Tension values, proved to be reliable in delivering data due to its particularly advantageous cost of about €20. However, it also exhibited a slow performance decline over time. Therefore, its application is not suitable for very long monitoring periods (greater than 1 year). Furthermore, its use in sandy soil is not particularly appropriate due to the high permeability of sand, which allows water to infiltrate quickly, generally maintaining low soil moisture levels. These conditions proved to be particularly disadvantageous for the Chameleon sensor, which, due to its porous material structure (gypsum), requires maintaining a minimum moisture level to avoid irreparable damage to the sensor. The sensor is also particularly affected by the salt content in the soil, so high salt values (> 4 dS/m) cause it to malfunction and require recalibration. In the laboratory, salt values were well below the limit indicated by the manufacturer, but conditions could be different in field applications.

5.1.2 Project limitations

The sensors project faced several challenges that slowed down the research, presenting continuous obstacles These included issues related to incorrect interactions between the soil and sensors, due to excessive drying of the soil, which led to the detachment of the sensors from the soil layers, and in some cases to inaccurate data collection or sensor failure.

Battery life was another significant concern; the sensors required consistent power to operate, and shorter battery lifespans necessitated frequent replacements, increasing maintenance efforts and measurement instability caused by energy fluctuations.

Additionally, various electronic problems were encountered, ranging from BOSL board malfunctions to difficulties in data transmission. These electronic issues disrupted the continuous monitoring of the raingardens, leading to gaps in data or incorrect performance assessments. Finally, limitations with the internet signal posed another challenge for real-time data transmission.

5.1.3 Future steps

The project has shown great potential, but further steps are needed to improve some critical aspects.

To tackle the issues encountered, future steps must focus on:

- conducting a comprehensive analysis that encompasses a review of the BoSL board code and communication protocols;
- evaluating and optimizing the power management systems to prevent the BoSL board from entering a "sleep" mode, ensuring its proper operation until the battery is fully drained;
- performing extensive tests on the BoSL board's internet connection to assess its performance across different battery charge levels and under various environmental conditions.

Addressing these challenges will significantly improve the reliability and performance of the sensor system, leading to enhanced data collection and more effective decision-making processes. This is crucial for the successful application of sensor technology in monitoring raingarden performance, and it involves not only selecting the appropriate technology and infrastructure but also developing strategies for regular maintenance and problem-solving to ensure the continuous and effective operation of the monitoring system.

5.2 Raingarden numerical model

The study on raingarden implementation in the city of Brescia urban context aimed to assess the effectiveness of raingardens in reducing peak flow and surface runoff within a highly impermeable urban catchment. The choice to use raingardens as green strategy to mitigate runoff volumes and peak flows was motivated by the urban characteristics of the study area, predominantly comprised of industrial facilities and extensive transportation infrastructure. The inherent geometric versatility of raingardens allows for their integration into urban landscapes in various forms, such as linear installations along sidewalks and roads, or as ornamental flower beds nestled between buildings. This adaptability makes raingardens an especially suitable solution for urban areas where space may be limited or highly segmented.

To assess the potential raingardens performances in the context of Brescia, a typical stratigraphic configuration complemented by an underdrain system was simulated. This setup was modelled using the Environmental Protection Agency (EPA) Storm Water Management Model (SWMM) software, specifically employing its Low Impact Development (LID) module.

The SWMM software, which is one of the most widely used tools for modelling the hydraulic and hydrologic processes involving drainage networks, was utilized to create the current state of the sewer network based on the geometric and flow data provided by the integrated water service management body A2A Ciclo Idrico. The model was then calibrated and validated based on flow rate values measured at some strategic points within the network. The model was subsequently implemented with raingardens whose physical characteristics were chosen based on the guidelines for the proper design of these systems.

The implementation of raingardens was evaluated based on different de-pavement scenarios corresponding to 2%, 3%, and 4% of the impermeable area of the urban catchment. The raingardens were incorporated into the model as individual subcatchments, operating as outlets for the existing sub-basins which were disconnected from the network nodes and were channelled into the raingarden, which in turn acts as a mitigation system before discharging back into the existing network.

The hydrologic response of the urban catchment and the hydraulic behaviour of the sewerage system were simulated under different rainfall events characterized by different return periods (2, 5 and 10 year), as well as continuous simulations spanning 12 months (rainfall data for the year 2022 and 2023), considering precipitation, air temperatures, and potential evapotranspiration values as input parameters.

The simulations were also carried considering future climate scenarios as well. Specifically, three climate scenarios corresponding to three different Representative Concentration Pathways (RCP) set by the IPCC (Intergovernmental Panel on Climate Change) were created: RCP 2.6, RCP 4.5, and RCP 8.5. These represent three future scenarios characterized by greenhouse gas concentration pathways equivalent to a radiative forcing of 2.6 W/m^2, 4.5 W/m^2, and 8.5 W/m^2, respectively. The future periods considered for the evaluations are those related to the decades 2040-2059 and 2080-2099. To assess the performance of raingardens in future climate contexts, seasonal correction factors were identified and used to derive design rainfall events on a seasonal scale (summer, autumn, winter, and spring).

Environmental benefits were estimated based on hydrologic performance indexes, including peak flow reduction, volume reduction, and hydrograph delay. The simulation results of the current state of the sewerage system revealed that the existing infrastructure is inadequate to handle the water volumes generated by meteorological events, even those with a two-year return period.

Regarding the results obtained in future climate scenarios, raingardens exhibited varied performance depending on the simulated seasons. Specifically, the greatest benefits were observed during the autumn and summer seasons, with peak reductions of up to 26%. In contrast, they proved less effective during the winter and spring seasons, with more

limited benefits, especially for a return period of 10 years where the average peak reduction was around 4%, and volume reduction was limited to 2%.

These findings underscore the critical importance of considering future climate scenarios in urban planning endeavours. It highlights the inadequacy of rain garden implementation covering less than 4% of the impermeable area to effectively manage water volumes under potential future climate conditions. Thus, it provides valuable insight for decision-makers, emphasizing the necessity of proactive measures to enhance urban resilience in the face of climate change.

Continuous simulations demonstrated significant reductions in runoff volumes over the year (up to 75.4 % for the 2022 and 52.5 % for the 2023 both considering the 4 % EIA conversion scenario) and a significant increase in the infiltration rates (up to 207 % for 2022 and 177.2 for 2023 still for the 4 % EIA conversion scenario). Less significant were the benefits in terms of evapotranspiration.

In event-scale simulations, raingardens proved more effective in mitigating the impact of medium to low-intensity events (with a two-year return period) compared to higher-intensity events (with a ten-year return period). Implementation of raingardens resulted in an average peak reduction at the outlet of approximately 15%, with a delay of 5-10 minutes, and a runoff volume reduction of 10%.

To conclude the evaluation of raingarden implementation across different de-pavement scenarios (2%, 3%, and 4% of impermeable area) elucidates their potential in mitigating urban stormwater issues. By incorporating raingardens as individual subcatchments within the existing drainage network that act as outlet for the drainage network subcatchments, significant reductions in runoff volumes and improvements in infiltration rates are observed. However, it is noted that the environmental benefits of raingardens vary across rainfall intensities considering the actual and the predicted future climate.

The modelling results highlight the essential role of raingardens in mitigating the impacts of urbanization and climate change on sewer systems. Results underscore the necessity of integrating Low Impact Development (LID) practices into strategic land use planning to achieve sustainable stormwater management objectives. These include minimizing the occurrence of overflow discharges, reducing the load of pollutants entering water bodies, and preventing drainage system failures. The adoption of raingardens, as demonstrated by the modelling approach, significantly contributes to reducing the overall flood risk, thereby advocating for their broader implementation in urban catchments.

Moreover, these findings contribute to a comprehensive understanding of the effectiveness of raingardens under various climatic conditions, offering valuable insights for future planning and adaptation strategies to be adopted in sustainable stormwater management. This evidence supports the argument for a strategic, widespread adoption of raingardens and similar green infrastructure as part of a holistic approach to urban water

management, aligning with sustainability goals and enhancing resilience against changing climate patterns.